Site specific traffic load factor approach for the assessment of existing bridges

by Sergi Pérez Sifre

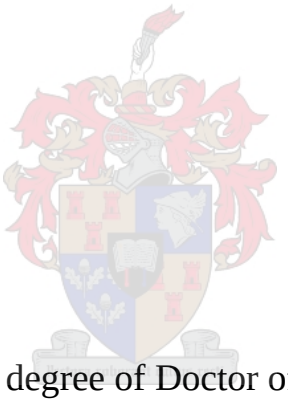

Dissertation presented for the degree of Doctor of Philosophy in the Faculty of Engineering at Stellenbosch University

Supervisor: Dr-Ing Roman Lenner

December 2020

DECLARATION

By submitting this thesis/dissertation electronically, I declare that the entirety of the work contained therein is my own, original work, that I am the sole author thereof (save to the extent explicitly otherwise stated), that reproduction and publication thereof by Stellenbosch University will not infringe any third party rights and that I have not previously in its entirety or in part submitted it for obtaining any qualification.

ABSTRACT

Maintenance of existing bridges is a matter of on-going concern for engineers and local authorities. In most developed countries, a large percentage of bridges in service nowadays was constructed decades ago. The design of these structures was executed using codes and guidelines that could be now outdated. In addition, owing to increased traffic loads, traffic intensity and deterioration of materials due to aggressive environments over time, it is necessary to evaluate bridge performance to assure the continuance of high levels of safety and comfort for users. Even though important advances have been accomplished in this matter, especially regarding the resistance side of this issue, there are still opportunities for enhancements of the traffic load models used for the assessment of existing bridges.

Recent technological advances as Weigh-in-Motion recordings and probabilistic approaches such as Monte Carlo simulations of artificial traffic allow for more accurate estimation of the traffic load effects on bridges. This is, however, not an option for the majority of practicing engineers and it is not desirable from the bridge-owners' perspective due to the potentially high associated cost of investigations.

In this contribution, an innovative, general and simple procedure for the estimation of the site-specific load effects on existing bridges is presented. Traffic design load model effects are modified through the application of various site-load factors in order to adapt the load effects to the specific conditions of the traffic circulating over the assessed bridge. In contrast to previous studies, the here developed method is based on simple observation of basic traffic descriptors such as average daily truck traffic, or percentage of long vehicles. These can be easily obtained, which presents a novel and simplified approach in comparison to WIM data based reduction factors.

The calibration of the site-load factors is performed using a new Monte Carlo routine based on bivariate copula functions. The simulation of artificial traffic not only allows for the generation of extreme events that are not usually recorded by WIM stations but also allows for the modification of certain variables in the traffic generated to evaluate its influence on the load effects. It therefore also allows for a simulation of traffic not encountered on major highways.

Shorter remaining service life is usually at play when assessing existing structures. This is usually taken into account by reduced reference periods and consequently lower characteristic values of the variable loads. Reduced target reliability levels and therefore, lower safety margins, are also considered in the assessment due to the increased cost of strengthening and

achieving an optimal cost of safety. Both concepts are applied here for the calibration of the partial safety factors.

Moreover, an additional partial safety factor is introduced in this thesis. Traffic flow is not constant and fluctuates with the time, therefore this affects the estimation of the traffic descriptors necessary for the calculation of the site-specific load effects. This new partial factor accounts for this uncertainty and mitigates its undesirable consequences.

The proposed procedure is validated using reliability analysis techniques to ascertain that the intended reliability levels are achieved in any scenario.

Lastly, a general framework for the calibration of the design traffic load models for the assessment of existing bridges is established here. The most important aspects of this work are discussed and summarised for its applicability in any other regions.

The presented results show the important modifications on the design load model load effects that can be achieved by taking into account site specific traffic conditions from simple traffic counts. Especially, the estimation of the traffic load effects in minor roads with very light traffic can be significantly improved. In addition, the new safety partial factors calibrated with reduced reference periods for shorter remaining service life and reduced target reliability indices allow for a more accurate assessment of existing bridges. The service life of the assessed bridges could be, therefore, extended or unnecessary and costly repairs avoided.

OPSOMMING

Die instandhouding van bestaande brûe is 'n saak wat die ingenieurs en die plaaslike owerhede deurlopend bekommer. In die meeste ontwikkelde lande is 'n groot persentasie brûe wat tans in diens is, dekades gelede gebou. Die ontwerp van hierdie strukture is uitgevoer met behulp van kodes en riglyne wat nou verouderd kon wees. Vanweë verhoogde verkeersbelasting en verkeersintensiteit en agteruitgang van materiale as gevolg van aggressiewe omgewings met verloop van tyd, is dit ook nodig om die prestasie van die brug te evalueer om die kontinuïteit van hoë veiligheid en gemak vir gebruikers te verseker. Alhoewel belangrike vooruitgang hiertoe bewerkstellig is, veral wat betref die weerstandkant van hierdie kwessie, maak die meeste lande steeds gebruik van ontwerpstandaarde vir die beoordeling van bestaande brûe.

Onlangse tegnologiese vooruitgang soos Weeg-in-Mosie stasie en waarskynlike benaderings soos Monte Carlo-simulasies van kunsmatige verkeer maak voorsiening vir 'n akkurate beraming van die effek op verkeersbelasting op brûe. Dit is egter nie 'n opsie vir die meerderheid praktiserende ingenieurs nie, en dit is ook nie wenslik uit die perspektief van die brug-eienaars nie as gevolg van die koste verbonde aan ondersoeke.

In hierdie bydrae word 'n innoverende en eenvoudige prosedure vir die beraming van die terrein-spesifieke laseffekte op bestaande brûe aangebied. Effekte van die vragmodel van die verkeersontwerp word gewysig deur die gebruik van verskillende terreinbelastingfaktore om die laseffekte voldoende toe te pas op die spesifieke omstandighede van verkeer wat oor die beoordeelde brug sirkuleer. Hierdie terreinbelastingfaktore is 'n funksie van basiese verkeersbeskrywers en kan maklik verkry word deur verkeerstellings.

Die kalibrasie van die terreinbelastingfaktor word uitgevoer met behulp van 'n nuwe Monte Carlo-roetine gebaseer op tweevoudige kopula-funksies. Die simulasie van kunsmatige verkeer maak nie net voorsiening vir ekstreme gebeure wat gewoonlik nie deur WIM-stasies opgeneem word nie, maar ook om die veranderlikes in die verkeer wat gegenereer word, te verander om die invloed daarvan op die laseffekte te evalueer.

Korter oorblywende lewensduur word gewoonlik ondervind by die beoordeling van bestaande strukture. Dit word gewoonlik in ag geneem deur verminderde verwysingsperiodes en gevolglik die laer waardes van die veranderlike vragte. Verlaagde teikenbetroubaarheidsvlakke en laer veiligheidsperke word ook oorweeg as gevolg van die hoër koste om bestaande strukture te versterk as dit met die ontwerpstadium vergelyk word. Beide konsepte word hier toegepas vir die kalibrering van die gedeeltelike veiligheidsfaktore.

Verder word 'n addisionele gedeeltelike veiligheidsfaktor in hierdie tesis bekendgestel. Verkeersvloei is nie konstant nie en wissel met tyd, daarom beïnvloed dit die beraming van die verkeersbeskrywers wat nodig is vir die berekening van die terrein-spesifieke laseffekte. Hierdie nuwe gedeeltelike faktor is verantwoordelik vir hierdie onsekerheid en verminder die ongewenste gevolge.

Die voorgestelde prosedure word gevalideer met behulp van tegnieke vir betroubaarheidsanalise om te bepaal of die beoogde betroubaarheidsvlakke in enige scenario bereik word.

Laastens word hier 'n algemene raamwerk vir die kalibrering van die ontwerp-verkeersbelastingmodelle vir die beoordeling van bestaande brûe ingestel. Die belangrikste aspekte van hierdie werk word bespreek en saamgevat vir die toepaslikheid daarvan in enige ander streek.

Die aangebied resultate toon die belangrike modifikasies op die lasbelastingeffekte van die ontwerpbelastingmodel wat bereik kan word deur die spesifieke verkeerstoestande in ag te neem uit eenvoudige verkeerstellings. Die beraming van die effek van die verkeersbelasting op geringe paaie met baie ligte verkeer kan veral aansienlik verbeter word. Daarbenewens het die nuwe veiligheidsgedeeltes wat gekalibreer is met 'n verminderde verwysingsperiode vir korter oorblywende lewensduur en verminderde teikenbetroubaarheidsindekse, 'n akkurater beoordeling van die bestaande brûe moontlik gemaak. Die gebruiksduur van die brûe se gebruiksduur kan dus verleng of onnodig en duur herstelwerk vermy word.

ACKNOWNLEDGMENTS

Firstly, I would like to express my gratitude to the Structures Division at Stellenbosch University, especially to my supervisor Dr.Ing. Roman Lenner, for granting me the opportunity to grow both as an engineer and as a person during the three years that I have dedicated to complete my PhD. Not only has the academic side of my period in South Africa been rewarding but living in such a wonderful place such as Stellenbosch and being able to enjoy this beautiful country is something that I will always remember. I will leave South Africa with a bag full of great experiences and amazing friends. Thank you to all of you as well. You have made this journey easier.

My special thanks goes to my mother, father and sister. They have been an unconditional support since the moment I decided to take on this opportunity. Being so far away from home for such a long time has been challenging for all of us. Despite not being always able to express my gratitude, I am truly grateful to you for helping me all the way to where I am.

Date: December 2020

TABLE OF CONTENTS

DECLARATION ..... **I**

ABSTRACT ..... **II**

OPSOMMING ..... **IV**

ACKNOWNLEDGMENTS ..... **VI**

TABLE OF CONTENTS ..... **VII**

CHAPTER 1: INTRODUCTION **1**

1.1 Objectives 3

1.2 Research Scope 4

1.3 Outline of the thesis 4

CHAPTER 2: LITERATURE REVIEW **8**

2.1 Concepts of probability and reliability of structures 8

2.1.1 Random variable 8

2.1.2 Estimation of distribution parameters 12

2.1.3 Reliability concepts 13

2.1.4 Reliability based partial factors 16

2.2 Uncertainty 20

2.3 Determination of extreme load effects 22

2.4 Assessment of existing bridges 26

2.4.1 Codes 28

2.4.2 Research publications and projects 37

2.5 A new design load model for South Africa 41

2.6 Artificial traffic generation using Monte Carlo techniques. 41

2.6.1 Gross vehicle weight and axle loads 41

2.6.2 Axle spacings 46

2.6.3 Vehicle gaps or headways 47

CHAPTER 3: TRAFFIC DATA PROCESSING **51**

3.1 WIM data 51
3.2 Data filtration 55
3.3 Truck tractor method 56
3.4 Traffic composition 60
3.5 Gross vehicle weight and axle load distributions per vehicle class 63
3.6 Axle spacings 66
CHAPTER 4: TRAFFIC MODELLING 69
4.1 The gross vehicle weight and axle loads 70
4.2 Axle spacing 76
4.3 Vehicle gaps 77
4.4 Algorithm 80
4.5 Operational days per year 81
4.6 Load effects - Comparison of recorded to simulated 82
CHAPTER 5: INFLUENCE OF THE TRAFFIC DESCRIPTORS ON THE LOAD EFFECTS 86
5.1 Average daily truck traffic – ADTT routine 87
5.2 Percentage of six- and seven-axle vehicles routine 89
5.3 Percentage of long vehicles routine 89
5.4 Results. 91
5.4.1 Average daily truck traffic 91
5.4.2 Ratio six- to seven-axle vehicles 92
5.4.3 Percentage of long vehicles 93
5.4.4 Conclusions 94
CHAPTER 6: SITE LOAD FACTORS 97
6.1 Two lane traffic simulations 103
6.2 Extrapolation of load effects 104
6.3 Results and comments 106
6.4 Validation 109

6.5 Conclusions 111

CHAPTER 7: UNCERTAINTY EVALUATION AND PARTIAL FACTORS 112

7.1 Uncertainty in the determination of the characteristic load effects. 116

7.2 Estimation of the traffic descriptors uncertainty 118

7.3 Reliability based partial factor 126

7.4 Model uncertainty 127

7.5 Final partial factors 128

7.6 Reliability verifications 128

7.6.1 Traffic load factor and partial factor layering verification 129

7.6.2 Sensitivity factors for loading 132

CHAPTER 8: APPLICATION OF THE SITE LOAD FACTOR APPROACH 138

CHAPTER 9: SUMMARY 142

9.1 Proposed framework and application in other regions 143

9.2 Recommendations 144

9.3 Future research 145

CHAPTER 10: REFERENCES 147

APPENDIX A 159

A.1 Vehicle classes and axle spacings 159

A.2 Vehicle loads 165

A.3 Generated and recorded axle load-GVW structure 172

A.4 Normal fit to tail of the GVW 176

A.5 Comparison recorded and simulated load effects. 178

A.6 Influence of the traffic descriptors on the load effects. 180

APPENDIX B 182

B.1 Extrapolation of load effects 182

B.3 Site load factors. 199

B.4 Validation load effects. 204

B.5 Traffic partial factors. 206

B.6 Reliability based partial factors. 207

B.7 Reliability analysis 217

CHAPTER 1: INTRODUCTION

A road transport network is essential for modern economies. In fact, a developed and safe transport system is a key factor for the economic growth and well-being of societies since an important percentage of the movement of people and goods are carried by roads.

National authorities, therefore, invest significant amounts of money in road networks, and bridges are one of their most vulnerable and expensive element. Bridges and similar structures allow roads to cross natural and artificial obstacles such as rivers, railways or other roads. Bridges are also effective structures that improve traffic flow at intersections and connect remote areas that would be inaccessible otherwise. In relative terms, the construction and maintenance of bridges requires a significant investment that is much more costly than other elements encountered in roads.

In most developed countries, a large percentage of bridges in service nowadays was constructed decades ago. The design of these structures was executed using codes and guidelines that could now be outdated. In addition, owing to increased traffic loads, traffic intensity and deterioration of materials due to aggressive environments over time, it is necessary to evaluate bridge performance to assure the continuance of high levels of safety and comfort for users. For these reasons, therefore, maintenance of existing bridges is a matter of an on-going concern for engineers and local authorities. Even though important advances have been accomplished, especially regarding the resistance side of this issue, there are still opportunities for enhancements of the traffic load models used for the assessment of existing bridges.

Design codes are calibrated to provide optimum safety levels for the design of a wide range of structures, heavily loaded routes and traffic scenarios. Conservatism for new bridges is widely accepted since the cost of increasing the strength is minimal at this stage; however, the design codes tend to be overly conservative and inefficient when the performance of existing bridges is evaluated. In addition, operations such as strengthening or the replacement along with restrictions of heavy traffic may become very costly and disruptive for the community. Consequently, assessed bridges may fail a contemporary evaluation using design codes but in reality, they could be carrying lighter traffic and exhibit satisfactory performance. More accurate evaluations, therefore, could help to avoid unnecessary repairs or replacements.

One advantage of the assessment of existing bridges is that real data can be collected, thus reducing the uncertainty in the variables involved in the analysis. During the design, values of

resistance of materials and loads are based on assumptions or detailed in codes that might not be representative for the site. Among the variable actions taken into account when designing or assessing a bridge, traffic load plays a decisive role and presents high uncertainty. Consequently, the accurate evaluation of existing bridges should consider the estimation of the real traffic that the bridge is currently carrying.

Technological advances such Weigh-in-Motion (WIM) systems facilitate the task of collecting traffic data. Traditional methods, such as static weight stations, do not provide the same amount of information possible with a modern WIM station. Furthermore, the disadvantage of static stations is that they can produce biased data sets since most of the overloaded vehicles tend to avoid them. In contrast, modern WIM stations are not visible to most road users and therefore, collect sustained traffic data that can authentically provide an extremely useful database for the investigation of the effects of road traffic on bridges. Moreover, not only are WIM stations capable of recording the gross vehicle weight but also all the information necessary to characterize the traffic flow: individual axle loads, axle spacings, length of the vehicle, speed and time stamps.

Although an important advance, the expense of installation and maintenance of WIM equipment makes this technology scarce and therefore its use is not yet extended in many countries. Consequently, the probabilistic approaches such as the Monte Carlo simulations are a way to overcome the issue of limited data. The most relevant variables of the traffic flow recorded by a few WIM stations can be accurately modelled and simulated for the generation of artificial traffic data. In addition, simulation of extensive convoys of vehicles enables the completion of traffic data, which especially increases the number of extremely heavy vehicles that are rarely recorded in real traffic flows.

Ideally, an accurate assessment of an existing bridge would require the evaluation of the real traffic circulating over the structure, and therefore allow for the calibration of a site-specific load model. However, the challenge with the site-specific traffic load model for existing bridges typically lies in complicated numerical procedures, WIM data setup and extensive knowledge of statistical extrapolation. This is not an option for the majority of practicing engineers and it is not desirable from the bridge-owners' perspective due to the associated cost of investigations - especially for smaller bridges located off main national highways. The motivation for this study, therefore, is to address this issue by developing a general procedure to modify the design load models based on site-specific traffic conditions. Research projects in the past had introduced a variety of reduction factors for the design load models based on WIM data and/or

extensive simulations. This thesis aims at developing a new framework for defining a site-specific load model based on, in contrast to previous studies, easily obtainable descriptors of crossing traffic.

1.1 Objectives

The main objective of this thesis is to establish a framework for the reliability calibration of traffic design load models for the assessment of existing bridges. This is done such manner that the methodology presented can be extracted from this thesis and applied to other countries. Four secondary but essential objectives/steps are highlighted hereafter. Once these four objectives are achieved, the establishment of the main objective is completed:

- **Development a Monte Carlo routine.** Monte Carlo simulations allow for the generation of artificial traffic streams by modelling the basic variables describing the traffic flow and the vehicles. The significant advantage of this is that basic traffic characteristics can be modified in the simulations and their influence in the load effects can be evaluated.
- **Calibration of site-specific traffic load factors based on the basic traffic descriptors**. The development of a detailed site specific load model based on measured WIM data is often impractical, expensive and prolonged. It is necessary to propose a new, simple and flexible approach that alleviates these problems by allowing to use easily obtainable basic traffic descriptors such as average daily truck traffic or percentage of long vehicles to derive a more representative model at the site.
- **Evaluation of the uncertainty and the calibration of the partial safety factors**. As the proposed approach is simplified, it is important to introduce necessary safeguards alleviating the uncertainty in estimation of the traffic descriptions as well as establishing partial factors for optimal safety performance.
- **Verification the concept of the proposed site load factors.** Once the method of load reduction is established, it is required to verify the proposed layering of site load factors as well as partial factors. This is achieved by formulating a limit state and performing a first order reliability analysis.

1.2 Research Scope

This research is limited to two lanes of traffic in the opposite directions. The calculations are focused on short- to medium-span lengths from 10 m to 50 m in 10 m increments and free-flowing conditions. Extreme scenarios on these lengths are commonly found under these traffic circumstances. The three load effects considered are:

- sagging moment on single span bridges;
- shear force on single span bridges; and
- hogging moment on double span bridges. The total lengths of the bridges considered are twice the span lengths indicated in each case.

The dynamic interaction of the vehicles with the bridge is not studied here. Vehicles with a number of axles larger than eight are also ignored in further chapters since the WIM station does not provide enough observations to model these vehicles accurately. Moreover, such heavy vehicles do not occur in the studied roads without a permit. The influence on the load effects of three traffic descriptors is studied, however, only the two most influential are retained for further calculations.

Only traffic data recorded in the South African road network is utilised in this thesis. Nevertheless, the procedure described hereafter is general and adaptable to any recorded traffic data.

1.3 Outline of the thesis

A brief description of the contents of this study's chapters is presented here. Moreover, Figure 1.1 summarises the alignment of the chapters and methodology followed herein to accomplish the research objectives.

Chapter 1 introduces the issue with the assessment of existing bridges and the objectives of this thesis. Thereafter, the core of the thesis contains eight further chapters whereby the complete process of the calibration of the site-specific assessment traffic load factors is presented.

Chapter 2 discusses the Literature review. Concepts about probability, reliability of structures and uncertainty are introduced. Several methods for the determination of extreme load effects are detailed. Moreover, the most recent national codes and research publications in the field of

assessment of existing bridges are discussed. Lastly, various approaches adopted for the generation of artificial traffic with Monte Carlo techniques are presented.

Chapter 3 contains the description of the traffic data recorded (gross vehicles weight, axle loads and axle spacings) by the main station used in this work and the process followed to assure the quality of the data, namely cleaning, filtering and calibration of the traffic.

In **Chapter 4** the details of the probabilistic modelling of the traffic variables involved in the Monte Carlo simulation are described. The innovative core of the presented Monte Carlo routine is the modelling of the correlation between gross vehicles weight (GVW) and axle loads using bivariate copula functions. The treatment of the axle spacings and the headway distances are also discussed. Finally, the accuracy of new presented algorithm is verified by comparing the load effects calculated using artificial traffic and the ones obtained directly from the recorded traffic.

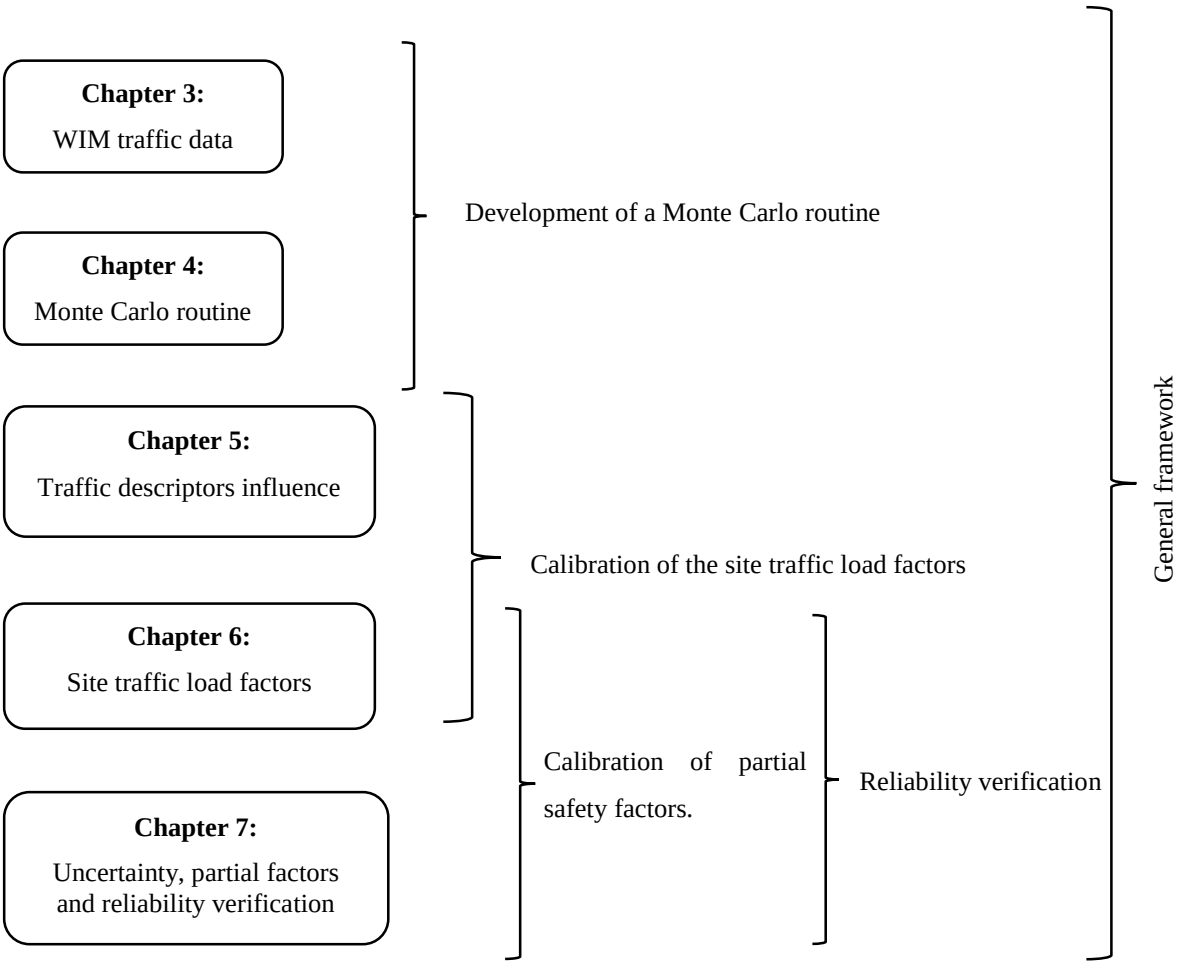

Figure 1.1. Alignment of chapters and research objectives

Chapter 5 discusses the general procedure to evaluate the influence of traffic descriptors on the load effects. Some of them might be selected for further calibrations of the site load factors. Average daily truck traffic (ADTT), percentage of long vehicles and ratio six- to seven- axle vehicles in the traffic flow are evaluated in this thesis. The ADTT is known for being a greatly influential factor on the load effects. The influence of the percentage of long vehicles and ratio six- to seven axle vehicles needs to be studied as well. Short vehicles are expected to be lighter than long vehicles. On the other hand, six- and seven-axle vehicles comprise more than 75% of the WIM traffic used in this work. Therefore, a certain correlation between these two factors and the load effects is expected.

The described Monte Carlo routine is coded to allow for the variation of the chosen descriptors and consequently for the generation of different traffic streams affected by these modifications. An evaluation on the extrapolated load effects obtained from the generated traffic is performed. The two most influential traffic descriptors are then selected to be part of the assessment site load factors.

Chapter 6 introduces the new site-specific load factors. The adaptability of this approach to the site traffic conditions is achieved through the modification of the characteristic load effects generated by the design load model. The original characteristic load effects obtained from the station used to calibrate the model are altered increasing or decreasing its values through the use of the calibrated site load factors. The site load factors are a function of the two traffic descriptors selected in the previous chapter.

This chapter then continues with the presentation of the site load factors for two-lane roads directions. The different simulations performed are detailed. The site load factors are calibrated using the characteristics values extrapolated from each simulated traffic flow. The extrapolation method used is discussed here. Furthermore, the new approach is also validated using traffic data recorded by several WIM stations. The characteristic load effects obtained directly from the recorded traffic are compared against the values modified following the previously described site-specific approach.

Chapter 7 evaluates the uncertainties. In reality, the site load factors have to be estimated using traffic counts of the traffic descriptors. Owing to the inherent variability of the traffic, the estimated descriptors might differ from the long term and more stable values and could be a source of uncertainty. A set of correction factors are then introduced. They are a function of the length of the measurements and are aimed at addressing the lack of accuracy caused by short

measurements. In addition, the reliability based partial factors and model uncertainty partial factors are calibrated considering reduced reference periods and target reliability values. The proposed site load factors and partial factors layering are verified using reliability analysis techniques.

Chapter 8 summarises the steps to be followed to apply the proposed site load factor approach and two numerical examples to clarify the concepts.

Chapter 9 provides a summary of the general procedure for the reliability calibration of the traffic design load models for the assessment of existing bridges based on the work presented here.

CHAPTER 2: LITERATURE REVIEW

2.1 Concepts of probability and reliability of structures

2.1.1 Random variable

The performance of a structural system can be described in mathematical physical terms in conjunction with empirical relations. The basic random variables are the parameters of the performance evaluation and should be able to represent the uncertainties tied to any quantity and idealise such quantity in a mathematical way (Faber, 2009). Uncertainties are detailed in Section 2.2.

Random variables are modelled using distribution functions and statistical parameters. The probability that a random variable X is equal or less than a value x is described by the cumulative distribution function (CDF):

$$F_X(x) = P(X < x) \tag{2.1}$$

The derivative of the CDF is the probability density function (PDF) and it describes the probability of the variable X to be within the interval $[x_1, x_2]$:

$$f_X(x) = \frac{dF(x)}{dx} \tag{2.2}$$

$$P(x_1 < X < x_2) = \int_{x_1}^{x_2} f_X(x) \tag{2.3}$$

The probability distributions can be described in terms of their moments. The PDFs and CDFs are often written as $f_X(x, p)$ and $F_X(x, p)$ respectively to indicate the paramenters of moments p of the distributions (Faber, 2009). The ith moment of a continuous random variable is defined as:

$$m_i = \int_{-\infty}^{+\infty} x^i \cdot f_X(x) dx \tag{2.4}$$

The mean μ_x or expected value of a random continuous variable is defined as the first moment:

$$\mu_X = E[X] = \int_{-\infty}^{+\infty} x \cdot f_X(x) dx \tag{2.5}$$

Similarly, the second moment describes the variance σ_x^2 of the random variable:

$$\sigma_X^2 = E[(X - \mu_X)^2] = Var[X] = \int_{-\infty}^{+\infty} (x - \mu_X)^2 \cdot f_X(x) dx \tag{2.6}$$

Taking the square root of the variance, the standard deviation σ_X is obtained. The ratio between the standard deviation and the mean is known as the coefficient of variation (CV). This is a good estimator of the variation of the random variable around its expected value:

$$CV[X] = \frac{\sigma_X}{\mu_X} \tag{2.7}$$

The most common probability distributions used in structural reliability for the modelling of both resistance and load variables are detailed in Table 2.1 (Zilch, 2001). This is followed by definitions of Normal distribution and the Extreme Value Theory.

Table 2.1. Statistical distribution functions in structural engineering.

Random variable	Probability distribution
Permanent loading	Normal
Variable loading (long range of values)	Gumbel
Variable loading (narrow range of samples)	Gamma
Material strength	Normal or Lognormal
Measurements	Normal
Fatigue working life	Weibull

Normal distribution

The Normal distribution is the most popular and studied of all the probability distributions for its simplicity and applicability in many practical problems. Random variables such as self-weight and geometrical properties are commonly modelled using Normal distributions. It is a suitable distribution for symmetrical variables with small dispersion. It can be defined using two parameters and its PDF is as follows:

$$f_X(x) = \frac{1}{\sigma_X \sqrt{2 \cdot \pi}} \int_{-\infty}^{x} exp\left(\frac{-1}{2}\left(\frac{x - \mu_X}{\sigma_X}\right)^2\right) dx \tag{2.8}$$

Extreme Value Theory

Extreme Value Theory (Fisher & Tippett, 1928; Gnedenko, 1943; Gumbel, 1935) is a statistical discipline concerned with developing techniques and models that can describe unusual events, either maximum or minimum (Coles, 2001). This theory is especially important in the civil engineering field since the design of structures always requires the estimation of the maximum extreme events that they are expected to suffer during its service life.

Extreme events are scarce and the current design prescriptions require levels of variables greater than have already been observed. Extreme value theory provides tools for the estimation of these unobserved extreme events from observed values.

Consider $X_1, X_2, \dots, X_n$ in Equation (2.9) a sequence of independent and identically distributed random variables with a cumulative distribution function F, the extreme value theory models the statistical behaviour of:

$$M_n = max(X_1, X_2, \dots, X_n) \tag{2.9}$$

X_i are usually observations of a process that occurs on a regular time-scale, e.g. hourly, daily or annually, therefore M_n represents the maximum observation over a period of time. The distribution of M_n can be derived theoretically:

$$\begin{aligned} &\Pr(M_n \leq x) = \Pr(X_1 \leq x, \dots, X_n \leq x) = \\ &= \Pr(X_1 \leq x) \cdot, \dots, \cdot \Pr(X_n \leq x) = [F(x)]^n \end{aligned} \tag{2.10}$$

This is not usually applicable in practice, since the distribution F is unknown. One but not recommended possibility is the estimation of F and its substitution into Equation (2.10). Very small discrepancies in the estimation can lead to important errors for F^n. Alternatively, it can be accepted that F is unknown and approximate F^n using the appropriate families of distributions, estimated only using extreme data. The theoretical background can be found in specialised literature (Castillo, 1988; Coles, 2001) but the implication of the Extreme Value Theory is that the distribution $G(x)$ of extremes M_n must belong to one of the following cumulative distribution families:

$$\text{I: } G(x) = exp\left\{-exp\left[-\left(\frac{x-b}{a}\right)\right]\right\}, \qquad -\infty < x < \infty; \tag{2.11}$$

$$\text{II: } G(x) = \begin{cases} 0, & z \leq b; \\ \exp\left\{-\left(\frac{x-b}{a}\right)^{-\alpha}\right\}, & z > b; \end{cases} \tag{2.12}$$

$$\text{III: } G(x) = \begin{cases} \exp\left\{-\left[-\left(\frac{x-b}{a}\right)^{\alpha}\right]\right\}, & z < b; \\ 1, & z \geq b; \end{cases} \tag{2.13}$$

where $a > 0$, b and for families II and III $\alpha > 0$ are the scale, location and shape parameters respectively. These distribution functions are widely known as Type I or Gumbel, Type II or Frechet and Type III or Weibull. It can be observed that the Gumbel distribution is defined on the entire real axis, the Frechet distribution is bounded on the lower tail and has a heavy upper tail and the Weibull distribution is bounded on the upper tail.

These three families of distributions can be combined into a single family known as the Generalised Extreme Value distribution (GEV) of the form:

$$G(x) = \exp\left[-\left(1 + \xi\left(\frac{x-\mu}{\sigma}\right)\right)^{-\frac{1}{\xi}}\right] \quad for \quad 1 + \xi\left(\frac{x-\mu}{\sigma}\right) > 0 \tag{2.14}$$

where μ, $\sigma > 0$ and ξ are the location, scale and shape parameters of the distribution. The shape parameter ξ dictates the behaviour of the distribution. Both Frechet and Weibull type distributions correspond to $\xi > 0$ and $\xi < 0$ respectively. For $\xi = 0$ the distribution approaches to the Gumbel family.

Figure 2.1 shows the PDF of the three types of extreme value families. The boundaries in each distribution mentioned before are appreciable on the tails.

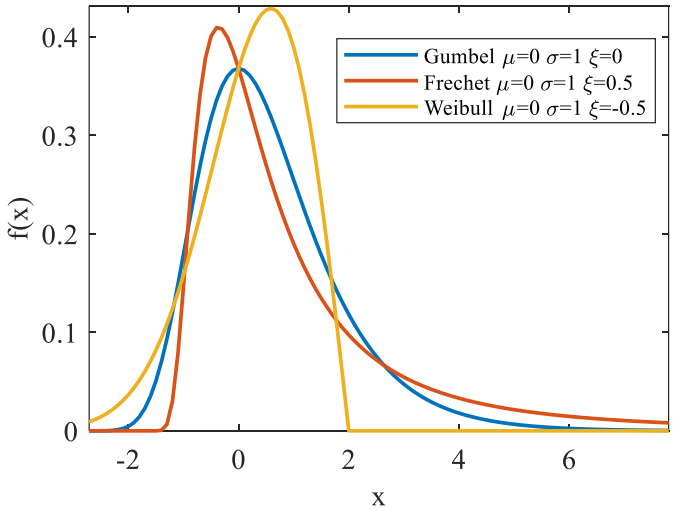

Figure 2.1. PDF of extreme value families.

2.1.2 Estimation of distribution parameters

Various techniques have been proposed for the estimation of the distribution parameters based on collected data; namely the Method of Moments and the Method of Maximum Likelihood as numerical approaches or graphical techniques based on probability plots. A brief description of these techniques is presented hereafter.

Probability plots

A probability plot is a graphical technique used to assess whether or not data follows a specific probability distribution. The data being studied is plotted on the x-axis while the y-axis is modified in such a way that if the data plotted follows a straight line it reveals good adherence to the distribution.

The plotting position of the data is based on the empirical cumulative distribution function of the data $x_1,\ldots,x_n$. Values are organised in increasing order and the position i is calculated as follows:

$$P[X \leq x_i] = \frac{i}{n} \approx \frac{i}{n+1} \tag{2.15}$$

This adjustment is made so that x_n does not have a value of 1. Other plotting positions are available in the literature (Castillo, 1988), however its influence is not remarkable as the fit is nowadays performed using numerical techniques. Assuming a Gumbel distribution the standard extremal variate (Gumbel Reduce Variate) y_i of the value x_i can be obtained from:

$$y_i = -\ln\left(-\ln\left(\frac{i}{n+1}\right)\right) \tag{2.16}$$

If the evaluated data follows a straight line, the location and scale parameters of the distribution can be estimated from the intercept and the slope of the fitted line.

The Method of Moments

Considering a random variable X with a probability density function $f_X(x;\boldsymbol{\theta})$ where $\boldsymbol{\theta} = (\theta_1, \theta_2, \ldots, \theta_k)^T$ are the distribution parameters, the first k moments $\boldsymbol{\lambda} = (\lambda_1, \lambda_2, \ldots, \lambda_k)^T$ can be written as follows:

$$\lambda_j(\boldsymbol{\theta}) = \int_{-\infty}^{+\infty} x^j \cdot f_X(x|\boldsymbol{\theta})dx \tag{2.17}$$

If the sample used in the estimation of the parameters of the distribution $\boldsymbol{\theta}$ are collected in the vector $\hat{\mathbf{x}} = (\hat{x}_1, \hat{x}_2, \dots, \hat{x}_n)^T$ the corresponding k sample of moments can be calculated as:

$$m_j = \frac{1}{n}\sum_{i=1}^{n} \hat{x}_i^j \tag{2.18}$$

Equating the k sample moments to the k equation of moments for the random variable a solution can be found solving the system of k equations and k unknown distribution parameters.

Method of Maximum Likelihood

The principle of the method is that the likelihood of the observed random sample is maximised by fitting the parameters of the distribution function.

Considering a random variable X with a probability density function $f_X(x;\boldsymbol{\theta})$ where $\boldsymbol{\theta} = (\theta_1, \theta_2, \dots, \theta_k)^T$ are the distribution parameters. Let the random sample collected be $\hat{\mathbf{x}} = (\hat{x}_1, \hat{x}_2, \dots, \hat{x}_n)^T$, the likelihood of the observed random sample is defined as follows:

$$L(\boldsymbol{\theta}|\hat{\mathbf{x}}) = \prod_{\boldsymbol{i=1}}^{\boldsymbol{n}} f_X(\hat{x}_i|\boldsymbol{\theta}) \tag{2.19}$$

Taking logarithms in the previous equation simplifies the problem:

$$l(\boldsymbol{\theta}|\hat{\mathbf{x}}) = \sum_{\boldsymbol{i=1}}^{\boldsymbol{n}} \ln(f_X(\hat{x}_i|\boldsymbol{\theta})) \tag{2.20}$$

The estimation of the parameters of the distribution can be achieved now by solving the optimisation problem of maximising the previous equation.

The combined use of approaches is common since the Method of Moments can be used as a first estimator of the parameters in the Maximum Likelihood Estimation.

2.1.3 Reliability concepts

The fundamental problem in the reliability of structures is the evaluation of the relationship between resistance R and load effects E. The assessment of this relationship should assure that the structure has enough resistance to carry the loads applied in its lifetime. This can be mathematically expressed as follows:

$$R > E \tag{2.21}$$

Rearranging the equation:

$$M = R - E > 0 \tag{2.22}$$

where M is commonly known as the margin of safety. From a probabilistic point of view, the reliability problem is assessed by considering the probability that the load effects exceed the resistance also known as the probability of failure:

$$P_f = P(E > R) = P(M < 0) \tag{2.23}$$

Owing to practical reasons and through the proper mathematical transformations the probability of failure can be expressed using the term reliability index β. The equation relating both terms is as follows:

$$\beta = -\Phi^{-1}(P_f) \tag{2.24}$$

where Φ^{-1} is the inverse standard Normal cumulative distribution function.

In Figure 2.2 a theoretical probability distribution of M is shown. The probability of failure is the area of the PDF of M below 0.

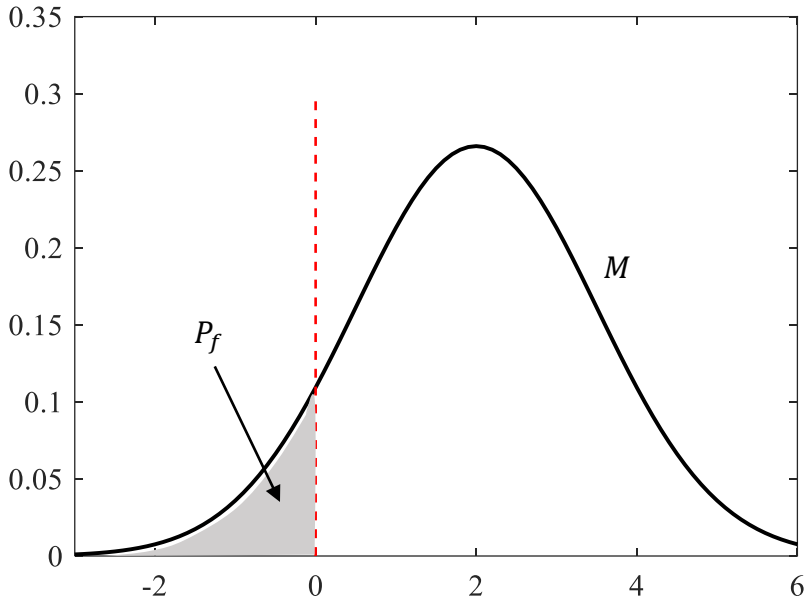

Figure 2.2. Probability of failure.

In reality, resistance and loading cannot be expressed by only two random variables but by functions of random variables:

$$R = f_1(X) \quad E = f_2(X) \tag{2.25}$$

where X is the vector of the n random variables. The previously indicated safety of margin can be indicated now as follows:

$$M = R - E = f_1(X) - f_2(X) = g(X) \tag{2.26}$$

The function $g(X)$ is commonly known as the limit state function. Negative values of the function are denoted as the failure region, positive values are denoted as the safe region. Setting $g(X) = 0$ defines a hyper surface in the space of the n random variables also known as the failure surface. The probability of failure can be determined by now solving the following multidimensional integral:

$$P_f = \int_{g(x)\leq 0} f_X(x)dx \tag{2.27}$$

where $f_X(x)$ is the joint probability density function for the vector of basic random variables X. The exact solution of the integral is not always easy to obtain and in most practical situations it is necessary to used approximate the solution by mathematical approaches. First (Lind & Hasofer, 1974) and second (Madsen, Krenk, & Lind, 2006) order reliability methods or Monte Carlo simulations (Rubinstein & Kroese, 2016) are some of the mathematical methods that can be utilised. An example of First Order Reliability Method (FORM) is shown in Figure 2.3 in the standard normal space, a requirement for the application of the method, where variables X become U. The original failure surface is linearised around the design point u^*. The reliability index β is the shortest distance from the origin to the failure surface. The design point u^* corresponds to the point with the minimum distance from the origin to the failure surface. The reliability β value can be split into its collaboration to the resistance and the load effect. Values α_1 and α_2 are known as the sensitivity factors and are fundamental for the calibration of the codes as they represent the influence of each variable in the probability of failure. They are usually taken as positive values when representing a resistance variable and negative when the variable is in the load side. The following equations hold for the sensitivity factors:

$$|\alpha_i| \leq 1; \quad \sum_i^n \alpha_i^2 = 1 \tag{2.28}$$

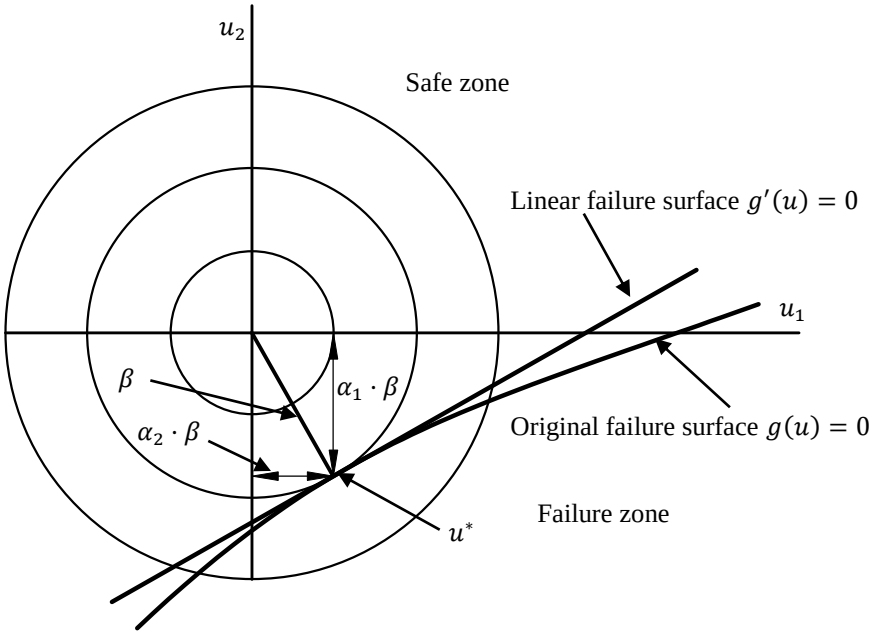

Figure 2.3. Linearised failure surface in FORM analysis.

2.1.4 Reliability based partial factors

The semi-probabilistic approach considered in modern design codes is schematically explained in Figure 2.4. The reliability or probability of failure P_f is given by the distance between mean values of R and E and the standard deviation of the distributions. The larger the distance between peaks the greater the reliability index and therefore lower probability of failure.

The semi-probabilistic concept in Eurocode (EN-1990, 2002) is based on the use of partial factors. The limit state equation can therefore be rewritten as:

$$\frac{R_k}{\gamma_R} - \left(\gamma_G \cdot G_k + \gamma_Q \cdot Q_k\right) = 0 \qquad (2.29)$$

where $\gamma_{R,}$ γ_G and γ_Q are the partial factors and R_k, G_k and Q_k are the characteristics values of the resistance, permanent loads and variable loads respectively. As can be seen from Figure 2.4 partial factors are defined as the difference between the design and the characteristics values.

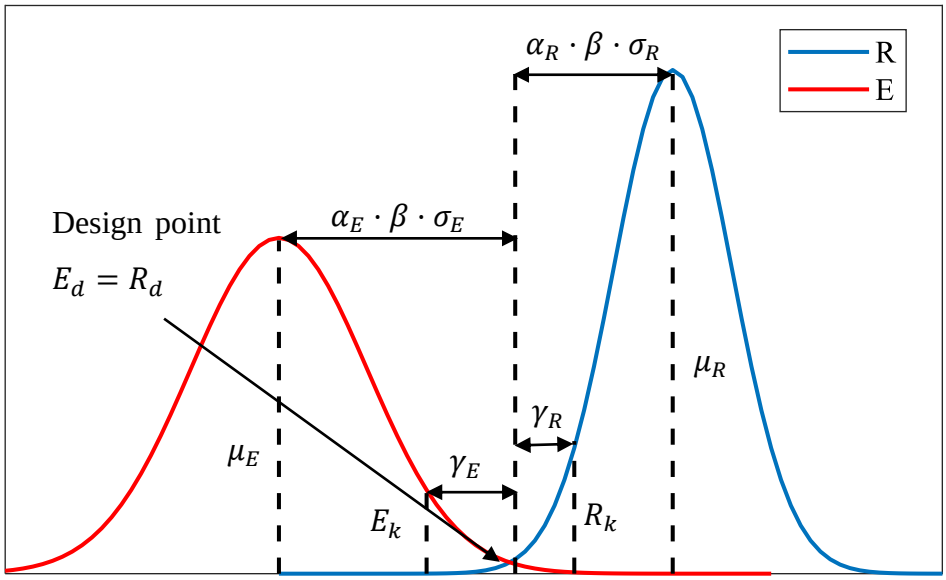

Figure 2.4. Semi-probabilistic safety concept.

Characteristic values of the variables are define as certain fractiles on the probability distributions modelling the specific variables. Generally, a 5% fractile is selected for resistance and a 95% fractile for loads. Statistically speaking this means that the selected characteristic value will not be higher or lower with a certain probability during the whole reference period.

Design values are calculated in the Eurocode as follows:

$$P(E > E_d) = \Phi(\alpha_E \cdot \beta) \tag{2.30}$$

$$P(R < R_d) = \Phi(-\alpha_R \cdot \beta) \tag{2.31}$$

where E_d and R_d are the load (permanent or variable) and resistance design values respectively.

The sensitivity factors α_E and α_R are -0.7 for leading variable actions and 0.8 for resistance according to Eurocode (EN-1990, 2002). Based on the FORM analysis the sensitivity factors are defined in the Eurocodes as follows:

$$\alpha_R = (\sigma_R)/\sqrt{\sigma_R^2 + \sigma_E^2} \tag{2.32}$$

$$\alpha_E = (-\sigma_E)/\sqrt{\sigma_R^2 + \sigma_E^2} \tag{2.33}$$

where σ_R and σ_E are the standard deviation of the resistance and the load respectively.

The Eurocodes fixes the sensitivity factors to the values indicated as long as the following condition is respected:

$$0.16 < \frac{\sigma_E}{\sigma_R} < 7.6$$

If this condition is not satisfied, then a value of $\alpha = \pm 1$ is recommended to be used for the variable with the largest variation. The simplified values selected in the Eurocodes indicated above are conservative as the sum of the squares is greater than one, therefore not complying with the value indicated in Equation (2.28).

Considering Normal, Lognormal and Gumbel distributions the design values can be directly calculated from the equations in Table 2.2.

Table 2.2. Design values according to Eurocode (EN-1990, 2002)

Distribution	Equation
Normal	$1 - CV \cdot \alpha \cdot \beta$
Lognormal	$\mu \cdot \exp(-\alpha \cdot \beta \cdot CV)$
Gumbel	$1 - CV \cdot \left[0.45 + 0.78 \cdot ln\left(-ln\left(\phi(-\alpha \cdot \beta)\right)\right)\right]$

Consequently, as anticipated before, the partial factors can be calculated using the following expression comparting characteristic and design values:

$$\gamma_R = \frac{R_k}{R_d} \tag{2.34}$$

$$\gamma_E = \frac{E_d}{E_k} \tag{2.35}$$

It can be observed that their values are highly influenced by the statistical properties of the random variable and the reliability index β. In practice, codes define what is known as the target reliability β_T used for calibrations. This value defines a minimum structural reliability and consequently, a maximum probability of failure required in any safe structure. Reliability indices are always tied to a reference period.

Target reliability levels can be calibrated from previous experiences (EN-1990, 2002). Alternatively, target reliability levels can be determined using cost optimisation methods that minimise the total working-life cost taking into account consequences of failure and cost of safety measures (Sýkora & Holický, 2011; Sýkora, Holický, Lenner, & Maňas, 2014).

Nonetheless, target reliability values are always constrained by minimum requirements for human safety from the individual or social point of view when the expected number of fatalities is taken into account (ISO 2394, 2015; Steenbergen & Vrouwenvelder, 2010).

Tables 2.3 and 2.4 show examples of target reliability levels implemented in the Eurocode (EN-1990, 2002) and ISO-2394 (2015). The Eurocode classifies the target reliability levels into three categories depending on the failure consequences. Values are provided for 1 and 50 years reference period. The ISO 2394 code, however, introduces a more detailed classification taking into account the relative cost of safety measures (annual reference period). This is especially important for existing structures due to higher upgrading cost. For an existing structure, one may use the values of one category higher (high instead of moderate).

Table 2.3. Target reliability values according to EN-1990 (2002)

Reliability class	Failure cons.	β (1 year)	β (50 years)	Examples
RC3	High	5.2	4.3	Significant bridges, public buildings
RC2	Medium	4.7	3.8	Bridges, residences, offices
RC1	Low	4.2	3.3	Agricultural buildings

Table 2.4. Target reliability values according to ISO-2394 (2015).

Relative cost of safety measures	Failure consequences		
	Minor	Moderate	Large
High	3.1	3.3	3.7
Moderate	3.7	4.2	4.4
Low	4.2	4.4	4.7

The reliability target β_T for a reference period of n years can be calculated from the following equation:

$$\Phi(\beta_n) = [\,\Phi(\beta_1)]^n \tag{2.36}$$

where β_1 is the annual target reliability, $\beta_{T,n}$ the target reliability for the desired reference period and Φ is the cumulative distribution function of the Standard Normal distribution. It should be emphasised that the values calculated using the previous equation correspond to the same reliability level but to different reference periods. The application of the previous equation is valid as long as the actions have independent statistical maxima in each year. In reality, this

is not always true and the maxima of actions in subsequent years are correlated. A more general expression is investigated by Holický, Diamantidis, & Sýkora (2018) concluding that the assumption of annual independence accepted in many codes may lead to larger failure probabilities:

$$\Phi(\beta_{nk}) = [\,\Phi(\beta_1)]^{n/k} \tag{2.37}$$

where β_{nk} is the reliability index for a n reference period and independence interval $k \leq n$ (mean time period for which the failures in subsequent periods of k years are considered to be mutually independent). The difficulty in the application of this equation is the definition of the independence interval k.

2.2 Uncertainty

Construction works are complicated technical systems that suffer from a number of significant uncertainties at all stages of execution (*Handbook 2 - Reliability Backgrounds*, 2005). Uncertainties from all essential sources must be evaluated and integrated in the basic variable model (JCSS, 2001). The sources of uncertainties are defined as follows (Kiureghian, 1989):

- **Natural variability**: randomness of the basic variables. Values cannot be fixed deterministically.
- **Statistical uncertainty**: arises from the use of insufficient data. Different sets of observations of a variable can lead to different statistical parameters. This error can be reduced by larger samples.
- **Model uncertainty**: is generally a random variable accounting for effects neglected in the mathematical models that try to represent the real life. It has two components: one due to the lack of understanding of the phenomena, and a second due to the simplifications in the mathematical models for practical reasons. Calibration of the models or more complex models can be adopted, which means that research is necessary to reduce this type of uncertainty. In structures, two types of model uncertainties can be distinguished; the load model uncertainty that captures the error introduced in the idealised representation of the loading phenomenon and the structural model uncertainty that accounts for the uncertain conversion of loads into load effects in a particular cross section due to mathematical simplifications.
- **Human error**: arises from errors made during the design, construction or operation processes in a structure. Quality assurance procedures may be useful to reduce this

uncertainty. Reassessment can reduce design errors, inspection and testing can detect construction errors and protection devices may mitigate operation errors. Usually excluded in reliability assessment owing to the quality assurance procedures mentioned.

The natural randomness and statistical uncertainties can be best described by probability and mathematical statistics. Nevertheless, the lack of data causes significant problems. Uncertainties in the theoretical models may be assessed to a certain extent on the basis of experimental research. Human error uncertainties, however, are complicated to evaluate although they are often the decisive causes of structural failure. In such cases, effective quality control procedures should be applied.

The theory of structural reliability has been developed to describe and analyse the afore-mentioned uncertainties and to consider them when designing or assessing a structure. Uncertainties in modern semi-probabilistic codes are accounted for by using the previously defined partial factors. According the Eurocodes (EN-1990, 2002) the loading partial factors, for both permanent and variable loads, can be split as follows:

$$\gamma_F = \gamma_{Ed} \cdot \gamma_f \tag{2.38}$$

where γ_{Ed} stands for the partial factor accounting for the model uncertainty in the estimation of the load effects from the load model and γ_f is the reliability-based partial partial factor accounting for the variability of the variable or permanent action, statistical uncertainty and uncertainties related to the model of variable or permanent action or traffic load effects in the context of this research.

In structural verifications the model uncertainty factor $\gamma_{Ed,q}$ can be assumed as 1.05 for unfavourable action and 1.0 for favourable action (Steenbergen & Vrouwenvelder, 2010). The fib Bulletin 80 (Allaix et al., 2016), suggests a value of 1.12 for unfavourable variable actions. Alternatively this partial factor can be estimated assuming a Lognormal distribution as indicated in Sýkora, Holický, & Marková (2013):

$$\gamma_{Ed} = \exp(-\alpha_E \cdot \beta \cdot CV) \tag{2.39}$$

where CV is the coefficient of variation of the model uncertainty and α_E and β the sensitivy factor and target reliability value detailed in the code. The recommended model uncertainties are shown in Table 2.5 as provided by the JCSS (2001).

Table 2.5. Recommended probabilistic model for model uncertainties.

Model type	Distribution	Mean value	CV
Moment in frames	LN	1.00	0.10
Axial force in frames	LN	1.00	0.05
Shear force in frames	LN	1.00	0.10
Moment in plates	LN	1.00	0.20
Forces in plates	LN	1.00	0.10

The reliability based partial factor can be calculated, as indicated in Section 2.1.4, as the ratio of the design to the characteristic value. Both values are obtained as specific fractiles from the probability distribution of maxima variable or permanent loading during the same reference period as used for the reliability index.

2.3 Determination of extreme load effects

An extensive variety of methods are available in the literature for the determination of extreme traffic load effects. This section reviews the most common approaches that include Extreme Value Distributions, Peaks over Threshold (POT), Box-Cox Method and Rice Formula.

Extreme value distributions

A common approach among researchers is the use of the classic extreme value distributions (Gumbel, Frechet, Weibull and GEV) to fit block maximum traffic load effects (daily, monthly or yearly maxima). Every distribution has a different behaviour towards the tail. The advantage of using the GEV distribution is that no assumptions must be made in terms of which extreme distribution fits the data better.

O'Connor and O'Brien (2005) fit extreme distributions of either Gumbel or Weibull to the maximum load effects. The appropriate distribution is selected by plotting the load effects on Gumbel or Weibull probability paper and assessing the linearity of the observations. This indicates good adherence to the distribution.

Getachew and O'Brien (2007) use the GEV distribution fitted to the daily maximum traffic load effects. This distribution is also used by Caprani, O'Brien and McLachlan (2008) and Caprani and O'Brien (2006) fitted to daily maximum values to obtain the extreme traffic load effects. The Composite Distribution Statistics (CDS) approach is used in the above mentioned research

papers. This approach considers every type of extreme events individually to ensure independent and identically distributed (iid) data and fits an extreme distribution to every one of them. The global load effect is achieved combining all the distributions together. This approach is also used by Enright (2010); however, Gumbel and Weibull distributions fitted to the tail of the CDF are used in this case. An evaluation of the effect of the length of the upper tail in the extrapolated values is also performed. The top 30% and top $2\sqrt{n}$ values are compared.

Raising the parent distribution of the load effects to a certain power $F(x)^n$ is also the usual approach to obtain the CDF of the maximum load effects over a certain period (Bailey, 1996; Ghosn, Moses, & Wang, 2003). Several publications indicate that a high precision in the evaluation of the $F(x)$ is necessary to obtain reliable results (Coles, 2001; Lenner, de Wet, & Viljoen, 2017). Instead, the approach presented by Bissell, Ang, & Tang (1979) is used in Soriano, Casas, & Ghosn (2016) and Ghosn, Sivakumar, & Moses (2011). It is stated that if the parent distribution of the initial variable S has a general Normal distribution with mean μ and standard deviation σ, then the maximum value after N repetitions approaches asymptotically an Extreme Value Type I (Gumbel) distribution. A series of expressions are presented to obtain the maximum load effect. Single load effects are plotted in Normal probability paper and the tail shows a clear linear trend indicating normality of the values.

Block maximum data are usually fitted with extreme value distributions, however, some researchers also use Normal distributions. Nowak (1993) finds the characteristics values by extrapolation the traffic load effects using a Normal distribution fitted to the values on Normal probability paper. Flint and Jacob (1996) fit half Normal distribution to the upper tail of the histogram of extreme values for the background work in the calibration of the Eurocode. O'Brien et al.(2015) also fit the Normal distribution to the tail of daily maximum data. The method is compared to other approaches explained.

Peaks over Threshold (POT)

An alternative to the classic extreme value distributions to model extreme events is the POT. As the name indicates, this approach calculates the maximum values of a series of data given a threshold above which a probability distribution is fitted. The preferred distribution among researchers is the Generalised Pareto distribution (GPD), which is proven to approximate the cumulative distribution function (CDF) of a POT data in Coles (2001). The GPD probability function is as follows:

$$H(x;\xi,\sigma) = \begin{cases} 1 - \left[1 + \xi\left(\frac{x-u}{\sigma}\right)\right]^{\frac{-1}{\xi}}, \xi \neq 0 \\ 1 - exp\left(-\frac{x-u}{\sigma}\right), \xi \to 0 \end{cases} \quad (2.40)$$

where u is the threshold, $\sigma > 0$ and $\xi > 0$ the scale and shape parameters respectively and $x > 0$ with $x - \frac{\sigma}{\xi} > 0$.

James (2003) applies this method to calculate extreme load effects on railway bridges. Crespo-Minguillon and Casas (1997) use the GPD to model the weekly maximum traffic load effects on bridges over a selected threshold. Other research papers (Gindy & Nassif, 2006; O'Brien et al., 2015) compare the extreme values of traffic load effects using the POT with other distributions. Zhou, Schmidt, and Jacob (2016) improve the POT approach with the GPD by individually analysing the traffic load effects generated by different loading scenarios. Assuming the same distribution for all of them contradicts the assumption of iid data necessary to apply the extreme value theory.

The key point of the method is the selection of an appropriate threshold. An excessive mixture of extreme events due to different loading scenarios can be encountered if a low threshold is selected. A high threshold can also be problematic as well since a few results are left above it, leading to unreliable results.

Several methods for the selection of thresholds are available. Graphical methods (Dargahi-Noubary, 1989) require high expertise and tend to be subjective. Simpler methods are based on order statistics (Pickands, 1975) or the selection of fixed values such as the 10% upper tail or similar. The optimal threshold is selected using the overall minimum least square value in (Crespo-Minguillón & Casas, 1997). Zhou et al. (2016) use a combination of goodness-of-fit test to calculate the optimal threshold.

The estimation of the distribution parameters can be done using several approaches as method of moments, probability weight method, maximum likelihood and Bayesian updating (de Zea Bermudez & Kotz, 2010) or weighted sum of squared errors (Crespo-Minguillón & Casas, 1997).

Box-Cox method

The Box-Cox transform (Box & Cox, 1964) is used by Bali (2003) and introduces a more general approach that combines the best of the GEV and the GPD. The Box-Cox distribution follows the equation below:

$$H(x) = \frac{1}{\lambda}\left[\left(exp\left(-\left(1-\xi\left(\frac{x-\mu}{\sigma}\right)\right)^{\frac{1}{\xi}}\right)\right)^{\lambda} - 1\right] + 1 \qquad (2.41)$$

The parameters of the distribution are the same as in the Generalised Extreme Value distribution. A model parameter λ is added. When $\lambda \to 1$ the distribution converges to the GEV; however when $\lambda \to 0$ it converges to GPD. Examples of the application of the Box-Cox method in the field of bridge engineering are found in Caprani and O'Brien (2010) and O'Brien et al. (2015).

Rice formula

The Rice formula, first introduced by Rice (1945), can be used to find a parametric fit to data. Considering the hypothesis suggested by Ditlevsen (1994) that traffic load effects on long span bridges can be modelled as a Gaussian random process, the mean rate V of up-crossing given a threshold level $x > 0$ during a reference period T_{ref} is found by the expression:

$$v(x) = \frac{\sigma^*}{2\pi\sigma} exp\left[-\frac{(x-m)^2}{2\sigma^2}\right] \qquad (2.42)$$

where x is the threshold of load effects, m the mean value, σ the standard deviation and $\sigma *$ the derivative of σ with respect to time.

The Rice formula is used by different researchers. Jacob (1991) uses the Rice formula for the prediction of characteristic traffic load effects on bridges for free and congested traffic. This work is the basis for the development of the Eurocode. Getachew (2003) also uses this approach to for the analysis of load effects on bridges using measured and simulated data. O'Connor and O'Brien (2005) compare Rice's formula with the Gumbel and Weibull extreme distributions.

Discussion

Of the four methods to determine the extreme load effects in bridges due to truck traffic described here, the most popular in the literature is fitting Extreme Value distributions to block

maximum data, either the tail or the complete series of data. The use of these distributions, including the GEV, is supported by the Extreme Value Theory. The generalization of the three Extreme Value distribution into the GEV facilitates the task of fitting distributions and eliminates the subjectivity in the process. Nevertheless, the implementation of the GEV distribution in computer software is not yet fully extended, which makes in some instances necessary the use of the three well-known Extreme Value distributions.

Peaks-over-threshold is also a popular method in some sectors to model extreme events. However, the method is not time-referenced and the selection of the threshold is a subjective process. Several methods for the determination of the appropriate threshold have been discussed previously in this section.

Box-Cox method is a hybrid of the POT and GEV. It has been used in a few instances mentioned before in the field of bridge engineering with successful results. Its more complicated formulation and its reduced presence in the most used mathematical software are disadvantages of this method.

The Rice formula is an indirect approach and it is the upcrossing frequencies that are fitted instead of the data. This method has been tested in the literature indicated before showing good performance, however, the use of the Rice formula for the determination of extreme load effects is not as extended as other approaches. The reasons mentioned for the Box-Cox method plus its indirect nature might explain this.

2.4 Assessment of existing bridges

Design codes are often based on conservative assumptions and are developed to perform well for any structural system. This is, however, not ideal when assessing existing bridges. Through the accurate structural evaluation, the lifetime of existing structures might be extended leading to substantial savings. According to Diamantidis (2001) and Wisniewski, Casas, & Ghosn (2012) the principles that differentiate the assessment of existing bridges from the design include:

1. Increasing the safety level of an existing structure usually involves more costs compared to the design phase. Lower reliability target values are accepted.
2. The remaining service life in existing structures leads to lower reference periods and consequently lower return periods for the variable loads. Load effects are decreased.

3. The reduction of the uncertainties encountered in the design stage can be achieved through the collection of available data. Actual structural conditions and load can be better measured and calibrated.
4. Advanced structural analysis techniques can be applied and justified by the significantly higher costs of upgrading or replacing the structure.
5. Proof load testing of existing bridges may serve to verify resistance models.

Great efforts towards the development of assessment codes have been made recently (BRIME, 2001; COST345, 2007; ISO 13822, 2001; Lenner, 2014; Rücker, Hille, & Rohrmann, 2006; SAMARIS, 2006). The advantages that an assessment code for existing bridges would provide are widely accepted.

The common idea behind the development of new assessment codes is the adoption of the well-known semi-probabilistic approaches found in modern design codes. The process of generalising the use of assessment codes for existing bridges among practising engineers should then be simple. The use of advanced techniques in a multi-level procedure is however proposed in multiple documents. If the load capacity of the existing bridge is not sufficient during the initial check, advanced techniques may be employed to accurately evaluate the performance of the bridge. Maljaars, Steenbergen, Abspoel, & Kolstein (2012) propose a four level assessment of existing bridges as follows:

1. Partial factors and load reduction factors for existing infrastructure based on reduced target reliability levels.
2. Current use of the structure. Actual loading conditions are considered accounting for the limiting geometry or shorter reference period.
3. Application of WIM technology along with load cells to quantify the loading and the response.
4. A full probabilistic assessment.

The resistance side of the equation have been widely studied. For example Fischer (2010) attempts to modify the partial factors of existing concrete structures reflecting their existing nature. Val and Stewart (2002) consider bridges and buildings in terms of resistance and capacity reduction factors whereby the Bayesian approach is used to recalibrate characteristics resistance and partial factors. Braml, Fisher, Keuser, & Schnell (2009) develop stochastic models to represent existing damaged of bridges. The work presented here, however, focused

on the loading side. An up-to-date review of the literature regarding the loading side of the assessment of existing bridges is therefore presented in this section.

2.4.1 Codes

CAN/CSA-S6-06

The Canadian load rating of existing bridges CAN/CSA-S6-06 (2006) is the current standard used in Canada for the assessment of bridges. The process begins with the selection of the appropriate target reliability level for a reference period of 50 years. Values depend on the system behaviour, the element behaviour and the inspection level. All values are shown in Table 2.6.

Table 2.6. Target reliability levels according to CAN/CSA-S6-06 (2006).

System behaviour	Element behaviour	Inspection level 50 years (annual)		
		Insp 1	Insp 2	Insp 3
S1	E1	4.00 (4.80)	3.75 (4.60)	3.75 (4.60)
	E2	3.75 (4.60)	3.50 (4.40)	3.25 (4.20)
	E3	3.50 (4.40)	3.25 (4.20)	3.00 (4.00)
S2	E1	3.75 (4.60)	3.50 (4.40)	3.50 (4.40)
	E2	3.50 (4.40)	3.25 (4.20)	3.00 (4.00)
	E3	3.25 (4.20)	3.00 (4.00)	2.75 (3.80)
S3	E1	3.50 (4.40)	3.25 (4.20)	3.25 (4.20)
	E2	3.25 (4.20)	3.00 (4.00)	2.75 (3.80)
	E3	3.00 (4.00)	2.75 (3.80)	2.50 (3.70)

Note: S1, element failure leads to total collapse; S2, element failure does not cause total collapse; S3, local failure only. E1, sudden loss of capacity with no warning; E2, sudden failure with no warning but with some post-failure capacity; E3, gradual failure. INSP1, component unable to inspect; INSP2, inspection records available to the evaluator; INSP3, inspections of the critical and substandard members directed by the evaluator.

The selected reliability index is not intended to be used as the target reliability in a full probabilistic analysis but only to recalibrate the load partial factors as seen in Table 2.7.

Table 2.7. Partial safety factors according to CAN/CSA-S6-06 (2006).

Load category	Symbol	Target reliability index β						
		2.50	2.75	3.00	3.25	3.50	3.75*	4.00
Permanent load D1	α_{D1}	1.05	1.06	1.07	1.08	1.09	1.10	1.11
Permanent loads D2	α_{D2}	1.10	1.12	1.14	1.16	1.18	1.20	1.22
Permanent loads D3	α_{D3}	1.25	1.30	1.35	1.40	1.45	1.50	1.55
Traffic loads	α_L	1.35	1.42	1.49	1.56	1.63	1.70	1.77

D1, factory produced components and cast in place concrete excluding decks; D2, casting place concrete decks; D3, bituminous surfacing with assumed standard thickness of 90 mm.*Target reliability index and the corresponding safety factors used also for the design of bridges.

These values are to be used in the evaluation of the bridge following the load rating parameter process, which compares resistance and load using the following equation:

$$F = \frac{U \cdot \mathrm{R_r} - \sum \alpha_D \cdot \mathrm{D} - \sum \alpha_A \cdot \mathrm{A}}{\alpha_L \cdot \mathrm{L} \cdot (1 + \mathrm{I})} \tag{2.43}$$

where R_r is the factored resistance, D the permanent load, A the secondary variable load, L the primary load, I the dynamic amplification factor, U the resistance adjustment and the corresponding load partial factors.

The prescribed traffic loads used in the assessment of existing bridges are similar to the loads used for the design stage. They consist of an 18 m long train of axles with a total weight of 625 kN or alternatively the same train with a load of 500 kN plus a uniformly distributed load of 9 kN/m per traffic lane. The code also specifies different uniformly distributed assessment loads for different road categories. Bridges that fail the initial assessment must be checked using either two or one unit vehicles with loads of 380 kN and 240 kN respectively. Consequently, the carrying capacity of bridges assessed using these reduced loads must be restricted.

AASHTO LRFR

The load and resistance factor load rating methodology (AASHTO LRFR, 2003) used for the evaluation of existing bridges in the US includes three different live load models:

- Design load: HL-93 according to LRFD (AASHTO LRFD, 2017).
- Legal loads: AASHTO legal loads.
- Permit load: permit vehicles.

Three rating factor procedures are specified in the manual based on the listed live load models using the following equation:

$$RF = \frac{C - \gamma_{DC} \cdot DC - \gamma_{DW} \cdot DW \pm \gamma_P \cdot P}{\gamma_L \cdot LL \cdot (1 + IM)} \tag{2.44}$$

where C is the capacity, DC the dead load effect, DW the dead load effect due to wearing surface and utilities, P the permanent load other than dead loads, LL the live load effects IM the dynamic load allowance and γ_i the load partial factors.

The design load (HL-93) provides a convenient and uniform basis for the design; however, it is not representative of the current traffic (Minervino, Sivakumar, Moses, Mertz, & Edberg, 2003). Furthermore, the site loads are often less aggressive than the ones obtained using the design load. If the assessed bridge fails the initial check using the design loads, the legal loads can be used as described hereafter.

The design load is used in the first step of the rating. Firstly, a reliability index of 3.5 (β_1=4.52) for a reference period of 75 years as in design is considered with a live load partial factor of 1.75. A second stage with a lower reliability index of 2.5 for a reference period of 5 years (β_1=3) leads to a partial factor of 1.35. This reference period is equivalent to the time between inspections of the bridges.

The third level of the assessment uses the legal loads with a reduced reliability index of 2.5. The partial factors depend on the ADTT as described in Table 2.8.

Table 2.8. Load factors as indicated in AASHTO LRFR (2003)

Traffic volume	Limit state	Load factor
Unknown	Strength	1.80
ADTT>5000	Strength	1.80
ADTT=1000	Strength	1.60
ADTT<100	Strength	1.40

If more traffic information is available, the load factors can be calculated using the following equations:

- For two or more lane loading case:

$$\gamma_L = 1.8\left[\frac{2 \cdot W \cdot t_{ADTT} \cdot 1.41\sigma^*}{240}\right] > 1.30 \tag{2.45}$$

- For single lane loading case:

$$\gamma_L = 1.8\left[\frac{W \cdot t_{ADTT} \cdot \sigma^*}{120}\right] > 1.80 \qquad (2.46)$$

where W is the mean truck weight for the top 20% of the truck sample, $\sigma^*$is the standard deviation of the already mentioned sample and t_{ADTT} is the fractile value appropriate for the maximum expected loading event from Table 2.9.

Table 2.9. t_{ADTT} fractiles.

ADTT	Two or more lanes	One lane
5000	4.3	4.9
1000	3.3	4.5
100	1.5	3.9

Danish Road Directorate

The Danish code for the classification of existing bridges (Danish Road Directorate, 2004) uses an uniformly distributed load of 2.5 kN/m and a set of two vehicles. Vehicles must be selected from the ones described in the code or defined by real vehicles found at the particular site. These vehicles are used to classify the bridges assessed according to the maximum weight of vehicles that they are able to carry. Furthermore, the code provides guidance for the development of fully probabilistic assessments.

ONR Richtlinie 24008, Verkehr and SIA 269 - 269/8

The Austrian (ONR Richtlinie 24008, 2014), German (Verkehr, 2011) and Swiss (SIA 269 - 269/8, 2011) codes accept a second level of assessment once the first one based on the codes for new bridges has failed. Permanent action partial factors can be reduced to 1.2 after weight is determined through measurements. In German and Swiss standards the double-axle load in the third lane it is not included however, a partial factor for live loads of 1.5 is used.

The Swiss code presents a detailed procedure for the assessment of existing bridges with different levels. If the bridge fails the initial assessment based on the design standards the next level of assessment is introduced with some differences. This is repeated as long as the verification fails and the partials factors, loads and other variables are updated in the process.

This code presents a set of adjustment factors that can be applied directly to the first and second tandem α_{Q1}, α_{Q2} and to the uniformly distributed load α_{qi} found in the LM1 (EN 1991-2, 2003). These factors depend on the type of structure and the span length as shown in Table 2.10.

Table 2.10. Load adjustment factors according to SIA 269 - 269/8 (2011).

Type of bridge structure		Span (m)	α_{Q1}	α_{Q2}	α_{qi}
Beams	Box	20-80	0.7	0.5	0.5
	Two webs	20-80			
	More webs	15-35			0.4
Slabs	Slabs	10-30			
Slab bridges and other type of bridges		5.3-10	0.6	0.4	0.4
		<5.3	0.5	0.4	0.4

The basis for the calibration of these reduction factors is the less aggressive traffic found in Swiss roads that leads to lower load effects in comparison to the LM1 more suitable for other European countries with heavier traffic. The reduction of the LM1 at the National level is allowed in the Eurocode (EN 1991-2, 2003).

BD 21/01

The design of bridges in the UK (BD 37/01, 2002) is performed using the Eurocode (EN-1990, 2002) however for the assessment of existing bridges the old assessment code is still used (BD 21/01, 2001). Reduction factors for the normal traffic loading (HA) are presented. These factors depend of the annual average hourly heavy goods vehicle flow (AAHHGVF) of the road and the roughness of the surface. Three categories of traffic flow are presented:

- High AAHHGVF>70
- Medium 70> AAHHGVF >7
- Low 7> AAHHGVF

This includes two categories of roughness:

- **Good**: in terms of ride quality, roads in good condition, no visible deterioration or low deterioration that need no action.
- **Poor**: in terms of ride quality, extensive or severe deterioration. Include roads with poor vertical alignment.

This adds up to six traffic situations. The code presents six diagrams where a K factor that has to be applied to the nominal uniformly distributed load (UDL) and the nominal knife edge load

(KEL) directly. The diagrams shows live loadings in six categories depending on the maximum GVW that the bridge should be capable to sustain. Weights are 40, 26, 18, and 7.5, fire engine loading and 3 tonnes. If the bridge fails the assessment for the highest category or weight restriction level then the factors from the following category must be applied. The process is completed when the K value found in the diagrams is lower than the C value according to the ratio:

$$C = \frac{Available\ live\ load\ capacity}{Capacity\ required\ Adjusted\ HA\ Loading} \tag{2.47}$$

Bridges are then restricted to the highest weight level that complies with the previous condition.

NEN8700

The Dutch Standard (NEN8700, 2011) establishes two levels of reliability for assessment. The target reliability index for new bridges can be reduced using Equation (2.48).

$$\beta_i = \beta_{new} - \Delta\beta_i \tag{2.48}$$

where β_i is the assessment target reliability and $\Delta\beta_i$ the reduction applied. A reduction of $\Delta\beta_{repair} = 0.5$ can be applied to bridges without significant deficiencies that do not have to be immediately repaired. Bridges considered unfit for use and require immediate measurements to be taken can adopt $\Delta\beta_{unfit} = 1.5$. These reductions have been obtained based on economic optimisations of the target reliability index (Steenbergen & Vrouwenvelder, 2010). Table 2.11 details all target reliability indices after the commented reductions. Note that the reference period for these values is 15 years.

Table 2.11. Target reliability indices in NEN8700 (2011).

Consequence class	Reference period	β_{new}	β_{repair}	β_{unfit}
CC1	15 (1)	3.3 (4.0)	2.8 (3.6)	1.8 (2.8)
CC2	15 (1)	3.8 (4.42)	3.3 (4.0)	2.5 (3.34)* Human criteria
CC3	15 (1)	4.3 (4.86)	3.8 (4.42)	3.3 (4.0)* Human criteria

A first analysis is suggested in the code based on the lower reliability indices and consequently the lower partial factors. Table 2.12 presents the modified permanent loads γ_g and traffic load γ_q partial factors based on the previous target reliability indices.

Table 2.12. Partial factors according to NEN8700 (2011).

Classification	Reference period	Partial factors			
		CC2		CC3	
		γ_g	γ_q	γ_g	γ_q
New	100	1.30	1.35	1.40	1.50
Repair	15	1.25	1.20	1.30	1.30
Unfit	15	1.10	1.10	1.25	1.25

More sophisticated techniques and updated information available based on the current condition and use of the bridge can be introduced in the second, third and fourth level of analysis.

ISO 13822

ISO 13822 (2001) specifies target values for the assessment of existing structures. It is indicated that the remaining working life of an existing structure determined at the assessment is considered equal to the reference period for serviceability and fatigue verifications, while the design working life is considered as a reference for a new structure. Even though the recommended assessment reference period of the target reliability indices for ultimate state limits is the design life, the standard states that a shorter reference period might be reasonable for ultimate limit states. Table 2.13 shows the recommended values.

Table 2.13. Target reliability indices recommended in ISO 13822 (2001).

Limit state	Target reliability	Reference period
Serviceability		
Reversible	0.0	Remaining working life
Irreversible	1.5	Remaining working life
Fatigue		
Can be inspected	2.3	Remaining working life
Cannot be inspected	3.1	Remaining working life
Ultimate		
Very low consequences of failure	2.3 (β_1=3.5)	L_s years (e.g. 50 years)
Low consequences of failure	3.1 (β_1=4.1)	L_s years (e.g. 50 years)
Medium consequences of failure	3.8 (β_1=4.7)	L_s years (e.g. 50 years)
High consequences of failure	4.3 (β_1=5.1)	L_s years (e.g. 50 years)

fib Bulletin 80

Recent approaches in the calibration of the partial safety factors for the assessment of existing structures are presented by Caspeele, Sýkora, Allaix, & Steenbergen (2013) and the fib Bulletin 80 (Allaix et al., 2016). Two alternative methods known as the Design Value Method (DVM) and the Adjusted Partial Factor Method (APFM) are proposed and verified using FORM analysis. The DVM uses the design format for the calibration of partial factors for new structures γ_X but accounting for the revision of some parameters as:

1. Reduced reference periods, which should be related to the design working life.
2. Adjusted target reliability levels for existing structures.
3. Adjusted probabilistic models for the variables, for example modified CV.
4. Adjusted model uncertainties.

Alternatively, the APFM consists of calculating adjusted partial factors γ_X^{exist} for the variables X of an existing structure, considering alternative reference periods t_{ref}, target reliability levels β_T and CV. The partial factor for existing structures for a given variable X is established by simply multiplying the partial γ_X for the design as provided in the Eurocode by an adjustment factor ω_γ as follows:

$$\gamma_X^{exist} = \omega_\gamma\left(t_{ref}, \beta_T, CV\right) \cdot \gamma_X \tag{2.49}$$

Expressions for the adjustment factor ω_γ are available in the mentioned literature. The proposed method is fully compatible with the current framework of the Eurocodes. The APFM requires less input information, it is therefore a simplified method if compared to the DVM.

Discussion

Modified reliability levels are considered in several codes. CAN/CSA-S6-06 (2006) establishes different reliability levels that can be selected based on three properties of the element being evaluated. These reliability levels are reflected in the calibration of various partial factors for both the permanent and the traffic loads. No further adjustments or recommendations are indicated for assessment. Reduced target reliability values for the assessment could be suggested among the proposed values to account for the lower level of safety allowed during the assessment of existing bridges. For instance, the selection of a lower element behaviour for the assessment could be adopted. The load and resistance factor load rating (AASHTO LRFR,

2003) only allows in a second evaluation stage for a reduction of the reliability accompanied with a reduced reference period of 5 years (time between inspections).

The Dutch Standard (NEN8700, 2011) introduces adjusted reliability levels for the assessment of existing bridges. This is an important aspect of this code as it allows for the reduction of the target reliability index in the assessment of existing bridges due to higher cost of upgrading as indicated previously. The reduced reliability levels have an impact in the calibration of the partial factors.

ISO 13822 (2001) does not provide a clear reference period for the reliability levels indicated, however an important detail is that shorter reference period (equal to the remaining service life) are accepted for serviceability and fatigue verifications as well as reduced reference periods for ultimate limit states. Alternatively, the ISO-2394 (2015) ties the reliability target values to the relatively cost of safety measures. This allows for the reduction of the reliability target values for higher relative cost, situation encountered in the assessment of existing bridges.

The fib Bulletin 80 section for the calibration of the partial factors for the assessment of structures compiles the most recent ideas in the field as indicated previously and gives a framework for the recalibration of the safety partial factors in codes. While the two approaches proposed require extensive knowledge to be applied, they can be adopted in codes for the adjustment of the partial factors for existing structures.

The reduction in the design traffic load model is accepted by the Canadian code CAN/CSA-S6-06 (2006) if the bridge fails the first evaluation. The reduction of the uniformly distributed loads and axles loads is indicated. Load restrictions on these bridges should be consequently applied. Similarly, the Danish Road Directorate (2004) allows for the classification of the bridges according to the maximum weight of the vehicles they are able to carry. These are straightforward approaches to classify the bridges, however, they are not a good estimation of the actual traffic being carried by the bridge but of the load carrying capacity. They require iterative calculations until the capacity is found to exceed the loads applied.

Site specific conditions are introduced in the AASHTO LRFR (2003) with modified live load factors that account for different ADTTs. These factors have been calibrated using recorded histograms of truck weights and probability of multipresence of trucks. The process followed does not allow for multipresence of events or weights of trucks not recorded by the WIM station, which could be non-conservative. More sophisticated approaches such as Monte Carlo simulations of continuous traffic streams could be used to verify the proposed values.

Moreover, the ADTT intervals lack accuracy and could be improved with a more information or a detailed representation of the variation of the live load factor with the ADTT. The use of WIM data is necessary for the calculation of more accurate live load factors using the equations detailed in the code.

The Eurocode (EN 1991-2, 2003) allows for the modification of the LM1 at the National Level to account for different traffic conditions. For instance, the Swiss code (SIA 269 - 269/8, 2011) presents a reduced LM1 traffic load model owing to reduce traffic loads found in Switzerland. Although, being a reduction of the LM1 for the national traffic conditions, this approach does not allow for further adjustments of the load model based on site specific traffic conditions that could be encountered in minor roads in the country.

National codes have been introducing concepts such as reduced target reliability levels, reduced reference periods, modified traffic load models and site specific traffic conditions, however none of them accounts for all the possible modifications, or their approaches present shortcomings in the calibration or applicability that can be potentially addressed.

2.4.2 Research publications and projects

Bailey

Bailey (1996) uses the concept of traffic load reduction factors. These factors are calibrated comparing the distribution of maximum load effects due to simulated traffic to the one obtained due to the Swiss design load model. A parametric study is performed to analyse the relationship between 13 traffic characteristics and the reduction factors. The six traffic characteristics below are defined as the most influential:

1. Maximum value of the heavy vehicle linear weight.
2. Mean value of the heavy vehicle linear weight.
3. Standard deviation of the heavy vehicle linear weight.
4. Proportions of heavy vehicles in the traffic.
5. Volume of traffic.
6. Percentage of free moving traffic.

These six traffic characteristics are transformed into six coefficients $c_1, \dots, c_6$ using the equations derived in Bailey (1996). An optimization process is performed to obtain the best

agreement between the calibrated reduction factors and the approximated ones. The six coefficients are combined together using the following expression:

$$\alpha_Q = 6 \cdot \frac{c_1 \cdot c_2 \cdot c_3 \cdot c_4 \cdot c_5 \cdot c_6}{(c_1 + c_2 + c_3 + c_4 + c_5 + c_6)} \tag{2.50}$$

Using the simplified method, 95% of the reduction factors are conservative and the remaining 5% do not overestimate the values by more than 5 %.

BRIME Report

The BRIME Report (2001) offers an extensive guideline for the assessment of existing bridges. Regarding the traffic load models, the document introduces an equation that can be used to modify the load effects:

$$\Delta S = (\ln(N_1) - \ln(N_2)) \cdot a \tag{2.51}$$

where ΔS is the variation of the load effect, N_1 is the number of heavy vehicles per year, N_2 is $365 \cdot 10^4$, which is the number of vehicles per year used in the simulations and a is a parameter of distributions of extremes for annual extreme values. This formula has been derived simulating traffic using recorded data from Germany, UK and France.

Maljaars et al.

Maljaars et al. (2012) present two reduction factors for the LM1 traffic load model. The first factor is based on a reduced reference period in comparison to the design load model. For existing bridges, a factor can be calculated using the equation calibrated for WIM data recorded in the Netherlands:

$$\psi_{rp} = \left(\frac{\ln(n_a \cdot t)}{\ln(n_a \cdot T)}\right)^{0.45} \tag{2.52}$$

where n_a is the number of heavy vehicles per year, t the desired reference period and T the reference period of the design traffic load model, equal to 100 years.

The second reduction factor ψ_t takes into account the increment in the axle loads and intensity of traffic that is assumed in the Eurocode LM1 (EN 1991-2, 2003). The Eurocode traffic load model is calibrated to consider these increments in the traffic to match the expected traffic loads in 2050. If shorter life spans are considered the LM1 can be reduced. The reduction factor ψ_t are calibrated following the above mentioned idea and using WIM data from the Netherlands.

The reduction factors are dependent on the year and the influence length (traffic load vs axle load) and range from 0.8 for the year 2010 and large influence lengths until 1, as years move towards 2050 or for shorter influence lengths.

Moses & Ghosn

Alternatively other models have been developed. Moses & Ghosn (1985) propose an empirical formula for the estimation of site-specific maximum load effects:

$$L_{max} = a \cdot m \cdot W_{95} \cdot H \tag{2.53}$$

where a is the load effect of the standard truck with unit GVW, m is a random variable that accounts for the variations in the geometry and axle load distributions compared to the standard truck, W_{95} is 95% percentile of the GVW at the site and H is a random variable accounting for the multiple presence of trucks on the bridge function of the ADTT and the span length. This approach was calibrated using WIM truck data in the US and using convolution methods to obtain the load effects. Despite being a simple approach, it needs WIM data to obtain some of the parameters involved in the equation.

ARCHES

The previous method is tested with European traffic data in ARCHES project (2009). The study concludes that the method is only recommended if the vehicle population contains a high number of extremely heavy vehicles, otherwise the comparison of the load effects with more sophisticated methods is not satisfactory.

Other sections in the same project present a way to reduce the traffic load models depending on the ADTT in one lane. Traffic recorded at five different sites in Europe is used of the calibration of this method. Reduction factors for the design stage are calculated considering that the return period of characteristic value of the load effects is proportional to the traffic volume at the site. For example, load effects at a site with an ADTT of a 50% of the one to calibrate the load model should be extrapolated to a return period of 500 years instead of the 1000 years used traditionally in the Eurocodes for design purposes. The assessment factors combine the previous method with the reduction of the return period that it is assumed to be 50 years, or 10% of exceedance in 5 years, for the assessment stage.

Table 2.14 shows the mentioned factors that are to be applied directly to the characteristic values obtained using the LM1. These factors are to be combined with the LM1 national reduction factors α as shown previously for the Swiss standard. The reference site to reduce the design characteristic load is considered the one used to calibrate the national model in each country.

Table 2.14. Reduction factors for reduced truck volumes and assessment.

Traffic volume as percentage of the reference site ADTT	Design reduction factors	Assessment reduction factors
10%	0.93	0.83
20%	0.95	0.85
30%	0.97	0.87
40%	0.97	0.88
50%	0.98	0.89
60%	0.99	0.89
70%	0.99	0.90
80%	0.99	0.90
90%	1.00	0.91
100%	1.00	0.91

Discussion

Bailey (1996) uses the concept of traffic load reduction factors to adapt the load effects to the site specific traffic characteristics. This concept is applied later in this thesis. The shortcoming of the proposed approach is that WIM data is needed for its application, therefore making it less interesting for industry.

BRIME Report (2001), Maljaars et al. (2012) and Moses & Ghosn (1985) propose different equations for the reduction of the traffic load effects based on various parameters. While the application of the equations is simple, some of the parameters must be obtained making used of WIM traffic data, not always available. The applicability and accuracy of these equations in other regions should be verified since they are simplistic and designed for a specific site. For instance, the equation proposed by Moses & Ghosn (1985) does not always perform well if European traffic is used.

Lastly, the reduction factors proposed in ARCHES are based on the assumption that the return period of the characteristic load effects is proportional to the traffic volume at the site. It is not clear how this assumption is considered as valid as the characteristic values of the load effects are the 95% fractile of the distribution of load effect and adopting a lower return period would

decrease this fractile. Furthermore, it is not mentioned if this has an impact on the design values. If the design values remain unmodified, the decrease of the characteristic values is irrelevant. Further work is required to determine the general applicability of the approach.

2.5 A new design load model for South Africa

A new design traffic load model for South Africa is simultaneously being developed with the present research at Stellenbosch University. This new model will substitute the current design model TMH-7 (1981) as it presents a cumbersome applicability and an unknown performance. In van der Spuy and Lenner (2019) the preliminary design traffic load model for one lane is presented. It consists of a tridem of axles of 160 kN each one separated 1.2 m and a uniformly distributed load UDL of 30 kN/m. The calibration of the model is performed using Weigh-in-Motion data. Daily maximum axle loads are extrapolated to a return period of 975 as done in the EN 1991-2 (2003) delivering a value of 158 kN that is rounded up to 160 kN for practical purposes. Uniformly distributed loads are calculated together with the previously mentioned tridem of axles to achieve the load effects for various span lengths that have been extrapolated using the WIM data. The maximum value of UDL is obtained for the hogging moment at 15 m span lengths. The adoption of this value is shown to be conservative for larger spans. It is however mentioned that conservatism in the traffic model on large spans is not a concern since they are dominated by the dead load. Conservative live loads provide a higher safety margin at low additional cost.

2.6 Artificial traffic generation using Monte Carlo techniques.

The generation of artificial traffic is one of the pillars of this study. The use of Monte Carlo techniques for the generation of traffic requires modelling all the variables involved in the traffic flow such as gross vehicles weights, axle loads, vehicle geometries and distances between adjacent vehicles. The mentioned variables have been modelled in the past using several techniques. This section reviews the most relevant approaches found in the literature.

2.6.1 Gross vehicle weight and axle loads

Bailey (1996) uses WIM measurements recorded at various sites in Switzerland. The traffic is separated into 14 different vehicles that comprise 99% of the recorded traffic flow.

Axle groups are modelled together instead of as individual axles since weight in axle groups is considered to be evenly distributed when the distance between axles is close. Bimodal beta distributions are fitted to the histogram of axle groups.

The GVW and its distribution among the axles or axle groups are based on the heaviest axle group, considered as the most influential on the GVW. Correlation between axles or axle groups is modelled as linear while allowing some randomness in the process. The mean and the standard deviation of the distribution of the axle or axle group are defined as a linear function of the axle groups already simulated. An example a vehicle consisting of a two-axle truck tractor and a tridem is generated as follows:

- The tridem is modelled using the bi modal beta distribution.
- The second axle is modelled by a Normal distribution. The mean and the standard deviation of the new distribution are modelled as a linear function of the previous axle:

$$Q_2 = N + Q_3 \cdot N \tag{2.54}$$

- The first axle is also modelled as a Normal distribution and function of the two previous generated axles:

$$Q_1 = N + (Q_2 + Q_3) \cdot N \tag{2.55}$$

where N is the Normal distribution with mean and standard deviation varying depending on the vehicles class and axle being generated.

Crespo-Minguillon and Casas (1997) use linear correlation between GVW and axles to generate the vehicles. The WIM data is used to obtain the measured CDF of the axle loads. Table 2.15 presents the correlation matrix used in the simulation of the vehicle class eight. Twenty-one vehicles classes are considered.

Table 2.15. Correlation matrix of weights for class 8 vehicles. W_i= axle weight, W_g =GVW.

	W_1	W_2	W_3	W_g
W_1	1	0.40	-0.74	-0.04
W_2	0.40	1	-0.89	0.11
W_3	-0.74	-0.89	1	-0.02
W_g	-0.04	0.11	-0.02	1

Grave (2001) and later Caprani (2005) classify vehicles per number of axles. Trucks over six axles are omitted since they represent less than 1% of the traffic flow. A bi- or tri-modal mix of Normal distributions is fitted to the GVW histograms. These histograms present two peaks, which represent loaded and unloaded vehicles and are perfectly fitted by bi-modal distributions. In some cases a third peak without a physical explanation appears, therefore the use of tri-modal distributions.

Correlation between GVW and its proportion among the axle loads is considered for four- and five-axle vehicles and ignored for the rest since it is not significant. Axle loads for these last vehicles are modelled using again bi- and tri-modal distributions.

For four- and five-axle vehicles, it is assumed that the individual axles in the rear tandem or tridem carry the same weight. The correlation between GVW and the rear axles it is not neglected. As the GVW increases, more proportion of the load is carried by the rear axles.

The GVW is divided in intervals of 5 t and Normal distributions are fitted to the proportion of GVW carried by individual axle or axle group encountered in every interval. Axle loads are rescaled at the end of the process to sum the initially generated GVW for the specific vehicle.

Allaix (2007) classifies the traffic into 31 vehicles types; firstly according first to the number of axles and then to the geometry of the trucks. The modelling of the GVW is just concerned about the loaded side of the histogram and the upper tail. The threshold that separated the loaded from the unloaded populations is chosen as the minimum value of the histograms between the two peaks. Truncated Lognormal, Gumbel, Frechet and Weibull distributions are used to fit the data. As other researchers have noticed, the GVW histograms sometimes present a third peak on the upper side. In this case, a bimodal distribution is fitted with two truncated distributions as mentioned before.

Full linear correlation between axle loads and GVW is assumed with the form of the equation:

$$Q_i = \alpha_i \cdot W + \beta_i \quad i = 1,2,\dots,n \tag{2.56}$$

where α_i and β_i are constants with the $\sum \alpha_i = 1$ and $\sum \beta_i = 0$ with n the number of axles in the specific vehicle class. Q_i is the axle load and W the GVW. Although the method is very simple, the author argues that the accuracy is sufficient for the purpose of the thesis.

The approach used by Enright (2010) for the generation of the GVW is a combination of two methods known as the semi-parametric fitting. This method uses the measured histogram up to

a point where a probability distribution is fitted to the tail of the histogram (Getachew & O'Brien, 2007). This has the advantage of improving the accuracy in the upper tail, allow for the interpolation between observed points (which can be scarce in this region), and provides a way to generate greater values than observed.

In later stages of his work, this concept is extended and an empirical bivariate distribution of GVW and number of axles is used up to a point where data is insufficient and a bivariate Normal distribution is fitted to the tail. This not only allows for the generation of heavier vehicles but for vehicles with more axles than recorded.

The generation of axle loads is performed using bimodal Normal distributions fitted to the histograms of the percentage of GVW carried by the axle loads. The loads of adjacent axles are highly correlated while the strength of the correlation decreases as the distance between axles increases. A correlation matrix is built for every vehicle class and multicorrelated random values are generated (Iman & Conover, 1982). Axle loads are obtained after the multicorrelated valued are transformed using the CDF of the previously fitted distributions.

Srinivas, Menon and Prasad (2006) use copula functions to model the dependence structure between axle loads of two- three- and four-axle vehicles using traffic data recorded in India. Multivariate copula functions are fitted to the recorded axle loads. The size of the copulas depends on the number of axles in the vehicles and the geometry. Bivariate copulas are used for two- and three-axle vehicles. Three-dimensional copulas are used for four-axle vehicles. Groups of axles are modelled as one load. Copulas are used to model the dependence structure between axles. The marginal distributions of each axle load or group of axles are used to obtain the real values in the last stage after the multivariate simulation of axles is performed. The resultant GVW is the sum of the simulated axle loads.

Discussion

Bailey (1996) models axle groups using bimodal beta distributions that fit well the data. The linear correlation between the distributions of axles or axle groups needs further explanation as it is not clear how the values are obtained. Moreover, this might not always be a valid assumption. Beta distributions present and upper bound, therefore the simulations are limited to the distribution boundaries and no greater axle loads are allowed. It is true that the heaviest axle group is determinant on the GVW, however, a certain correlation between GVW and axle load should have been incorporated since it is not validated that the sum of axle loads is actually

equal to the distribution of recorded GVW. A comparison of recorded and simulated load effects to ascertain the accuracy of the simulated traffic is missing.

Crespo-Minguillon and Casas (1997) use the correlation matrix between all the axle weights and the GVW for each vehicle class. This accounts for the complexity of the distribution of loads in trucks. The simulations are limited to the values recorded since no distributions are fitted to the observed histograms. There could be extremely heavy vehicles no recorded by the WIM station that are therefore excluded from the simulations.

Grave (2001) and Caprani (2005) fit bi- and tri-modal normal distributions to the histograms of axle load and GVW or proportions of GVW carried by axle loads. This can be problematic on the upper tails since the fit is not always accurate in this region. The correlation between GVW and axle loads is included with a simple division of the GVW histogram in intervals. The selection of 5 t intervals for the GVW histograms seems a subjective decision that could affect the accuracy of the results. The comparison of the recorded and simulated load effects is not shown to validate the simulations.

Allaix (2007) shows a good effort to classify the vehicles into different categories. Several multimodal distributions are considered to fit the recorded histograms of GVW and the importance of the upper tail is mentioned. The linear correlation between axle loads and GVW assumed is a simple approach, however, it could be inaccurate since the dependence structure might not always be linear as shown in Section 4.1.

The semi-parametric fitting adopted by Enright (2010) for the modelling of the GVW is an important innovation since it allows for the generation of heavier vehicles and with more axles than recorded. The multicorrelated approach account for the complex correlation structure in vehicles and the comparison of recorded and simulated load effects shows that the method is accurate.

Srinivas, Menon and Prasad (2006) propose the use of copula function for the modelling of the complex dependence structure between axle loads in trucks. This has been an inspiration for the presented thesis. Their work is limited to vehicles up to five axles and uses multivariate copulas. As explained in Section 4.1 multivariate copulas with high dimensions are less flexible than bivariate copulas. This could lead to inaccurate fittings if vehicles with more axle were studied.

2.6.2 Axle spacings

Bailey (1996) models vehicular geometries using beta distributions for each of the axle spacings and overhangs of each type of truck in the classification. Since axle groups are modelled together, the axles spacing modelled are the distances between the centre of gravity of the axle or axle groups.

Graves, O'Brien and O'Connor (2000) and Jacob and Flint (1996) use fixed axle spacings.

Allaix (2007) models the distance between axles using Normal distributions fitted to the measured data. Similarly, O'Brien, Caprani and O'Connell (2006) use combinations of Normal distributions. In the last-mentioned research, axle spacings are measured for each vehicle class and bi- or tri-model Normal distributions are then used to model the variables. Axle spacings are considered independent of direction.

Srinivas, Menon and Prasad, (2005) use Normal distributions to model axle distances and model correlation between spacings using copula functions.

Enright (2010) ranks axle spacings for all vehicles in descending order. In the simulation, the maximum axle spacing is obtained from an empirical distribution depending on the number of axles and the GVW. For the rest of the axle spacings trimodal Normal distributions are fitted to the measured histograms. The position of each of the ranked spacings on the vehicle is also modelled in the simulation using empirical distributions for all spacings in each vehicle class. The magnitude and position of all axle spacings for extrapolated vehicle classes are modelled using trimodal Normal distributions fitted to measurements.

Discussion

Most of the approaches to model axle spacing consist of fitting probability distributions to the histograms of recorded axle spacings, usually classified in different vehicles classes. As seen in Section 3.6, this is sometimes difficult due to the complex shape of the some histograms. Graves, O'Brien and O'Connor (2000) and Jacob and Flint (1996) use fixed axle spacings. Some of these magnitudes usually present most of the observations around one value and can be treated as deterministic, especially spacings between axles in groups and spacings in vehicles with high number of axles. This is supported by the fact that truck manufacturers produce vehicles and trailers with constant magnitudes.

More complex approaches are proposed by Srinivas, Menon and Prasad, (2005) and Enright (2010). The last approach is designed to model vehicles with more axles than recorded, thus its complexity.

2.6.3 Vehicle gaps or headways

Modelling vehicles gaps is a crucial step in the generation of artificial traffic. Distances between following trucks determine the number of vehicles over the bridge at a specific time and consequently they are greatly influential on the load effects. Special detail is required when modelling short gaps since maximum load effects are expected to occur during multiple and closely distanced vehicle events.

The most remarkable approaches in the literature assuming free-flowing traffic conditions are described hereafter. The term gap is considered as the distance from the rear axle of the leading vehicles to the front axle of the following vehicles. The headway is the gap plus the length of the leading vehicles.

Exponential distributions are used to model headways in Bailey (1996) and Grave (2001). Often, this distribution is shifted to the right to allow for a minimum headway (Shifted Exponential Distribution in Equation (2.57)) as extremely short gaps are physically impossible:

$$F(t) = 1 - \exp[-\gamma \cdot (t - t_0)] \tag{2.57}$$

$$\gamma = \frac{\lambda}{(\lambda \cdot t_0 - 1)} \tag{2.58}$$

where t_0 is the minimum headway and λ is the hourly vehicle flow rate. Bailey (1996) adopts a minimum value of 0.25 sec at a speed of 22 m/s (80 km/h) which is equivalent to 5.5 m. Equation (2.57) models the distance between vehicles (bumper to bumper) and not the distance between rear and front axle of following vehicles.

Gable, Moses and Record (1976) assume that the PDF of short headways is constant and equal to the average traffic flow per unit time. This is expressed using the negative exponential distribution as:

$$F(t) = 1 - e^{-\lambda \cdot t} \approx \lambda \cdot t \tag{2.59}$$

where λ is the traffic flow in trucks per hour. An improvement to the exponential distribution is the Gamma distribution that ensures small probabilities for small headways:

$$F(t) = \frac{\Gamma(k, \gamma \cdot t)}{\Gamma(k)} \tag{2.60}$$

where $\Gamma(k, \gamma t)$ is the incomplete Gamma function and γ and t are the location and scale parameters. This distribution is widely used in the background research for the development of the Eurocode traffic load model for bridges (Bruls, Calgaro, Mathieu, & Prat, 1996; Getachew, 2003; Jacob & Flint, 1996; O'Connor, Jacob, O'Brien, & Prat, 2011). This distribution however passes thought the origin therefore a physical limitation to small headways must be taken into account. These researchers above consider a minimum distance of 5 m from the rear axle of the leading truck to the front axle of the following truck. Harman and Davenport (1979) adopt a minimum headway of 7.32 m.

An alternative approach is based is based on the driver's behaviour. Vrouwenvelder & Waarts (1993) assume that, in free flowing conditions, the headway randomly lies in the range:

$$L \leq h \leq 30 - L \tag{2.61}$$

where L represent the length of the vehicle.

Buckland et al., (1980) propose a simple equation to calculate the headway function of the speed and minimum distance for long span bridges:

$$h = 1.5 + \frac{v}{16} \cdot L \tag{2.62}$$

where v is the velocity (km/h) and L is the truck length (m).

Nowak (1993) derives the maximum load effect of a two-truck meeting on the bridge calculating the maximum value of different scenarios. Headways (rear axle to front axle) are varied from 5 to 30 m and different correlations between the weights of the trucks, 0 (no correlation), 0.5 (partial correlation) and 1 (full correlation). Observations show that, on average, every 50th truck is followed by a truck with headway less than 30 m (Nowak, Nassif, & DeFrain, 1993).

Various authors have linked headways and truck traffic flow (Bailey, 1996; Samuel Grave, 2001), however instead of fitting individual distributions for each flow, Crespo-Minguillón & Casas (1997) consider a normalised headway, defined as the headway divided by the average headway for a given traffic flow. This normalised distribution can be adapted for the desired traffic flow.

O'Brien and Caprani (2005) introduce the Headway Distribution Statistics. This is based on traffic data, for each hour of each day, headway data and the corresponding hourly flow (mean flow in an hour). Data from different hours are combined according to intervals of hourly flow and cumulative distribution functions calculated for each interval.

Almost no correlation between hourly flow and headways for values lower than 1.5 seconds is observed therefore, a distribution independent of the flow is assumed. For small headways, these are determined by truck driver's behaviour of safe distance rather than the traffic flow (Lieberman, 1992). Two quadratic equations are fitted to the distribution of headways lower than 1.5 seconds. For values between 1.5 and 4 seconds, correlation between headway and traffic flow is noticeable. Headways are combined into intervals of 10 veh/h and the headways CDF are calculated for each interval as commented before.

O'Brien and Caprani (2005) use Grave's (2001) normalised headway distribution to model gaps larger than 4 seconds. It is argued that for medium span bridges up to 50 m headways larger than 4 seconds are not critical, therefore they do not need to be modelled accurately. Enright (2010), on the other hand, uses a negative exponential distribution to model these larger gaps. Also mentioned is that, the following truck for these large gaps is unlikely to be located on the bridge at the same time as the leading truck.

Daily variation of the truck flow is modelled by calculating the average hourly flow for each weekday. A quadratic equation is fitted to the measured headway CDF closest to the average hourly flow AHF for each hour. Other studies do not consider hourly variation of the traffic flow (Bez & Bailey, 1995) or consider a typical day with variable hourly flow (Caprani et al., 2008; Cooper, 1995). Temporal variations are modelled using Weibull distributions (Stathopoulos & Karlaftis, 2001).

Enright (2010) alternatively fits a Weibull distribution to the histogram of the ADTT and generates random values of the ADTT which allows for a daily variation of the ADTT. Once the ADTT is generated the average hourly flows recorded are scaled to match the ADTT and from them the vehicle headways are generated using the Headway Distribution Statistics.

Discussion

The use of Exponential distributions to model headways in Bailey (1996) and Grave (2001) allows for the simulation of closer headways at higher flow rates. The use of shifted distribution defines a low boundary for headways. This distribution, however, gives very high probabilities

to headway values close to the minimum allowed. An enhanced version of the previous model is the Gamma distribution model used in the background studies for the Eurocode.

Drivers behaviours models as proposed by Buckland et al., (1980), Vrouwenvelder & Waarts (1993) and Nowak (1993) might be a good site specific representation of the traffic where they were developed, but it seems unlikely that they can be generalised to other locations.

The normalised headway is a simple approach that avoids the use of multiple distributions for each flow rate, grouping all of them in one normalised distribution.

The Headway Distribution Statistics is the most complex approach to model this variable reviewed here and adopted in O'Brien and Caprani (2005) and Enright (2010). Different models are considered for different intervals of headways, acknowledging the high importance of the short gaps with an accurate modelling. Less accurate models are adopted for larger gaps that are relatively less critical on short to medium span lengths. The correlation between headway and hourly flow is accounted for fitting equations to the measured data and avoiding the use of empirical or subjective formulations. This approach is general and can be applied to any traffic.

CHAPTER 3: TRAFFIC DATA PROCESSING

The use of WIM traffic data have been introduced in the last decades for the calibration of traffic load models, design of road pavements, enforcement of the legal truck weights or estimation of the tolling fees. Even though being an important source of traffic data, the traffic records have to be treated carefully as they can present inaccuracies and therefore, they could lead to incorrect conclusions and inefficient measures. Two post-recording processes are necessary to ascertain the quality of the data. A first filtration process eliminates incorrect WIM records. Previous experience and general criteria based on similar work can be followed to determine the filtration process. Incorrect calibration of the WIM station usually leads the observation of a systematic error in the records. The comparison of constant known values with the WIM records is a way to proceed to eliminate the systematic error. Although general criteria can be extracted, both processes are recommended to be develop for the specific characteristics of the traffic being used, as the regional properties of the vehicles cannot always be extrapolated to other countries. Sections 3.2 and 3.3 describe the methods used for the specific traffic in this thesis along with reference to similar methods used previously.

Furthermore, the processed traffic data should be separated in the different lanes recorded and classified into different vehicles classes (same geometry). Plotting axle loads, GVW and axle spacings per lane is a recommended step that facilitates to understand the data and helps in future modelling of the variables.

3.1 WIM data

The present research makes use of different WIM stations located in South Africa and managed by the local authorities that provided the traffic data. The research is mainly based on the Roosboom WIM station, however; the approach proposed here is validated in several steps using other stations that present different traffic characteristics. All the WIM stations evaluated in this research are located on national roads and are described below:

- **Roosboom**: this main station used in the research is located on the N3 approximately 250 km from Durban, KwaZulu-Natal. This road connects the city of Durban with Johannesburg. The first city serves as an important maritime port while Johannesburg is the financial and commercial capital of the country. This road, therefore, is populated with a high percentage of trucks and which then makes the Roosboom WIM station suitable for obtaining records of highly aggressive traffic (Lenner et al., 2017). The N3

has two lanes in each direction, however, only the slow lanes in each direction are instrumented and therefore not all the traffic on this national road is recorded.

- **Wilge**: WIM station on the N3 south of the town of Villiers, about 120 km from Johannesburg. This is station similar to Roosboom as the cross-section of the road is the same and only the slow lane is instrumented.
- **Kapmuiden**: station located in the province of Mpumalanga on the N4 between Nelspruit and Matsulu. The N4 runs from the border with Botswana until the border with Mozambique, passing through Pretoria, the administrative capital of the country. The section of the road where the WIM station is located has one lane per direction and both are instrumented.
- **Komatipoort**: located in the city of Komatipoort on the N4, a few kilometres away from the previous station and outside the Komatipoort dry port. This city lies on the Mozambique border.
- **Zeerust**: located on the N4 in the proximity of Zeerust, North-West Province. This part of the road is representative of the heavy traffic circulating from Gauteng (Pretoria and Johannesburg) to Botswana. It is the station with the lowest ADTT provided for this research. The road contains one lane per direction and both are instrumented.
- **Witbank**: station located on the N12 east of Johannesburg, close to the municipality of Emalahleni (formerly Witbank) in the province of Mpumalanga. The N12 highway runs from the city of George in the province of the Western Cape to Emalahleni passing through Kimberly and Johannesburg. This is a four-lane road however only the slow lanes are instrumented.

An example of the format of the files received from the authorities is shown in Figure 3.1.The first rows of the file are irrelevant for the purpose of this research since they include information on the location and data format in which the WIM station records. Valuable data are located in lanes commencing for the number 13. The number corresponds to the type of information being recorded, in this case axle weights and axle spacing. Every line is a single vehicle record and contains multiple values providing information about it. The rest of the lines contain information that is not useful and it is therefore ignored.

```
H0 200 002 RSA Data Format Version 2.00
S0 3022     3022              Roosboom
I0 RT8010 Fam 110909MN
D0 M L
D1 160101 000000 160101 240000 150512 122300 151231 070151 160101 240000
D3 20160101 000000 20160101 240000 20150512 122300 20151231 070151 20160101 240000
L0 04 04
L1 01 0 1 00 2 1 1 1 1 1
L1 02 0 2 00 2 1 1 1 0 0
13 08 18 05 05 000000 030 020
30 15 15 08 18
21 15 15 30 060 070 080 090 100 110 120 130 140
70 15 15 05 030 020
H9
MS 0 160101 000000 01 0 137
MS 0 160101 000000 01 1 08 40792 40658 31923 31568 31889 32142 39933 41035
13 0 160101 00050400 04 04 1 116 0710 999 1 0 1 0 00 02 00
13 0 160101 00104140 01 01 1 105 1390 999 3 0 1 0 06 03 03 050 0738 086 0139 045
13 0 160101 00123810 04 04 1 112 0730 999 2 0 1 0 05 01 02 018 0418 020
13 0 160101 00144200 04 04 1 100 1400 999 3 0 2 0 06 03 03 052 0710 081 0136 042
30 0 160101 0015 15 01 0000 0000 0003 0000 0000 0000 0001 0000 0000 0000 0000 0000 0000 0000 0000
30 0 160101 0015 15 02 0000 0000 0001 0000 0000 0000 0000 0000 0000 0000 0000 0000 0000 0000 0000
21 0 160101 0015 15 04 0000 0000 0001 0001 0006 0003 0007 0001 0000 0000 000289 001 002 000 0002
```

Figure 3.1. Example of txt file produced by the WIM station.

The length of these lines depend on the number of axles that the recorded vehicles contain. The data provided in a line can be summarised as follows:

- **Individual Vehicle Data Record (Axle Weights & Spacing):** describes the data being recorded. As mentioned above, only number 13 is of interest for this research.
- **Edit Code:** value from 0 to 3 describing the status of the specific record. Normal, edit, invalid or bad and filled (manufactured to fill missing data) respectively.
- **Arrival Date:** year, month and day (YYMMDD) indicating the date of recording.
- **Arrival Time:** time of arrival in hours, minutes, seconds and 100th of a second (hhmmsscc).
- **Physical Lane Number**: lane on which a vehicle is physically detected irrespective of the direction in which the vehicle was moving. On a four lane road is normally be labelled as 01, 02, 03 and 04.
- **Logical Lane Number:** lane number assigned to the vehicles depending on the direction the vehicle is travelling. If the vehicle is traveling forward, it is equal to a physical lane number, otherwise, it can be reassigned to another physical lane or to a ghost lane number. The number of logical lanes can never be less than the physical lanes.

- **Direction Code:** indicates whether a vehicle was travelling in the forward or reverse direction to the normal traffic flow as defined for the physical lane. Can adopt 0 (not recorded), 1 (forward) and 2 (reverse).
- **Speed (km/hr):** speed of the vehicle measured at the front bumper or first axle (3 digits).
- **Length (centimetres):** length of the vehicles measured from bumper to bumper. This is measured using magnetic loops and the values are not very accurate (4 digits).
- **Bumper to first axle spacing:** distance between the front bumper and the first axle measured in cm. The magnetic loops is used to detect the bumper and an axle sensor to detect the axle. The accuracy in the detection of the bumper is low (4 digits).
- **Chassis Height Code:** loops can also detect the height of the chassis. Values range from 0 to 3 indicating no record, high, medium and low chassis height.
- **Tag Code:** some special vehicles can be marked in the data.
- **Following Vehicle Code:** this value indicates whether the vehicle is a following vehicle or not (gap time between vehicles is less than 3 seconds).
- **Failure Code:** the system may detect a physical or logical error while the vehicle is detected. If the value differs from 0 then there is an error in the record.
- **Vehicle Class Code I and II:** field used to classify the vehicles if a classification scheme is implemented.
- **Number of Axles:** number of axles in the recorded vehicle.
- **Axle Weight 1 (100xkg):** weight of the first axle (3 digits).
- **Axle Spacing 1 (centimetres):** distance between axle 1 and axle 2 (4 digits).
- **Axle Weight 2 (100xkg):** weight of the second axle (3 digits).
- **Axle Spacing n-1 (centimetres):** distance between the second last and the last axle (4 digits).
- **Axle Weight n (100xkg):** weight of the last axle in the vehicle (3 digits).

The monthly txt files of traffic data provided are loaded into Matlab (R2017b, 2017), the main software used in the research. The data are cleaned of unnecessary or bad information in order to reduce the size of the files. All the files containing records from the same WIM station are combined together into one large file.

3.2 Data filtration

After obtaining a WIM data set, the application of a basic filtration to the WIM data can commence to remove potentially incorrect values that could disrupt the results.

WIM data collection in South Africa is governed by several specifications of Committee of Transport Officials (TMH 14, 2013; TMH 3, 2013; TMH 8, 2014). The South African Standard Automatic Data Collection Format (TMH 14, 2013) specifies the data collection format and according to it, the following criteria must be applied to reject invalid records:

1. Truck travelling at less than 5 km/h or more than 150 km/h.
2. Truck length less than 4 m or greater than 26 m.
3. Truck with fewer than two axles.
4. Truck with gross vehicle weight (GVW) less than 3.5 t.
5. Truck with any individual axle heavier than 16 t.
6. Truck with any axle spacing shorter than 0.53 m or larger than 10 m.

Although the derivation of the presented criteria is not entirely clear, it is widely applied by the South African authorities that manage the WIM stations throughout the country. Furthermore, the present criteria is used in line with the steps followed for the calibration of the new design traffic load model (van der Spuy & Lenner, 2018). This avoids inconsistencies that could arise from the use of different filtering and cleaning criteria in this thesis. For comparison, similar research (Enright & O'Brien, 2011) presents alike criteria, only with minor deviations due to regional variations in the traffic. It makes use of vehicle images to improve the filtration process, contrary to South Africa, where the technology is currently not available. Additional criteria are therefore introduced in this contribution to complement the filtration process:

7. Recorded number of axle spacings must equal to recorded number of axles minus one.
8. Day and time stamp attached to the all truck records must be chronologically sorted.

From the initial 1,600,347 trucks recorded over the period of one year at Roosboom, 1,359,300 remain after the filtration process. This value corresponds to the two lanes, one instrumented in each direction on a four-lane road, recorded by the station. Table 3.1 details the number of vehicles removed by each criteria.

Table 3.1. Number of vehicles removed by each criteria.

Criteria	Vehicles deleted
1	18
2	2973
3	241274
4	5661
5	28
6	3666
7	73
8	0

The significant number of vehicles filtered by criteria 3 is caused by the presence of records without axles in the raw WIM files. The reason why the station is registering vehicles in these cases is, however, unknown. Although the criteria do not filter all the vehicles with more than eight axles, these are excluded in the analysis. Moreover, such vehicles typically do not occur in South African roads without a permit. Table 3.2 shows the number of vehicles removed from both lanes of traffic.

Table 3.2. Number of vehicles with more than eight axles deleted.

Number of axles	Vehicles deleted
9	398
10	185
11	107
12	6
13	1
14	1

3.3 Truck tractor method

The Truck Tractor method (TT method), developed by de Wet (2010) is mandatory and regulated by South African authorities when using WIM data. Non-calibrated WIM data can be misinterpreted and misused and may result in inaccurate designs of pavements, calibration of load models or overload control efforts.

Two errors arise from the use of WIM data: the systematic and the random error. The TT method is used in this research to eliminate the systematic error in the axle load records that might be produced by the WIM station's inaccurate calibration. The random error is not eliminated by the application of the TT method. Moreover, the nature of the error makes it very difficult to predict and correct (de Wet, 2010).

Calibration procedures are typically developed based on measurements of known static weight of a specified truck (either a two-axle and or a five-axle for E1318 (2002) and a three-axle for COST 323 (2002)). The TT method requires the application of the k_{TT} calibration factor, which is calculated iteratively using Equation (3.1), along with the truck tractor axle loads of six- and seven-axle vehicles conforming to a specific axle spacing criteria (selected trucks). The average monthly truck-tractor mass of the selected truck is a known constant value of 21.8 t according to de Wet (2010).

$$k_{TT} = \frac{T_{target}}{T_{TT}} \tag{3.1}$$

where T_{TT} is the average truck-tractor mass of selected trucks in each iteration and T_{target} is the target truck-tractor mass (21.8 t). The factor k_{TT} is applied to all the axle loads in the WIM file and therefore a new T_{TT} can be calculated. The calibration is finalized when the k_{TT} is equal to 1 and consequently T_{TT} and T_{target} are equal. The systematic error is now suppressed. Table 3.3 presents the k_{TT} values for every month and iteration. The factor converges to 1 always after 6 iteration as also suggested by de Wet (2010). Figure 3.2 shows the variation in the GVW after the application of the TT method. The largest peak in the histogram is clearly lower and moves from 53 t to 50.3 t. The mean of the GVW decreases from 37.6 t to 36 t.

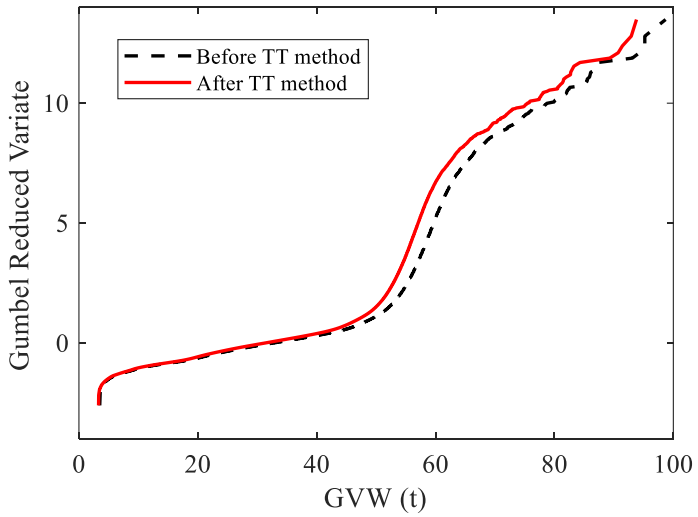

Figure 3.2. Distribution of GVW before and after the application of the TT method.

Table 3.3. k_{TT} factors per month and iteration.

Month	Iteration					
	1	2	3	4	5	6
January	0.9814	0.9958	0.9990	0.9997	1	-
February	0.9701	0.9931	0.9987	0.9999	1	-
March	0.9613	0.9910	0.9982	0.9994	0.9999	1
April	0.9655	0.9920	0.9982	0.9999	1	-
May	0.9691	0.9930	0.9986	0.9996	0.9998	1
June	0.9742	0.9950	0.9989	0.9997	1	-
July	0.9770	0.9946	0.9988	0.9999	1	-
August	0.9675	0.9929	0.9989	0.9995	1	-
September	0.9649	0.9915	0.9984	0.9995	0.9999	1
October	0.9615	0.9900	0.9980	0.9996	0.9997	1
November	0.9584	0.9906	0.9981	0.9996	0.9999	1
December	0.9558	0.9894	0.9979	0.9995	1	-

The influence of the TT method on the load effects is evaluated in this work using traffic data before and after the application of the method and running them through simple span bridges and double span bridges with same span length and sagging moment, shear force and hogging moment calculated. The reduction on the GVW seen before it is reflected in the load effects as well. Table 3.4 shows the comparison of the mean and maximum values in percentage terms. Load effects present variations from 4% to 13.52%, which proves that the TT calibration has a significant influence that should not be neglected.

Table 3.4. Mean and maximum difference between load effects before and after TT method.

Span length (m)	Sagging		Hogging		Shear	
	Mean (%)	Max (%)	Mean (%)	Max (%)	Mean (%)	Max (%)
10	4.39	4.60	4.39	3.95	4.40	3.95
20	4.38	3.82	3.93	3.32	4.47	4.68
30	4.40	3.85	5.62	9.75	4.44	4.51
40	4.40	3.98	5.72	6.33	4.63	4.03
50	4.17	4.93	5.20	13.52	5.04	3.89

The verification of the accuracy of the WIM data is completed with three data checks recommended by de Wet (2010):

1. The standard deviation of the front axle loads (F_{TT}) and the truck tractors loads (T_{TT}) should be below 0.8 t and 1.9 t respectively for the data to qualify as "Good". Good data are typically those that would achieve at least COST 323 accuracy class C(15) if a random sample of trucks from the road was used to verify the accuracy (de Wet, 2010)
2. Stability of the calibration factors k_{TT}: the calibration factor rarely differs more than 3% from the average factors of the past five months. Sudden changes or gradual drifts of the factor can be indicators of deterioration of the pavement around the WIM station.
3. The average front axle loads of the post calibration selected trucks should be in the range of 5,6 t to 6,6 t. The calculated value for the used data is found to be 6,4 t.

Figure 3.3 shows the standard deviation of the front axle loads (F_{TT}) and the truck tractors loads (T_{TT}) obtained using Roosboom traffic data. Values are below the warning thresholds mentioned previously, therefore, the Roosboom WIM station data are classified as Good and belongs, at least, to the accuracy class C(15). The influence of the accuracy of the WIM data in the prediction of extreme traffic load effects has been previously studied. O'Connor & O'Brien (2005) recommend a minimum class C(15) for the prediction of extreme load effects for spans <50 m.

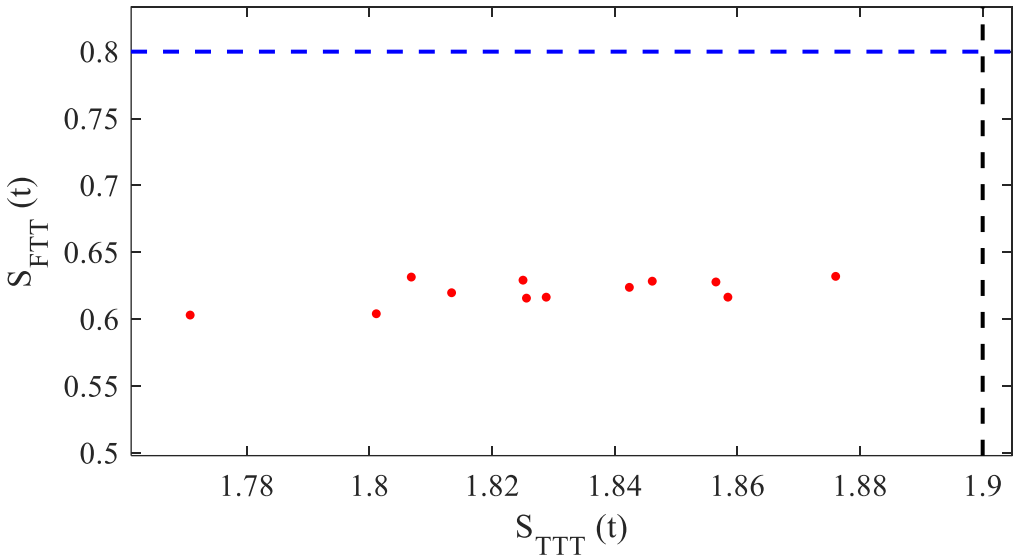

Figure 3.3. Monthly standard deviation of F_{TT} and T_{TT}.

Table 3.5 shows the differences between the calibrated k_{TT} in a month and the average factor from the previous five months. The average factor according to data check 2 can only be

estimated from June, hence the number of values in Table 3.5. All the differences are below the 3% indicated before.

Table 3.5. k_{TT} differences as indicated in data check 2.

Month	Difference (%)
June	0.48
July	0.92
August	0.19
September	0.59
October	0.93
November	1.09
December	1.04

The recorded data at Roosboom station, once cleaned and calibrated, comply with all the recommendations in de Wet (2010) and are suitable for being utilised in further calculations.

3.4 Traffic composition

After filtering and cleaning the data, vehicles need to be classified into different categories, usually based on the vehicles geometry. This in an important step that influences future modelling of variables. If vehicles are not classified properly, truck variables could present complex structures that might be difficult to model accurately, therefore affecting further calculations.

Regarding the data used in this document, lane 1 of the Roosboom WIM station presents 356 days of trucks with an ADTT of 2025 vehicles a day. Owing to the filtration process and the fact that the station lacks data during some days, the number of days recorded is lower compared to the 365 days in a year. The reason for selecting Lane 1 over Lane 2 for use in upcoming sections is that Lane 1 presents approximately 80 000 more vehicles when compared to Lane 2. Furthermore, heavier vehicles are recorded in Lane 1 as can be seen in Figure 3.4.

The percentage composition of the traffic regarding the number of axles per vehicle (vehicle class) is listed in Table 3.6, where 1 stands for a single axle, 2 for a double and 3 for a tridem. Table 3.6 clearly shows traffic dominated by the six- and seven-axle trucks, which together form more than 75% of the flow. Subclasses of trucks can be defined by taking into account the geometry and axle spacings. However, most of the vehicles belong to one sub-class for every

vehicle class while the rest of the sub-classes contain a relatively small number of trucks. Only main subclasses are modelled for simplicity. The amount of trucks forming the neglected sub-classes is less than 1% of the total traffic flow recorded.

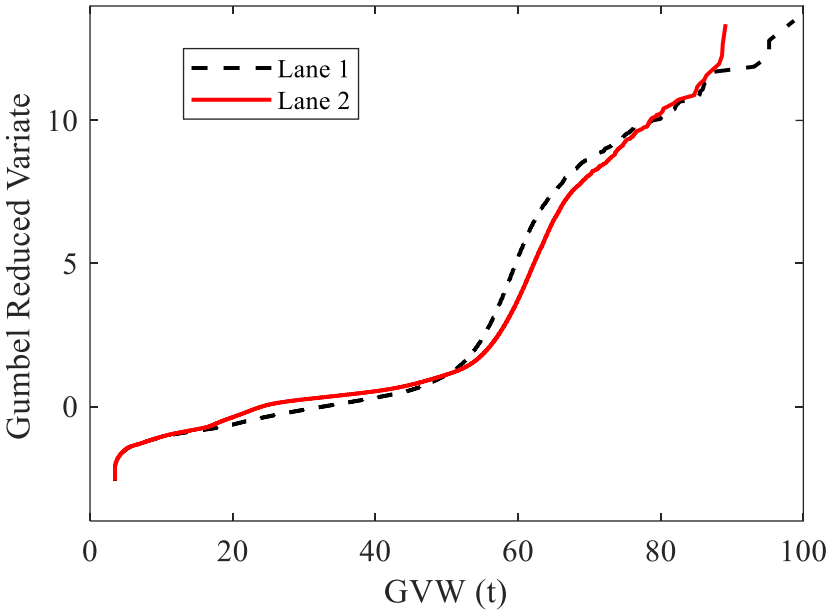

Figure 3.4. CDF of GVW for lane 1 and lane 2

Table 3.6. Traffic composition.

Number of axles	Axle geometry	Frequency (%)
2	1-1	7.87
3	1-2	5.97
4	1-1-2	4.00
5	1-2-2	4.74
6	1-2-3	31.11
7	1-2-2-2	45.10
8	1-2-3-2	1.13

Table 3.7 shows the composition of the traffic considering all the subclasses encountered in the data. This classification is based on the number of axles and distribution of them in single or group of axles. The assumption is that the maximum distance between adjacent axles in groups is 2 m. Axles further apart are considered to be isolated. Figure 3.5 shows the histogram of axle spacing between the forth and the fifth axle on a seven-axle vehicle considering all subclasses. The histogram shows a large peak around 1.4 m, which suggests that these values correspond to the commonly found tandem in these and other trucks.

Table 3.7. Traffic composition considering all the geometries.

Number of axles / Axle geometry	Frequency (%)
2/1-1	7.87
3/1-1-1	0.77
3/1-2	5.20
4/1-1-1-1	0.39
4/1-1-2	3.31
4/1-2-1	0.31
4/1-3	-
5/1-1-2-1	0.51
5/1-2-1-1	0.33
5/1-2-2	3.01
5/1-1-3	0.83
6/1-1-2-1-1	-
6/1-1-2-2	0.15
6/1-2-1-2	0.17
6/1-2-2-1	0.20
6/1-2-3	30.59
7/1-2-2-1-1	0.20
7/1-2-2-2	44.23
7/1-2-4	-
7/1-2-3-1	0.71
7/1-3-3	-
7/1-1-2-1-2	-
7/1-1-2-3	-
7/1-2-1-3	-
8/1-2-2-3	0.23
8/1-2-3-2	0.87
8/1-3-2-2	-
8/1-3-4	-
8/1-2-3-1-1	-

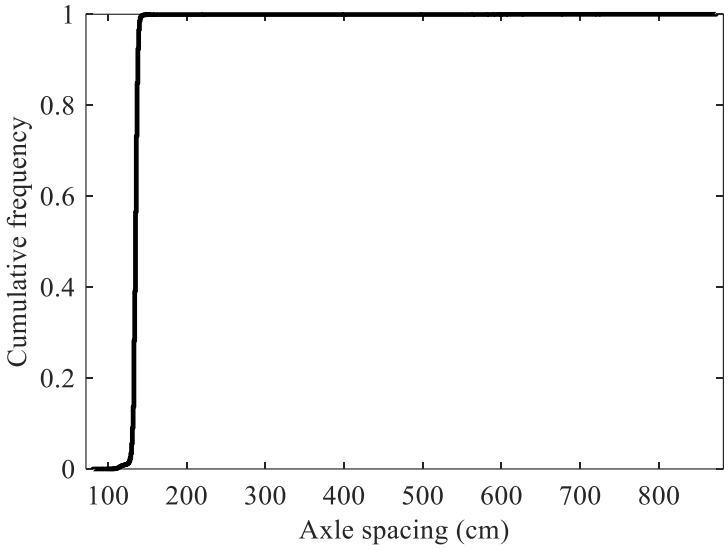

Figure 3.5. Axle spacing 4th to 5th axle on 7-axle vehicles.

Although the percentage of the eight-axle vehicles is slightly inferior to 1%, this class is not neglected. The amount of eight -axle vehicles is scarce but sufficient to characterise the vehicle class variables and the GVW of the vehicles suggests that they could generate determinant load effects.

3.5 Gross vehicle weight and axle load distributions per vehicle class

The following section presents a summary of the distribution of gross vehicle weights (GVW) and axle loads. Relative histograms are used to describe the variables. Figures not portrayed in this section are shown in Appendix A.2. Although the geometry of the vehicles is different between classes, there are similarities in the distribution of the load among the axles:

- The GVW's distributions show that most of the vehicles are loaded since the unloaded peaks in the distributions are always smaller than the loaded peaks and in some cases almost imperceptible. In many other cases, the threshold between loaded and unloaded vehicles is not clear. The tendency is to load the vehicles for economic reasons. Regions of the distributions below the loaded peak correspond to partially loaded vehicles. The GVW distributions are a mixture of dominating loaded vehicles and less important unloaded and partially loaded vehicles.

- The steering axle is mostly influenced by the weight of the engine. All histograms present unimodal distributions with a minimum of 0.9 t and maximum of 10 t, whereas most of the values are around 6 t as shown in Figure 3.6. The unusual low steer axle loads (1 t) are mostly found in two, three and four axle vehicles. Vehicles geometries suggest that they could be cars, buses or vans towing a single or double axle trailer. The minimum GVW threshold of 3,5 t is exceeded in these cases and therefore these vehicles are recorded by the station. These small loads are also observed in very small quantities in larger vehicles, which present standard axle spacing configurations and axle loads. The influence of the recorded vehicles with unusual low steer axle load on the extreme load effects is neglected due to the small number of these vehicles present in the data. The accuracy of the WIM data has been estimated in Section 3.3 providing acceptable results, however, further investigations are recommended in the future to clarify the source of these uncommon records.

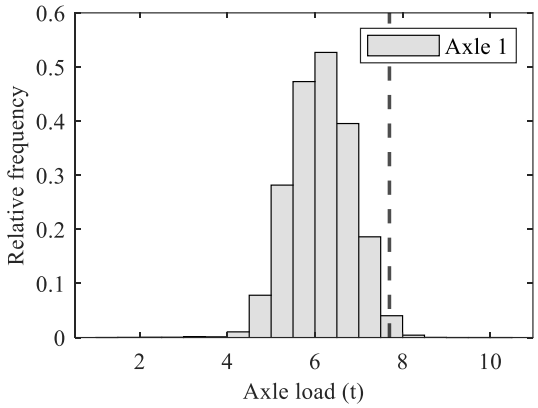

Figure 3.6. Histogram of the load on the steering wheel - six-axle vehicles.

- The rest of the axles recorded present values between 0.9 t and 14-15 t for all the vehicles consisting of three or more axles. Distributions are unimodal or bimodal depending on the number of unloaded vehicles but all of them present the largest peak around 6-7 t. Figure 3.7 shows two examples of different histograms of single axle loads.

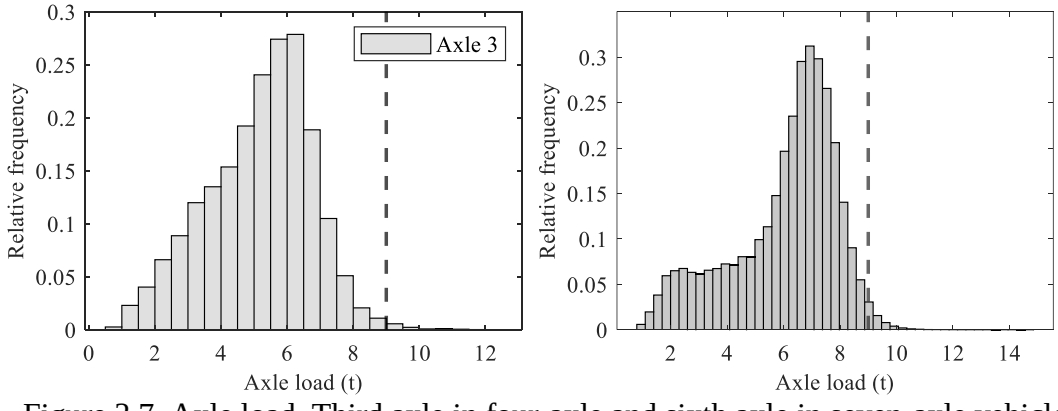

Figure 3.7. Axle load. Third axle in four-axle and sixth axle in seven-axle vehicles.

- Tandems present minimums around 2 t and maximums between 24 t and 29.7 t. Main peaks are located between 12 t and 15 t. A greater peak of 17 t is found on the tandem for the six axle vehicles. Figure 3.8 shows two examples of histograms on five- and seven-axle vehicles. Although the shape is different, the largest peak is similar.

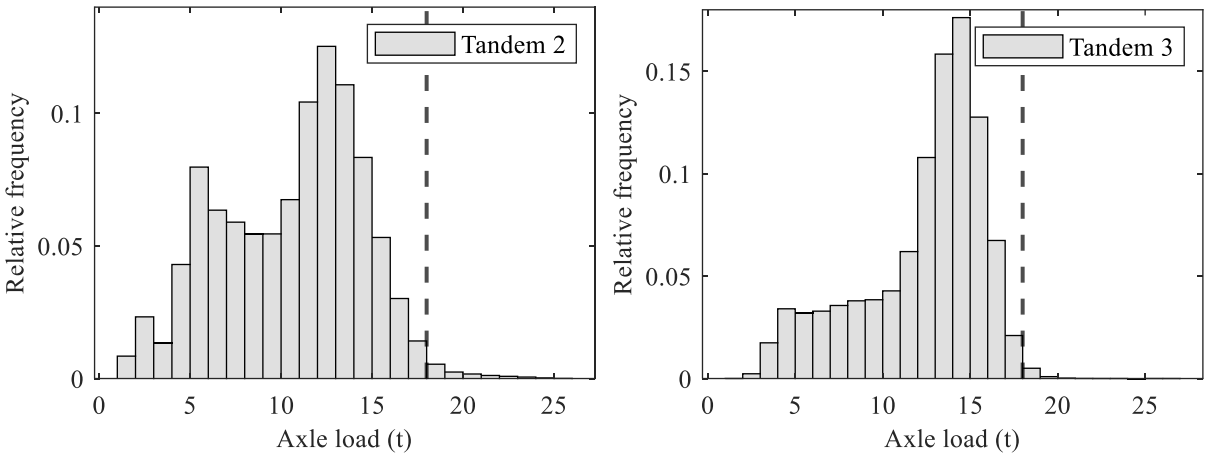

Figure 3.8. Tandem load histograms. Second tandem in five-axle vehicles and third tandem in seven-axle vehicles.

- Only six- and eight-axle vehicles present tridem in the traffic analysed. Minimums are at 3-4 t while maximum are 35.1 t for eight-axle and a greater 41.7 t for six-axle vehicles. Both distributions show similar peaks at around 21 t. Figure 3.9 shows the tridem for six- and eight-axle vehicles.

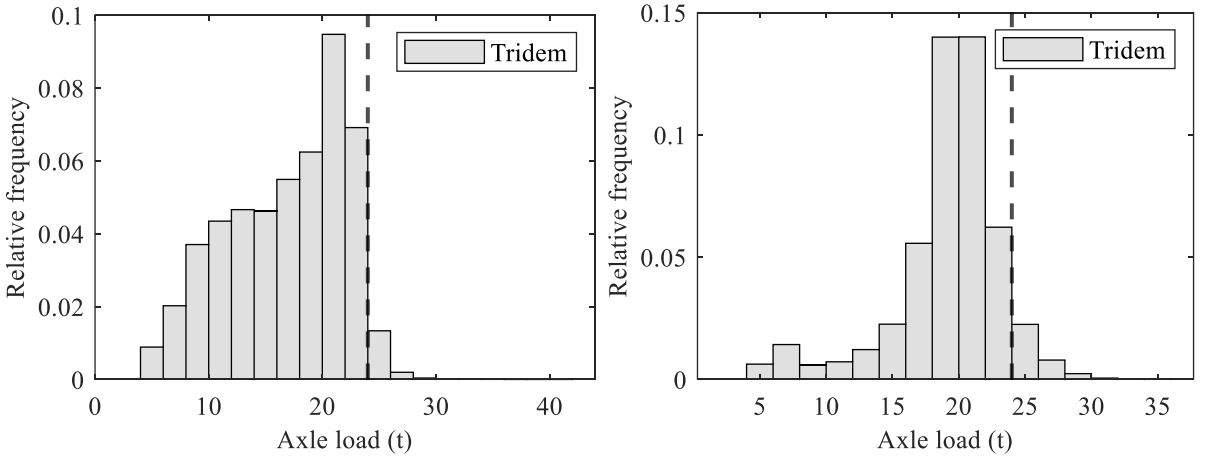

Figure 3.9. Tridem load histograms. Six-axle vehicles and eight-axle vehicles.

- Over loading is present in the traffic recorded at Roosboom WIM station. The TRH 11 (2009) published by the Department of Transport in South Africa provides the axle or axle group mass limitations in the country. As mentioned, the maximum GVW is 56 t, value that six-, seven- and eight-axle vehicle overpass. Axle mass limitations are 7.7 t

for steering wheels and 8 t or 9 t for non steering single axles with one or two wheels per side respectively. Tandems are limited to twice the previous masses and tridem to 24 t. Limitations are generally respected by most of the vehicles, as shown by the peaks in the histograms, which are found closer to the maximum legal masses, however, maximums surpass the legal upper limits by far. Maximum single axles of 15 t, tandems closer to 30 t and tridems of 42 t have been recorded which proves this behaviour. It is unfortunately not possible to know whether these records correspond to permit vehicles or simply overloaded normal traffic. The fact that these records belong to vehicles with eight or less axles suggests that overloading is a general practice in the country.

3.6 Axle spacings

Vehicles formed by five or more axles are powered by a three-axle truck tractor with a single front steering wheel and a read tandem. The distance between the steering wheel and the first axle of the tandem presents a minimum of 2.4 m to a maximum around 6 m. Two major peaks are located around 3.15 m and 3.7 m. The distance between the front and the rear axle in two-axle truck tractor is also commonly found to be 3.7 m. Figure 3.10 shows examples of both cases.

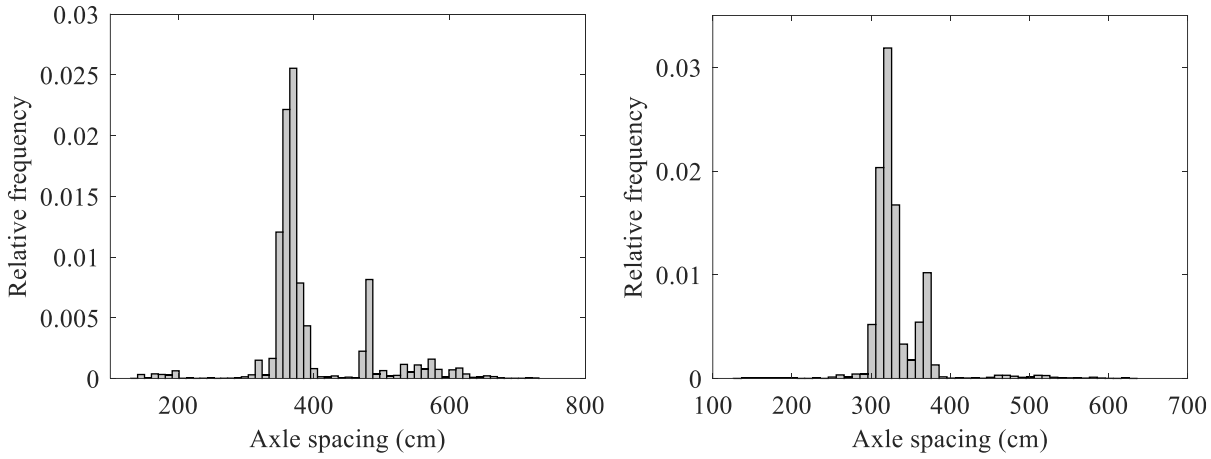

Figure 3.10. Axle spacing histograms. Large distance in two-axle and three-axle truck tractors.

Distances between axles forming axle groups (tandems or tridems) are usually between 0.5 m and 2 m with most of the values around 1.35 m as can be seen in Figure 3.11 for tandems and tridems. This is independent of the vehicle class.

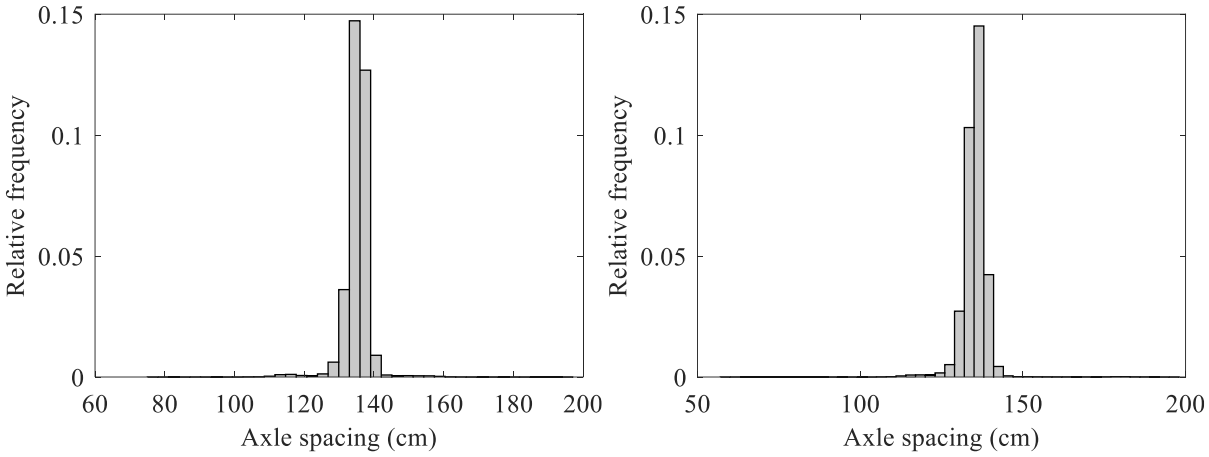

Figure 3.11. Axle spacing histograms of adjacent axles in groups. Third tandem in seven-axle vehicles and tridem in six-axle vehicles.

The spacing between rear and front wheel of adjacent axle groups presents high variability and slight differences between vehicles classes. Values are usually larger than 4 m and always lower than 10 m due to the filtration criteria. Common distances are around 7 m. Figure 3.12 shows an example of axle spacings for six- and eight-axle vehicles.

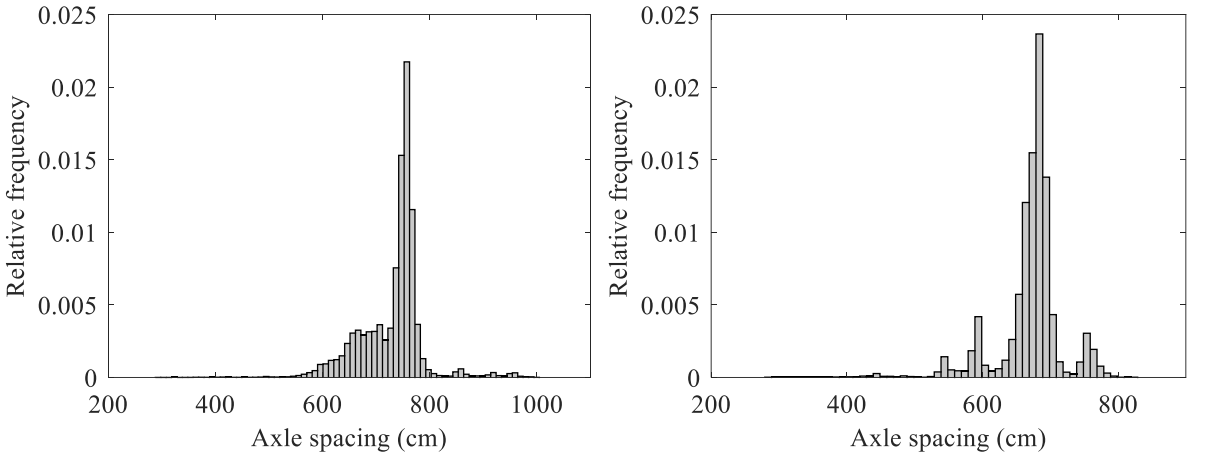

Figure 3.12. Axle spacing histograms - distance between adjacent axle groups. Tandem and tridem in six- and eight-axle vehicles.

The histogram of axle spacings for two- and three-axle vehicles (except for the tandem in the latter class) do not present any specific shape and are quite erratic as can be seen in Figure 3.13.

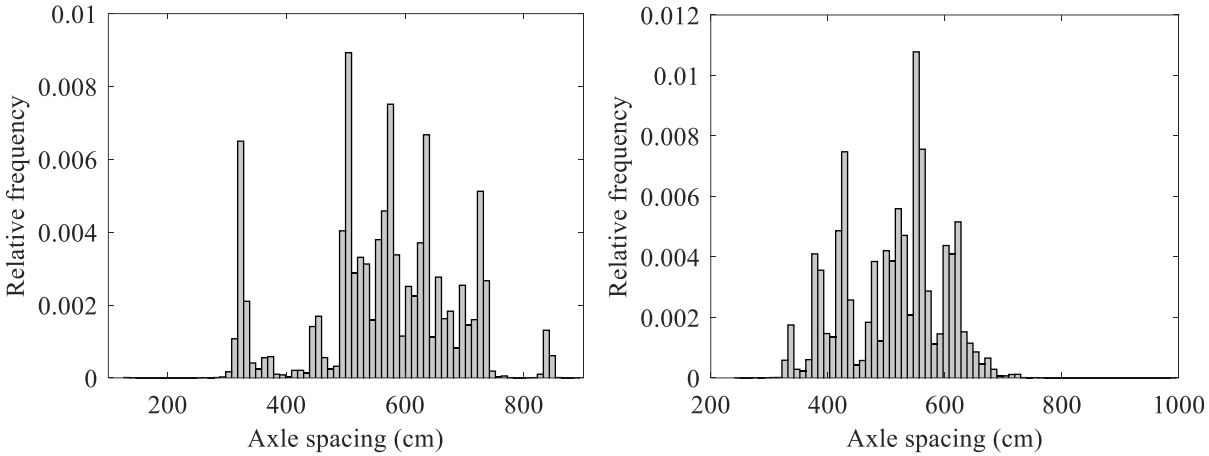

Figure 3.13. Axle spacing histograms. Two-axle vehicles and large spacing – three-axle vehicles.

The histograms of axle spacings portrayed in this section show that the recorded axle spacings do not follow any specific probability distribution and are either erratic or most of the values are concentrated around some values. These features are important as they influence the way that this variable is going to be treated in the Monte Carlo routine. Further details regarding the modelling of axle spacings can be found in Section 4.3. Other histograms not shown here are available in Appendix A.2.

CHAPTER 4: TRAFFIC MODELLING

The amount of traffic data usually available do not provide enough observations of heavy trucks due to the limited period of recording, therefore, a Monte Carlo routine can be used to increase the number of heavy vehicle observations. This method requires modelling the available data, thus artificial traffic can be simulated for the desired period. The first sections of this chapter are focused on the description of the methods used to model the traffic variables necessary for the generation of artificial traffic. The modelled variables are:

1. GVW and its distribution among the axle loads.
2. Axle spacing.
3. Vehicles gaps.

Developing a Monte Carlo routine also allows for the variation of the traffic characteristics in the generated flow and the evaluation of its impact in the traffic load. This is an important concept of this study as the aim is to identify the main parameters of the traffic flow and quantify their influence on the load effects. One year of recorded traffic is used in this study as it presents enough data to model vehicles with up to eight axles. However, the developed routine described hereafter and already introduced in Pérez Sifre & Lenner (2019), can be applied to any type of vehicle recorded. The flowchart shown in Figure 4.1 summarises the Monte Carlo routine detailed in the following sections.

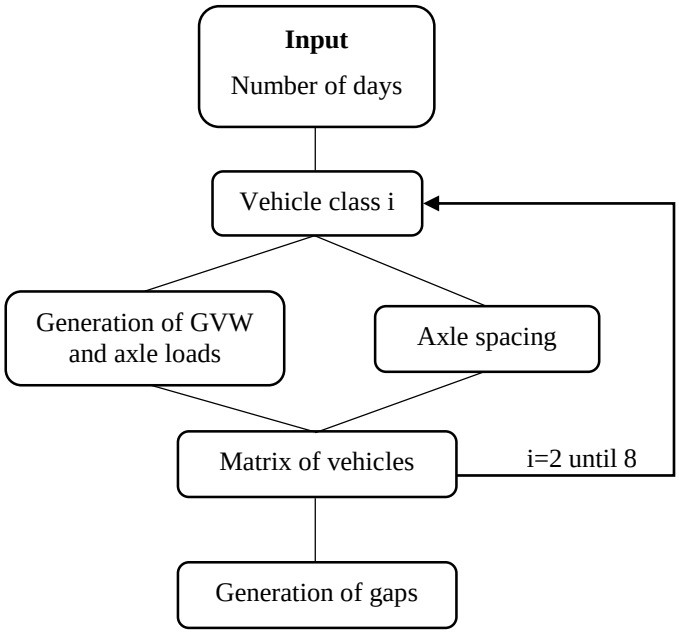

Figure 4.1. Flowchart – Monte Carlo routine.

4.1 The gross vehicle weight and axle loads

The approach used in this research to model the distribution of the GVW among the axle loads is based on the use of copula functions. Copulas were first introduced by Sklar (1959) and have become a very popular tool in many fields that demand the modelling of multivariate correlated variables. Copulas establish a link between the multivariate probability distribution and the univariate margins. Sklar's theorem states that if F is n dimensional joint cumulative distribution function with $F_1, F_2, \dots, F_n$ the marginal cumulative distributions, then there exists a copula C such all $x = (x_1, x_2, \dots, x_n)$:

$$F(x) = C\big(F_1(x_1), \dots, F_n(x_n)\big) \tag{4.1}$$

where C is unique if $F_1, F_2, \dots, F_n$ are continuous. Conversely, it means that if there is a copula C and the marginal cumulative distributions$F_1, F_2, \dots, F_n$, the joint distribution function F is defined. C could also be interpreted as the cumulative distribution function of a n-dimensional random variable on the $[0,1]^n$ space with uniform margins.

Linear correlation between the GVW and axle load is commonly used for the generation of axle weights as a simple approach (Allaix, 2007; Bailey, 1996; Crespo-Minguillón & Casas, 1997), and provides reasonable results especially when dependence is similar to the one in multivariate Normal or t-distributions. Nevertheless it could produce uncertain results when this is not the case (Embrechts, Lindskog, & McNeil, 2003). Truck loads present a wide variety of distributions and combinations, therefore, the linear approach is likely to introduce errors. This can also be alleviated by more complicated relationships between the GVW and axle loads; for example by generating multivariate random numbers using correlation matrixes and Cholesky factorisation (Enright, 2010). The practical implication of Sklar's theorem is that copula functions enable the separation of the marginal distributions (which can be of any type) and the dependence structure. Such a characteristic makes it an appropriate approach when simulating correlated variables.

Previous researchers have used multivariate copulas to account for the correlation between axles for up to four-axle vehicles (Srinivas et al., 2006). This essentially requires a four-dimensional copula (one dimension per axle). High dimension multivariate copulas present inflexible structures (Brechmann & Schepsmeier, 2013) and could not accurately model the dependence structure of vehicles with high number of axles.

To alleviate the issue of high dimension copulas and to address the problem of the high percentage of six- and seven-axle vehicles in the local traffic, it is proposed here to develop an alternative approach. The new method presented is based on the use of bivariate instead of multivariate copulas. Bivariate copulas are used to simulate the dependence structure between the GVW and every axle or group of axles for up to eight-axle vehicles. However, if truck data with a larger number of axles are available, the proposed procedure can be adapted. While Srinivas et al. (2006) fit multivariate copulas to simulate the structure dependence between axles, studying the correlation between the GVW and independent axle loads means that only bivariate copulas are necessary. The later approach reduces the problem to the use of bivariate copulas. The rich variety of available bivariate copula families enables them to accurately fit any dependence structure that the data presents. This is another advantage over high dimension copulas with less variety of families (Brechmann & Schepsmeier, 2013).

Bivariate copulas are fitted to the data using the CDVine package (Brechmann & Schepsmeier, 2013) available on the statistical software R. This software allows for the use of Maximum Likelihood or Method of Moments for estimation of the copula parameters. Once all the parameters for every family available are obtained, objective criteria can be then used to select which copula best fits the data. The Akaike Information Criteria AIC (Akaike, 1974) estimator is used to select the best fit to the data:

$$AIC = 2k - 2\log(L) \tag{4.2}$$

where k represents the numbers of parameters in the model and L the maximum value of the likelihood function. The model with the lowest AIC value is selected as the best fit.

As an example of bivariate copulas, Figure 4.2 shows the dependence structure between the recorded GVW of a four-axle vehicle and the 4th axle load and the GVW of a six-axle vehicles and its tandem in terms of pseudo values. As stated by Sklar's theorem, copulas are defined in the $[0,1]^n$ space with uniform margins, hence real values must be transformed into pseudo values or values contained in the previous interval, to observe the dependence structure. A region on the left side of the scatter plot indicates values clearly not following the structure. This discordance is found to be caused by trucks that are unevenly loaded, thereby indicating that some axles are overloaded while others are not loaded to the same extent. In short, this means that some axles exhibit small loading even when the whole truck is technically loaded. While the left dependence structure could seem linear, the right scatter plot does not show the

same clear linear correlation. Moreover, the density of points is not constant throughout the graph and some sections present higher probability as observed in the density plots (graphs below scatter plots) of the fitted copulas. Copula functions can capture this phenomenon.

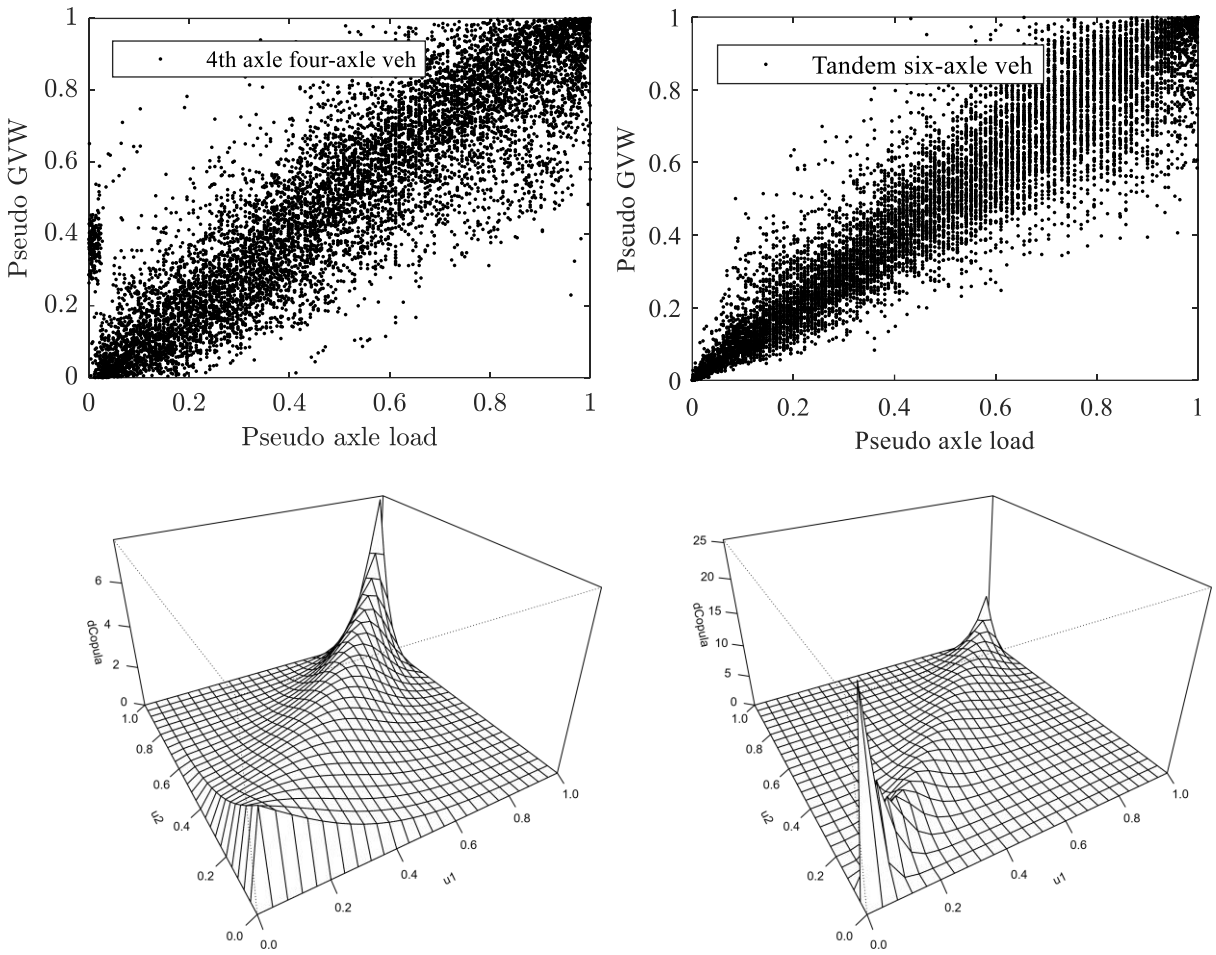

Figure 4.2. Pseudo observations - dependence structure and densities.

A total of 23 bivariate copulas are fitted to the pairs of vectors:

- GVW to axle load or
- GVW to individual axle group (tandem and tridem in this case).

During the calibration of the Monte Carlo routine, it was found that modelling the entire axle groups for the five-, six-, seven- and eight-axle vehicles and distributing the load evenly among axles in the group results in a better fit when compared to the individual treatment of each axle in the group. This effectively implies a full correlation of the load among the individual axles in the group. This is supported by axle group modelling done by Caprani (2005). Table 4.1 contains the bivariate copulas fitted to the each vehicles class and their parameters.

Table 4.1. Copula fitted to pairs of vectors axle load - GVW.

Axle or axle group/ vehicle class	Copula family	Parameter 1	Parameter 2
Steering wheel/2	Frank	12.81	N/A
Rear axle/2	Frank	22.05	N/A
Steering wheel/3	Student t	0.71	28.58
First axle tandem/3	Rotated-Survival BB8	6	0.88
Second axle tandem/3	Rotated-Survival BB8	4.25	0.94
Steering wheel/4	Rotated-Survival BB1	0.06	1.53
Second single axle/4	Rotated-Survival BB8	4.43	0.9
First axle tandem/4	Rotated-Survival BB1	0.23	2.78
Second axle tandem/4	Rotated-Survival BB8	6	0.82
Steering wheel/5	Student t	0.57	30
First tandem/5	Student t	0.78	24.64
Second tandem/5	Frank	11.65	N/A
Steering wheel/6	Frank	4.65	N/A
Tandem/6	Rotated Tawn 1 180^{o}	4.41	0.983
Tridem/6	Rotated Tawn 2 180^{o}	5.97	0.99
Steering wheel/7	BB1 Copula	0.71	1.11
First Tandem/7	Rotated-Survival BB8	4.14	0.99
Second Tandem/7	Rotated-Survival BB8	4.21	0.99
Third Tandem/7	Rotated-Survival BB8	4.25	0.98
Steering wheel/8	Rotated-Survival BB8	2.1	0.94
Tandem/8	Rotated-Survival BB8	3.03	0.65
Tridem/8	Rotated-Survival BB8	3.49	0.97
Tandem/8	Student t	0.77	5.7

It therefore follows, that by knowing the number of trucks per vehicle class, the simulation continues using the bivariate copula fitted to the pair of values GVW – last axle load for one vehicle class. A pair of correlated vectors containing what is commonly known as ‘pseudo values’ can then be simulated. The pseudo GVW is then used in the next step in the simulation, which involves the bivariate copula fitted to the next axle. A correlated vector for the pseudo

axle load is obtained for the same pseudo GWV used in the previous step. The length of the above mentioned vectors is equal to the number of trucks that the simulated vehicles class contains. The process continues successively until all the pseudo axle loads are simulated for the vehicle class.

The last step in the simulation of GVWs and axle loads is to calculate real values using the pseudo axle loads, the pseudo GVWs, and empirical cumulative density functions (CDF) for every variable involved.

One year of data provides a limited insight in the distribution of extremely heavy vehicles. To overcome this, it is necessary to generate heavier trucks than recorded by the WIM station to obtain heavier observations. Consequently, Normal distributions, which are asymptotic towards zero probability, are fitted to the tail of the GVW distribution of every vehicles class. The same approach with Normal distributions is adopted by Enright (2010), O'Brien, Enright, & Getachew (2010) and Zhou, Schmidt, & Jacob (2012). The tail fitting is not performed on two- and three-axle vehicles as their influence on the extreme load effects is negligible. As an illustration, Figure 4.3 shows the Normal probability plot and the Normal fit for the six-axle vehicle class. This effectively means that GVWs are generated using the empirical CDF until the selected threshold, from where the fitted Normal distribution applies. This is known as semi-parametric fitting (O'Brien et al., 2010).

The threshold is selected as the point in the tail of the distribution of GVW where the Pearson correlation coefficient R is closer to 1. The correlation coefficient R is a good estimator of the strength of the linear relationship between two variables, in this case the GVW observations and their position in the Normal probability paper represented by the Normal Reduce Variate Z. Values of R range from -1 (negative linear relationship) to 1 (positive linear relationship), Values close to 0 represent weak linear relationship. R is calculated iteratively increasing the size of the variables GVW and Z adding more tail observations, starting from the highest GVW recorded. Figure 4.4 shows the variation of R with the length of the tail and a detail of the area of interest for six-axle vehicles. The correlation coefficient reaches its maximum value when 250 observations in the tail are considered. The changes in the gradient after this point seen in Figure 4.3, cause a gradual decrease of the value R indicating a weakening in the linear relationship. Table 4.2 shows the thresholds – fractiles and number of tail values - for the rest of the vehicles.

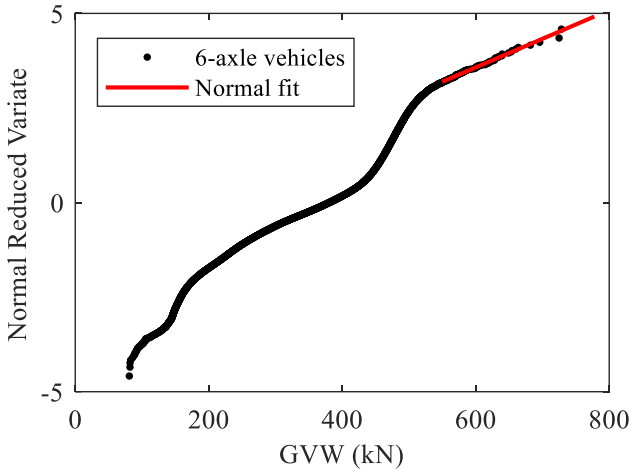

Figure 4.3. GVW with Normal probability distribution fitted to the tail.

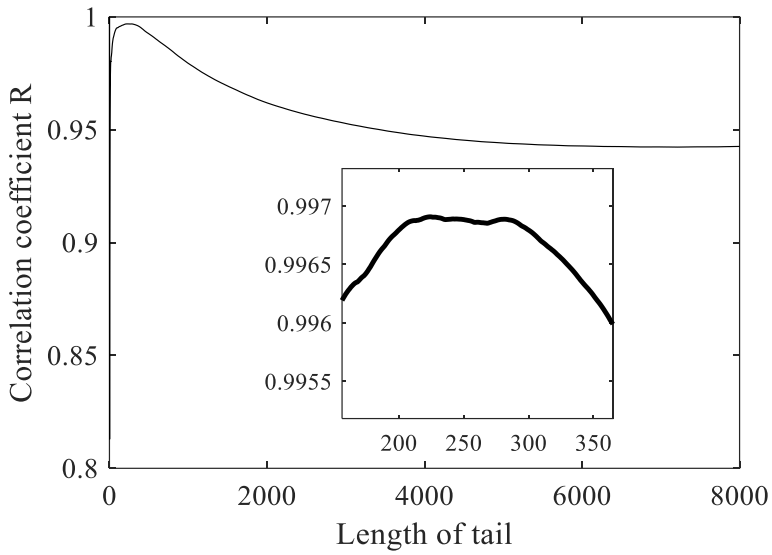

Figure 4.4. Variation of correlation coefficient with length of the tail.

Table 4.2. GVW thresholds (fractiles) from where the Normal fit is performed.

Vehicles class	*R*	Threshold (fractile)	Length of the tail	GVW (kN)
five-axle	0.9972	0.9623	818	371.8
six-axle	0.9969	0.9990	223	539.8
seven-axle	0.9855	0.9999	41	648.8
eight-axle	0.9884	0.9884	577	564.8

In the case that the sum of the axle generated loads do not exactly match the value of the originally generated GVW (due to the inherent randomness of the here developed process) every axle load of that vehicle is rescaled by the same factor so that the desired GVW is achieved.

Figure 4.5 shows the scatter plot comparing the dependence structure between the generated and recorded pair of values 4th axle - GVW for the four-axle vehicle. As can be observed by the cluster of only black points and lack of red data points there, the routine does not allow for uneven loading of vehicles.

The described process is then repeated for each vehicle class until all the classes required at the beginning of the routine are generated.

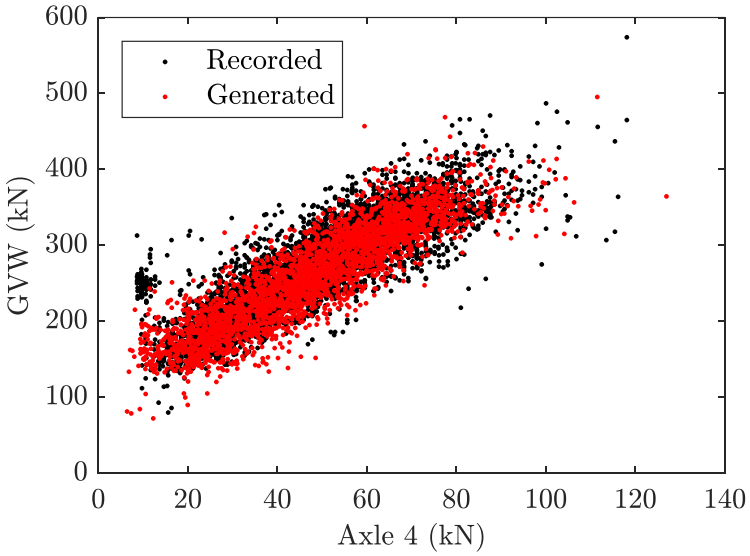

Figure 4.5. Scatter plot of recorded and generated fourth axle load - GVW for four-axle vehicles.

4.2 Axle spacing

The Monte Carlo algorithm begins with the simulation of GVWs and axle loads in relation to the selected vehicle class as a function of number of axles. As previously discussed, vehicles comprising less than 1% of the total flow are not considered in the model. The same approach is used for the rest of the vehicle classes.

Figure 4.6 shows the relative histograms of the axle spacing for the second tandem and the spacing between the 3rd and the 4th axle of seven-axle vehicles. All the values are located around 1.35 m with a low variability for the tandem. The 3rd to 4th axle spacing histogram shows two clearly divided populations, the first one and most frequent around 5.8 m and the second around 7.5 m. As a result, it is proposed in this Monte Carlo routine to use the geometry of real recorded vehicles instead of generating a random shape. The shape and form of vehicles on the roads is in-fact limited and it is therefore not appropriate to generate trucks that do not resemble real

vehicles in terms of axle spacings and lengths. Correlations between adjacent axle spacing or other sophisticated approaches could be used to generate individual axle spacings (Bailey, 1996; Enright, 2010; Srinivas et al., 2006) but given the large amount of vehicles recorded, the random selection of the recorded vehicle geometries covers the geometries observed in a simple manner.

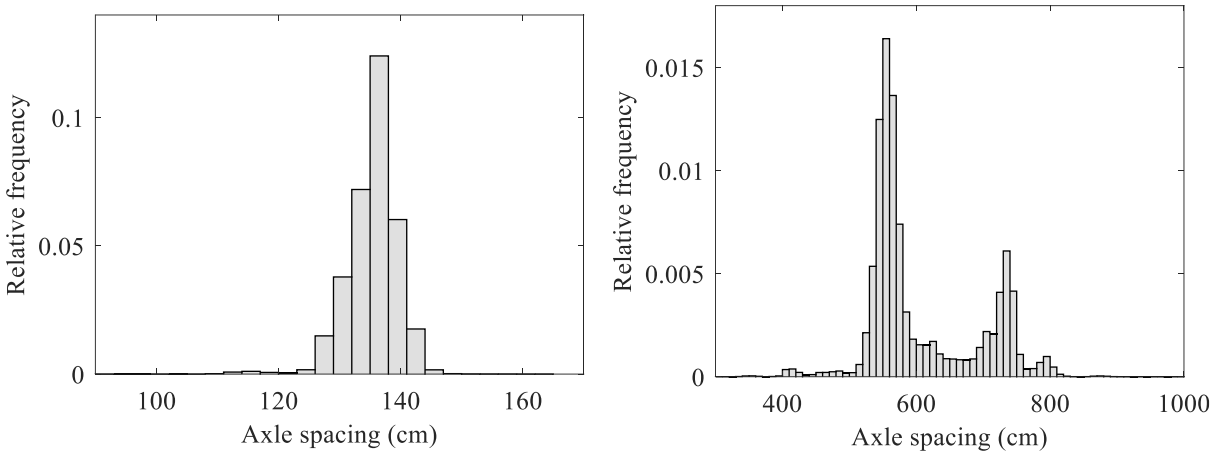

Figure 4.6. Axle spacing second tandem and 3rd to 4th axle on 7-axle vehicles.

4.3 Vehicle gaps

The generation of artificial convoys involves a simulation of headways (distance or time between front axles) or gaps (distance or time between rear and front axle of the following vehicles) between trucks. As mentioned before, the ADTT of the station used as a basis for this study is 2025 veh/day per lane. Traffic flow is not constant throughout the day and the gaps change. It is therefore important to consider an hourly variation of the flow (HF). The average hourly flow (AHF) of the station is 84.4 veh/h. Using this value and considering the average hourly flow for every hour of the day, a coefficient c to compare both values can be calculated from the following Equation (4.3):

$$c = HF/AHF \tag{4.3}$$

where HF is the average hourly flow for a specific hour of the day and AHF is the average hourly flow of the station. Figure 4.7 shows the c values obtained for the Roosboom station. This patterns is assumed constant for all traffic scenarios of free flow and is therefore used for all the simulations in this study.

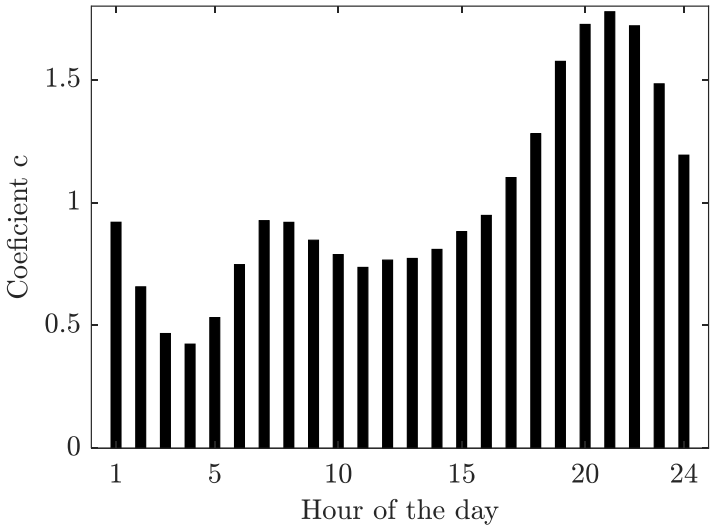

Figure 4.7. Coefficient c of the hourly flow variation.

As suggested by by O'Brien and Caprani (2005) gaps recorded at hours with the same hourly flow are combined together using intervals of 10 veh/h. The empirical CDF for every interval is obtained from the recorded vehicles gaps. This allows for the use the CDF for the simulation of gaps. Linear interpolation between gaps not recorded is used to smooth the shape of the CDFs. The AHF is obtained by dividing the selected ADTT by 24. Following the inverse process explained here, the proposed parameter *c* and the AHF are multiplied resulting in 24 different values that represent the hourly flows for the complete day. As explained, every value would fall into one of the gap intervals and consequently the simulation of gaps for every hourly flow is straightforward using its gap CDF. Figure 4.8 shows the CDF of vehicle gaps for different hourly flows and detail of the small gaps. As expected, the correlation between gap and hourly flow is inverse, gaps decrease as HF increases.

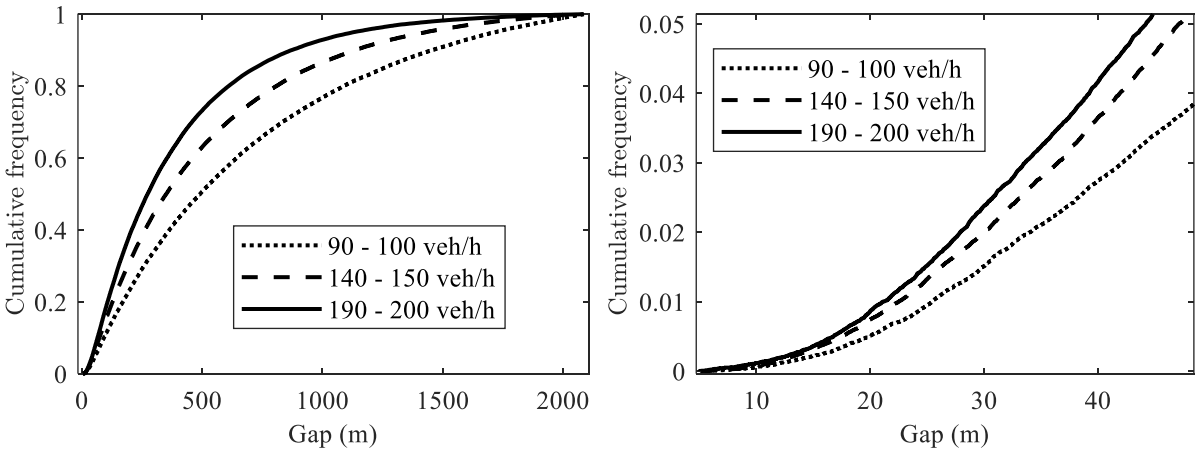

Figure 4.8. Complete and detailed CDF of gaps - variation with hourly flow.

As can be seen in Figure 4.9, where the recorded values of hourly flow are plotted against the average speed of the vehicles, Roosboom station is able to provide the CDF for hourly flow up to 260 veh/h. The corresponding speed for the maximum HF is 79 km/h what indicates that the road can sustain free-flowing traffic for an HF of 260 veh/h. Records for speeds below 70 km/h are removed to avoid the use of congested gaps. Applying the maximum value of c=1.78, the maximum ADTT that can be simulated is 3500 veh/day. Roosboom station does not provide enough vehicle gap information and other stations are, therefore, analysed in order to complete the database allow the routine to generate ADTTs up to 4000 veh/day. Two piezoelectric stations, Wilge Plaza and Bergville, which only record vehicle and axle distances, help to obtain the required CDF.

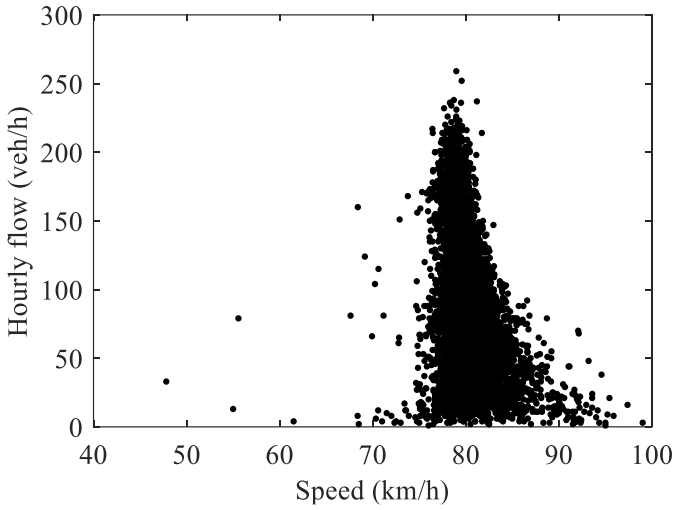

Figure 4.9. HF and average vehicle speed.

Figure 4.10 shows the CDF of the recorded gaps in comparison to the generated gaps using the same ADTT. Only gaps up to 100 m are displayed to improve the quality of the graph. A detailed graph of short gaps is also displayed.

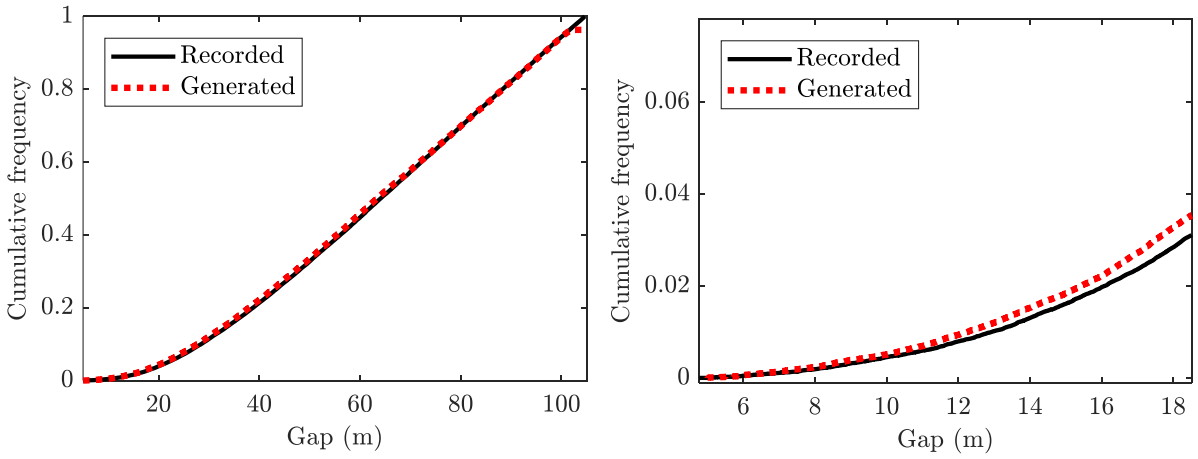

Figure 4.10. CDF of recorded and generated vehicle gaps up to 100 m and detail.

4.4 Algorithm

The algorithm able to generate the artificial traffic is described here. The modelling of the variables involved explained in the previous sections is as follows:

1. All the information necessary for the generation of the artificial traffic are loaded. This includes CDF of axle loads and GVW, copula parameters previously calculated axle spacings and headways.

2. The algorithm requires inputs on the number of years to be generated, the days per year and the ADTT of the artificial traffic. The traffic composition is also preliminary information necessary for the generation.

3. Once the total number of trucks and the traffic composition are known, it is straightforward to calculate the number of trucks per vehicle class. The generation of vehicles in every class can then be start.

4. For every vehicles class the generation of trucks begins with the simulation of pseudo random values (GVW and axle load) using the bivariate copula corresponding to the axle a_n or rear axle of the vehicle. The pseudo GVW simulated is used in the next step to simulate the axle load of the following axle a_{n-1}. The generation continues likewise until all the pseudo axle loads are generated $(a_1, a_2, \dots a_n)$.

5. Pseudo values are contained in the space $[0,1]^n$. To obtain real axle load and the GVWs generated are transformed using empirical cumulative density functions (CDFs) for every variable involved.

6. Axle loads are then rescaled so that the sum of its values matches the generated GVW.

7. Random axle configurations are selected from the database and assigned to the trucks from the corresponding vehicles class.

8. All the vehicles generated are added together in a matrix of traffic and they are randomly mixed since until this moment they are categorised per vehicles class.

9. Vehicles gaps are calculated using the ADTT and the hourly flow variation.

10. The vehicle gaps are added in a column at the end of the matrix and a column representing the day of arrival is included. This is important for the calculation of the daily maxima load effects.

11. The generated traffic is saved in individual files containing 1 year of information. These files are to be loaded into Matlab, software used to write the algorithm that calculates the traffic load effects.

The pseudo-random number generator used in the whole process is the Mersenne-Twister (Matsumoto & Nishimura, 1998) with a period of 2^{19937}-1. Initially there is no seed and a new one is created from the current time and process ID when required, therefore, different sessions give different simulation results, by default.

4.5 Operational days per year

The number of operational days in a year is assumed to be 365 in the context of this thesis. This assumption influences future simulations of traffic and extrapolation of load effects. Although in previous publications years are considered of 250 days after deducting holidays and weekends with light or non-existent heavy traffic (Allaix, 2007; Caprani, Grave, O'Brien, & O'Connor, 2002; Enright, Caprani, & O'Brien, 2011), the reality in South Africa is that heavy traffic is observed throughout the week, therefore years of 365 days are considered as a conservative measure since it delivers higher load effects (details in Appendix B.1). Moreover the same number was used in the derivation of the design traffic load model (van der Spuy & Lenner, 2019).

The assumption of 365 operational days is here supported by the values portrayed in Figure 4.11 that shows the ADTT for each day of a selected standard week. The red line contains all the vehicles and the black line contains only vehicles with more than five axles. Minimum traffic intensity is recorded on Saturday and it increases gradually reaching its peak from Tuesday to Thursday. An important decrease in the traffic flow is observed during Friday, which presents similar values to Monday and Sunday. The decrease of the traffic intensity around weekends is noticeable, however, the economic activity is still substantial, and equivalent to some weekdays, with an important percentage of heavy vehicles in the traffic flow (black line). Whether the traffic activity in a day is sufficient for it to be considered as operational is, however, a subjective decision that could be better defined in future research.

The distinction of weekdays and weekends is, in the data used here, not entirely clear and all the days recorded are considered in further sections.

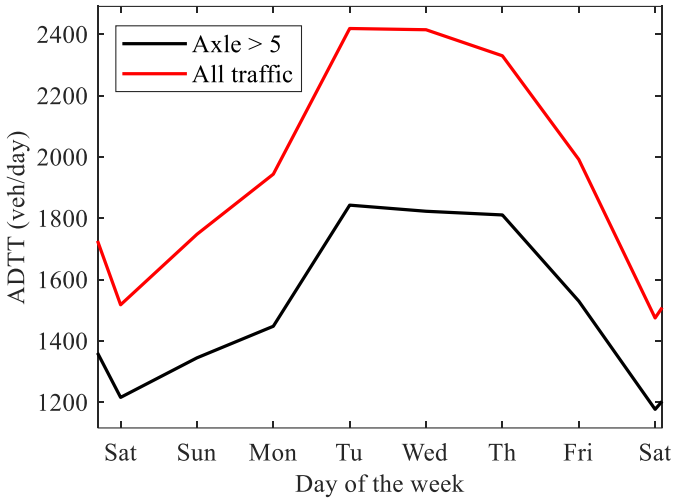

Figure 4.11. ADTT during a week.

4.6 Load effects - Comparison of recorded to simulated

To validate the proposed Monte Carlo routine, one year of artificial traffic with the same ADTT as the recorded traffic is generated for a single lane loading. As mentioned in the previous section, a year of 365 days is considered – this essentially results in 739125 artificial vehicles per year.

Load effects are calculated here by means of appropriate influence lines, (detailed in Table 4.3) where the axle loads act as point loads while convoys of vehicles with appropriate gaps are moved across the required span lengths. Vehicle gaps are maintained throughout the process and the overlapping of vehicles is not allowed. A simple scheme of a three-axle vehicle followed by a six-axle vehicle with the corresponding axle spacings s_{ij} and vehicle gap g_h is shown in Figure 4.12.

Calculations are performed for sagging moment and shear force at simple spans while the hogging moment is investigated for continuous beams of equal span lengths. The obtained load effects for the artificial traffic are compared to the load effects calculated from the recorded traffic on Gumbel probability paper in Figure 4.13.

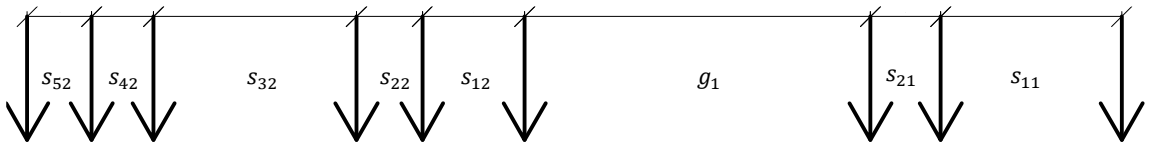

Figure 4.12. Axle load – vehicles gap scheme.

Table 4.3. Influence lines.

Influence line	Equation
Sagging 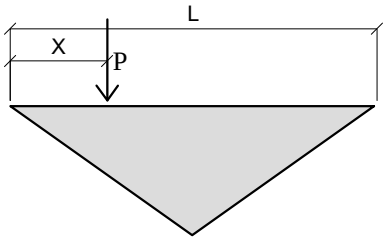	$M(x) = \begin{cases} \frac{P \cdot x}{2} & \text{for } 0 < x < \frac{L}{2} \\ \frac{P \cdot (L - x)}{2} & \text{for } \frac{L}{2} < 0 < L \end{cases}$
Shear 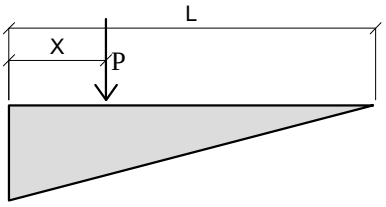	$V(x) = P \cdot (-\frac{x}{L} + 1) \quad \text{for } 0 < x < L$
Hogging 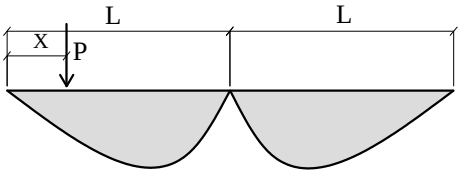	$M(x) = \begin{cases} \frac{P \cdot x \cdot (L^2 - x^2)}{4L^2} & \text{for } 0 < x < L \\ \frac{P \cdot (L^2 - (2L - x)^2) \cdot (2L - x)}{4L^2} & \text{for } L < x < 2L \end{cases}$

Figure 4.13 presents the daily maximum sagging moments for 10 to 50 m span range with shorter spans on the left. Load effects from recorded and generated traffic corresponding to be same span length overlap in the plot owing to its similarity. Due the fact that the WIM station presents some days with a few records producing non-representative load effects, differences can be observed at the lower tail of the distribution. In reality, the developed model is not intended to replicate the values at the lower tail accurately, as the focus of this study is on the extreme values. However, the inherent randomness of the Monte Carlo simulation also produces discrepancies at the upper tail. Consequently, different simulations present different upper tails. This issue can be addressed by simulating longer periods than required as shown by Enright (2010), where the tail loses importance as the sought-after values are at lower quantiles.

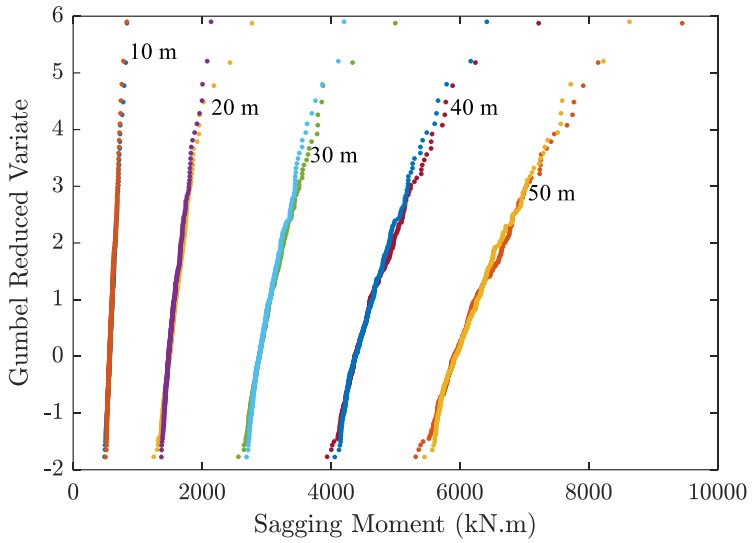

Figure 4.13. Gumbel plot of daily maximum sagging moment 1 year recorded vs 1 year simulated.

By considering the presented results, the developed routine is able to replicate the load effects obtained from the recorded traffic. A measure of the accuracy of the simulation in terms of mean difference between the simulated and the recorded load effects with the same reduce variate is shown in Table 4.4. The difference is higher for shorter spans and it becomes negligible as the span length increases. Mean differences are calculated following Equation (4.4):

$$Dif(\%) = \frac{1}{n}\sum_{i=1}^{n}\frac{LE_{Ri} - LE_{Si}}{LE_{Si}} \cdot 100 \qquad (4.4)$$

where i is the order of the n load effects in the plot from 1 to n, LE_{Ri} is the recorded load effect in the position i and LE_{Si} the simulated load effect in the position i.

Table 4.4. Mean differences between recorded and simulated load effects in percentage terms.

Span length (m)	Sagging	Shear	Hogging
10	1.43	2.19	0.33
20	1.36	1.13	-0.62
30	0.51	0.7	-1.57
40	0.30	0.07	-0.06
50	0.17	0.49	0.42

To further validate the proposed Monte Carlo routine, the previous comparison is repeated using the traffic recorded by another WIM station available in the country, Kaapmuiden with an ADTT of 1100 veh/day. The traffic recorded by this station differs from the Roosboom station and therefore, shows the adaptability of the proposed Monte Carlo routine. The process followed is the same as the one explained in previous sections. Results are available in Appendix A.5.

In addition, the introduced Monte Carlo routine does not only highlight the accuracy of simulating load effects based on WIM data but traffic parameters can also be modified so it is possible to assess their influence on the load effects. This routine is suitable for other research topics such as fatigue of bridges or performance of road pavements. It provides a steady stream of vehicles that can be treated in different ways through the appropriate mathematical models, therefore, allowing for the calculation of the sought-after results.

The algorithm responsible for the calculation of the load effects and written in Matlab is described as follows:

1. Traffic files are used to generate a vector of axles and a vector of distance between axles. This last vector includes the headways, therefore, a convoy of axles following the real disposition of the vehicles is generated. The above mentioned pair of vectors is one day of traffic so the daily maxima load effects are easier to obtain.
2. The vectors described are run over the influence lines detailed before to obtain load effects. The convoy of axles is moved over the influence lines in steps of 0.5 m.
3. In every step, the algorithm checks if the new load effects are greater or lower than the previous load effects. In the case of being greater, the maximum load effects are updated. At the end of the convoy, the maximum values are stored as the daily maximum load effects for the specific day.
4. The process is repeated for every day of traffic generated and for the five span lengths analysed in this study.
5. The results are stored in three matrixes corresponding to the sagging moment, hogging moment and shear force. Each matrix has five columns for span lengths from 10 to 50 m and a number of lines equal to the number of days of traffic used in the calculations.

CHAPTER 5: INFLUENCE OF THE TRAFFIC DESCRIPTORS ON THE LOAD EFFECTS

The aim of this chapter is to isolate parameters of the traffic flow that are influential on the load effects. For that purpose, several routines based on the same developed Monte Carlo simulation have been coded. Various traffic descriptors can be selected to evaluate their influence on the load effects. The selection of the traffic descriptors to be studied is, a priori, a subjective step based on engineering judgement or previous research. The general steps for the evaluation of the influence of a specific traffic descriptor are detailed hereafter:

1. Selection of the traffic descriptors to be evaluated.
2. Development of algorithms suitable for the generation of artificial traffic that allows for the modification of the traffic descriptors.
3. Simulation of the artificial traffic. Different sets of traffic with variable traffic descriptors are generated to capture its influence in the load effects.
4. Selection of a return period for the comparison of the load effects. Extrapolation of the load effects to the selected return period.
5. Evaluation of the influence of the individual traffic descriptors by calculating the variation of the load effects in percentage terms. The load effects corresponding to the lowest and the highest values of the parameters being studied in each analysis should be used to assess the variation.
6. Selection of the most influential traffic descriptors by analysis of the variations previously calculated.

When considering simple traffic descriptors that are easily obtainable from the traffic counts, it is proposed to study in this thesis the ADTT, ratio of six- to seven-axle vehicles and the percentage of long over short vehicles. Data such as axle loads, GVW, headways and vehicle lengths are only obtainable by the installation of expensive equipment; therefore, they are not variables that a simple approach should consider.

Initially 100 years of traffic are simulated, therefore, 100 years of daily maxima are shown in Figures 5.3, 5.4 and 5.6 on Gumbel probability paper. The process requires more resources and time as the number of years simulated increases. One hundred years provides insight on how the load effects are affected by the traffic descriptors studied and the results are relatively fast to obtain. In further sections longer simulations are carried out as well as a discussion of the

adequate length of the simulations to alleviate the variation of the upper tail for the acquisition of accurate results.

5.1 Average daily truck traffic – ADTT routine

The routine that simulates the variation of the ADTT follows the previously highlighted principles. The percentage of each vehicle class in this particular simulation is maintained, while the ADTT and the desired period of the simulation are the inputs. Therefore, it is straightforward to calculate the AHF from the selected ADTT and consequently the hourly flow for every hour of the day using the established parameter c.

Figure 5.1 presents the hourly flows for different ADTT studied. All the curves present the shape of the parameter c increased by the corresponding AHF. The vehicle gaps for every hour of the day are defined according to the gap database and the hourly flow. The generated gaps are plotted in Figure 5.2 for every value of ADTT. The negative correlation between vehicle gaps and ADTT is noticeable. This is expected to influence the load effects as with lower vehicle gaps more chances of having scenarios when two or more vehicles are located at the same time on the bridge, consequently increasing the load effects.

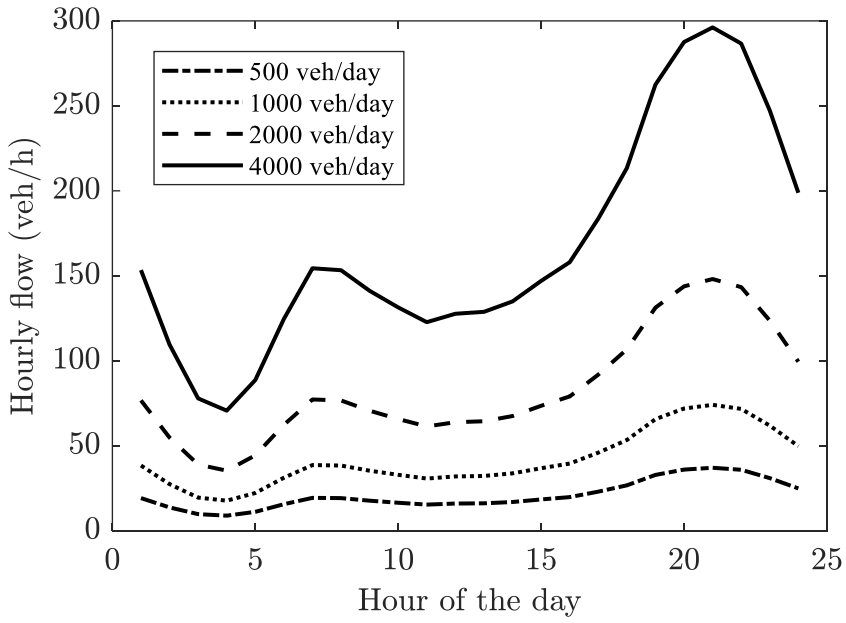

Figure 5.1 Variation of the hourly flow with the ADTT

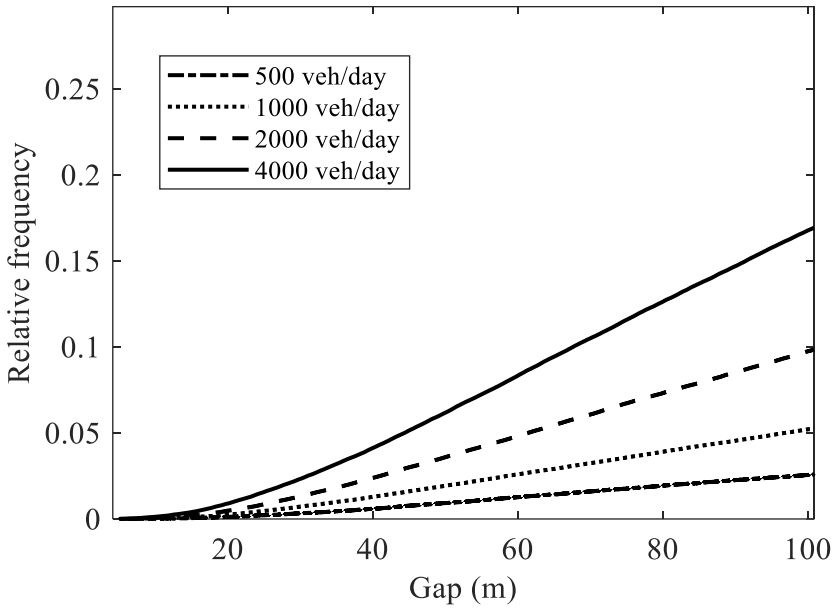

Figure 5.2. CDF of gap - variation with the ADTT.

Figure 5.3 shows the variation of the sagging moment as a function of the ADTT, ranging from 100 veh/day to 4000 veh/day per lane. As could be expected, the load effects increase with the ADTT. Note that although the increase of the load effects is clear, overlapping is present at the upper tail, which is addressed in the upcoming sections.

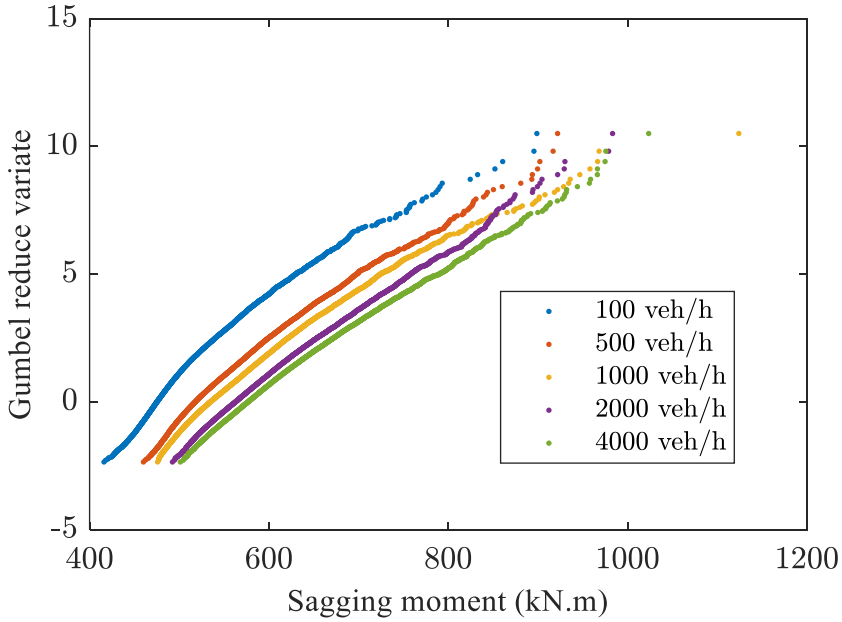

Figure 5.3. Variation of sagging moment with ADTT - 10 m span.

5.2 Percentage of six- and seven-axle vehicles routine

The input for this round of simulations is the ratio of six- to seven-axle vehicles. As mentioned before 76% of the vehicles recorded by the WIM station are six- or seven-axle vehicles, consequently they are expected to be influential on the load effects. The percentage value as well as the ADTT at 2025 veh/day is retained during the course of this simulation. The percentage of six-axle vehicles is varied in the different simulations from 0% to 76%. Consequently, the seven-axle vehicles compose the rest of the flow. Figure 5.4 shows the sagging moment of 100 years of traffic for 10 m span as an example.

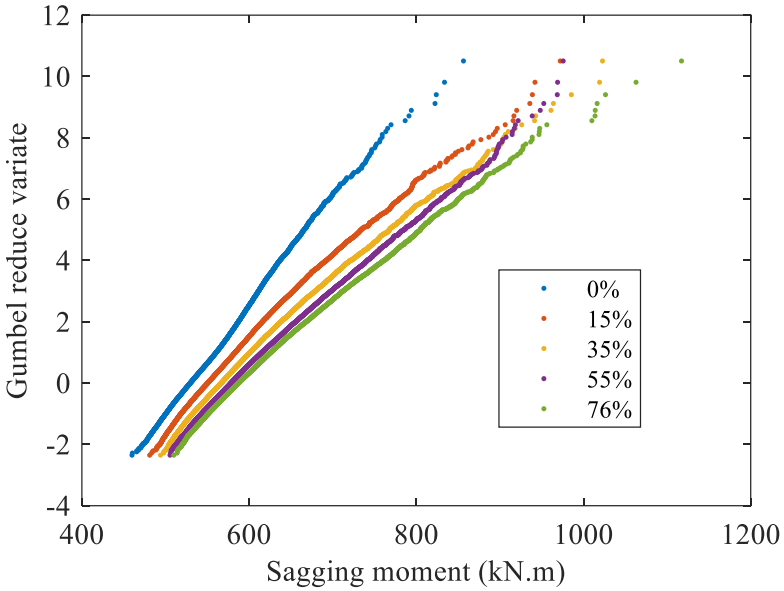

Figure 5.4. Variation of sagging moment with percentage of 6-axle vehicle - 10 m span.

5.3 Percentage of long vehicles routine

This round of simulations requires the definition of long and short vehicles. Based on the data available the threshold is selected at 14 m. Figure 5.5 clearly shows the length of most of the six-axle vehicles above the selected threshold value. It effectively means that when varying the percentage of long vehicles the number of six- and higher axle vehicles is automatically changed. The percentage of long and short vehicles for every vehicles class is shown in

Table 5.1, with most of long vehicles distributed in six-, seven- and eight-axle vehicle classes. Results for the variation of load effects as a function of percentage of long vehicles are shown in Figure 5.6 for sagging moment. The larger the percentage, the more six-, seven- and eight-axle vehicles are generated and, as expected, the load effect increases. Values from 0% to 100%

of long vehicles are investigated with 100 years of generated traffic, while the ADTT is set at 2025 veh/day.

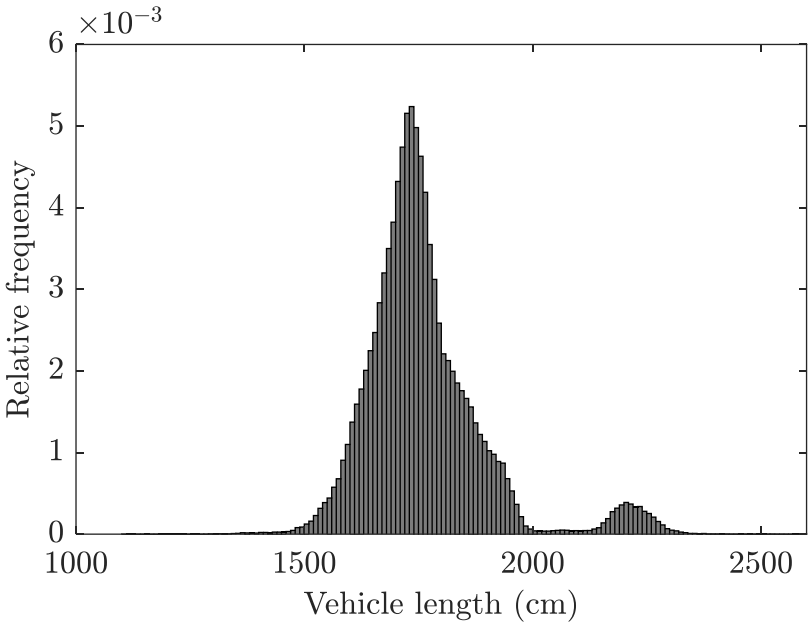

Figure 5.5. Histogram of 6-axle vehicle length.

Table 5.1 Percentage of long and short vehicles per vehicle class.

Number of axles	Long vehicles	Short vehicles
2	0.07	58.37
3	1.14	37.22
4	4.38	1.56
5	5.21	1.72
6	35.74	1.10
7	52.12	0.002
8	13.05	0.002

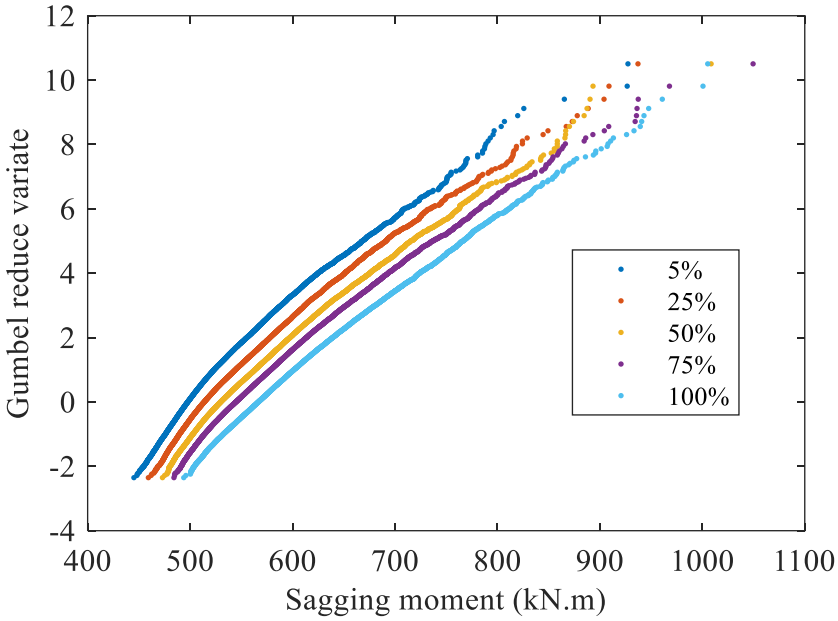

Figure 5.6 Variation of sagging moment with percentage of long vehicles – 10 m span.

5.4 Results.

In this section, a summary of the performed investigation is presented by means of unit sagging moment plotted in relation to the investigated parameter as shown in Figure 5.7, Figure 5.8 and Figure 5.9 for various span lengths in increments of 10 meters. For study purposes, the results correspond to a chosen return period of 1 year that does not require extrapolation. Characteristic load effects can be obtained directly from the 100 years already simulated. At this stage of the research only one lane of traffic is analysed along with a reduced return period. This allows for the evaluation of the influence of the traffic descriptors on the load effects avoiding long simulations. Only the selected traffic parameters will be used in further sections.

5.4.1 Average daily truck traffic

Figure 5.7 shows the variation of the sagging moment with the ADTT that points to a larger gradient of the curves at lower values of ADTT. As the ADTT increases, the probability of heavier vehicles present in the traffic flow increases and therefore, initially at low ADTT, there is a strong correlation to increased load effects, but at a high number of vehicles, the tendency of load spectrum is sufficiently covered by a variety of heavy vehicles. Consequently, the internal force tends to be less sensitive. Similar results are obtained for shear and hogging moment.

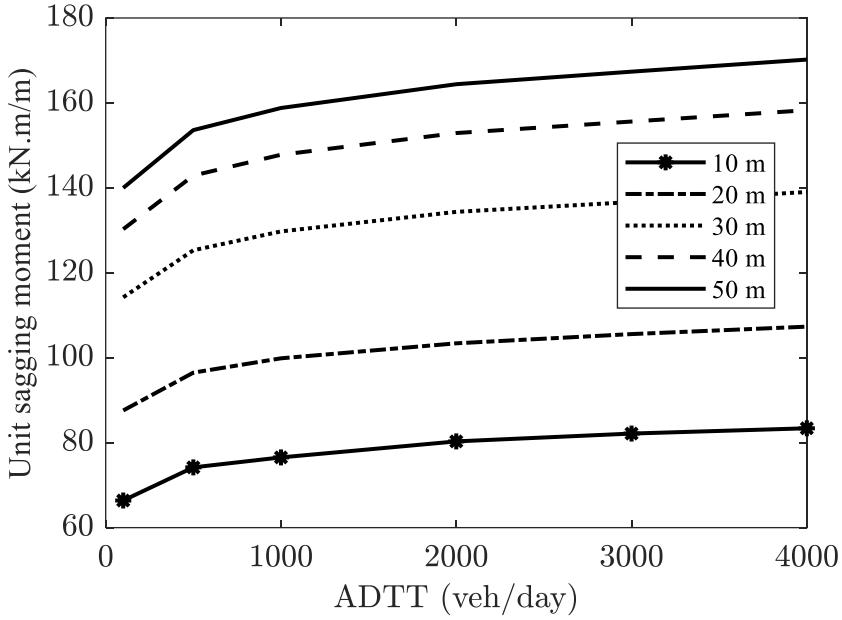

Figure 5.7 Variation of sagging moment with ADTT.

5.4.2 Ratio six- to seven-axle vehicles

Figure 5.8 shows the variation of load effects as a ratio of six- to seven-axle vehicles, with the total of both classes equal to 76% of the entire traffic flow. The only real apparent change in the load effects is at short spans, where sagging moment increases with the increased percentage of six-axle vehicles. Typically, longer vehicles tend to produce lower load effects at shorter spans due to the spread of the loading, but it this case the tridem axle group of the six-axle vehicles dominates the response. The same tendency is observed for shear and hogging moments. For longer spans, the longer and heavier seven-axle vehicles are dominant, which effectively means a slight decrease of the load effects with the increased percentage of six-axle vehicles. The decrease on the load effect when the percentage of seven-axle vehicles is increased is logical since the probability of having two or more seven-axle vehicles over the bridge at the same time is lower. Yet the sagging moment tends to be relatively constant, which means that the load effects are not sensitive to the exact ratio of six- to seven- axle vehicles; except at short spans.

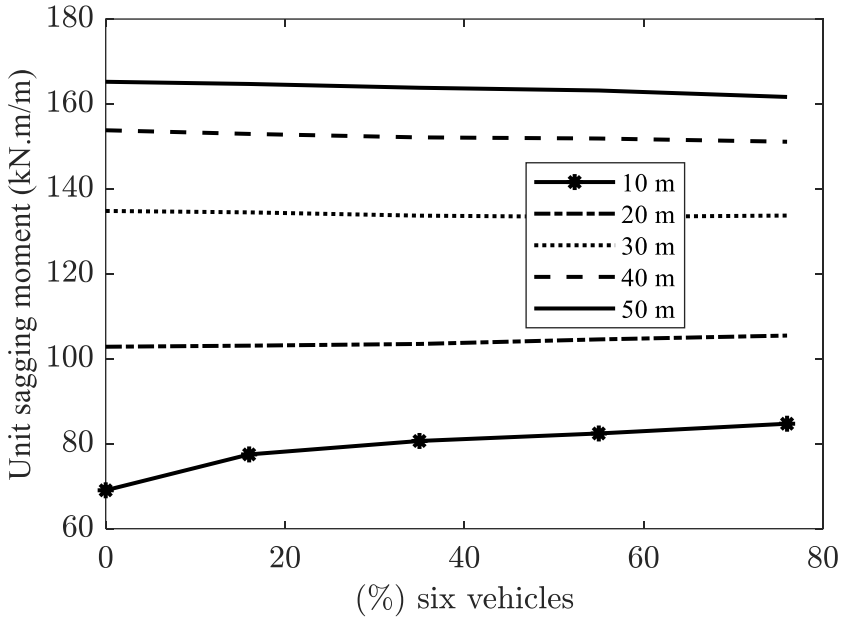

Figure 5.8 Variation of sagging moment with percentage of 6- and 7-axle vehicles.

5.4.3 Percentage of long vehicles

The variation of sagging moment as the percentage of long vehicles is shown in Figure 5.9, where a low percentage of long vehicles results in a low value of load effects. This is a very important result indicating that even a small increment of percentage of long vehicles results in substantial increase of load effects, however, with saturation of long vehicles on the roads, the gradient indicating an increase of load effects is lower. As discussed previously, six-, seven- and eight-axle vehicles fall under long axle vehicles category. Increasing the percentage of long vehicles implies the increase of six-axle vehicles in the flow. For short spans, the tridem axle is found to dominate the response of the structure, hence the results observed. For longer spans, it is the GVW the variable that creates the maximum load effects, since the entire vehicle is loading the bridge deck. Long vehicles are expected to be heavier, thus the increase in the load effects with the percentage of long vehicles.

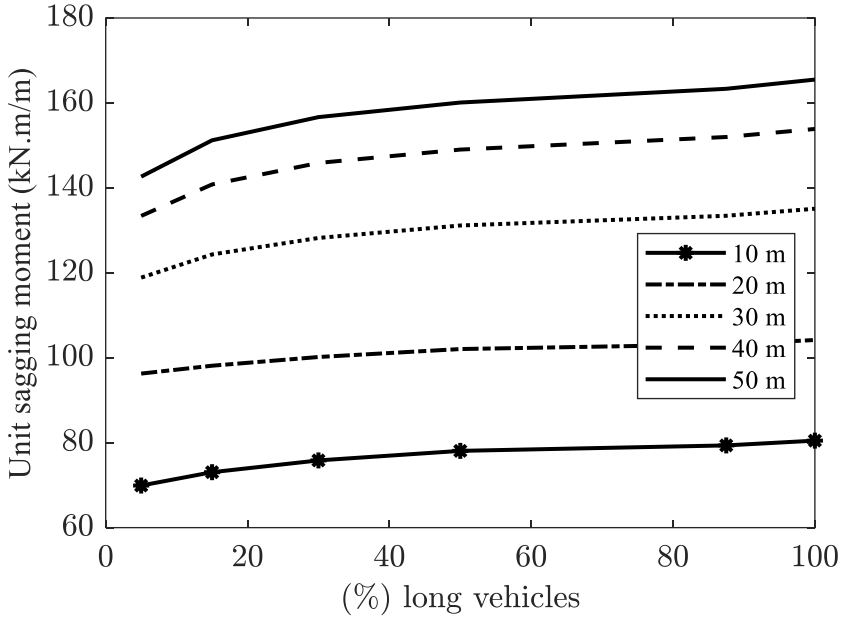

Figure 5.9 Variation of sagging moment with percentage of long vehicles.

5.4.4 Conclusions

The results presented in this chapter show the influence of selected traffic descriptors on the load effects. Especially the analysis of ADTT and percentage of long vehicles exhibits variation for all span lengths. The ratio of six- to seven-axle vehicles is mainly important under 20 m span length due to dominant tridem axle of six-axle vehicle class. Figure 5.10, Figure 5.11 and Figure 5.12 summarise the variation of load effects with the parameters studied in percentage terms for all span lengths. Mean, maximum and minimum variations of all the span lengths are portrayed together. The percentages have been obtained using load effects calculated from the lowest ($min(LE)$) and the largest ($max(LE)$) value of the parameter evaluated in each analysis as indicated in Equation (5.1) . Positive values mean an increase while negative mean a decrease of the load effects. Mean values are obtained as the mean variation of all span lengths.

$$\% = \frac{\max(LE) - \min(LE)}{\min(LE)} \cdot 100 \qquad (5.1)$$

Figure 5.10 shows the variation of the load effects with the ADTT. Sagging moment and shear force presents a mean variation of 24.6 and 24.7% respectively with both minimums around 23% and maximums at 28%. Following the tendencies described before the hogging moment presents larger variations when the ADTT increases. The mean variation is 49% with a maximum of 74% for the two 50 m span of a continuous bridge deck. This can be attributed to

the fact that at low ADTT only one vehicle is generating the extreme load effect, while for high ADTT the extreme value is driven by two or more vehicles in each span.

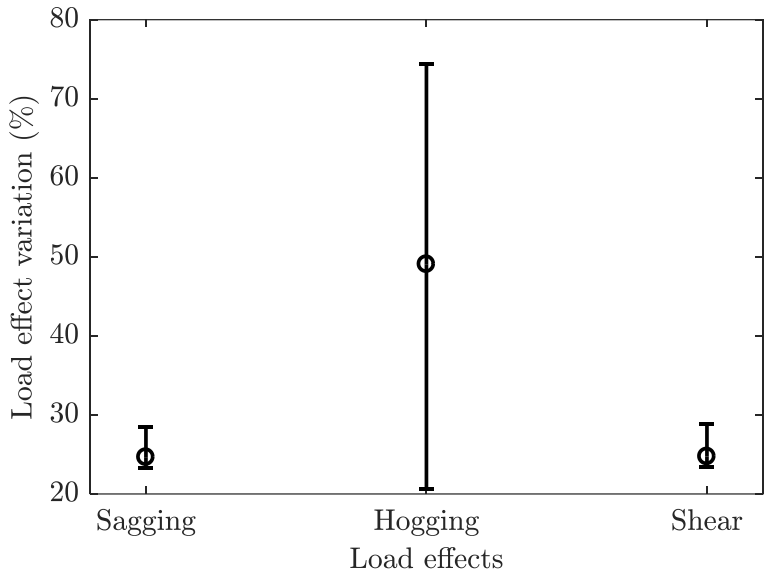

Figure 5.10. Mean, maximum and minimum variation of the load effects with the ADTT for all span lengths.

Figure 5.11 shows the results obtained in the ratio six-to seven-axle vehicles analysis. Both sagging moment and shear present means around 4% while hogging moment has a mean variation of -3.3%. Higher values correspond to smaller span lengths and lower values and negative values to larger spans specially 40 and 50 m.

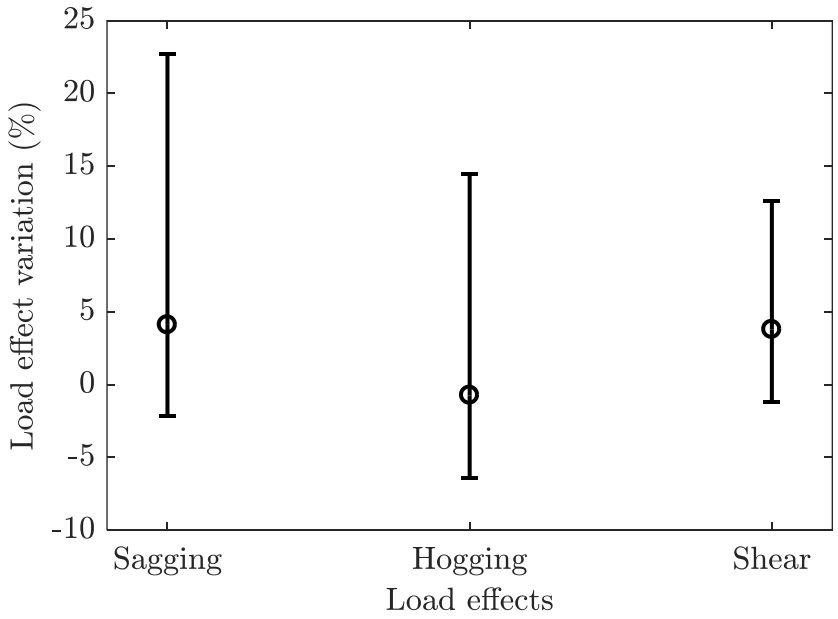

Figure 5.11 Mean, maximum and minimum variation of the load effects with the percentage of six-axle vehicles and for span lengths.

Figure 5.12 shows the results of the last traffic descriptor studied. The percentage of long vehicles is showing mean variations around 14% for all load effects, minimums of 8% and maximum of 15 %. No clear differences are found between span lengths and the variations are quite constant.

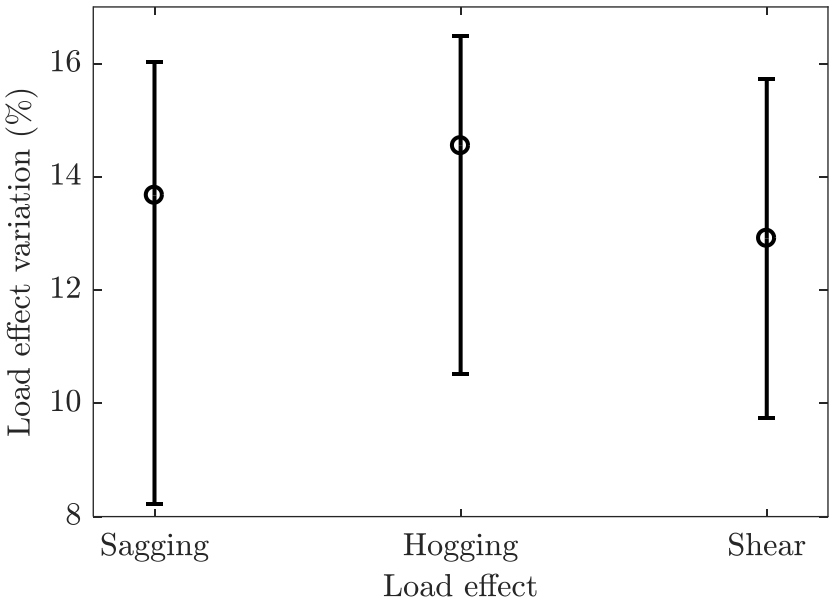

Figure 5.12. Mean, maximum and minimum variation of the load effects with the percentage of long vehicles for all span lengths.

Following the trends observed in the previous figures, the perceived influence of the ADTT is numerically quantified to be the most important. The percentage of long vehicles is found to be quite influential; however, the ratio between six- and seven-axle vehicles does not show important variations for all the spans lengths analysed and it is therefore rejected for further investigations.

Overall, the results presented above show that the exact traffic characteristics are important for the assessment of existing bridges. Remarkable differences in the load effects are observed when basic parameters are varied in the traffic flow. The selected parameters are easily obtainable by simple vehicle counts and no expensive instrumentation is required. The preliminary results point to the fact that site-specific load factors, based on simple traffic counts, can be developed for the assessment. Therefore, conservatism in the design load model can be alleviated to some extent.

CHAPTER 6: SITE LOAD FACTORS

The site load factor approach offered in the proposed framework is based on the calibration of individual factors that are to be applied to the design traffic load model to better estimate the actual traffic loads being carried by a bridge. The traffic flow characteristics at a specific location may differ from the recordings at the reference station used to develop the design the load model. Therefore, there is an opportunity to modify the load model and assess the performance of the bridge more accurately following the process.

Site load factors are a function of the traffic characteristics and accompanying descriptors selected previously as most influential on the traffic loads. The calibration of the respective site load factors is performed by comparing the load effects according to the reference WIM station and the load effects obtained from the specific simulation. The goal is to evaluate the influence of a specific traffic characteristic that leads to a modification of the reference load as detailed by Equation (6.1):

$$LF_i(x) = \frac{LE_i(x)}{LE_R} \quad with\ i = 1, \dots, n \tag{6.1}$$

where LF_i and LE_i are the reduction factor and the characteristic load effect respectively for the $i = 1, \dots n$ site load factors that correspond to the n traffic descriptors selected, with x the value of the descriptor for which the reduction factor is to be obtained. LE_R is the characteristic load effect obtained from the reference station. The calculated site load factor estimates the difference between the load effects and therefore the influence of the traffic descriptor.

Traffic design load models are usually calibrated by extrapolating load effects (characteristic load effects) to a certain return period RP, which corresponds to a probability of exceedance α exceedance in a reference period N. The return period can be calculated using Equation (6.2):

$$RP = \frac{1}{1 - (1 - \alpha)^{1/N}} \tag{6.2}$$

Lower reference periods tied to the remaining service life can be determined when assessing existing structures (Caspeele et al., 2013; ISO 13822, 2001). The reference simulation load effects can be extrapolated to lower return periods and compared to the characteristic load effects obtained from the design traffic load model. An extra site load factor is introduced to capture the influence of lower reference periods:

$$LF_{n+1}(x) = \frac{LE_R(x)}{LE_D} \tag{6.3}$$

where LF_{n+1} is the return period factor, LE_R is the characteristic load effect from the reference simulation for x years of return period and LE_D the characteristic load effect obtained from the design traffic load model.

The individual site load factors have to be combined together to account for the all the properties of the traffic being assessed. A simple multiplication of the factors could be appropriated assuming no correlation between the factors. Other combinations of the factors can be explored otherwise as for instance the expression proposed by Bailey (1996).

A two-step verification of the approach is recommended. In the first verification, the characteristic load effects obtained using the proposed approach should be compared to the values obtained using traffic data from different WIM stations. This should confirm that the variations in the characteristic load effects due to different traffic conditions (different stations) are actually observed in the real traffic and not only in the load effects obtained from artificial traffic. The estimated load effects using the calibrated site load factors should be equal or greater than the observed load effects, meaning that the approach is conservative. A second verification by means of a reliability analysis should be performed together with newly calibrated partial factors to ascertain that the intended reliability levels are accomplished.

The following steps summarise the general process explained in this section:

1. Selection of the most relevant traffic descriptors based on previous calculations.
2. Selection of the probability of exceedance and reference period used to extrapolate the characteristic load effects to a return period.
3. Simulation of the desired traffic varying the selected traffic descriptors.
4. Extrapolation of the load effects to the previously selected return periods (characteristic load effects).
5. Calibration of the site load factors according to Equation (6.1) and Equation (6.3).
6. Validation of the selected combination of site load factors making use WIM data recorded at other locations.

The site load factors proposed in this study are based on the specific WIM data used in this thesis (Roosboom) with the main variables:

1. The ADTT.

2. Percentage of long vehicles.

3. Reference or return period.

As mentioned above, the ADTT and percentage of vehicles are the descriptors that mostly influence the load effects and at the same time, they are easily obtainable from basic traffic counts. Moreover, the remaining service life of the bridge is usually lower than the initial service life, therefore, the reference period can be reduced. This means that the load effects can be further adjusted to the characteristics of the bridge being assessed.

The first two factors are derived considering that Roosboom WIM station as the basis for the calibration (reference station), therefore any station with the same traffic characteristics should not be affected by any reduction or increase of its load effects. The load effects obtained from the ADTT and percentage of long vehicles simulations described previously are compared to the reference simulation (Roosboom WIM traffic parameters) given a return period to obtain the characteristic values. Load factors are calculated using Equation (6.1) repeated here:

$$LF_i(x) = \frac{LE_i(x)}{LE_R} \quad with\ i = 1{,}2$$

where sub index *i* can be either 1 for the ADTT or 2 for percentage of long vehicles and *x* is value of the descriptor for which the reduction factor is to be obtained. For instance, the RF_1 (1000 veh/day) is calculated dividing the load effects obtained from the ADTT analysis using a value of 1000 veh/day and the load effects obtained from the reference simulation (2000 veh/day).

The preliminary design traffic load model (van der Spuy & Lenner, 2019) is calibrated by extrapolating load effects to a return period of 975 years (characteristic load effects), which corresponds to 5% exceedance in 50 years. This return period has been previously adopted in the Eurocode (EN 1991-2, 2003). Using Equation (6.2) a return period of 975.3 years is obtained (this is commonly rounded at 975). Assuming different remaining service lives and a probability of exceedance of 5%, the reduced return periods are shown in Table 6.1, whereas Figure 6.1 shows an example of the different return periods on Gumbel probability paper. Any reference period could be in principle selected, for instance annual reference period, however, if the reference period is related to the remaining service life of the bridge as discussed previously, does not seem practical to evaluate the performance of bridges with a remaining service life of one year. A minimum service life of 10 years is selected here.

Table 6.1. Return periods for various reference periods and probability of 5% of exceedance.

Reference period (years)	Return period characteristic values (years)
50	975
40	780
30	585
20	390
10	195

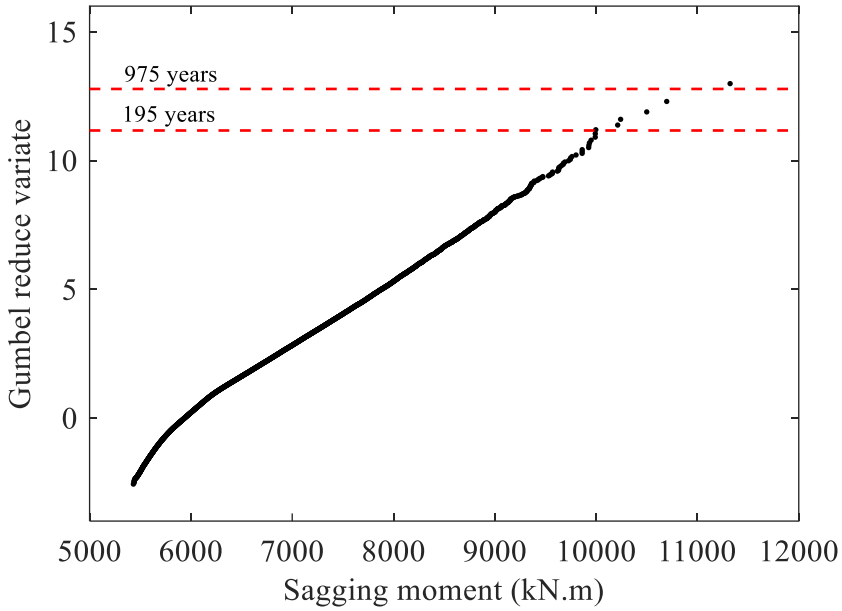

Figure 6.1. Extrapolation of load effects to various return periods - sagging moment on Gumbel probability paper - one lane of traffic.

Furthermore, the preliminary one lane design load model (van der Spuy & Lenner, 2019) is calibrated using the 15 m span length hogging moment as mentioned in Section 2.5. For the rest of the spans the load model is consequently over-conservative. The return period site load factors LF_3 based on Equation (6.3) account for this conservatism and therefore adapt the load effects depending on the span length, which can also be useful during the design stage. These factors allow for the calculation of more accurate characteristic load effects depending on the span length:

$$LF_3(x) = \frac{LE_R(x)}{LE_D}$$

Figure 6.2 schematically explains the concept of site load factors presented here. The distance between the design load model and the reference simulation (Roosboom) represents the reference period site-load factor LF_3 and the distance between the reference simulation and any other simulation performed represents (figure shows ADTT=100 veh/day simulation) the ADTT factor LF_1 or the percentage of long vehicles factor LF_2.

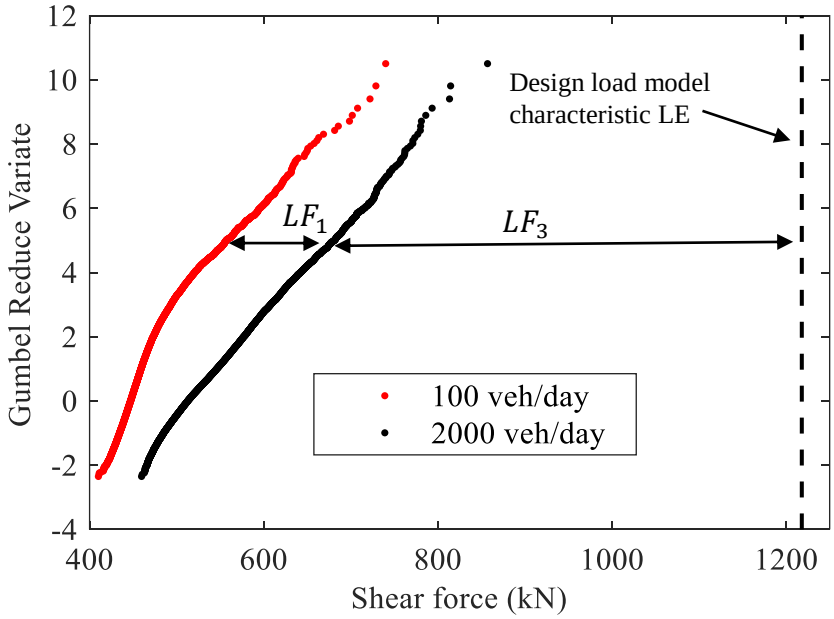

Figure 6.2. Site load factors concept.

The site load factors are combined together using Equation (6.4). Multiplication of the factors is considered appropriate, as they are independent from each other. Figure 6.3 shows the scatter plot of % of long vehicles and ADTT where clear dependency between these two variables is observed for the Roosboom data.

$$E_{ka} = E_{kd} \cdot \prod_{i=1}^{3} LF_i \tag{6.4}$$

where E_{ka} is the assessment characteristic load effect, E_{kd} the design characteristic load effect, and LF_i the site load factors. The site load factors should in principle belong to the same reference period when applying this formula. However, in section 6.3 site load factors LF_1 and LF_2 are found to stable and independent of the reference period for the range of periods considered.

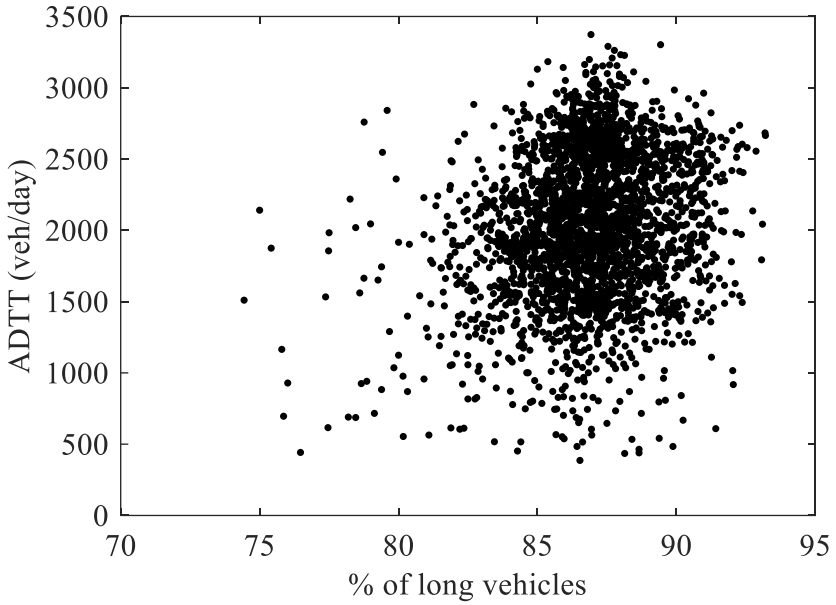

Figure 6.3. Scatter plot of % of long vehicles and ADTT – Roosboom WIM station.

A similar approach with reduction factors can be found in the Eurocode (EN 1991-2, 2003). The load model LM1 can be adjusted at national levels and for different route classes. The adjustment factors α_{Qi} and α_{qi} increase or decrease the concentrated forces and the uniformly distributed load respectively depending on the national requirements. The standard recommends following the minimum values of 0.8 for the α_{Qi} and 1 for the α_{qi} when $i > 1$. Further, two road categories are specified, namely:

1. Roads where heavy industrial traffic is expected: factors equal to 1.

2. Common traffic: moderate reduction can be applied. Suggested factors reduce loads between 10% and 20%.

Although most of the countries have adopted the LM1 without any site load factors, some of them have recalibrated the load model and apply factors to the uniformly distributed load (BD 37/01, 2002; Danish Road Directorate, 2004; NF-EN-1992-2, 2008). Furthermore, a revision of the adjustment factors for traffic loads on bridges in the Czech Republic is performed by Markova (2013).

E. O'Brien, O'Connor and Arrigan (2012) present a procedure for the calibration of the national load models. The characteristic load effects for different influence lines can be extrapolated and compared to the load effects obtained using the LM1. Therefore, a factor can be calculated using the following Equation (6.5):

$$\alpha = \frac{LE_k}{LE_{LM1}} \tag{6.5}$$

where LE_k is the characteristic load effect obtained using the national traffic and LE_{LM1} is the same load effect calculated using the LM1. This approach is similarly applied here, however, the presented site load factors depend on the estimation of traffic descriptors and not generic rules. The methodology presented in this thesis could be considered to further calibrate the national traffic load models in any country for different traffic conditions, given different routes can be characterised by these proposed traffic descriptors.

6.1 Two lane traffic simulations

The results presented in previous sections are based on the traffic simulations and load effects of the single slow lane from the reference station. In reality, roads present one lane per direction or multiple lanes with one slow lane that carries most of the traffic. The results already achieved in Pérez Sifre & Lenner (2019) are enhanced and generalized for real traffic scenarios hereafter.

The calculations performed in this section are based on the previously detailed Monte Carlo routine and generated traffic using the Lane 1 data from the reference station. Two lanes of traffic with exactly the same traffic characteristics are run over the same influence lines and span lengths detailed in previous sections. This assumption is motivated by the similar traffic conditions in the recorded traffic for lanes with traffic in the opposite directions.

Table 6.2 shows the ADTT and percentage of long vehicles for both lanes of the WIM stations detailed in Section 3.1. This condition leads to the most extreme loading scenarios. The global load effect is calculated superimposing the load effects on both lanes at the same time step.

Table 6.2.Traffic characteristics of WIM stations.

Station	ADTT (veh/day)		Percentage of long vehicles (%)	
	Lane 1	Lane 2	Lane 1	Lane 2
Roosboom	2025	1859	87.5	86
Wilge	1790	1637	86	85
Witbank	1318	1258	67	70
Kapmuiden	1101	1010	70	70
Komatiport	545	484	83	81
Zeerust	430	416	67	68

Load effects are calculated for different traffic conditions. The ADTT is varied from 100 veh/day to 4000 veh/day and the percentage of long vehicles from 5% to 100%.

6.2 Extrapolation of load effects

Maximum life-time load effects are obtained by extrapolating the values obtained from the artificial traffic. Various methods of extrapolation are discussed in the literature review. The here provided discussion aims at providing details about calculation of the characteristic load effects as well as proposing a suitable method of extrapolation.

The inherent randomness of the Monte Carlo simulations requires a special attention to the largest load effects calculated due to the variability of the obtained values. The successive simulations of the same traffic do not deliver the same value of the highest generated load effects. This variability can be alleviated by simulating very long periods of traffic (Enright, 2010). To illustrate this issue, 5000 years of Roosboom traffic are simulated. Figure 6.4. shows, for instance, the variation in the tail of the simulated load effects if hundred samples of 50 years (left graph) of sagging moment on a 50 m span length are considered compared to a reduced dispersion of the load effects if five samples of 1000 years are used (right graph). Note that samples are taken from the 5000 years simulated and the colours represents different samples. This variation is especially noticeable in the upper tail and can lead to inaccurate results.

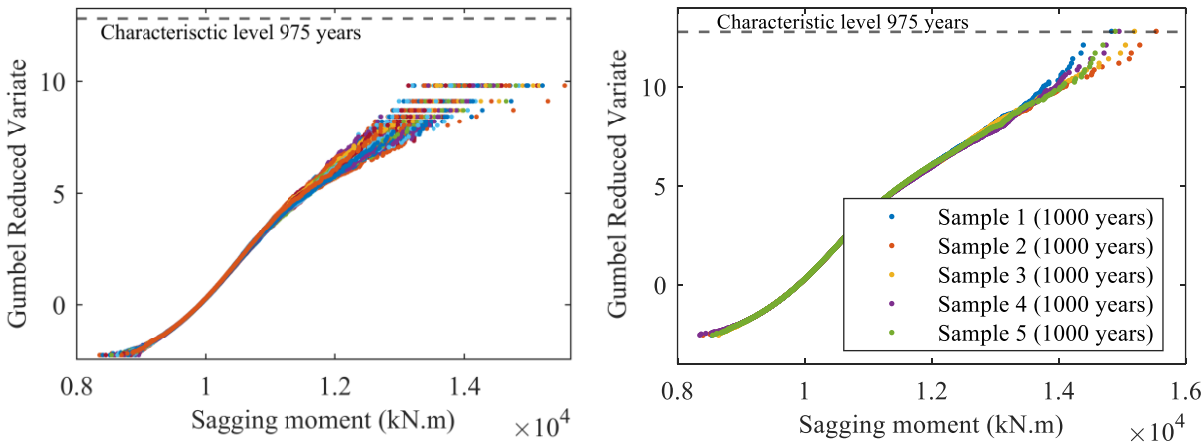

Figure 6.4. Variation of the simulation – 50 years and 1000 years samples.

Ideally, thousands of years of traffic can be simulated avoiding the need for extrapolation of the load effects to the desired return period. In reality, this is highly time consuming and shorter simulations can be performed. As suggested by Enright and O'Brien (2013), using 1000 years of artificial traffic as the basis for the extrapolation delivers a good approximation to the characteristic load effects (975 years return period) obtained directly from the very long

simulations. This approach alleviates the issue of the variability of the tail and avoids the need of longer simulations.

The application of the extreme value theory requires the use of independent and identically data (iid) as explained in section 2.1. In practice, this is sometimes difficult to achieve as seen in Figure 6.4. Many researchers focus on the upper tail of the plot where distributions can be fitted. For instance Enright (2010) fits Weibull and Gumbel distributions to upper $2\sqrt{n}$ and 30% tail of the load effects and, as mentioned before, finds consistent values if compared to the long simulations. Moreover, the Composite Distribution Statistics (CDS) proposed by Caprani and O'Brien (2006) applied on the upper tail is also compared to the previous approach (Enright (2010)). The CDS method assesses the different loading events that occur on a bridge separately. The global load effect on the bridge is obtained by combining each of the extreme distributions fitted to the iid loading events. The characteristic values delivered by the CDS method, Gumble and Weibull extrapolation are found to be very similar in Enright (2010).

A comparison is performed here between the characteristic load effects (975 years return period) obtained using Weibull and Gumbel distributions fitted to the upper tail of 1000 years (rounded 975 years) of the daily and annual maxima with the values directly obtained from the long simulation of 5000 years. If 5000 years are generated and blocks of 1000 years are selected, 5 characteristic values for each load effect can be calculated. Long simulation load effects are obtained directly from the probability paper without the need of extrapolation methods. They serve as a reference to validate the extrapolation method. Mean bias calculated as indicated in Equation (6.6) (difference between the 5000 years load effects and the extrapolated load effects using 1000 years) and mean CV in percentage terms for all span lengths and the five extrapolations for daily and annual maxima are shown in Table 6.3. The length of the tail selected is $2\sqrt{n}$ as suggested by Castillo (1988). The determination of this rule is not entirely clear, however, the results presented hereafter confirm that the approach delivers accurate results.

$$Bias\ (\%) = \frac{1}{5}\sum_{i=1}^{5}\frac{LE^{5000} - LE_i^{1000}}{LE_i^{1000}} \cdot 100 \qquad (6.6)$$

where LE^{5000} is the characteristic load effect obtained using 5000 years and LE_i^{1000} the characteristic load effects using 1000 years (five blocks of 1000 years).

Table 6.3. Gumbel and Weibull extrapolation - bias and CV in percentage terms.

Gumbel fit	Daily		Annual	
	Bias (%)	CV (%)	Bias (%)	CV (%)
Sagging	1.21	0.93	1.02	1.61
Shear	1.17	0.66	1.12	1.66
Hogging	-2.43 (-0.69)	0.73	1.03	2.15
Weibull fit	**Daily**		**Annual**	
	Bias (%)	CV (%)	Bias (%)	CV (%)
Sagging	-2.77	0.68	-1.04	1.25
Shear	-2.66	0.65	1.10	1.43
Hogging	-3.02 (-1.38)	0.68	-1.00	1.73

The results show that fitting Gumbel distributions to daily maxima delivers less bias than the Weibull distributions. It should be mentioned that the larger bias on the hogging moment observed for both distributions is caused by the change of behaviour of the load effects between short and large spans. From 10 to 30 m span lengths, hogging moments are fitted with Gumbel distribution and for 40 and 50 m spans, Weibull delivers the best approximations. Mean bias of 10-30 m span lengths for the Gumbel fit and 40-50 m span lengths for the Weibull fit are shown in brackets. If the characteristic values extrapolated from daily and annual maxima values are compared, it can be concluded that both methods deliver similar bias, however, higher CV are observed on the annual maxima fits. This is caused by the fewer observations involved in the annual fits. The estimation of the parameters of the distribution becomes more unstable, hence the increase in the CV. Detailed results are available in Appendix B.

Based on the results presented in this section, further extrapolations are performed fitting Gumbel distributions to the tail of 1000 years of daily maxima. Exceptionally, Weibull distributions are fitted to hogging moments on large spans. Nevertheless, extrapolations are evaluated individually in case occasional special treatment is needed.

6.3 Results and comments

Table 6.4 shows the characteristic load effects for a reference period of 50 years obtained from the reference station and the ratios two-lane LE/single lane LE. Load effects are not twice the single lane load effects. Those scenarios where two or more vehicles capable of generating the largest load effects in one lane are mirrored in the second lane are extremely rare.

Table 6.4. Two-lane load effects vs single lane load effects.

Span length(m)	Sagging		Hogging		Shear	
	LE	Ratio	LE	Ratio	LE	Ratio
10	1418	1.31	1001	1.30	584	1.29
20	3761	1.37	2503	1.41	934	1.46
30	7564	1.43	4654	1.52	1114	1.44
40	11425	1.42	7713	1.62	1187	1.39
50	15306	1.42	10133	1.57	1298	1.44

Ratios are between 1.31 and 1.46 for sagging and shear. The hogging moment shows higher values for spans larger than 30 m. This happens because having two spans larger than 30 m increases the chances of having two or more vehicles at the same time over the bridge, hence increasing the hogging moment.

Load site factors are obtained using the equations detailed previously that compare the characteristics load effects from the reference simulation with the rest of the simulations performed for two lanes of traffic. Tables 6.5 and 6.6 present the sagging moment site load factors LF_1 and LF_2. Even though, LF_1 and LF_2 are in principle function of the reference period, constant values for these two factors are obtained independently of the reference period. These constant values mean that that the relative distances between the characteristic values in different simulations are maintained independently of the reference periods considered here. The detailed factors for the rest of the load effects are presented in Appendix B.2.

Table 6.5. ADTT site load factors LF_1 – sagging moment.

Span length (m)	ADTT (veh/day)				
	100	500	1000	2000	4000
10	0.89	0.92	0.97	1.00	1.03
20	0.89	0.93	0.98	1.00	1.05
30	0.88	0.93	0.97	1.00	1.04
40	0.87	0.93	0.97	1.00	1.04
50	0.87	0.93	0.96	1.00	1.05

Table 6.6. Percentage of long vehicles site load factors LF_2 – sagging moment.

Span length (m)	Long vehicles (%)				
	5	25	50	87.5	100
10	0.83	0.88	0.90	1.00	1.01
20	0.91	0.94	0.95	1.00	1.01
30	0.85	0.93	0.96	1.00	1.01
40	0.83	0.93	0.96	1.00	1.01
50	0.83	0.93	0.96	1.00	1.01

Table 6.7 shows the site load factor LF_3 for all the reference periods. These values have been calibrated comparing global load effects using the design load model in van der Spuy & Lenner (2019) and a reduction factor for the second lane of 0.75 (van der Spuy, Lenner, de Wet, & Caprani, 2019). In Appendix B.2. the LF_3 factors for lane 1 and lane 2 are detailed. Although the same reduction is achieved, the separated factors can be used in a more detailed structural analysis.

Table 6.7. Reference period site load factors LF_3 – sagging moment.

Span length (m)	Reference period (years)				
	10	20	30	40	50
10	0.55	0.57	0.57	0.58	0.59
15	0.53	0.54	0.55	0.56	0.56
20	0.55	0.56	0.57	0.58	0.58
30	0.60	0.62	0.63	0.63	0.64
40	0.58	0.60	0.61	0.61	0.62
50	0.55	0.56	0.57	0.57	0.58

The drastic reductions observed in the LF_3 factors are caused, as mentioned earlier in this section, by the fact that the design load model is calibrated using the 15 m span length hogging moment (LF_3 also calibrated for this span length). For the rest of the span lengths and load effects the design load model is over estimating the real characteristic load effects. The influence of the reference period is, therefore, diminished and only appreciable differences are found between 50 and 10 years reference period.

6.4 Validation

The proposed approach is validated in two stages using five stations. The reduction achieved through the application of the site load factors (first validation) is evaluated by comparing the modified load effects E_{ka} against the characteristic load effects from the reference station (Roosboom). Moreover, the recorded traffic in the selected stations is used to obtain its characteristic load effects using the same extrapolation method detailed before. These values are, therefore, compared against the modified load effects E_{ka} (second validation). The comparison gives an estimate of the accuracy of the approach. The five stations and traffic flow characteristics used for verification have been already detailed in Table 6.2.

One year of traffic is available per WIM station under consideration. Verifications are performed based on the assumption that the traffic descriptors are equal on both lanes. The stations are specifically chosen as they present values of ADTT and percentage of long vehicles that substantially diverge from the reference station. The verification is therefore robust since both heavy and light traffic conditions are evaluated.

Validation 1

Figure 6.5 shows the comparison of the characteristic load effects (975 years) from the reference station and the modified characteristic load effects E_{ka} after the application of the site load factors LF_1 and LF_2 using the traffic parameters from the previously detailed WIM stations. For instance, the left graph on Figure 6.5 only displays the modified and the reference hogging moment for all the span lengths and the selected Komatiport station, while the right graph shows the individual differences obtained comparing reference and modified load effects in percentage terms using the five WIM stations. The values presented are an estimation of the reduction in the load effects achieved with the presented method. As can be seen, sagging and shear present mean values ranging from slightly over 0 to maximums around 13% with means of 6.4 and 5.5% respectively. The hogging moment shows more variability with a maximum closer to 20% and a mean of 8.5%. Lower values are representative of stations with traffic similar to the reference station and the larger values correspond to the stations with lighter traffic.

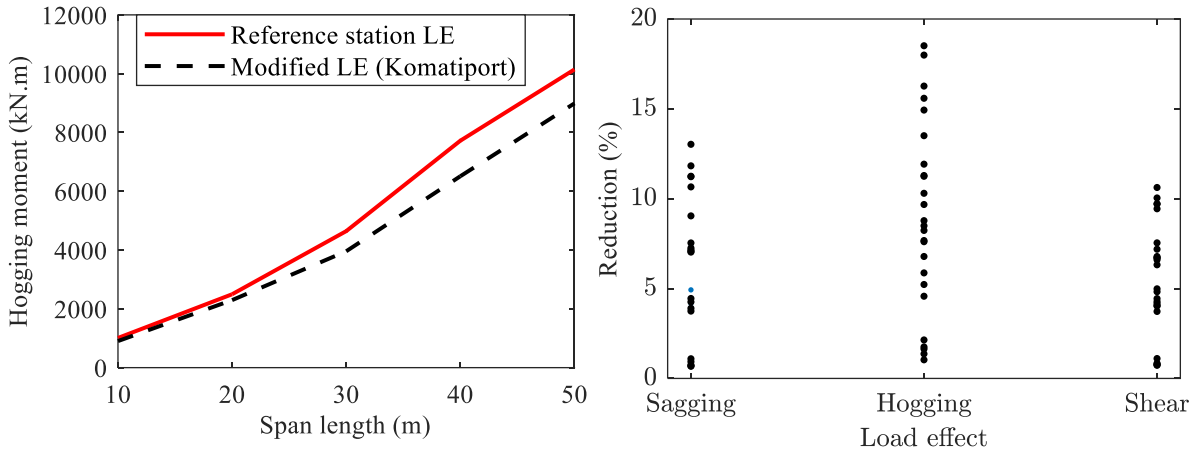

Figure 6.5. Comparison reference and modified characteristic load effects.

Validation 2

The validation continues comparing the modified load effects E_{ka} and the characteristic load effects (975 years) obtained using the recoded traffic from all the stations mentioned before. The characteristic values from each station should be lower than the modified values, essentially meaning that the approach leads safe reductions. The left graph in Figure 6.6 shows the characteristic load effects from Komatiport station compared with the modified load effects E_{ka}. As can be seen, the extrapolated load effects are higher than the reduced for 30 and 50 span lengths bridges. The right graph shows the individual differences for the five WIM stations and in percentage terms. This can be interpreted as the proximity or accuracy of the proposed approach to the reality.

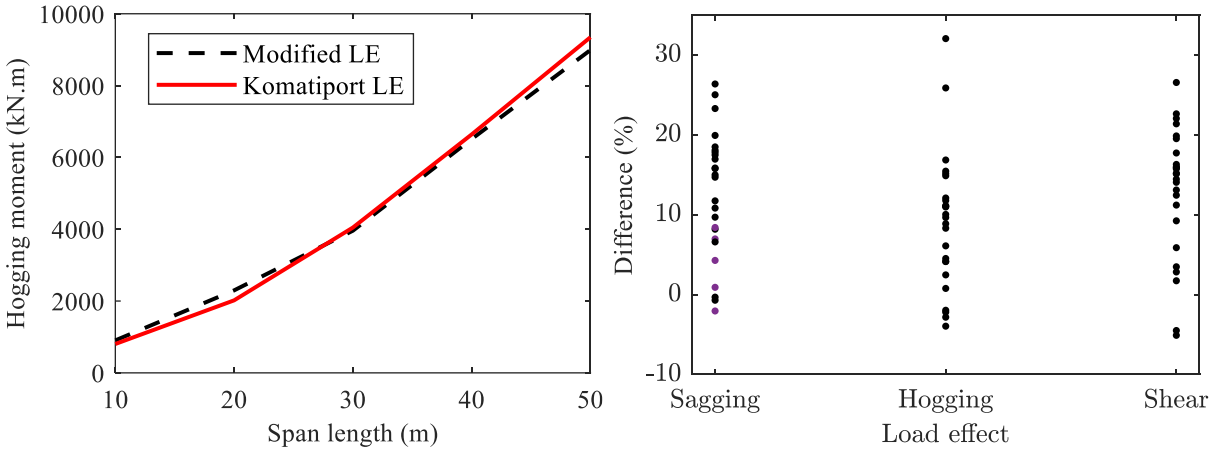

Figure 6.6. Comparison modified and extrapolated characteristic load effects.

The three load effects present means around 10% and maximum values over 25%, slightly higher for the hogging moment. Minimum values are slightly below zero. The assessment method is therefore failing to provide safe values of these specific load effects. The negative values are relatively low, furthermore, the variability of the extrapolation methods should be

especially acknowledged here. The periods of traffic recorded are insufficient to determine the characteristic values of the load effects for the rest of the stations with a great deal of accuracy. Slight variations in these values certainly should be taken into consideration when judging the accuracy of the presented approach. Detailed values are available in section B.4.

6.5 Conclusions

The results show that the new assessment approach can be applied with significant reductions of the reference station load effects. The reduction is especially noticeable when using traffic parameters recorded by the WIM stations with very light traffic (ADTT<1000 veh/day). Reductions over 10% are achieved in these cases. Less significant are the reductions for stations with heavier traffic closer to the reference traffic as expected from the site load factors presented previously. Further reductions can, however, be obtained by accepting reduced reference periods, as seems reasonable when assessing existing structures.

The approach presented is simple and in general the real extrapolated values are not replicated accurately. Scenarios where the characteristic values obtained from the real traffic are higher than the modified load effects have been observed. Differences are, however very low and can be attributed to the inaccuracies in the determination of the characteristic load effects from short WIM data sets as performed for the validation stations. Moreover, if the differences are observed at longer span lengths, where the dead load dominates the response of a structure and traffic load is less critical.

CHAPTER 7: UNCERTAINTY EVALUATION AND PARTIAL FACTORS

The definition of simple semi-probabilistic approaches that are suitable for its application in the industry requires the evaluation of the different sources of uncertainties that affect the simplified calculations. Semi-probabilistic approaches found in most of the codes use the concept of partial factors to account for all uncertainties. The introduction of the partial factors assures the achievement of the desired levels of safety in structures. The general procedure to be followed to evaluate uncertainties and calibrate partial factors is summarised here:

1. Assess the sources of uncertainty. A general list of the sources of uncertainty is included in Section 2.2 and can be found in the specialised literature(*Handbook 2 - Reliability Backgrounds*, 2005; JCSS, 2001; Kiureghian, 1989). Moreover, if the specific approach or methodology introduces extra sources of uncertainties in the model, these should be identified.
2. Calculate the uncertainty usually introduced in the model as a random variable. The multiplicative relationship as in Equation (7.1) is commonly preferred (Holický, Retief, & Sýkora, 2016) but the additive relationship can be considered:

$$R = \theta \cdot R_{EST} \tag{7.1}$$

   where R is the real value of the variable, θ is the uncertainty and R_{EST} is the estimated value. The random variable representing the uncertainty should be modelled using a probability distribution.
3. Calculate the individual partial factors as a fractile of the previous probability distribution with a certain probability of exceedance. The probability of exceedance is commonly determined as the value $\Phi(\alpha \cdot \beta_T)$ with α the sensitivity factor obtained from the FORM analysis and β_T the desired target reliability specified in the codes. Different reference periods can be considered leading to multiple partial factors.
4. The single final partial factor is obtained from the multiplication of the individually obtained partial factors. A reliability analysis should be performed finally to ascertain that the intended reliability level is accomplished through the application of the calibrated partial factors. Furthermore, the verification of the validity of the assumed sensitivity factors in the calibration of the partial factors is recommended. Recalibrations of the partial factors might be necessary.

When assessing the accuracy of the results achieved in this specific work the following sources of uncertainty should be taken into account apart from the variability considered by the reliability based partial factors:

1. **Statistical uncertainty due to the lack of recorded traffic data**. This is partially mitigated since the lack of traffic data is compensated for by the generation of hundreds of days of traffic. Consequently, large samples of load effects can be calculated thereby enhancing the results that would be obtained by only using the recorded WIM data. However, the recorded data are used to model the variables necessary to generate the artificial traffic flow. If insufficient data are collected the variables cannot be modelled with the accuracy desired, therefore, eventually affecting the results obtained in the simulations. For instance, the number of eight-axle vehicles recorded is insufficient. The statistical parameters of the variables present in the simulations can be updated as more traffic information is recorded and therefore the uncertainty reduced.
2. **Accuracy of the WIM data**. The accuracy of the recorded traffic data is an important aspect that can have sustainable implications in the determination of the extreme load effects as proven by O'Connor & O'Brien (2005) and might require a calibration of the data or a correction of the load effects through a partial factor. A minimum class C(15) is recommended for span <50m and less accurate data can be used for spans >50 m. The WIM data used here have been recalibrated as detailed in Section 3.3 and the accuracy evaluated following the criteria available in de Wet (2010). The accuracy is determined as Good or at least class C(15), which according to the review literature avoids the need for further corrections.

Particular aspects discussed in this chapter include:

3. **Structural model uncertainty.** The model uncertainty has been introduced in Section 2.2. The mathematical models used in the structural verifications are an idealization of the real phenomena. This uncertainty corrects the deviations in the results caused by these simplifications and is estimated using the recommendations found in the specialised literature.
4. **Statistical uncertainty in the determination of the characteristic load effects.** Monte Carlo simulations present a variability especially visible towards the upper tail of the load effects distributions as explained previously. The selection of different tails used in the extrapolation, therefore, deliver different characteristic load effects. The simulation of long periods of traffic to some extent alleviates this problem, however,

this uncertainty is evaluated and considered in the determination of the characteristic traffic load effects.

5. **Statistical uncertainty in the estimation of the traffic descriptors.** The method developed requires the basic estimation of the ADTT and the percentage of long vehicles for the calculation of the site-specific load effects. Undoubtedly, measuring these descriptors for a short period might incur errors in the estimation, as the traffic flow is not constant throughout all periods. Errors can lead to incorrect selection of the site load factors and therefore the potentially incorrect values of the site specific load effects.

Modern semi probabilistic codes address the issue with the variability of the load models by the implementation of partial factors accounting for the different sources of uncertainty. The formulation adopted here is variation of the one adopted for instance in Caspeele et al. (2013) and Lenner (2014):

$$\gamma_Q = \gamma_{Ed,q} \cdot \gamma_q \cdot \gamma_e \cdot \gamma_l \tag{7.2}$$

where γ_Q is the partial safety factor of the variable action, $\gamma_{Ed,q}$ stands for the partial factor accounting for the model uncertainty in the estimation of the load effects from the load model, and γ_q is the reliability-based partial factor accounting for the variability of the variable action, statistical uncertainty and uncertainties related to the model of variable action or traffic load effects in the context of this research. The additional partial factors γ_e and γ_l account for the uncertainty in the calculation of the characteristic load effects and the variability in the estimation of the traffic descriptors necessary for the application of the model, respectively.

The calibration of the partial factors in this contribution is performed based on the same concepts applied for the calibration of the design partial factors, also known as the design value method (Caspeele et al., 2013). As previously mentioned reduced reference periods t_{ref} are considered. Furthermore, adjusted reliability levels are recommended for the assessment of existing structures for the reasons highlighted previously. Retief, Viljoen and Holický (2019) propose the target reliability values β_T (50 years) as shown in Table 7.2. Values for the assessment of existing structures and determined by optimizing societal risk, are compared to the design values in SANS 10160-1 (2009).

Table 7.1. Proposed target reliability indices β_T.

SANS 10160-1	RC2	RC3
Design	3.00 (β_1=4.04)	3.50 (β_1=4.43)
Assessment	2.00 (β_1=3.31)	2.60 (β_1=3.74)
Required	1.60 (β_1=3.05)	2.60 (β_1=3.74)

RC2 and RC3 refer to the failure consequences class (medium and high consequences of failure respectively) as proposed in the Eurocodes. The calibration of partial factors is performed here using the reliability level for the design and assessment of existing structures for the RC2 class. RC3 class is omitted from the calibration as the presented work focuses on short to medium span length bridges that are generally fall under RC2 class.

The shorter remaining service life in existing structures is captured using the reduced reference periods detailed in Table 7.2. Using Equation (7.3) detailed in section 2.1.4, the target reliability values can be obtained for different reference periods. All the target reliability indices below correspond to the same annual probability of failure,

$$\Phi(\beta_{T,n}) = \left[\Phi(\beta_{T,1})\right]^n \tag{7.3}$$

Table 7.2. Target reliability indices – various reference periods.

Reference period (years)	Target reliability index	
	Design	Assessment
1	4.04	3.31
10	3.46	2.61
20	3.27	2.36
30	3.15	2.21
40	3.07	2.09
50	3.00	2.00

The sensitivity factor for the loads needed to calibrate the partial factors are the following values as suggested in the Eurocode:

$$\alpha_E = -0.7\ (dominant\ loads)$$

$$\alpha_E = -0.28\ (nondominant\ loads)$$

The use of these values is commonly accepted in practice for the calibration of the partial factors for a wide range of engineering structures (König & Hosser, 1982).

The partial factor and traffic load factors layering proposed here are validated in this section using reliability analysis to assure that the intended reliability levels are accomplished. Furthermore, the validity of the assumed sensitivity factors for dominant variable loads α_E is corroborated covering the studied span lengths.

7.1 Uncertainty in the determination of the characteristic load effects.

The generation of artificial traffic data using Monte Carlo simulations has an inherent variability, which essentially means that the results obtained in every simulation are different. The selection of different simulations used to extrapolate the load effects delivers different characteristic values of the load effects. Long run simulations are a way to reduce the variability of the results, however, they are extremely time-consuming and are not always an option. By means of generating hundreds or thousands years of traffic, it is possible to improve the accuracy of the extrapolated results. Long run simulations are therefore required to obtain the sought-after results.

Figure 7.1 shows the sagging moment on a 50 m span length calculated from a 2000 veh/day of artificial traffic. From the 5000 years of simulated traffic, hundred samples of 50 years traffic are drawn and used to calculate the load effects, thereby obtaining different curves (each sample shown with a different colour) from each sample as anticipated in Section 6.2. The graph on the right in Figure 7.1 shows the relative histogram of the characteristic sagging moments obtained from each of the 50 years samples.

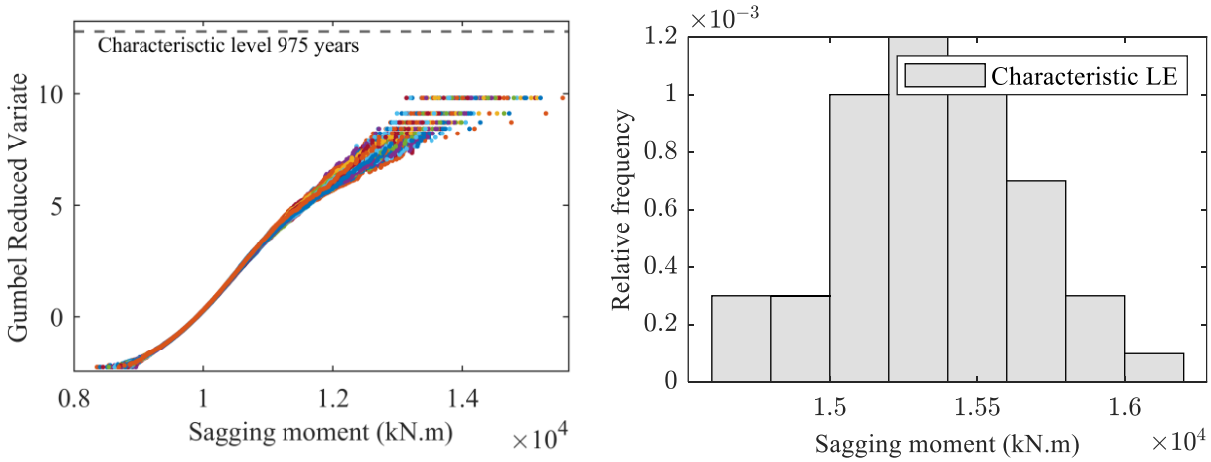

Figure 7.1. Uncertainty in the estimation of the characteristic load effects.

This extrapolation is repeated for different block sizes and for the various ADTT simulated. The mean and CV of the all the extrapolated load effects are calculated in every case at a return period of 975 years. For instance, if 1000 years are simulated and 100 years is selected as a block size, 10 different characteristic values can be calculated. Figure 7.2 shows the mean of the sagging moment for a 50 m span length bridge and different ADTTs and the mean CV for all the span length for the reference simulation as examples. The rest of the spans and simulations present similar results. Values clearly converge for all the ADTTs portrayed when the length of the simulations is increased. Short simulations are not reliable and deliver inconsistent results as can be seen on the left graph where 100 veh/day sagging moment is higher than 500 veh/day sagging moment. The mean CV varies from approximately 9% for one year samples and decreases gradually to reach values lower than 1% after simulations of 1000 years. The plotted values show that the simulation of long periods of traffic reduces the uncertainty of the extrapolated LE as previously stated.

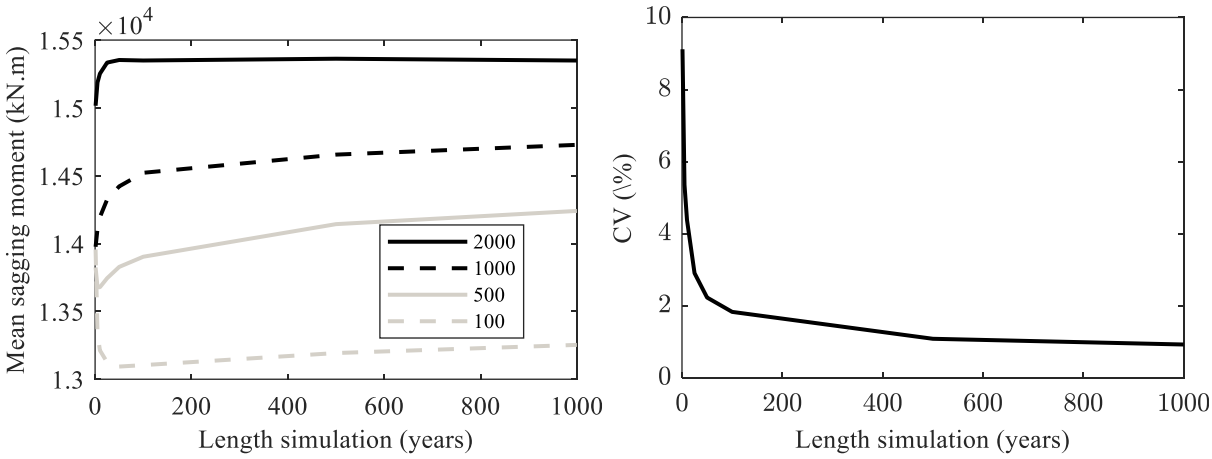

Figure 7.2. Mean and CV variation with the length of the simulations.

The partial factor γ_e accounting for this uncertainty is calibrated using the 2000 veh/day simulation as is the largest of the simulations perfomed with 5000 years of traffic. Samples of 100 years are selected from the 5000 years and used for the calculation of the characteristics values of the three load effects, delivering 50 values per load effect and span length. Selecting shorter samples would provide with a higher number of observations, however, could overestimate the partial factor γ_e (higher CV as seen in Figure 7.2). If larger samples were selected the number of observations would be insufficient to fit a probability distribution and model the uncertainty. The calibration of the partial factor γ_e is performed fitting Normal distributions to the mentioned histograms of load effects and selecting a high fractile as in Equation (7.4):

$$\gamma_e = 1 - CV \cdot \alpha_E \cdot \beta_T \tag{7.4}$$

where CV is the coefficient of variation of the Normal distribution, $\alpha_E = -0.7$ is the sensitivity factor and $\beta_T = 3$ is the reliability index fixed to this value for simplicity. The values of γ_e show in Table 7.3 are to be generalised for the evaluation of this type of uncertainty regardless the traffic conditions, reference period or reliability level adopted.

Note that the partial factors shown in this section are a pre-calibration based on the assumed sensitivity factor α_E. The actual influence of this uncertainty might differ from α_E significantly, therefore affecting the sensitivity value and leading to a recalibration of the factors proposed here. Section 7.6 presents more details.

Table 7.3. Fitted distributions and partial factor γ_e.

Load effect	Span length	Distribution	Mean	Standard deviation	γ_e
Sagging	10	Normal	1412	25.6	1.04
	20	Normal	3780	68	1.04
	30	Normal	7589	140	1.04
	40	Normal	11470	183	1.03
	50	Normal	15349	322	1.04
Shear	10	Normal	577	12	1.04
	20	Normal	931	23.1	1.05
	30	Normal	1118	22.7	1.04
	40	Normal	1188	25	1.04
	50	Normal	1304	21.5	1.03
Hogging	10	Normal	990	16	1.03
	20	Normal	2493	48.3	1.04
	30	Normal	4476	106.5	1.05
	40	Normal	7758	142.5	1.04
	50	Normal	10267	103.6	1.02

7.2 Estimation of the traffic descriptors uncertainty

The proposed assessment approach relies on the idea that the engineer is able to obtain basic information from the traffic flow for the bridge assessed. The ADTT and percentage of long vehicles are necessary for the application of the method. Both parameters are easily obtainable either manually or by the installation of simple equipment on the roads.

Traffic flow is not stable and it presents daily, weekly and seasonal fluctuations. Measuring traffic on different dates may lead to different values of the traffic descriptors and therefore variable values of the load effects after the application of the site load factors. Both the ADTT and percentage of long vehicles are values that tend to stabilise with the increasing number of days measured. Ideally, long measurements should be taken, thus obtaining values with a great deal of accuracy. In practise, this is not always possible and just a few days of data might be available.

This section analyses how the estimation of the traffic descriptors is affected depending on the length of the measurements and proposes correction factors γ_l (traffic factors) that account for the uncertainty in the process, consequently mitigating the problem.

The values of ADTT and percentage of long vehicles are obtained from the reference station. Seven years of data were made available by the authorities in the late stages of this work and are therefore used in this section. Different intervals of time are used to calculate the traffic descriptors and the changes in the distributions are observed. For instance, from a station with 500 days recorded it is possible to calculate 100 different values of traffic descriptors with a time interval of 5 days or 50 values of an interval of 10 days. The longer the interval, the fewer the values that can be calculated, however, more stable values are always obtained.

Intervals of 1, 5, 10, 30, 60 and 90 days are considered. Values located outside of the interval detailed in Equation (7.5) are considered outliers and therefore excluded from the calculations. This is one of the many conditions that can be applied to the data to remove outliers.

$$outliers\ boundaries = \mu \pm 3 \cdot \sigma \tag{7.5}$$

where μ is the mean and σ is the standard deviation of the set of values. The probability of occurrence of an observation outside this interval considering the Normal distribution is less than 0.3%. This condition therefore filters extremely rare events.

The Figures 7.3 and 7.4 shown below correspond to the reference station since it provides the largest data set. The ADTT and percentage of long vehicles for 1 and 30 days are shown. As can be seen the longer the time interval the narrower the histogram becomes. This essentially means less dispersion of the values and less uncertainty in the determination of the descriptor, which slowly approaches the long run value. This is observed for both traffic descriptors, however, the percentage of long vehicles presents lower variability.

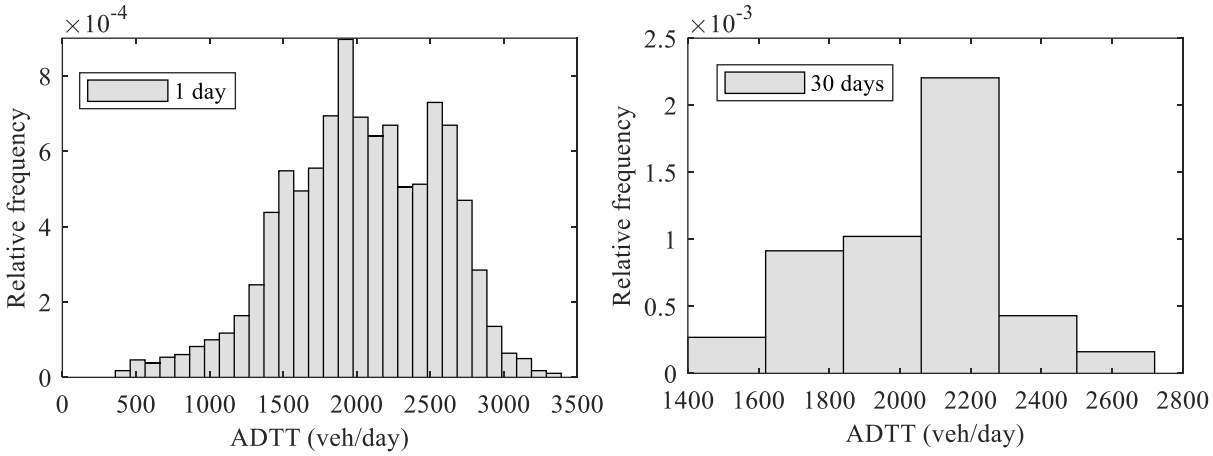

Figure 7.3. Histograms of measured ADTT. One day vs thirty days.

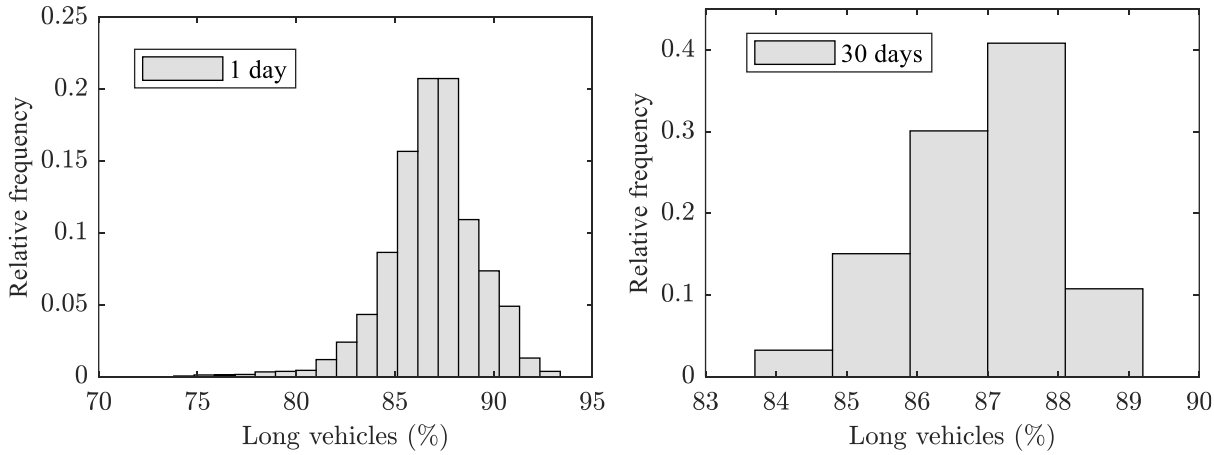

Figure 7.4. Histograms of measured percentage of long vehicles. One day vs thirty days.

The peaks of the histograms are always located around the long run values, which are 2025 veh/day and 87.5% of long vehicles for this station, however, the dispersion of the histograms is noticeable.

Figure 7.5 shows the CV of the ADTT and the percentage of long vehicles against the length of the measurements. The values clearly shows the larger variability presented by the ADTT. The decrease with the length of the measurements presented in both pictures indicates an improvement in the estimation of the traffic descriptors.

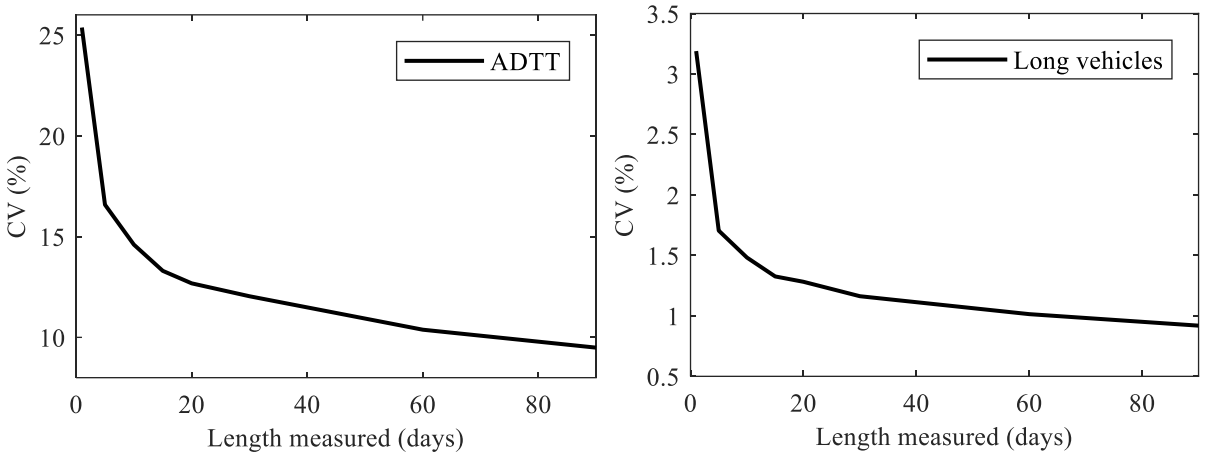

Figure 7.5. Variation of CV for ADTT and percentage of long vehicles with the length of the measurements.

The uncertainty in the estimation of the traffic descriptors eventually affects the estimated LE for the site being assessed. The values of the ADTT and percentage of long vehicles are transformed into site load factors using the appropriate values as shown in Section 6.3, where the correlation between site load factors and traffic descriptors is presented.

Figure 7.6 shows the relative histograms of site load factors obtained from 5 days of measurements for the two traffic descriptors being evaluated as an example. For simplicity, only the sagging moment factor for a span length of 50 m is portrayed.

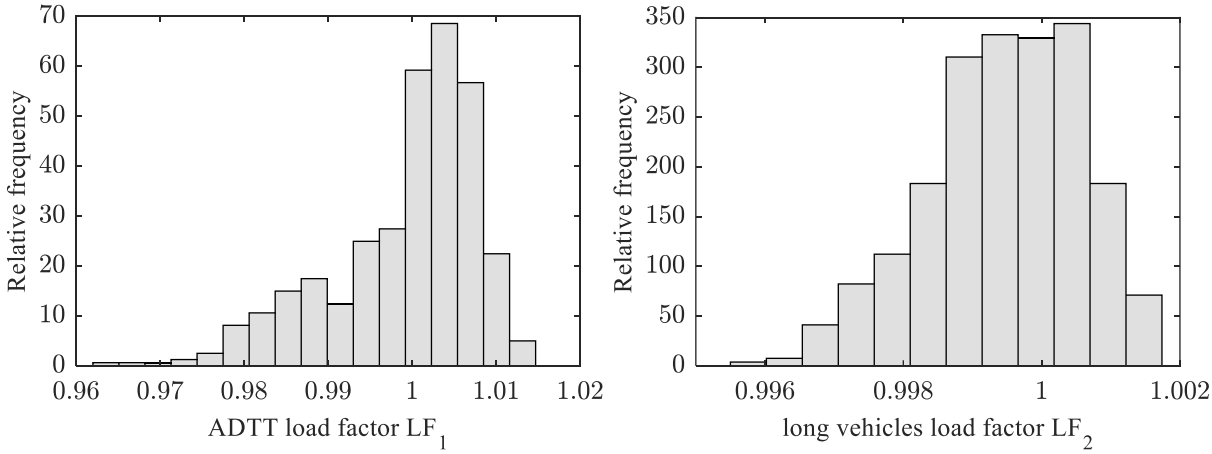

Figure 7.6. Relative histograms of LF_1 and LF_2.

The peaks of both histograms are located around 1 as expected. The dispersion of the ADTT load factor is larger than the percentage of long vehicles as anticipated before with the observation of the CV of the raw traffic descriptors.

The multiplication of both LF_1 and LF_2 factors leads to the combined site load factor. This is achieved by sampling from the empirical CDF and randomly multiplying values from both distributions. Figure 7.7 shows the combined site load factors for the same load effect, the span length and number of days measured mentioned before. As can be observed the combined distribution is close to the distribution of the LF_1 factor. This fact confirms the higher importance of the LF_1 in the approach here proposed.

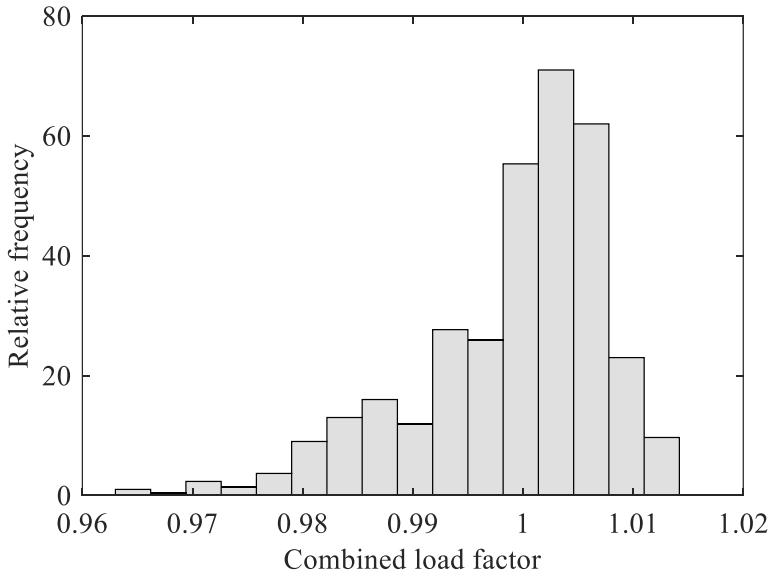

Figure 7.7. Relative histogram of combined load factor.

Distributions of modified load effects are calculated using Equation (7.6). This equation is equivalent to the Equation (6.4) previously presented but differs in that distributions of load effects and site load factors are used here instead of deterministic values. The input values are the characteristic load effects at 975 years, therefore LF_3 is omitted. The influence of the variation of the traffic descriptors on the load effects for other return periods is equivalent since the LF_1 and LF_2 are independent of the reference period (Section 6.3).

$$E_{ka} = E_{kR} \cdot \prod_{i=1}^{2} LF_i \tag{7.6}$$

where E_{ka} stands for the distribution of the assessment characteristic load effects, E_{kR} the reference station characteristic load effects, and LF_i the distributions of site load factors. Figure 7.8 shows an example of the histogram obtained and the fitted probability distribution using maximum likelihood estimation. Given the shape of the histogram, GEV of minima is a good fit to the data. The peak of the histogram is the most probable characteristic load effect, equal

to E_{kR}. Long measurements of the traffic descriptors with low variation deliver $\prod_{i=1}^{2} LF_i = 1$, as seen in Figure 7.7, and therefore $E_{ka} = E_{kR}$.

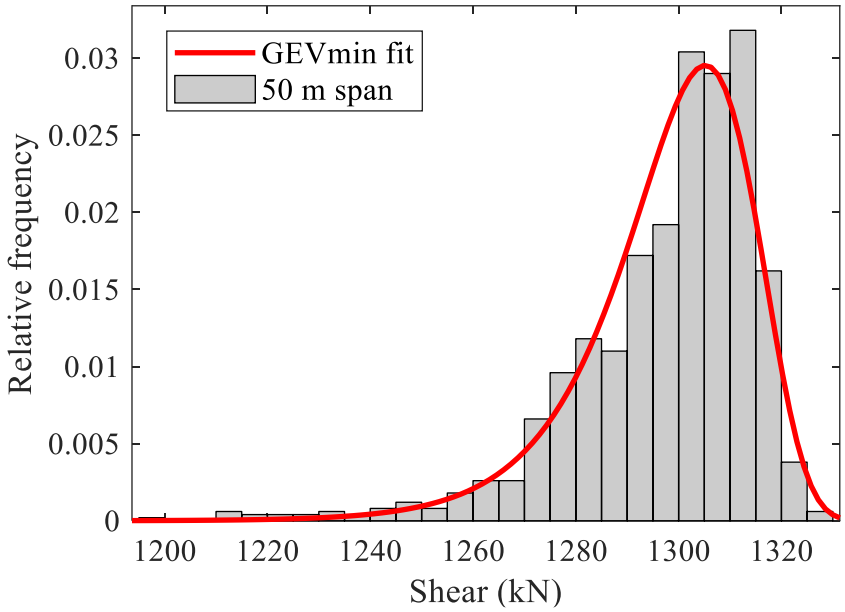

Figure 7.8. Relative histogram of modified shear force and fitted distribution.

The shape of the histogram is explained not only by the dispersion of the traffic descriptors but also by the shape of load factors functions. These curves present higher gradients for lower values of the traffic descriptors and vice versa. Two values of traffic descriptors located the same distance from the mean but each one on each side of the histogram would lead to the same modification of the load effects in absolute terms if the correlation was linear. However, due to the variations in the gradient, lower values induce higher modifications, thus the histograms tend to present larger lower tails. Figure 7.9 clarifies this concept.

Two values of ADTT shown in the figure above are 1000 veh/day apart from the original ADTT (2000 veh/day) on the left and right side, however, the site load factors obtained lead to a modification of 4% for the lower ADTT and 1.02% for the higher ADTT. It is therefore clear now that lower ADTTs produce higher modification, hence the shape of the histograms.

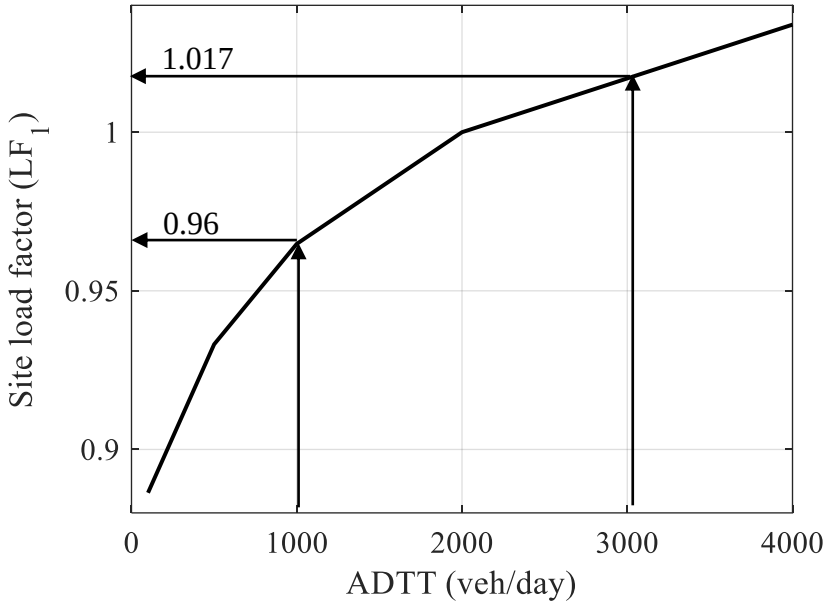

Figure 7.9. Site load factor LF_1- shear force 50 m span length.

The partial factor γ_t accouting for the uncertainty in the estimation of the traffic parameters is introduced here. The goal of this partial factor is to compensate for combinations of traffic descriptors that potentially lead to extreme reductions of the original characteristic load effects and therefore unsafe scenarios. This can be mathematically expressed as indicated in Equation (7.7):

$$P(E_k < E_{kR}) = \Phi(-\alpha_E \cdot \beta_T) \tag{7.7}$$

where E_k is the assessment characteristic low effect estimated using short measurements of the traffic descriptors and E_{kR} is the actual assessment characteristic load effect based on long measurements of the traffic descriptors (peak of the histogram in Figure 7.8). Equation (7.7) is equivalent to saying that the probability of observation of a characteristic load effect E_k below the real value E_{kR} is very low.

It is the lower tail of the histogram of the modified load effects (Figure 7.8) that captures the required probability, therefore the partial factor is calculated as a low fractile as indicated in the following equation:

$$\gamma_l = \frac{E_{kR}}{F_{GEV}^{-1}\left(\Phi(-\alpha_E \cdot \beta_T)\right)} \tag{7.8}$$

where E_{kR} the reference station characteristic load effects that normalises the partial factor, F_{GEV}^{-1} is the inverse CDF of the GEV minima distribution, Φ is the CDF of the Standard Normal distribution, α_E the sensitivity factor and β_T the target reliability index. The selected β_T is 3

that corresponds to a 50 years reference period. Selecting different β_T for each reference period leads to a high number of factors. This is equivalent to the selection of a fixed fractile for the calibration. Tying these partial factors to the sensitivity factor and the target reliability index is a way to avoid subjectivity in the selection of the fractile.

Figure 7.10 shows the mean value of the traffic partial factors γ_t of all the span lengths for the three load effects evaluated at $\beta_T = 3$ (design 50 years reference period). Partial factors decrease with the period measured reflecting the reduction in the uncertainty in the estimation of the traffic descriptors mentioned previously. Sagging moment and shear force partial factors are lower than hogging moments. The hogging moment is greatly affected by the span length of the bridge and the ADTT. For short structures and lower ADTTs only single truck scenarios are creating the most extreme events. For larger spans and higher ADTT scenarios involving more trucks gain importance. This consequently affects the site load factors creating substantial variations in their gradient, thus leading to larger reductions of the hogging moment (higher uncertainty) than observed in the other two load effects by increasing the traffic partial factors. This uncertainty is greatly mitigated when the measurements are extended.

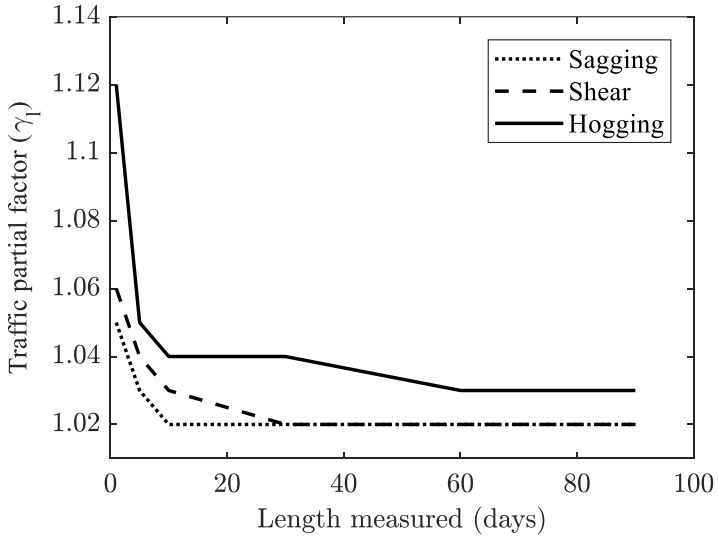

Figure 7.10. Mean traffic partial factors – all span lengths and load effects.

Ideally, the traffic descriptors should be estimated using extensive data sets. In these cases, the uncertainty can be neglected and the traffic partial factor γ_t can be considered 1. Otherwise, measuring for periods larger than ten days does not lead to substantial variations in the traffic partial factors. On average and with reasonable accuracy, five days could be used. This period should be considered as a minimum for the estimation of the traffic descriptors. The use of short periods for the estimation partially undermines the benefits of the reductions achieved with the

application of the site-load factors and is therefore not recommended. To avoid biased estimations, measurements should be always taken on working days in months where the economic activity is normal.

Note that the partial factors shown in this section are a pre-calibration based on the assumed sensitivity factor α_E. The actual influence of this uncertainty might differ from α_E significantly, therefore affecting the sensitivity value and leading to a recalibration of the factors proposed here. Section 7.6 presents more details.

7.3 Reliability based partial factor

The reliability-based partial factors γ_q can be obtained comparing the assessment E_d and characteristic E_{ka} values of the load effects as in Equation (2.35) conveniently repeated here:

$$\gamma_q = \frac{E_d}{E_{ka}} \tag{2.35}$$

The characteristic load effects are obtained as the values with a probability of exceedance of 5% in the selected reference period. The design load effects, however, are a function of the reliability target beta β_T and the sensitivity factors α_E leading to a probability of exceedance P_{exd}:

$$P_{exd} = \Phi(-\alpha_E \cdot \beta_T) \tag{7.9}$$

where Φ is the CDF of the Standard Normal distribution. If the concept of return period is applied to the calculation of the design values, the probabilities of exceedance for the design and assessment and the reference periods considered lead to the return periods RP in Table 7.4. Note that the concept design values of the load effects, calculated as a high fractile of the distribution of load effects, should not be confused with the design (versus assessment) evaluation scenario, that refers to the reliability level.

The design load effects are obtained by extending the extrapolations to detailed return periods for all the simulations previously performed. The reliability based partial factors γ_q can be now calculated based on the previous results.

Table 7.4. Design values return periods for design and assessment and characteristic return period (years) – various reference periods (years).

Reference period	Design RP	Assessment RP	Characteristic values RP
10	1291	289	195
20	1798	396	390
30	2180	475	585
40	2497	539	780
50	2774	594	975

Table 7.5 shows the chosen partial factors for every reference period and reliability level. These partial factors have been chosen to simplify the method as the maximum values among all the span lengths and load effects. The values obtained remain quite constant and differences of 3% are observed, value that justifies the simplification. Moreover, the selection of the maximum values gives an extra safety margin in certain scenarios. The observation of values equal and below 1 for the assessment can be easily understood observing the return periods on Table 7.4. For reference periods of 20 years and longer the characteristic return period is higher than the assessment return period, thus the partial factors obtained.

Table 7.5. Reliability-based partial factors γ_q.

Reference period (years)	Design	Assessment
10	1.09	1.02
20	1.07	1.00
30	1.06	1.00
40	1.05	0.99
50	1.05	0.99

7.4 Model uncertainty

According to the fib Bulletin 80 (Allaix et al., 2016), the model uncertainty partial factor $\gamma_{Ed,q}$ can be assumed as 1.12 for unfavourable variable actions. This value is also assumed here for the calibration of the partial factors.

7.5 Final partial factors

The previously introduced model uncertainty and reliability based partial factors can be multiplied to obtain the final partial safety factors. Equation (7.10) is rewritten here as follows:

$$\gamma_Q = \gamma_Q^* \cdot \gamma_t \cdot \gamma_e \quad with \quad \gamma_Q^* = \gamma_{Ed,q} \cdot \gamma_q \tag{7.10}$$

where the factor γ_Q^* is equivalent to the usual partial safety factor γ_Q that in the context of this thesis is modified by the additional factors γ_t and γ_e . The intermediate partial factor γ_Q^* in Table 7.6 avoids the need of multiplying two factors that in practice always appear as one value. Factors are rounded for simplicity but the exact values are available in Appendix B.6. When the assessment of a specific bridge is executed the last step to obtain the final partial factor γ_Q is to multiply the intermediate factor γ_Q^* by the traffic factor γ_t and γ_e.

Table 7.6. Intermediate partial factors γ_Q^*.

Reference period (years)	Design	Assessment
10	1.22	1.14
20	1.20	1.12
30	1.19	1.12
40	1.18	1.11
50	1.17	1.11

7.6 Reliability verifications

The proposed layering of partial factors and traffic load factors are verified in this section using reliability principles. A reliability analysis assures that the developed methodology with the proposed site load factors and newly calibrated partial factors achieves the desired level of reliability for the traffic loads (Section 7.6.1). Prior to the calculation of the reliability indices, the influence of the proposed uncertainties is evaluated to verify the pre-calibrated partial factors.

An assumed sensitivity factor $\alpha_E = -0.7$ is utilised in the previous section for the calibration of the partial factors. Given the important influence of the sensitivity factors in the calculation of the reliability based partial factors, the value α_E is to be verified in a second reliability exercise (Section 7.6.2). A simple beam with various ratios of permanent to variable load is utilised to cover for both short and medium span lengths and assure the validity of the assumed sensitivity factor α_E.

The reliability verifications are performed using FORM analysis implemented in the package UQLab (Marelli & Sudret, 2014) for Matlab.

7.6.1 Traffic load factor and partial factor layering verification

The here proposed reliability analysis of the traffic load factor and partial factor layering only considers the traffic load effects by means of isolating the design load and the actual traffic load. The desired target reliability level β_T can be split into the resistance and the load effect part. The relative importance of the load effects is initially expressed with the assumed sensitivity factor $\alpha_E = -0.7$, therefore the reliability level of the traffic load effects is $\beta_E = -\alpha_E \cdot \beta_T$. The failure mode is defined here as the instance where the design traffic loads are exceeded by the actual traffic load effects. This can be mathematically expressed using the limit state Equation (7.11):

$$Z = E_{kd} \cdot \gamma_Q^* \cdot \frac{\theta_t}{E_{kR}} \cdot \theta_e \cdot \prod_{i=1}^{3} LF_i - \theta_{E,Q} \cdot E_Q \qquad (7.11)$$

where E_{kd} is the characteristic load effect of the design traffic load model (van der Spuy & Lenner, 2019) ,γ_Q^* the partial factor as detailed in Equation (7.10), θ_t / E_{kR} the traffic descriptors uncertainty (Section 7.2), θ_e the uncertainty in the calculation of the characteristic load effects (Section 7.1) , LF_i the traffic load factors (Appendix B.3), $\theta_{E,Q}$ the model uncertainty (Table 2.5) and E_Q the distribution of the load effects obtained from the long simulations performed in previous chapters and they are tied to a reference period.

In the limit state Equation (7.11) the uncertainty in the determination of the characteristics values θ_e as well as the uncertainty of the traffic descriptors θ_t are initially introduced to evaluate its importance through the sensitivity factors α delivered by the FORM analysis. The assumed $\alpha_E = -0.7$, used in the pre-calibration of the partial factors accounting for these uncertainties, can differ from the actual importance of these variables. This first set of reliability analysis is intended to evaluate the importance of the uncertainties and recalibrate the factors, if necessary, before proceeding into the verification of the partial factors and site load factors layering.

The variables used here are obtained from the artificial traffic generated previously with the reference station traffic conditions (Roosboom) and a reference period of 50 years. The

complete description of all the variables involved in this and further FORM analysis are detailed in Appendix B.7. Table 7.7 presents the results of interest (sensitivity factors) for the span lengths and load effects considered here.

Table 7.7. Sensitivity factors FORM.

Load effect	Span Length	α_e	α_t
Sagging	10	0.17	0.07
	20	0.17	0.08
	30	0.17	0.06
	40	0.17	0.07
	50	0.18	0.08
Shear	10	0.17	0.07
	20	0.17	0.06
	30	0.17	0.06
	40	0.17	0.06
	50	0.17	0.06
Hogging	10	0.18	0.05
	20	0.17	0.06
	30	0.17	0.12
	40	0.18	0.07
	50	0.19	0.06

Given the difference between the previously assumed sensitivity factors (0.7) for the calibration of the partial factors accounting for these two uncertainties, it is necessary to recalibrate the values previously obtained. The partial factor γ_e (uncertainty in the determination of the characteristic load effects) is recalibrated using the formulation in Section 7.1 and the sensitivity factors α_e achieving a value of 1.01 (Table 7.3 contains the original values) . Owing to the very low values of the sensitivity factor α_t, the importance of this uncertainty in the global reliability is negligible and the partial factors γ_t are, therefore, excluded from the assessment method proposed here. It should be noted that the low influence of the uncertainty in the estimation of the traffic descriptors θ_t has been determined with an assumed length of measurements of five days. For the exclusion of this uncertainty from the model to be valid, a minimum of five days are necessary for the estimation of the traffic descriptors from traffic counts. Shorter periods of observation could lead to a decrease in the reliability levels. The exclusion of the partial factors γ_t is based on the results obtained is this thesis using the local traffic and cannot be generalised.

Other countries applying the proposed approach are advised to verify the influence of the traffic descriptors uncertainty before discarding it.

The main goal of this section is, as already introduced, the verification of the partial factors and traffic load factors layering. This can be now evaluated using a slightly modified version of the limit state Equation (7.11), where the uncertainty θ_e is substituted for the recalibrated partial factor γ_e and θ_t is eliminated given its low influence. The failure mode is defined here as the instance where the design traffic loads used in the structural verification (characteristic values and recalibrated partial factors) are exceeded by the actual traffic load effects:

$$Z = E_{kd} \cdot \gamma_Q^* \cdot \gamma_e \cdot \prod_{i=1}^{3} LF_i - \theta_{E,Q} \cdot E_Q \qquad (7.12)$$

The result of interest delivered by the FORM analysis are the probability of failure p_f (the probability that the actual loads exceed the design loads) or the equivalent reliability index β. The verification is successful if the reliability index β obtained in the FORM analysis is higher that the target reliability index for the traffic load effects $\beta_E = -\alpha_E \cdot \beta_T$, therefore the maximum probability of failure intended is not exceeded.

Three traffic scenarios are considered in this verification. These scenarios cover for different traffic conditions (light and heavy traffic) and evaluation conditions (design and assessment with different reference periods):

- **Scenario 1:** Newly generated traffic with an ADTT of 500 veh/day, 25% of long vehicles and an assessment evaluation with a reference period of 10 years. This traffic would be representative of a minor road in a rural area with a very light traffic. Target reliability index for load effects $\beta_{E,10}$=1.83 ($\beta_{E,1}$=2.31).
- **Scenario 2:** ADTT=100 veh/day and % of long vehicles= 87%, long traffic data available (traffic uncertainty excluded) and design evaluation with a reference period of 10 years. Target reliability index for load effects $\beta_{E,10}$=2.42 ($\beta_{E,1}$=2.83)
- **Scenario 3:** Reference station traffic conditions (Roosboom) and design evaluation with a reference period of 50 years. Target reliability index for load effects $\beta_{E,50}$=2.1 ($\beta_{E,1}$=2.83)

The distribution of load effects are obtained for every scenario fitting probability distributions to the traffic generated previously. The rest of the variables have been determined in previous

sections. The complete description of all the variables involved in the FORM for each scenario is detailed in Appendix B.7. Table 7.8 shows the reliability indices obtained for the load effects, the span lengths studied and the three scenarios described before.

Table 7.8. Reliability indices.

Load effect	Span Length	Scenario 1 $\beta_{E,10}$=1.83	Scenario 2 $\beta_{E,10}$=2.42	Scenario 3 $\beta_{E,50}$=2.10
Sagging	10	1.83	2.69	2.35
	20	2.12	2.62	2.40
	30	2.24	2.56	2.40
	40	2.21	2.53	2.39
	50	2.34	2.69	2.50
Shear	10	1.81	2.54	2.32
	20	2.03	2.69	2.39
	30	2.11	2.58	2.41
	40	2.18	2.54	2.35
	50	2.29	2.61	2.37
Hogging	10	1.80	2.68	2.30
	20	1.95	2.5	2.29
	30	1.86	2.44	2.36
	40	2.14	2.71	2.35
	50	2.42	2.89	2.24

The intended reliability index for traffic loads β_E is accomplished in all cases and, therefore, the partial factors (γ_Q^* in Table 7.6 and γ_e=1.01) and traffic load factors (LF_1, LF_2 and LF_3 found in Table B.13 to Table B.17) along with their layering (Eq. 6.4. and Eq. 7.2) are validated. The differences found between the reliability index achieved and the intended reliability level β_E can be attributed to rounding and simplifications of the partial factors as well as the difference between the design values obtained using the methodology presented previously and the design values obtained as the fractile $\Phi(-\alpha_E \cdot \beta_T)$ from the distribution of load effects E_Q.

7.6.2 Sensitivity factors for loading

The validity of the assumed sensitivity factor $\alpha_E = -0.7$ used in the calibration of the partial factors for loading is assessed here using a general bending limit state of a reinforced concrete beam as indicated in Equation (7.13) with R representing resistance and E load effect:

$$Z = R - E = 0.9 \cdot d \cdot A_s \cdot f_y \cdot \theta_R - \left(\theta_{E,G} \cdot E_G + \theta_{E,Q} \cdot E_Q \right) \qquad (7.13)$$

where $0.9 \cdot d$ is the simplified distance between the reinforcement and the centroid of the concrete block with d the reinforcement depth, A_s the area of reinforcement, f_y the yield strength, θ_R the resistance model uncertainty, $\theta_{E,G}$ and $\theta_{E,Q}$ the model uncertainties for the permanent and the variable loads and E_G the permanent load bending moment and E_Q the variable load bending moment due to traffic loads. This theoretical exercise is similar to the one performed by Lenner (2014) but adapted to the specific properties of the distributions of the variable loading studied in this thesis.

A simple cross section as shown in Figure 7.11 and a beam length of 10 m are selected, as an example, for the analysis. The design of the beam is performed using the partial factor for the variable load calibrated previously and the recommendations of the (TMH -7, 1981) for the permanent loads ($\gamma_G = 1.32$) and the partial load for yielding of steel ($\gamma_R = 1.15$). For the calculation of the needed area of reinforcement, the design resistance R_d is considered equal to the total design load effect E_d as indicated in Equation (7.14), where the characteristic values of the load effects are introduced:

$$R_d = \frac{A_s \cdot f_y \cdot 0.9 \cdot d}{\gamma_R} = \gamma_G \cdot E_{kG} + \gamma_Q \cdot E_{kQ} \qquad (7.14)$$

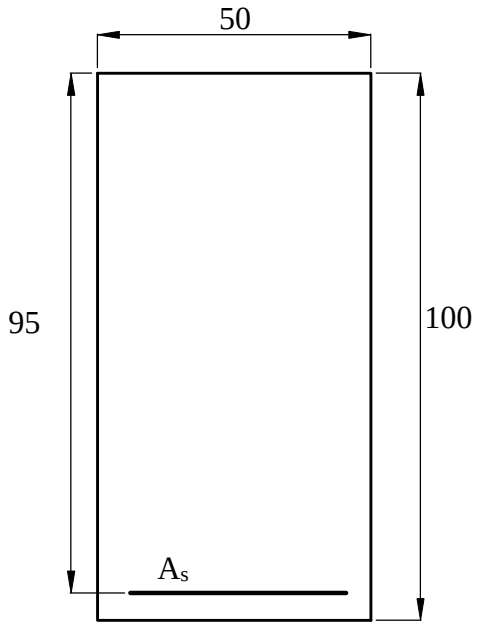

Figure 7.11. Cross section considered in the reliability analysis. Dimensions in cm.

In order to cover for a wide spectra of loading scenarios, the load ratio κ, describing the relationship between the characteristic load effects is introduced (Caspeele et al., 2013; Lenner, 2014; Lenner & Sýkora, 2017). The load ratio approach avoids the issue of using different structures and the mentioned publications show its clear influence on the sensitivity factors:

$$\kappa = \frac{E_{kG}}{E_{kG} + E_{kQ}} \tag{7.15}$$

With only one geometry and beam length considered, the characteristic permanent load effect E_{kG} is constant and the characteristic variable load effect E_{kG} can be calculated using Equation (7.15) and the load ratios, which range from 0.3 to 0.8. Low load ratios are representative of short spans (dominant variable load) and high load ratios are indicative of dominant dead load, commonly found in long spans. With all the variables defined, the design of the beam can be completed after the calculation of the area of reinforcement. Values are determined isolating A_s from Equation (7.14). Table 7.9 summarises the properties of all the beams used in the reliability analysis.

Table 7.9. List of beams used in the reliability analysis,

κ	d (m)	E_{kG} (kN.m)	E_{kQ} (kN.m)	A_s (cm^2)
0.3	0.95	156.25	364.58	19.46
0.4	0.95	156.25	234.38	14.71
0.5	0.95	156.25	156.25	11.86
0.6	0.95	156.25	104.17	9.96
0.7	0.95	156.25	66.96	8.61
0.8	0.95	156.25	39.06	7.59

The stochastic properties of the variables describing the limit state in Equation (7.13) are shown in Table 7.10. The variable load effects are modelled as a Gumbel distributions as done in the previous exercise and based on the simulations performed in previous chapters. As indicated in Appendix B.7 the CV of the fitted distributions for a 50 years reference period vary from approximately 2% to 6%. The variability of the sensitivity values is assessed making used of these two values as maximum and a minimum variance of the distributions of variable load effects. The rest of the properties are selected from the available literature (FIB, 2011; Holický, 2009; JCSS, 2001; Lenner, 2014). The means μ of the Gumbel distributions modelling the variable loads with characteristic values from Table 7.9 and CV of 2% and 6% are shown in Table 7.11.

Table 7.10. Stochastic properties of the variables in the limit state equation.

Variable	Unit	Distribution	μ	CV
d	m	Normal	0.95	0.02
A_s	m^2	Normal	1.02×Table 7.9	0.02
f_y	kN/m^2	LogNormal	499350	0.06
θ_R	-	LogNormal	1	0.06
E_G	kN.m	Normal	Table 7.9	0.05
E_Q	kN.m	Gumbel	Table 7.11	0.02-0.06
$\theta_{E,G}$	-	Normal	1	0.07
$\theta_{E,Q}$	-	LogNormal	1	0.1

Table 7.11. Mean of Gumbel distributions.

E_{kQ} (kN.m)	$\mu\ (CV = 0.02)$	$\mu\ (CV = 0.06)$
364.58	351.48	327.92
234.38	225.95	210.81
156.25	150.64	140.54
104.17	100.42	93.69
66.96	64.56	60.23
39.06	37.66	35.13

The results of the FORM analysis are plotted in Figure 7.12 For low load ratios the variable load is dominant and as the load ratio increases, the importance of the variable load decreases and the permanent load plays a major role in the performance of the bridge. The selection of a constant sensitivity factor for variable load $\alpha_E = -0.7$ is conservative for all the load ratios above 0.4 and slightly non-conservative for lower values of load ratio. Nevertheless, such low load ratios might only happen in very short bridges (<10 m). A simple example of a 10 m length bridge with a slab of 7×0.5 ($\frac{l}{h} = 20$ and two lanes) with a self-weight of 875 kN.m and a characteristic sagging moment of 1418 kN.m (Table 6.4) delivers a load ratio of 0.38. This value could rapidly increase if other permanent loads, such as barriers of asphalt layers, omitted here were included in the estimation.

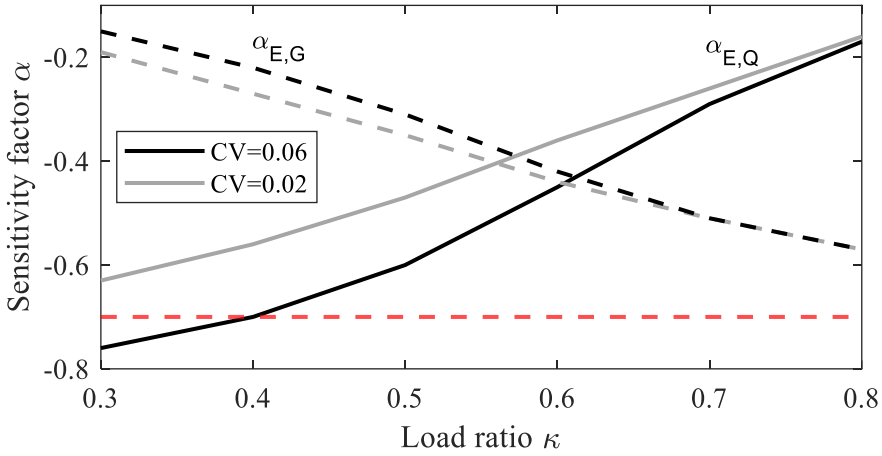

Figure 7.12. Variation of the sensitivity factors with the load ratio.

During the design stage of a bridge, both permanent and variable loads are estimated. With these values clearly defined, the load ratio can be calculated. Given the curves in Figure 7.12, there is an opportunity to obtain the appropriate sensitivity factors for the design conditions considered. With this new information, the reliability based partial factors could be recalibrated in every case and the design resistance R_d isolated from Equation (7.14). This could be an alternative to the adoption of unique sensitivity factors, for all spans lengths, adopted in design codes. Without involving complex calculations, selecting different sensitivity factors could be especially beneficial for longer bridges.

The assessment of an existing bridge, however, implies a more complicated procedure. The design resistance and characteristic permanent load are known variables in Equation (7.14). The partial factors and the characteristic variable load are unknown. An iterative process should be, therefore, performed for an accurate selection of the sensitivity factors. The iteration is as follows:

1. Assumed load ratio κ and calculation of the characteristic variable load effect E_{kQ1}.
2. Determination of the sensitivity factors from curves in Figure 7.12.
3. Calibration of the partial safety factors for permanent and variable loads.
4. Calculation of a second characteristic variable load effect E_{kQ2}, isolating this value from Equation (7.14).
5. The iteration continues similarly until $E_{kQ2} = E_{kQ1}$.

Alternatively, if basic traffic data information can be collected, the characteristic value of the variable load can be estimated as proposed in this thesis and the partial factors recalibrated as

explained for the design stage. In this instance, the bridge will successfully pass the evaluation if the design loads are inferior to the design resistance.

The selection of a conservative sensitivity factors is a commonly adopted way of simplifying the process of calibrating the partial factors. The process to ascertain the accuracy of the partial factors in every specific design or assessment case is to perform a reliability analysis. The sensitivity factors obtained in the analysis can be compared with the sensitivity factors used in previous calibrations of the partial factors. This is currently not an option for practising engineers. Advanced methods such as reliability analysis are only recommended in meaningful bridges where simplified methods do not deliver satisfactory results.

CHAPTER 8: APPLICATION OF THE SITE LOAD FACTOR APPROACH

The general procedure for the application of the site load factor approach is summarised below. Table 8.1 contains the partial factors to be used:

1. Collection of the necessary information for the application of the approach. A remaining service life of the structure together with a reliability level (design or assessment) must be set. This decision can be evaluated based on the age or the state of the bridge. Traffic measurements have to be taken to estimate the relevant traffic descriptors, in the case of this document the ADTT and the % of long vehicles. As mentioned previously a minimum of five days is recommended.
2. Table B.13 to Table B.17 are used together with the estimated traffic descriptors to obtain the site load factors LF_1, LF_2 and LF_3 for each of the three load effects considered. The hogging moment can be omitted if the structure is simply supported. The new characteristic load effect is obtained using Equation (6.4) repeated here for convenience, where E_{kd} is the characteristic load effect obtained using the design load model (van der Spuy et al., 2019):

$$E_{ka} = E_{kd} \cdot \prod_{i=1}^{3} LF_i$$

3. The design value of the load effects is finally obtained multiplying E_{ka} by the final partial factors γ_Q shown in Table 8.1 that contains all the individual partial factors calibrated previously. The reference period and reliability level are inputs in this table.

Table 8.1. Partial factors γ_Q.

Reference period	Design	Assessment
10	1.24	1.15
20	1.21	1.13
30	1.20	1.13
40	1.19	1.12
50	1.18	1.12

Two examples of the application of the site load factor approach are presented in this section to clarify the explained procedure.

Example 1 – simply supported bridge.

The first example is based on a simply supported bridge with one lane per direction located in a minor road with relatively low traffic. The structure does not present deficient performance, however, owing to its age (over 50 years old) the evaluation is performed for the lowest reference period and reliability level (assessment). These are the least aggressive loading conditions. Table 8.2 summarises the characteristics of the structure and traffic used for this example.

Table 8.2. Summary of data for the bridge evaluation.

Bridge arrangement	Simply supported
Span length	20 m
ADTT (one lane)	750 veh/day
Percentage of long vehicles (one lane)	70%
Remaining service life (reference period)	10 years
Reliability level	Assessment

The site load factors LF_1, LF_2 and LF_3 are obtained from the tables provided in Appendix B.3 only for the relevant internal forces on simply span bridges, the sagging moment and the shear force. Interpolation between the values provided in Appendix B.3 is performed to acquire the factors for the required site descriptors. In this instance, interpolation is needed to obtained both factors (500<750<1000 veh/day; 50<70<87.5% long vehicles). Table 8.3 details the load factors LF_1, LF_2 and LF_3, the final global factors and the modified UDL (30 kN/m first lane and 22.5 kN/m second lane) and tridem load (160 kN each axle first lane and 120 kN each axle second lane).

Table 8.3. Site load factors and modified load model.

Load effect	LF_1	LF_2	LF_3	Global	UDL (kN/m)	Axle load (kN)
Sagging	0.955	0.976	0.55	0.51	26.8	143×3 axles
Shear	0.955	0.976	0.66	0.62	32.5	174×3

The modified UDL and the axle load are obtained multiplying the site load factors by the design UDL and axle load for both lanes. The reference period factor LF_3 could be selected per lane for a lateral distribution of loading. The comparison of the characteristic load effects obtained from the design load model and the modified model are presented in Table 8.4.

Table 8.4. Comparison of characteristic load effects.

Load effect	Design LM	Modified
Sagging (kN.m)	6489	3310
Shear (kN)	1314	815

The partial safety factor according to the previous data is γ_Q =1.15. The design load effects are finally obtained multiplying the modified load effects by the partial factor γ_Q.

Example 2 – continuous two span bridge deck.

This example considers a continuous two span bridge deck with 20 and 30 m span lengths and one lane per direction. It is located in a minor road with low traffic. The bridge is relatively new, however, it was designed using an outdated design traffic load model. An evaluation should be performed to assess if the structure fulfils the current requirements. Design level and 50 years of reference period are therefore selected in a first stage. Table 8.5 summarises the characteristics of the structure and traffic used for this example.

Table 8.5. Summary of data for the bridge evaluation.

Bridge arrangement	Two span bridge deck.
Span lengths	20 and 30 m
ADTT (one lane)	500 veh/day
Percentage of long vehicles (one lane)	70%
Remaining service life (reference period)	50 years
Reliability level	Design

The site load factors to be estimated on a continuous beam are the sagging moment, hogging moment and the shear force. The hogging moment must be modified by selecting the site load factors according to one of the spans. Using the 20 m span length instead of 30 leads to conservative values owing the way the design load model has been calibrated using the 15 m span hogging moment as explained previously. The shear force and sagging moment can be modified separately on each span. Alternatively, the site load factors between the two span lengths with the lower reduction can be selected as conservative values. Table 8.6 shows the selected site load factors.

Table 8.6. Site load factors and modified load model.

Load effect	LF_1	LF_2	LF_3	Global	UDL (kN/m)	Axle load (kN)
Hogging (20 m)	0.92	0.98	0.59	0.53	27.8	148×3
Shear (30 m)	0.93	0.98	0.70	0.64	33.6	180×3
Shear (20 m)	0.94	0.976	0.70	0.64	33.6	180×3
Sagging (30 m)	0.93	0.98	0.62	0.55	28.9	154×3
Sagging (20 m)	0.93	0.976	0.56	0.50	26	140×3

For simplicity and adopting conservative values the load effects in this example are calculated using the highest global factor, which is the value obtained from the shear force factors. The design and modified load effects are shown in Table 8.7. Alternatively, the load effects can be calculated applying the individual site load factors. This simpler approach, however, still delivers important reductions.

Table 8.7. Comparison of characteristic load effects.

Load effect	Design LM	Modified
Sagging (kN.m)	8735	5603
Shear (kN)	1762	1130
Hogging (kN.m)	7488	4800

The partial safety factor selected from Table 8.1 is $\gamma_Q = 1.18$. The design load effects are finally obtained multiplying the modified load effects by the global partial factor γ_Q.

CHAPTER 9: SUMMARY

A general framework for the calibration of the design traffic load models for the assessment of existing bridges is presented in this thesis. It is shown that a robust Monte Carlo simulation with bivariate copulas is an original and suitable tool for the investigation. The real advantage is the possibility of transforming recorded traffic into artificial flows exhibiting different traffic characteristics. It is therefore possible to observe the influence of selected parameters on the resulting load effects. At the same time, the results clearly show increased internal forces due to increased ADTT and/or percentage of long vehicles in the traffic flow. The variation is most apparent for continuous beams and hogging moments due to the increased total bridge length, yet is still important to both sagging moments and shears at single spans. The simulated traffic is used to calibrated three site specific traffic load factors.

Although the contribution of the mentioned traffic descriptors on the load effects was known before, this work presents a new procedure to quantitatively evaluate and calibrate it. Consequently, these results can be numerically applied to the design load model using several factors. Therefore, if a specific bridge is assessed, site-specific load factors for assessment based on the basic descriptors collected by means of traffic counts can be applied to the design model. The main assumption is that the design model is conservative and up-to-date reflecting the heaviest traffic observed to account for all situations, so the load model can be modified for the assessment at a specific site. The real advantage of this approach is its easy applicability avoiding the installation of expensive equipment, the treatment of recorded traffic data and the extensive statistical knowledge necessary to obtain reliable results.

The method as presented has been verified using the traffic recorded by other WIM stations available showing that important modifications in the characteristic load effects can be achieved. It shows good adaptability to any traffic conditions.

A detailed evaluation of the uncertainties is presented in Chapter 7. Along with the reliability-based and model uncertainty partial factors two new factors are calibrated (γ_t and γ_e) for the evaluation of the individual uncertainties considered. The estimation of the influence of these two new uncertainties is assessed using FORM analysis leading to a recalibration of the factors based on the new sensitivity factors. The verification of the proposed partial factors and site load factors layering is carried out to assure the intended reliability levels. A reliability exercise with a simple supported beam is used to validate the assumed sensitivity factors for the loading.

9.1 Proposed framework and application in other regions

Figure 9.1 shows the general steps to be followed if the method proposed here is to be applied in other regions. Details comments on every step can be found below.

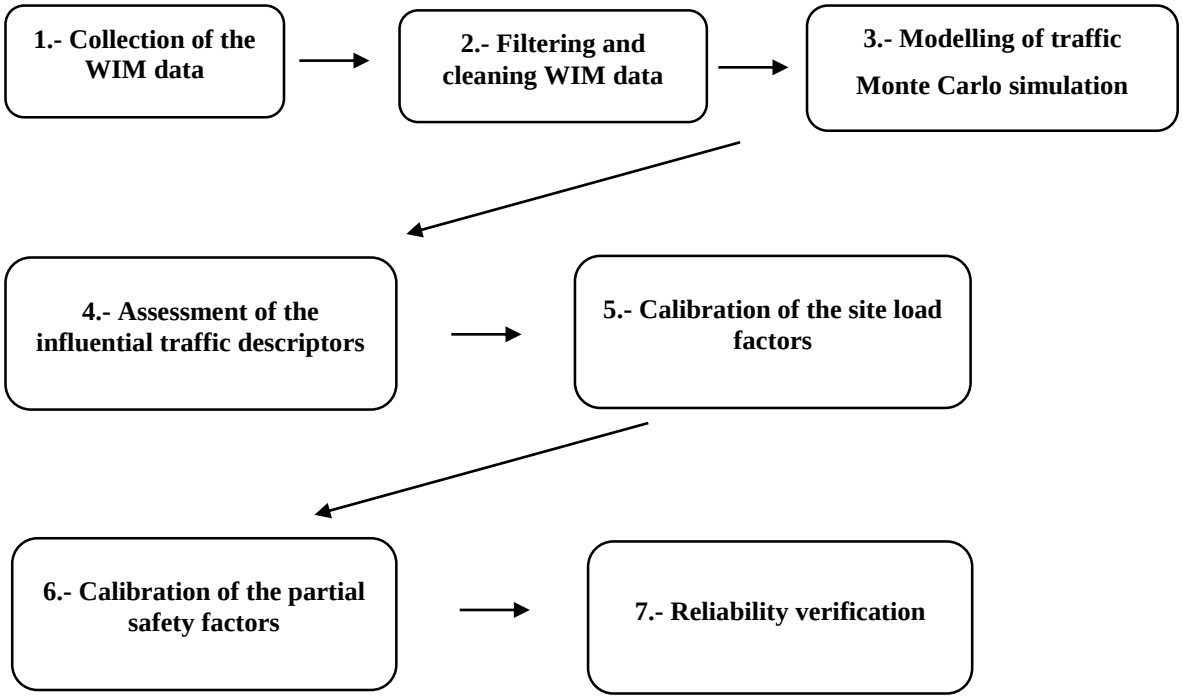

Figure 9.1. Flowchart of the proposed method.

1. **Collection of extensive WIM data.** The most aggressive traffic registered by the WIM stations is recommended for further calculations. The selected WIM data should be the basis for the calibration of the general design load model that can be later modified for lighter conditions using the site load factors. Other station can be used in verifications.
2. **Filtration and calibration of the WIM data.** Traffic data must be properly filtered and cleaned from erroneous or unnecessary records. The regional properties of the traffic are important for the application of filtration criteria and previous experiences must be taken into account. Moreover, accuracy of the WIM data should be checked and the systematic error introduced by the WIM station removed. Details can be found in Sections 3.2 and 3.3.
3. **Monte Carlo routine.** The development of the Monte Carlo routine requires the modelling of truck and traffic variables. The literature review and Chapter 4 both discuss several approaches. The similarity between the load effects calculated from the recorded and the generated traffic should be verified.

4. **Definition of the traffic descriptors to be studied.** An evaluation of the influence of various traffic descriptors on the traffic load effects should be performed. The most influential variables should be included in further calibrations. Chapter 5 details this step.
5. **Simulations concerning the most influential traffic descriptors.** Long simulations are recommended to increase the accuracy of the tail of the load effects distributions. The simulated load effects are utilised to determine the characteristic values and a calibration of the site load factors should follow as detailed in Chapter 6. A first verification of the site load factors at a characteristic load effects level can be performed using alternative stations.
6. **Uncertainty estimation.** The use of simple semi-probabilistic approaches requires the estimation of the uncertainties involved in the process and the quantification of the partial factors accounting for these uncertainties as done in Chapter 7.
7. **Reliability verifications.** A reliability verification of the proposed site load factors and partial factors is recommended along with a validation of the assumptions involved in the calibration of the partial factors (sensitivity values). The reliability analysis assures that the intended reliability level β_E for the traffic loads is accomplished. Recalibrations might be necessary if the assumed sensitivity factors highly differ from the calculated values.

The initial steps explained here for the calibration of the site load factors can be identically followed in the calibration of the design load model. Ideally, both calibrations can be performed simultaneously. The design load model requires a general applicability and a conservative nature. On the other hand, in the assessment of existing bridges certain variables can be modified during the calibration of the design load model to readjust its load effects to the site specific conditions. If the simultaneous calibration is not possible, both processes should, at least, base the calculations on the same WIM data, filtered and calibrated similarly to avoid discrepancies.

9.2 Recommendations

The assessment of a specific bridge can be firstly executed using the design load model. Should the structure fail the evaluation further adjustments can be applied. Site traffic conditions can be obtained and effectively reduced the design loads especially for light traffic conditions. If a remaining service life for the structure is set, the reference period can be adjusted to further

reduce the traffic loads. The use of the assessment partial safety factors calibrated using lower target reliability indices can be considered if the bridge fails all the previous evaluations. The entire evaluation process should in principle proceed from the design situation with its inherent conservative nature to techniques sequentially adapting to the site specific conditions and removing some of the unnecessary conservatism.

On simple supported bridges and two span bridges with equal lengths the site load factors can be applied to either the model in form of the UDL and to the tridem of axles or the equivalent load effects generated. The results are the same. On different arrangements, the factors should be applied to the UDL and axle load to later proceed with the calculation of the load effects.

If the assessment of multiple span bridges with different span lengths is encountered the recommendation is to use the higher site load factors corresponding to each individual span length. This provides an extra safety margin in this specific span arrangement.

9.3 Future research

The assessment of existing bridges is a topic in constant evolution and open to further development. The recalibration of the site load factors and partial safety factors can be achieved in the future if larger sets it traffic data are used. This might be achieved using Bayesian updating methods. The combination of the multiple lane reduction factors and site load factors as proposed in this thesis is an open investigation as well.

The definition of a day with economic activity or operational day should be investigated. Days without traffic or with very low traffic should not be considered, however, the reduction in the traffic intensity for a day to be considered non-operational could be better defined. Moreover, the influence in the characteristic load effects of years with different number of days could be evaluated. The selection of the number of economical days is a critical aspect that could lead to underestimations of the real load effects (lower economical days), therefore affecting the safety of the bridge, or to overestimations (higher economical days) with the consequent higher cost of construction.

The complex distribution of the vehicular loads among the axles might be better modelled using advanced copula techniques known as Vine Copulas. This approach allows for the study of the dependence structure (graphically represented by trees or vines) of multivariate data using bivariate copulas (higher number of families if compared to multivariate copulas).

The economic implications of the new assessment approach could be evaluated as well if the repercussions on a bridge or set of bridges after the use of the design load model and the assessment approach are compared.

CHAPTER 10: REFERENCES

AASHTO LRFD. (2017). *LRFD Bridge Design Specification*. Washington, D.C.: American Association of State Highway and Transportation Officials.

AASHTO LRFR. (2003). *Guide Manual for Condition Evaluation and Load and Resistance Factor Rating (LRFR) of Highway Bridges*. Washington D.C.: American Association of State Highway and Trasportation Officials.

Akaike, H. (1974). A New Look at the Statistical Model Identification. *IEEE Transactions on Automatic Control*. https://doi.org/10.1109/TAC.1974.1100705

Allaix, D. L. (2007). *Bridge Reliability Analysis with an Up-to-Date Traffic Load Model*. (Doctora dissertation, Politecnico di Torino).

Allaix, D. L., Botte, W., Diamantidis, D., Engen, M., Faber, M., Hendriks, M., … Vrouwenvelder, A. (2016). *fib Bulletin 80. Partial factor methods for existing concrete structures*. (R. Caspeele, R. Steenbergen, & M. Sýkora, Eds.). fib. The International Federation for Structural Concrete. https://doi.org/10.35789/fib.BULL.0080

ARCHES. (2009). *Assessment and Rehabilitation of Central European Highway Structures - Final activity report* (Vol. 54). Institute, Road and Bridge Research.

ASTM E1318-02. (2002). *Standard Specification for Highway Weigh-in-Motion (WIM) Systems with User Requirements and Test Methods.* West Conshohocken, PA. Retrieved from https://www.astm.org/DATABASE.CART/HISTORICAL/E1318-02.htm

Bailey, S. F. (1996). *Basic Principles and load models for the structural safety evaluation of existing road bridges*. (Doctoral dissertation, Ecole Polytechique Federale de Lausanne).

Bali, T. G. (2003). The generalized extreme value distribution. In *Economics Letters* (Vol. 79, pp. 423–427). North-Holland. https://doi.org/10.1016/S0165-1765(03)00035-1

BD 21/01. (2001). *The assessment of highway bridges and structures* (Vol. 3). Department of Transportation. United Kingdom.

BD 37/01. (2002). *Design manual for roads and bridges*. Department of Transportation. United Kingdom. Retrieved from http://www.standardsforhighways.co.uk/ha/standards/dmrb/vol1/section3/bd3701.pdf

Bez, R., & Bailey, S. F. (1995). Site specific traffic load models for bridge evaluation.

International Association for Bridge and Structural Engineering, *73/1/73/2*. Retrieved from http://dx.doi.org/10.5169/seals-55276%0ANutzungsbedingungen

Bissell, D., Ang, A. H. S., & Tang, W. H. (1979). *Probability Concepts in Engineering Planning and Design: Vol. I-Basic Principles. The Statistician* (Vol. 28). Wiley. https://doi.org/10.2307/2987875

Box, G. E. P., & Cox, D. R. (1964). An Analysis of Transformations. *Journal of the Royal Statistical Society.Series B (Methodological)*, *26*(2), 211–252. Retrieved from http://about.jstor.org/terms

Braml, T., Fischer, A., Keuser, M., & Schnell, J. (2009). Beurteilung der Zuverlassigkeit von Bestandstragwerken hinsichtlich einer Querkraftbeanspruchung. *Beton- Und Stahlbetonbau*. Berlin: Verlag Ernst & Sohn.

Brechmann, E. C., & Schepsmeier, U. (2013). Modeling Dependence with C- and D-Vine Copulas: The R Package CDVine. *Journal of Statistical Software*, *52*(3). https://doi.org/10.18637/jss.v052.i03

BRIME. (2001). *Final Report - Deliverable D14*. Bridge management in Europe.

Bruls, A., Calgaro, J.-A., Mathieu, H., & Prat, M. (1996). ENV 1991 Part 3: The main models of traffic loads on road bridges; Background studies. *IABSE Colloquium: Basis of Design and Actions on Structures; Background and Application of Eurocode 1*, 215–228.

Buckland, P. G., Navin, F., Zidek, J. J. V., McBryde, J. P., G. Buckland, P., P.D. Navin, F., & Zidek, J. J. V. (1980). *Proposed vehicle loading of long-span bridges*. *ASCE J Struct Div* (Vol. 106). Retrieved from https://www.semanticscholar.org/paper/PROPOSED-VEHICLE-LOADING-OF-LONG-SPAN-BRIDGES-Buckland-Navin/a9527a2544758bf161c7b55665f9f2d9c497f2e5

CAN/CSA-S6-06. (2006). *Canadian Highway Bridge Design Code*. Canadian Standards Asociation.

Caprani, C. C. (2005). *Probabilistic analysis of highway bridge traffic loading*. (Doctoral dissertation, University College of Dublin).

Caprani, C. C., Grave, S., O'Brien, E. J., & O'Connor, A. J. (2002). Critical Loading Events for the Assessment of Medium Span Bridges. In *Sixth International Conference on Computational Structures Technology* (pp. 1–11).

Caprani, C. C., & O'Brien, E. J. (2006). Statistical Computation for Extreme Bridge Traffic Load Effects, (January 2014). https://doi.org/10.4203/ccp.83.139

Caprani, C. C., & O'Brien, E. J. (2010). Estimating Extreme Highway Bridge Traffic Load Effects. *Safety, Reliability and Risk of Structures, Infrastructures and Engineering Systems*, (October 2016), 2015–2019.

Caprani, C. C., O'Brien, E. J., & McLachlan, G. J. (2008). Characteristic traffic load effects from a mixture of loading events on short to medium span bridges. *Structural Safety*, *30*(5), 394–404. https://doi.org/10.1016/j.strusafe.2006.11.006

Caspeele, R., Sýkora, M., Allaix, D. L., & Steenbergen, R. (2013). The design value method and Adjusted Partial Factor Approach for existing structures. *Structural Engineering International*, *23*(4), 386–393. https://doi.org/10.2749/101686613X13627347100194

Castillo, E. (1988). *Extreme value theory in engineering*. Academic Press. Retrieved from https://books.google.co.za/books?hl=en&lr=&id=CyFd42CkOmMC&oi=fnd&pg=PP1&dq=extreme+value+theory+in+engineering&ots=A3rxpz0Aju&sig=FHo8hC1We7g-MLHAau06P3ETzwA#v=onepage&q=extreme value theory in engineering&f=false

Coles, S. (2001). *An Introduction to Statistical Modeling of Extreme Values*. London: Springer London. https://doi.org/10.1007/978-1-4471-3675-0

Cooper, D. (1995). The dertermination of highway bridge design loading in he United Kingdom from traffic measurements. Retrieved from https://trid.trb.org/view/426887

COST 323. (1998). *Weigh-in-Motion of Road Vehicles*. Paris.

COST345. (2007). *Procedures for Assessing Highway Structures, Final report of the COST 345 action*. Retrieved from http://cost345.zag.si/Reports/COST_345_WG23.pdf

Crespo-Minguillón, C., & Casas, J. R. (1997). A comprehensive traffic load model for bridge safety checking. *Structural Safety*, *19*(4), 339–359. https://doi.org/10.1016/S0167-4730(97)00016-7

Danish Road Directorate. (2004). *Reliability Based Classification of the Load Carrying Capacity of Existing Bridges, Guideline Document, Report 291*. Denmark: Ministry of Transport.

Dargahi-Noubary, G. R. (1989). New Method for Prediction of Extreme Wind Speeds. *Journal*

of Engineering Mechanics, *115*(4), 859–866. https://doi.org/10.1061/(ASCE)0733-9399(1989)115:4(859)

de Wet, D. P. G. (2010). *Post-Calibration and Quality Management of Weigh-in-Motion Traffic Data*. (Master's thesis, Stellenbosch University). Retrieved from http://scholar.sun.ac.za/handle/10019.1/4205

de Zea Bermudez, P., & Kotz, S. (2010). Parameter estimation of the generalized Pareto distribution—Part II. *Journal of Statistical Planning and Inference*, *140*(6), 1374–1388. https://doi.org/10.1016/J.JSPI.2008.11.020

Diamantidis, D. (2001). Report 32: Probabilistic Assessment of Existing Structures-A publication for the Joint Committee on Structural Safety (JCSS). Retrieved from https://books.google.co.za/books?hl=es&lr=&id=aTTWQM7ZvY8C&oi=fnd&pg=PR6&dq=rilem+diamantidis+probabilistic+assessment&ots=jXl-NlR9va&sig=jiYZglqI7pqX-ulzRqol8oOZgoo

Ditlevsen, O. (1994). Traffic Loads on Large Bridges Modeled as White-Noise Fields. *Journal of Engineering Mechanics*, *120*(4), 681–694. https://doi.org/10.1061/(ASCE)0733-9399(1994)120:4(681)

Embrechts, P., Lindskog, F., & McNeil, A. (2003). Modelling Dependence with Copulas and Applications to Risk Management. *Handbook of Heavy Tailed Distributions in Finance*, 329–384. https://doi.org/10.1016/B978-044450896-6.50010-8

EN-1990. (2002). *Eurocode - Basis of structural design*. European Comittee for Standardization. Retrieved from https://www.phd.eng.br/wp-content/uploads/2015/12/en.1990.2002.pdf

EN 1991-2. (2003). *Eurocode 1: Actions on structures - Part 2: Traffic loads on bridges*. Brussels: European Comittee for Standardization. Retrieved from https://www.phd.eng.br/wp-content/uploads/2015/12/en.1991.2.2003.pdf

Enright, B. (2010). *Simulation of traffic loading on highway bridges*. (Doctoral dissertation, University College of Dublin).

Enright, B., Caprani, C. C., & O'Brien, E. J. (2011). Modelling of Highway Bridge Traffic Loading : Some Recent Advances. *Applications of Statistics and Probability in Civil Engineering (ICASP 11)*, (2002), 397–405.

Enright, B., & O'Brien, E. J. (2011). *Cleaning Weigh-in-Motion Data: Techniques and Recommendations*. University College Dublin. Retrieved from http://www.is-wim.org/doc/wim_data_cleaning_ie.pdf

Enright, B., & O'Brien, E. J. (2013). Monte Carlo simulation of extreme traffic loading on short and medium span bridges. *Structure and Infrastructure Engineering*, *9*(12), 1267–1282. https://doi.org/10.1080/15732479.2012.688753

Faber, M. (2009). *Risk and Safety in Engineering*. https://doi.org/10.4324/9780203477199

FIB. (2011). *Model Code 2010*. *fib Model Code for Concrete Structures 2010*. https://doi.org/10.1002/9783433604090.ch6

Fischer, A. (2010). Bestimmung modifizierter Teilsicherheitsbeiwerte zur semiprobabilistischen Bemessung von Stahlbetonkonstruktionen im Bestand. *Fachbereich Architektur / Raum- Und Umweltplanung / Bauingenieurwesen*, *Dr.-Ing.*(D 386).

Fisher, R. A., & Tippett, L. H. C. (1928). Limiting forms of the frequency distribution of the largest or smallest member of a sample. *Mathematical Proceedings of the Cambridge Philosophical Society*, *24*(2), 180–190. https://doi.org/10.1017/S0305004100015681

Gable, G., Moses, F., & Record, A. P. (1976). Applications of a bridge measurement system. *Transportation Research Board, National Research Council*. Washington D.C. Retrieved from https://trid.trb.org/view/46985

Getachew, A. (2003). *Traffic Load Effects on Bridges Statistical Analysis of Collected and Monte Carlo Simulated Vehicle data*. (Doctoral dissertation, Structural Engineering Royal Institute of Technology).

Getachew, A., & O'Brien, E. J. (2007). Simplified site-specific traffic load models for bridge assessment. *Structure and Infrastructure Engineering*, *3*(4), 303–311. https://doi.org/10.1080/15732470500424245

Ghosn, M., Moses, F., & Wang, J. (2003). *Design of highway bridges for extreme events*. *NCHRP Report*. National Academy Press. Retrieved from https://trid.trb.org/view/645961

Ghosn, M., Sivakumar, B., & Moses, F. (2011). *Protocols for Collecting and Using Traffic Data in Bridge Design*. https://doi.org/10.17226/14521

Gindy, M., & Nassif, H. (2006). Compartison of traffic load models based on simulation and measuted data. In *Joint International Conference on Computing and Decision Making in Civil and Building Engineering*. Montreal. Retrieved from http://www.irbnet.de/daten/iconda/CIB21071.pdf

Gnedenko, B. (1943). Sur La Distribution Limite Du Terme Maximum D'Une Serie Aleatoire. *The Annals of Mathematics*, *44*(3), 423. https://doi.org/10.2307/1968974

Grave, Samuel. (2001). *Modelling of site-specific traffic loading on short to medium span bridges*. (Doctoral disseratation, Trinity College Dublin).

Grave, Sarah, O'Brien, E. J., & O'Connor, A. J. (2000). The Determination of Site-Specific Imposed Traffic Loadings on Existing Bridges. *The Fourth International Conference on Bridge Management*, (January).

Gumbel, E. J. (1935). Les valeurs extrêmes des distributions statistiques. *Annales de l'institut Henri Poincaré*, *5*(2), 115–158. Retrieved from http://www.numdam.org/item/AIHP_1935__5_2_115_0/

Handbook 2 - Reliability Backgrounds. (2005). Prague: Leonardo da Vinci Pilot Project CZ/02/B/F/PP-134007.

Harman, D. J., & Davenport, A. G. (1979). A statistical approach to traffic loading on highway bridges. *Canadian Journal of Civil Engineering*, *6*(4), 494–513. https://doi.org/10.1139/l79-063

Holický, M. (2009). *Reliability analysis for structural design* (Vol. 111). Stellenbosch: SUN MeDIA. https://doi.org/10.1192/bjp.111.479.1009-a

Holický, M., Diamantidis, D., & Sýkora, M. (2018). Reliability levels related to different reference periods and consequence classes. *Beton- Und Stahlbetonbau*, *113*, 22–26. https://doi.org/10.1002/best.201800039

Holický, M., Retief, J. V., & Sýkora, M. (2016). Assessment of model uncertainties for structural resistance. *Probabilistic Engineering Mechanics*, *45*(January 2016), 188–197. https://doi.org/10.1016/j.probengmech.2015.09.008

Iman, R. L., & Conover, W. J. (1982). A distribution-free approach to rank correlation. *Communications in Statistics - Simulation and Computation*. https://doi.org/10.1080/03610918208812265

ISO 13822. (2001). *Basis for design of structures - Assessment of existing structures*. Geneva: ISO.

ISO 2394. (2015). *ISO 2394:2015 - General Principles on Reliability for Structures*. *International Organization for Standardization*. https://doi.org/10.1007/s11367-011-0297-3

Jacob, B. (1991). Methods for the prediction of extreme vehicular loads and load effects on bridges. Report of Subgroup 8, Eurocode 1. Traffic Loads on Bridges. Paris, France LCPC.

Jacob, B., & Flint, A. R. (1996). Extreme traffic loads on road bridges and target values of their effects for code calibration. *IABSE*.

James, G. (2003). *Analysis of Traffic Load Effects on Railway Bridges*. (Doctoral dissertation, Structural Engineering Division Royal Institute of Technology).

JCSS. (2001). *Probabilistic Model Code*. Zurich: Joint Comittee of Structural Safety.

Kiureghian, A. (1989). Measures of structural safety under imperfect states of knowledge. *Journal of Structural Engineering*. Retrieved from http://ascelibrary.org/doi/abs/10.1061/(ASCE)0733-9445(1989)115:5(1119)

König, G., & Hosser, D. (1982). *The Simplified Level II Method and its Application on the Derivation of Safety Elements for level I.* Lausanne: CEB Bulletin: 147. International Federation for Structural Concrete.

Lenner, R. (2014). *Safety Concept and Partial Factors for Military Assessment of Existing Concrete Bridges*. (Doctoral dissertation, Universitat der Bunderwehr Munchen).

Lenner, R., de Wet, D. P. G., & Viljoen, C. (2017). Traffic characteristics and bridge loading in South Africa. *Journal of the South African Institution of Civil Engineering*, *59*(4), 34–46.

Lenner, R., & Sýkora, M. (2017). Partial factors for imposed loads in areas for storage and industrial use. *Structure and Infrastructure Engineering*, *13*(11), 1425–1436. https://doi.org/10.1080/15732479.2017.1285328

Lieberman, E. (1992). Traffic Simulation', Chapter in The Theory of Traffic Flow, Turner-Fairbank Highway Research Center, Federal Highway Administration, Eds. AK Rathi, CJ.

Lind, N. C., & Hasofer, A. M. (1974). An exact and invariant first order reliability format.

Journal Eng. Mech. Division (ASCE), *100*(July), 111–121. Retrieved from http://books.google.pt/books?id=wZfmSgAACAAJ

Madsen, H. O., Krenk, S., & Lind, N. C. (2006). Methods of structural safety, 407. Retrieved from https://books.google.co.za/books/about/Methods_of_Structural_Safety.html?id=e8sZjD7so-AC&redir_esc=y

Maljaars, J., Steenbergen, R., Abspoel, L., & Kolstein, H. (2012). Safety Assessment of Existing Highway Bridges and Viaducts. *Structural Engineering International*, *22*, 112–120. https://doi.org/10.2749/101686612X13216060213716

Marelli, S., & Sudret, B. (2014). UQLab: A Framework for Uncertainty Quantification in Matlab. In *Vulnerability, Uncertainty, and Risk: Quantification, Mitigation, and Management - Proceedings of the 2nd International Conference on Vulnerability and Risk Analysis and Management, ICVRAM 2014 and the 6th International Symposium on Uncertainty Modeling a*. https://doi.org/10.1061/9780784413609.257

Marková, J. (2013). Reliability Assessment of Traffic Load Models on Road Bridges. *IABSE Symposium Report*, *99*, 600–5. https://doi.org/10.2749/222137813806481446

MATLAB (R2017b). (2017). *The MathWorks Inc.* https://doi.org/10.1007/s10766-008-0082-5

Matsumoto, M., & Nishimura, T. (1998). Mersenne Twister : A 623-dimensionally equidistributed uniform pseudorandom number generator. *Discrete Mathematics*.

Minervino, C., Sivakumar, B., Moses, F., Mertz, D. R., & Edberg, W. (2003). New AASHTO Guide Manual for Load and Resistance Factor Rating of Highway Bridges. *Journal of Bridge Engineering*, *9*(1), 43–54. https://doi.org/10.1061/(asce)1084-0702(2004)9:1(43)

Moses, F., & Ghosn, M. (1985). A comprehensive study of bridge loads and reliability. Final report. Retrieved from https://trid.trb.org/view/274062

NEN8700. (2011). *Nederlands Normalisatie Instituut - Assessment of existing structures in case of reconstruction and disaproval - basic rules*. Nederlands Normalisatie Instituut.

NF-EN-1992-2. (2008). *Annexe Nationale. Eurocode 1 – Actions sur les structures – Partie 2: Actions sur les ponts, dues au trafic.* AFNOR. Retrieved from https://www.isba.fr/wp-content/uploads/2018/09/21-NF-EN-1991-2-NA.pdf

Nowak, A. S. (1993). Load model for highway bridges. *Structural Safety 13(1-2): 53-66.*

Retrieved from http://dl.acm.org/citation.cfm?id=717257

Nowak, A. S., Nassif, H., & DeFrain, L. (1993). Effect of Truck Loads on Bridges. *Journal of Transportation Engineering*, *119*(6), 853–867. https://doi.org/10.1061/(ASCE)0733-947X(1993)119:6(853)

O'Brien, E. J., & Caprani, C. C. (2005). Headway modelling for traffic load assessment of short to medium span bridges. Retrieved from http://hdl.handle.net/10197/2313

O'Brien, E. J., Caprani, C. C., & O'Connell, G. J. (2006). Bridge assessment loading: a comparison of West and Central/East Europe. *Bridge Structures*, *2*(1), 25–33. https://doi.org/10.1080/15732480600578451

O'Brien, E. J., Enright, B., & Getachew, A. (2010). Importance of the Tail in Truck Weight Modeling for Bridge Assessment. *Journal of Bridge Engineering*, *15*(2), 210–213. https://doi.org/10.1061/(ASCE)BE.1943-5592.0000043

O'Brien, E. J., O'Connor, A. J., & Arrigan, J. E. (2012). Procedures for calibrating Eurocode traffic Load Model 1 for national conditions, (August 2015), 2597–2603. https://doi.org/10.1201/b12352-397

O'Brien, E. J., Schmidt, F., Hajializadeh, D., Zhou, X. Y., Enright, B., Caprani, C. C., … Sheils, E. (2015). A review of probabilistic methods of assessment of load effects in bridges. *Structural Safety*, *53*, 44–56. https://doi.org/10.1016/j.strusafe.2015.01.002

O'Connor, A. J., Jacob, B., O'Brien, E. J., & Prat, M. (2011). Report of Current Studies Performed on Normal Load Model of EC1 Report of Current Studies Performed on Normal Load Model of EC1 Part 2 . Traffic Loads on Bridges, *5119*. https://doi.org/10.1080/12795119.2001.9692315

O'Connor, A. J., & O'Brien, E. J. (2005). Traffic load modelling and factors influencing the accuracy of predicted extremes. *Canadian Journal of Civil Engineering*, *32*(1), 270–278. https://doi.org/10.1139/l04-092

ONR Richtlinie 24008. (2014). *Bewertung der Tragfähigkeit bestehender Eisenbahn- und Straßenbrücken*. Strassenbrucken, Bewertung der Tragfahigkeit bestehender Eisenbahn - und.

Pérez Sifre, S., & Lenner, R. (2019). Bridge assessment reduction factors based on Monte Carlo routine with copulas. *Engineering Structures*, *198*(August), 109530.

https://doi.org/10.1016/j.engstruct.2019.109530

Pickands, J. (1975). Statistical inference usign extreme order statistics. *The Annals of Statistics*, *3*, 119–131.

Retief, J. V., Viljoen, C., & Holický, M. (2019). Standarized basis for assessment of existing structures. In *Advances in Engineering Materials, Structures and Systems* (pp. 779–780). Cape Town: Taylor & Francis.

Rice, S. O. (1945). Mathematical Analysis of Random Noise. *Bell System Technical Journal*, *24*(1), 46–156. https://doi.org/10.1002/j.1538-7305.1945.tb00453.x

Rubinstein, R. Y., & Kroese, D. P. (2016). *Simulation and the Monte Carlo Method*. Hoboken, NJ, USA: John Wiley & Sons, Inc. https://doi.org/10.1002/9781118631980

Rücker, P. W., Hille, D. F., & Rohrmann, D. R. (2006). F08a Guideline for the Assessment of Existing Structures. Berlin: SAMCO.

SAMARIS. (2006). State of the art report on the assessment of structures in selected EEA and CE countries. Brussels: Sustainable and Advanced Materials for Road Infrastructure.

SANS-10160-1. (2009). *Part 1: Basis of structural design*. South African Bureau of Standards.

SIA 269 - 269/8. (2011). *Grundlagen der Erhaltung von Tragwerken,*. Zurich: Schweizerischer Ingenieur - und Architekten Verein.

Sklar, M. (1959). *Fonctions de Répartition a N Dimensions Et Leurs Marges*. Université de Paris.

Soriano, M., Casas, J. R., & Ghosn, M. (2016). Simplified probabilistic model for maximum traffic load effect from weight-in-motion data. *Structure and Infrastructure Engineering*, 1–39.

Srinivas, S., Menon, D., & Prasad, A. M. (2005). Modelling of highway traffic for bridges in India. Retrieved from https://abdn.pure.elsevier.com/en/publications/modelling-of-highway-traffic-for-bridges-in-india

Srinivas, S., Menon, D., & Prasad, A. M. (2006). Multivariate Simulation and Multimodal Dependence Modeling of Vehicle Axle Weights with Copulas. *Journal of Transportation Engineering*, *132*(12), 945–955. https://doi.org/10.1061/(ASCE)0733-947X(2006)132:12(945)

Stathopoulos, A., & Karlaftis, M. (2001). Temporal and Spatial Variations of Real-Time Traffic Data in Urban Areas. *Transportation Research Record: Journal of the Transportation Research Board*, *1768*(1), 135–140. https://doi.org/10.3141/1768-16

Steenbergen, R., & Vrouwenvelder, A. (2010). Safety philosophy for existing structures and partial factors for traffic loads on bridges. *Heron*, *55*(2), 123–140.

Sýkora, M., & Holický, M. (2011). Target reliability levels for assessment of existing structures. *Applications of Statistics and Probability in Engineering*, 1048–1056.

Sýkora, M., Holický, M., Lenner, R., & Maňas, P. (2014). Target reliability levels for existing bridges considering emergency and crisis situations. *Advances in Military Technology*, *9*(1), 45–57.

Sýkora, M., Holický, M., & Marková, J. (2013). Verification of existing reinforced concrete bridges using the semi-probabilistic approach. *Engineering Structures*, *56*, 1419–1426. https://doi.org/10.1016/j.engstruct.2013.07.015

TMH -7. (1981). *Parts 1 and 2: Code of Practice for the Design of Highway Bridges and Culverts in South Africa*. Pretoria: Deparment of Transport. https://doi.org/ISBN 0 7988 2158 2

TMH 14. (2013). *South African Standard Automatic Traffic Data Collection Format Version 3.00*. Pretoria: The South African National Roads Agency Limited. Retrieved from www.nra.co.za/content/TMH14 (2013) TrafData.pdf

TMH 3. (2013). *Specifications for the Provision of Traffic and Weigh-in-Motion Monitoring Service*. Pretoria: The South African National Roads Agency Limited.

TMH 8. (2014). *Traffic and Axle Load Monitoring Procedures*. Pretoria: The South African National Roads Agency Limited.

TRH-11. (2009). *Dimensional and mass limitations and other requirements for abnormal loadTransport, Department of vehicles*. Pretoria: Department of Transport.

Val, D. V., & Stewart, M. G. (2002). Safety factors for assessment of existing structures. *Journal of Structural Engineering*, *128*(2), 258–265. https://doi.org/10.1061/(ASCE)0733-9445(2002)128:2(258)

van der Spuy, P. F., & Lenner, R. (2018). Developing a new bridge live load model for South

Africa. In *Proceedings of the Ninth International Conference on Bridge Maintenance, Safety and Management (IABMAS 2018)*. Melbourne.

van der Spuy, P. F., & Lenner, R. (2019). Towards a New Bridge Live Load Model for South Africa. *Structural Engineering International*, *29*(2), 292–298. https://doi.org/10.1080/10168664.2018.1561168

van der Spuy, P. F., Lenner, R., de Wet, D. P. G., & Caprani, C. C. (2019). Multiple lane reduction factors based on multiple lane weigh in motion data. *Structures*, *20*(April), 543–549. https://doi.org/10.1016/j.istruc.2019.06.001

Verkehr, B. für. (2011). *Bau und Stadtentwicklung - Abteilung Strassenbau*. (Nachrechnungsrichtlinie), Richtlinie zur Nachrechnung von Strassenbrücken im Bestand.

Vrouwenvelder, A., & Waarts, P. H. (1993). Traffic Loads on Bridges. *Structural Engineering International*, *3*(3), 169–177. https://doi.org/10.2749/101686693780607796

Wisniewski, D. F., Casas, J. R., & Ghosn, M. (2012). Codes for safety assessment of existing bridges-current state and further development. *Structural Engineering International: Journal of the International Association for Bridge and Structural Engineering (IABSE)*, *22*(4), 552–561. https://doi.org/10.2749/101686612X13363929517857

Zhou, X. Y., Schmidt, F., & Jacob, B. (2012). Extrapolation of traffic data for development of traffic load models: Assessment of methods used during background works of the Eurocode. *Bridge Maintenance, Safety, Management, Resilience and Sustainability - Proceedings of the Sixth International Conference on Bridge Maintenance, Safety and Management*, 1503–1509. Retrieved from https://www.scopus.com/inward/record.url?eid=2-s2.0-84863910210&partnerID=40&md5=9f55301396367add6bfbba56aa7d0508

Zhou, X. Y., Schmidt, F., & Jacob, B. (2016). A Mixture Peaks over Threshold Approach for Predicting Extreme Bridge Traffic Load Effects. *Probabilistic Engineering Mechanics*, *43*, 121–131. Retrieved from https://hal.archives-ouvertes.fr/hal-01498789/document

Zilch, K. (2001). *Handbuch für Bauingenieure : Technik, Organisation und Wirtschaftlichkeit ; Fachwissen in einer Hand*. Berlin: Springer.

Appendix A

A.1 Vehicle classes and axle spacings

The general properties of the vehicles and axle spacings have been explained previously. All the histograms and geometries not shown before and found hereafter.

- **Two-axle vehicles:** the third largest class recorded, although with a small number of records compared to six- and seven-axle vehicles. The common geometry of two-axle vehicles is shown in Figure A.1. The histogram of the axle spacing does not present any specific shape and cannot be modelled with a probability distribution.

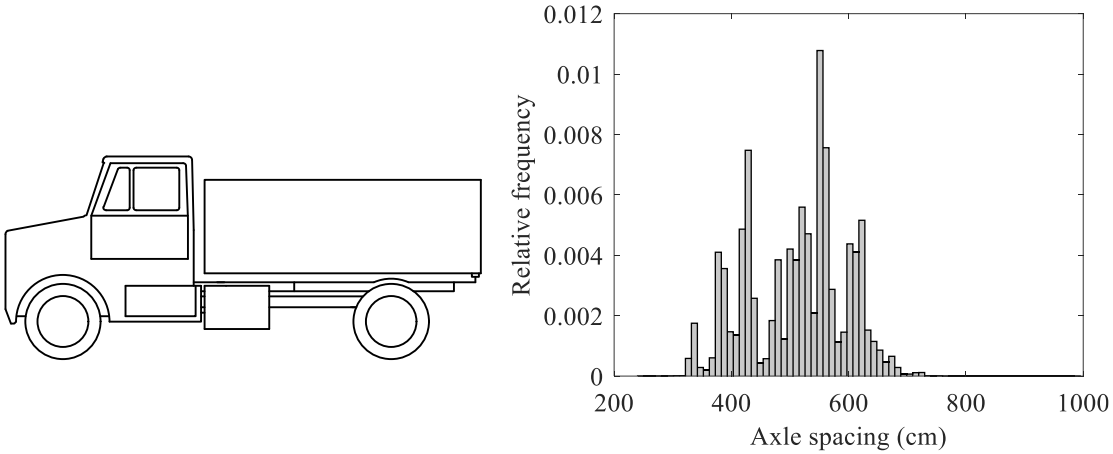

Figure A.1. Two axle-truck geometry and axle spacing.

- **Three-axle vehicles:** the vehicle geometry consists of a front single axle and a rear tandem as shown in Figure A.2. The first axle spacing does not present any specific shape and has high variability and the second axle spacing is located around 1.35 m as expected for a tandem.

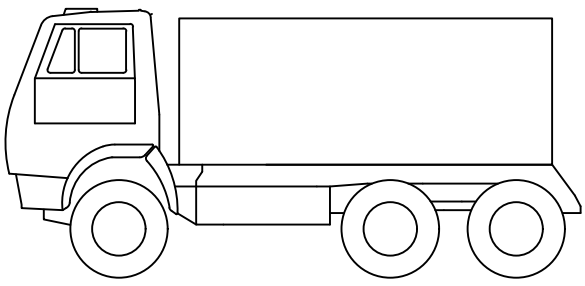

Figure A.2. Three-axle truck geometry.

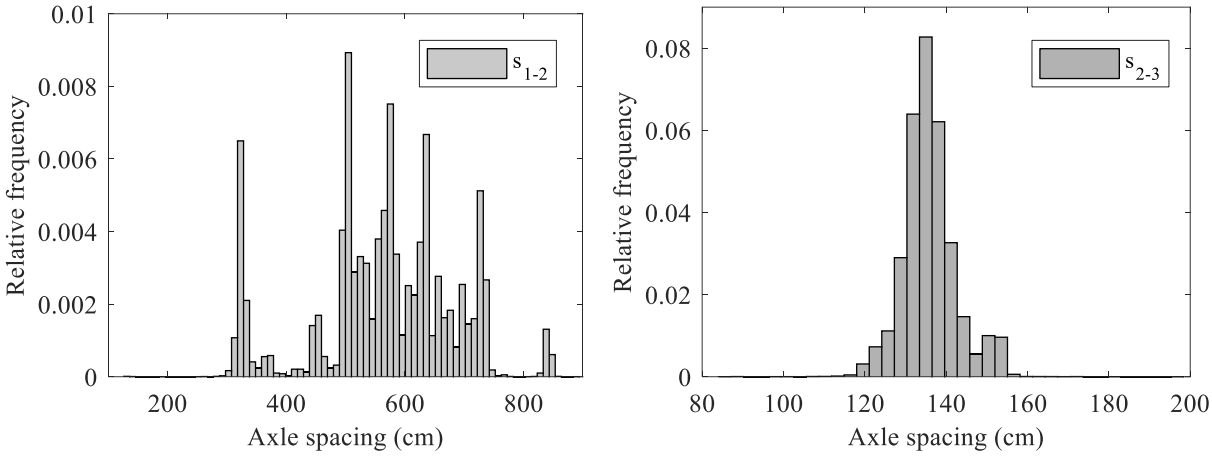

Figure A.3. Axle spacing – three axle vehicles.

- **Four-axle vehicles:** this vehicle geometry consists of two first single axles and a rear tandem as shown in Figure A.4. Except for the more constant distance in the tandem, the first and second axle spacing are high variable.

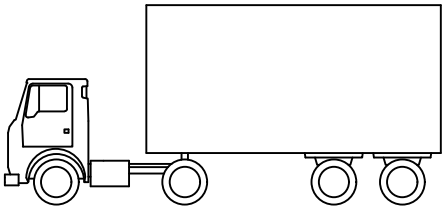

Figure A.4. Four-axle truck geometry.

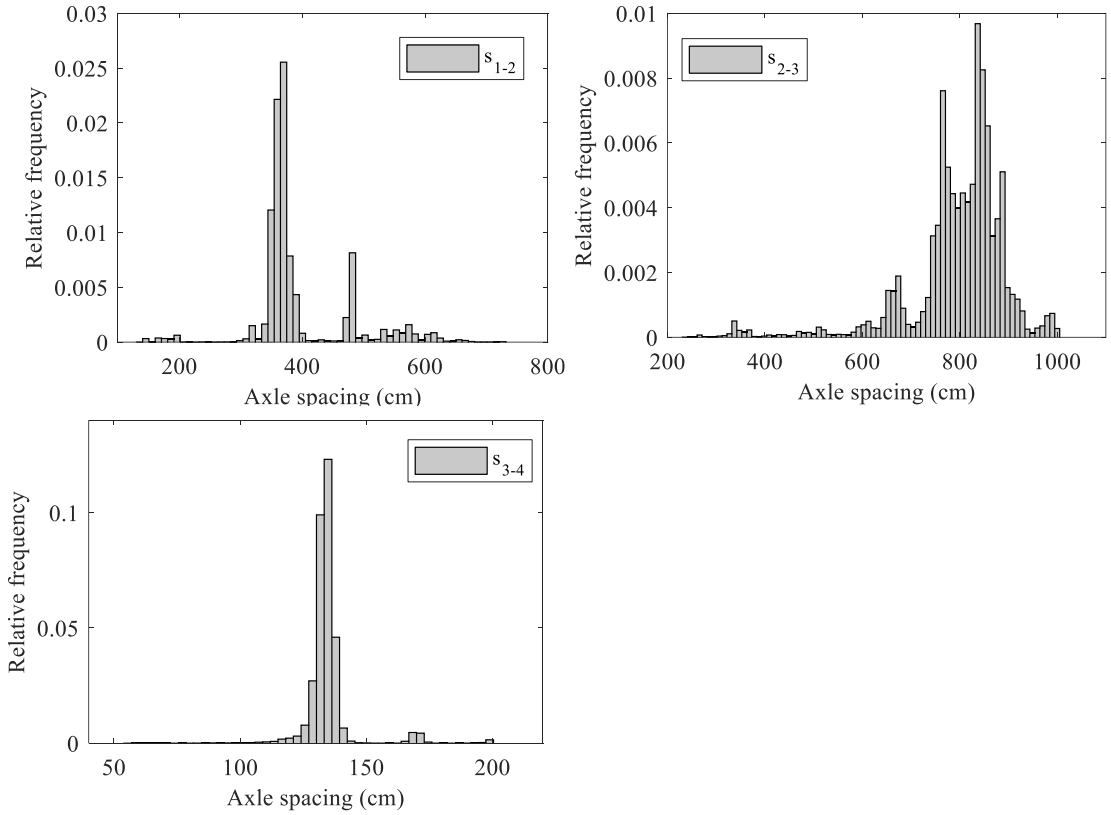

Figure A.5. Axle spacing - four-axle truck.

- **Five axle vehicles:** these vehicles consist of a truck tractor with a single axle, a tandem, and a second rear tandem a shown in Figure A.6. Spacing between tandems are around 1.35 m as observed previously. The first spacing in the truck tractor shows two peaks (two models of truck tractors) and the third axle presents high variation, caused by different types of trailers used.

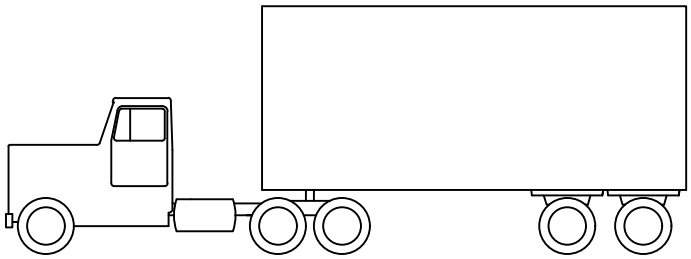

Figure A.6. Five-axle truck geometry.

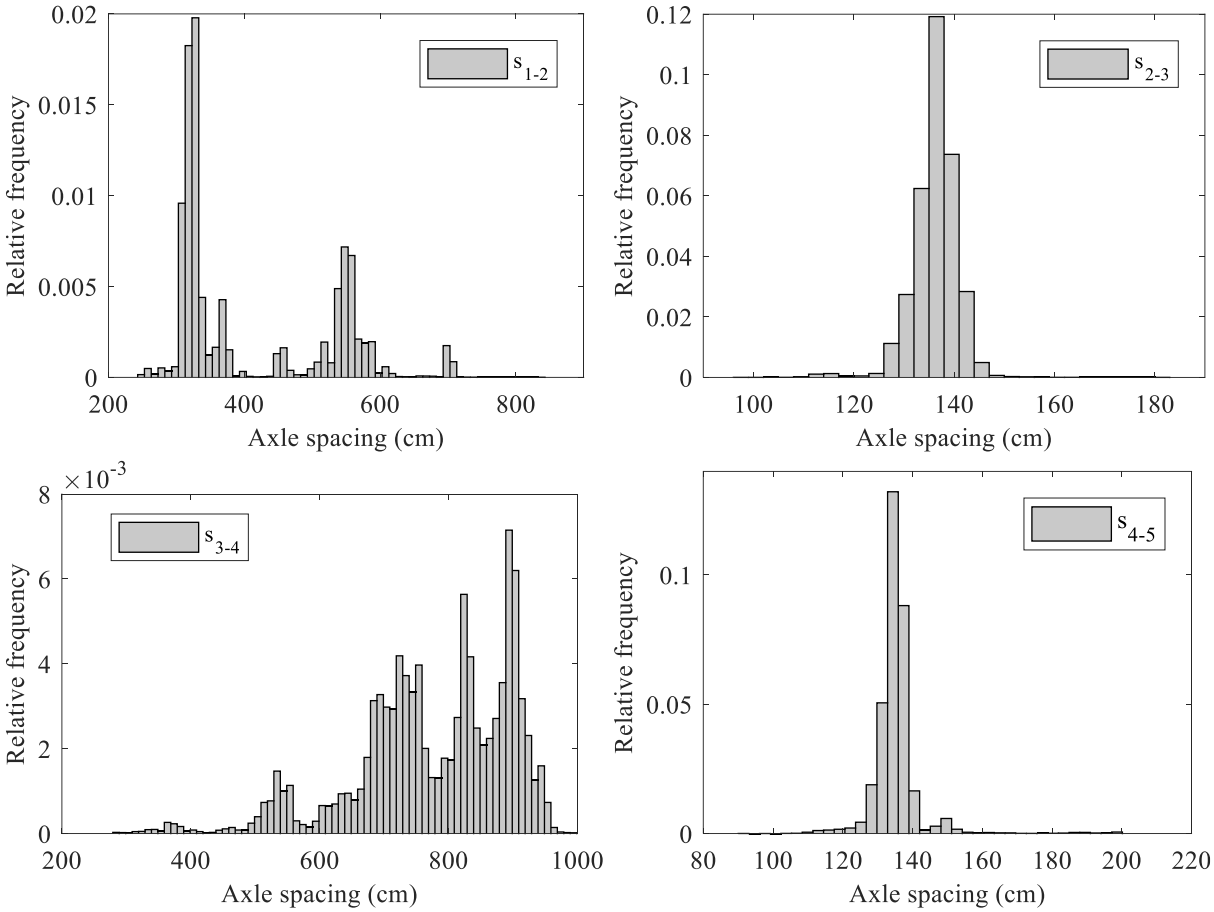

Figure A.7. Axle spacing – five-axle vehicles.

- **Six axle vehicles** are those vehicles formed by truck tractor of single axle and read tandem plus one tridem at the back of the vehicle (Figure A.8). In larger vehicles the axle spacing are observed around specific values. A reduced number of manufacturers produce these type of vehicles and trailers.

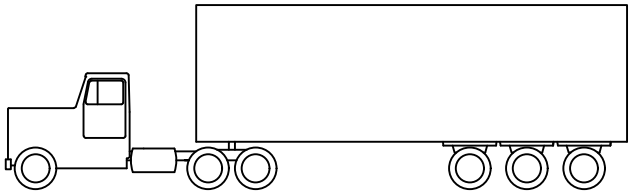

Figure A.8. Six-axle truck geometry.

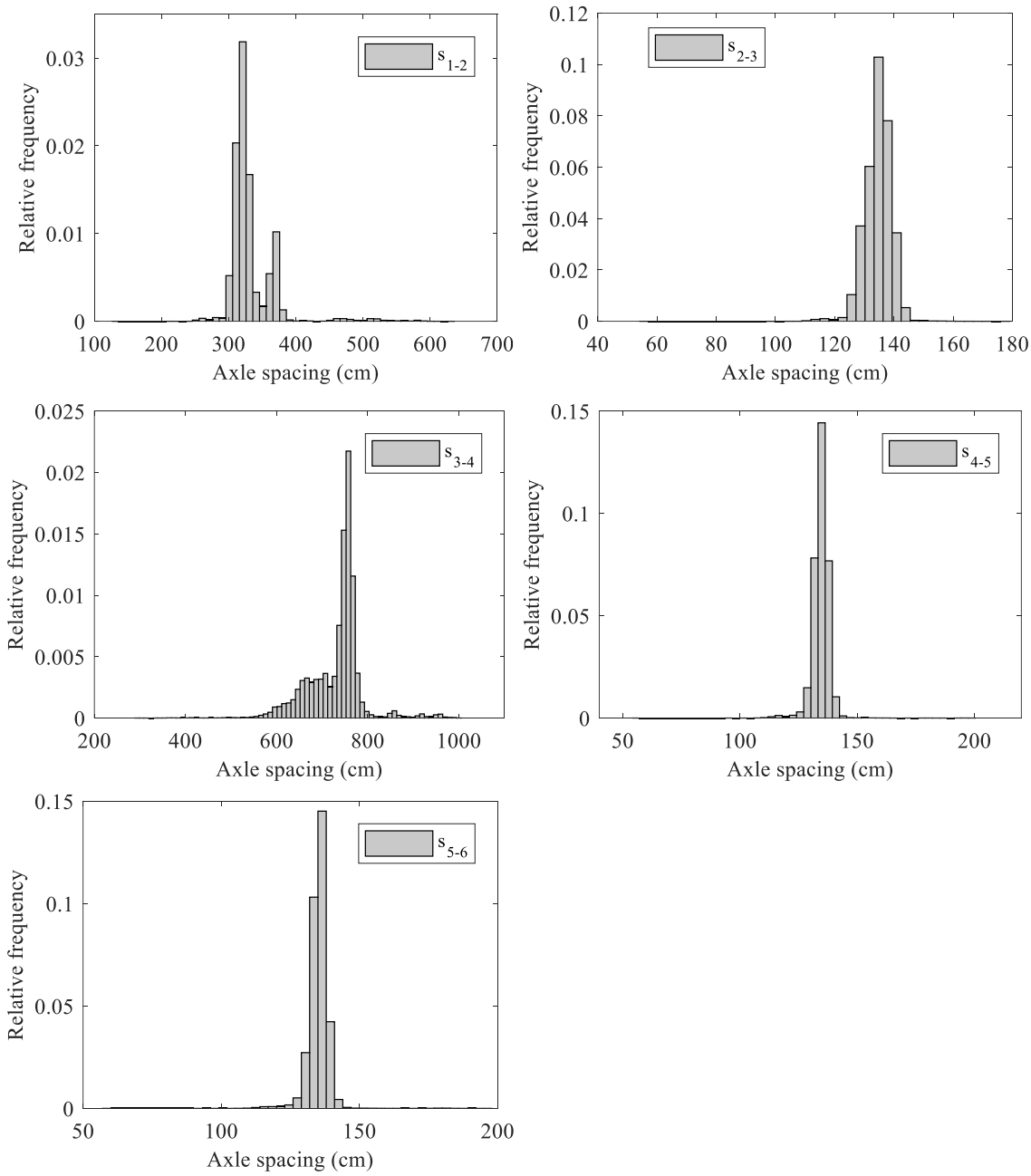

Figure A.9. Axle spacing – six-axle vehicles.

- **Seven-axle vehicles** are those vehicles that consist of the truck tractor and two rear tandems as shown in Figure A.10. The location of spacings around specific values is also observed here.

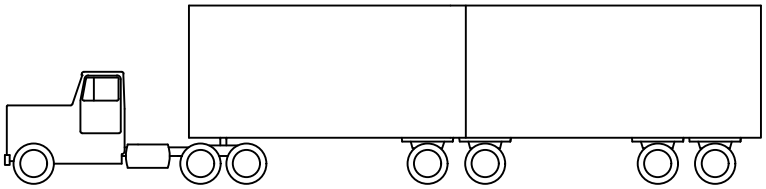

Figure A.10. Seven-axle truck geometry.

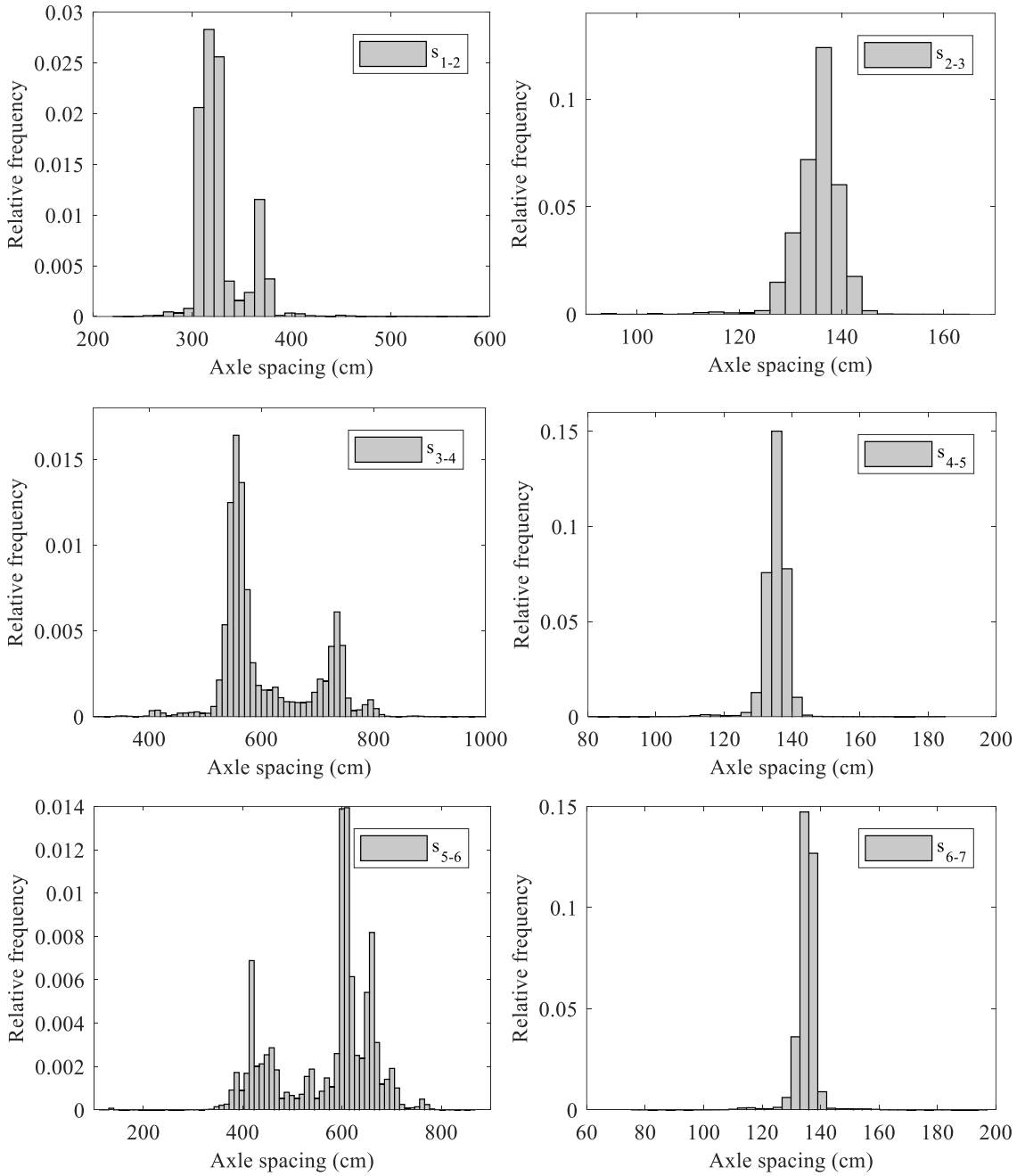

Figure A.11. Axle spacing – seven-axle vehicles.

- **Eight axle vehicles:** the vehicle geometry consists of the typical truck tractor plus one tridem and one tandem. Spacings remain relatively constant as observed before in large vehicles.

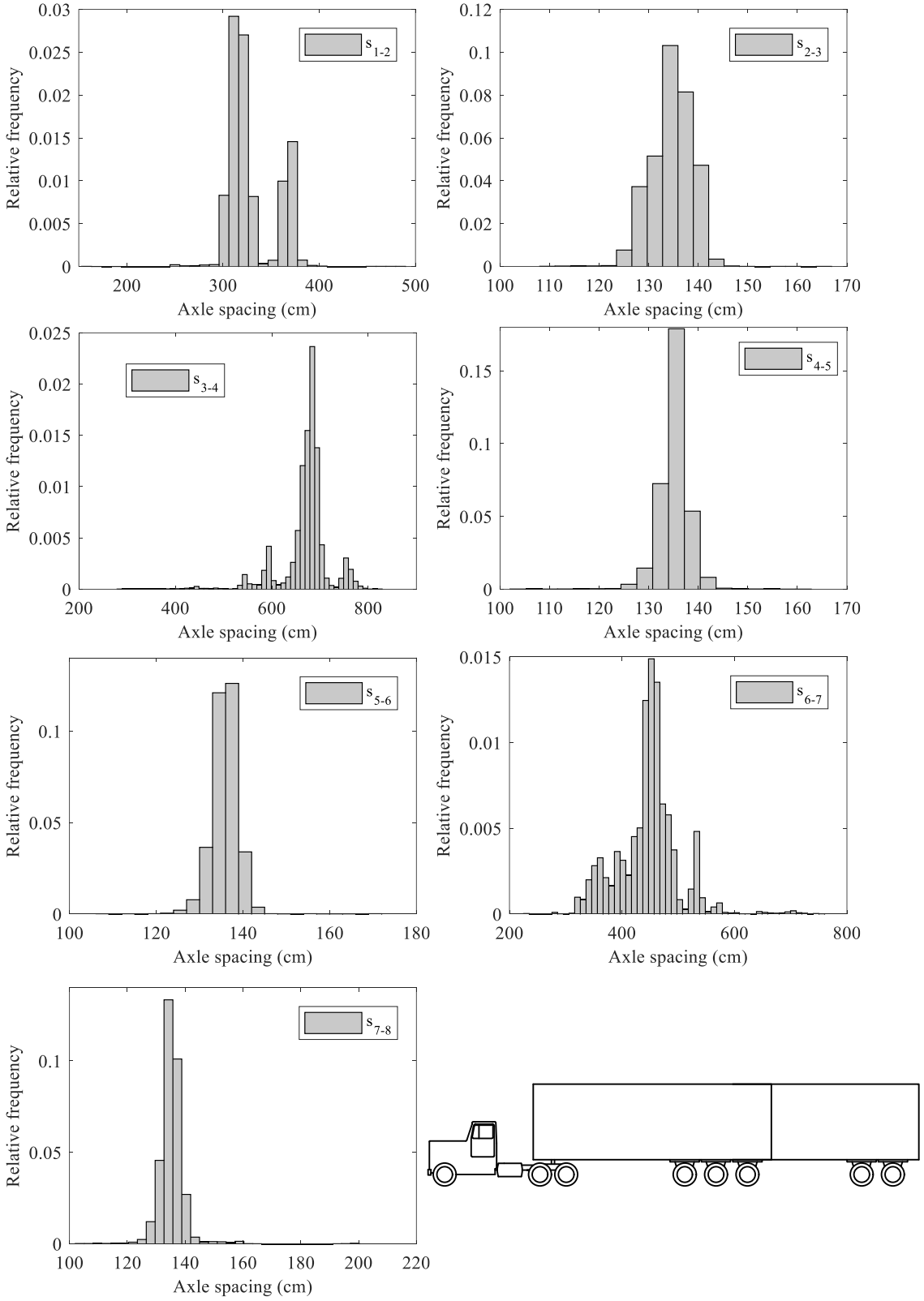

Figure A.12. Axle spacing and truck geometry – eight-axle vehicles.

A.2 Vehicle loads

- **Two-axle vehicles:** GVW varies from a minimum of 3.5 t (value imposed by the filtering criteria), to a maximum of 21 t, with most of the vehicles weighting between 4 t and 12 t. The histogram of GVW does not present a bimodal shape. This suggests that either trucks are usually circulating loaded or there is not a clear difference in weight between loaded and unloaded vehicles. Both axle loads present a minimum of 0.9 t, while the maximum for the first axle is 9.4 t and for the second axle 15.1 t. This is logical since the goods are usually located at the back of the vehicles, thus increasing the load supported by the rear axle. Legal limits are indicated with a black vertical line.

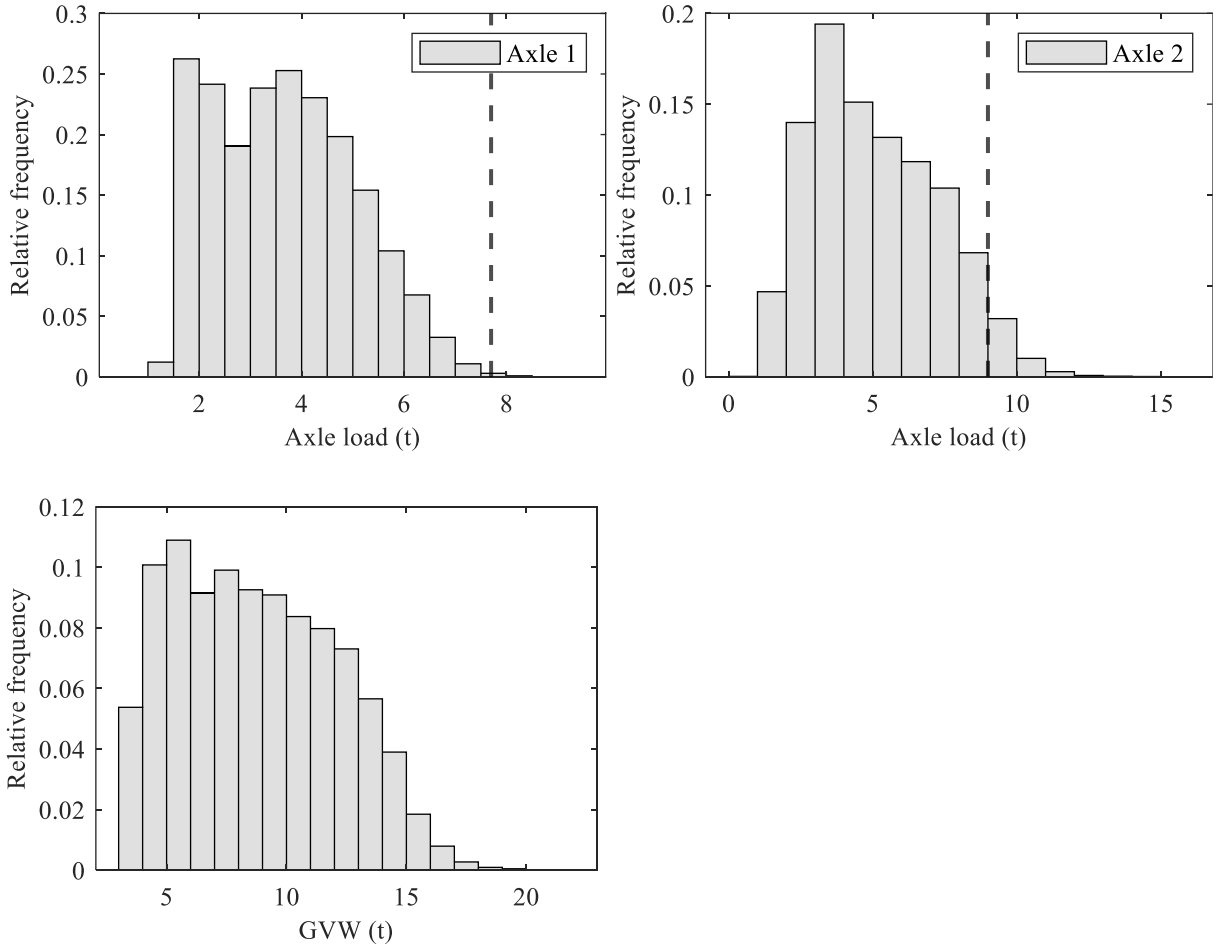

Figure A.13. Histograms of axle loads and GVW – two-axle vehicles.

- **Three-axle vehicles:** The GVW is clearly bimodal, with a first peak around 9 t and a second peak around 20 t corresponding to the peaks of the unloaded and the loaded population of vehicles respectively. Minimum GVW is 3.5 t, value again forced by the filtering criteria, and a maximum of 33.5 t. Front axle weight varies from 0.9 t to 10.9 t

with a unimodal distribution and peak around 6 t, similar values to the two-axle vehicle front axle. Individual axle weights in the tandem vary from 0.9 t to 13 t. The combination of both axles varies from 2 t to 25 t with a clear bimodal distribution. The first peak is located around 4 t and a second peak around 14 t. Slight overloading of axles loads is observed.

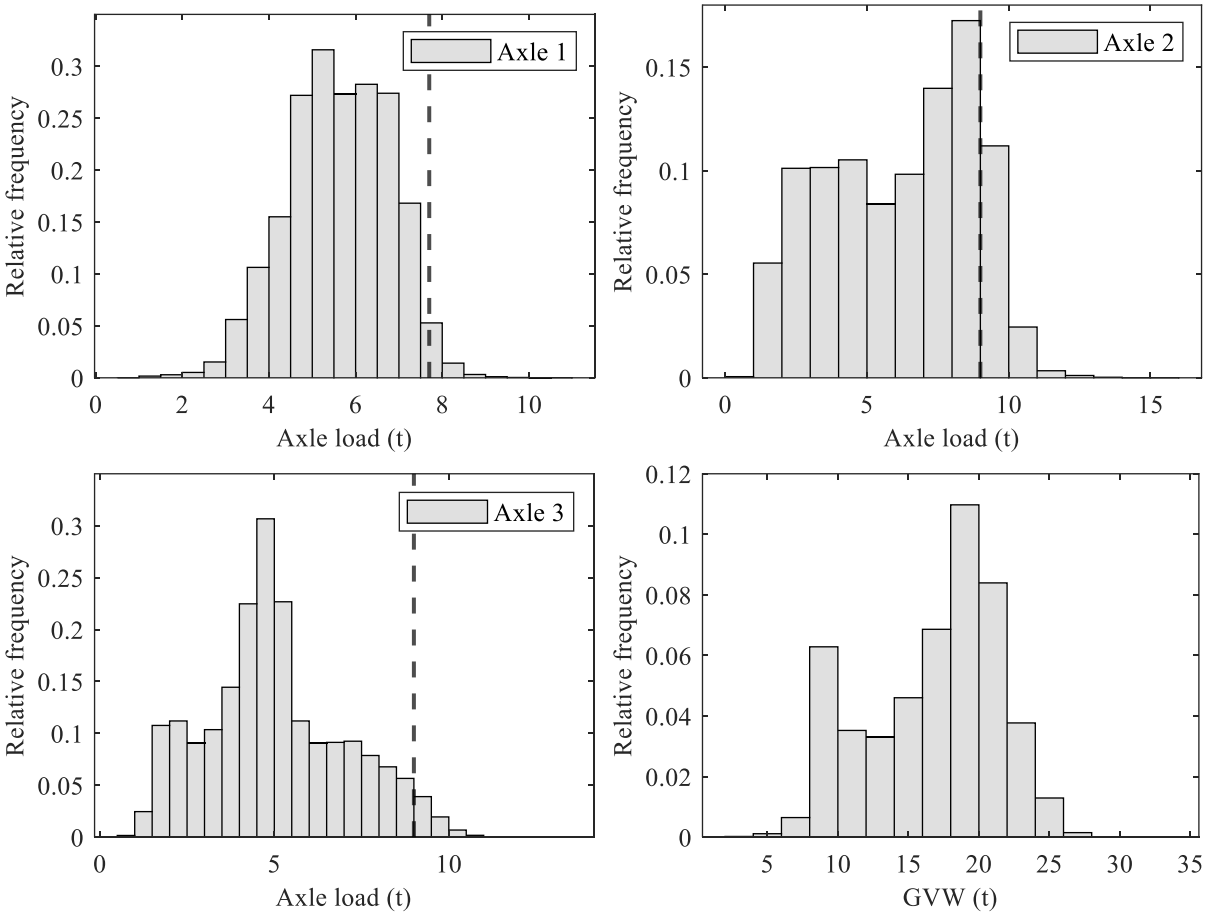

Figure A.14. Histograms of axle loads and GVW - three-axle vehicles.

- **Four-axle vehicles:** The GVW is clearly unimodal with a minimum of 4 t and a maximum of 40 t. All axle loads are unimodal as well. All of them present a minimum weight of 0.9 t and a maximum weight around 14 t except for the first axle that carries less weight and the maximum is around 8.6 t. Peak values are located between 6 t and 7 t, slightly less for the first axle. The tandem weight is between 1.8 t and 23.6 t with a peak at 12 t.

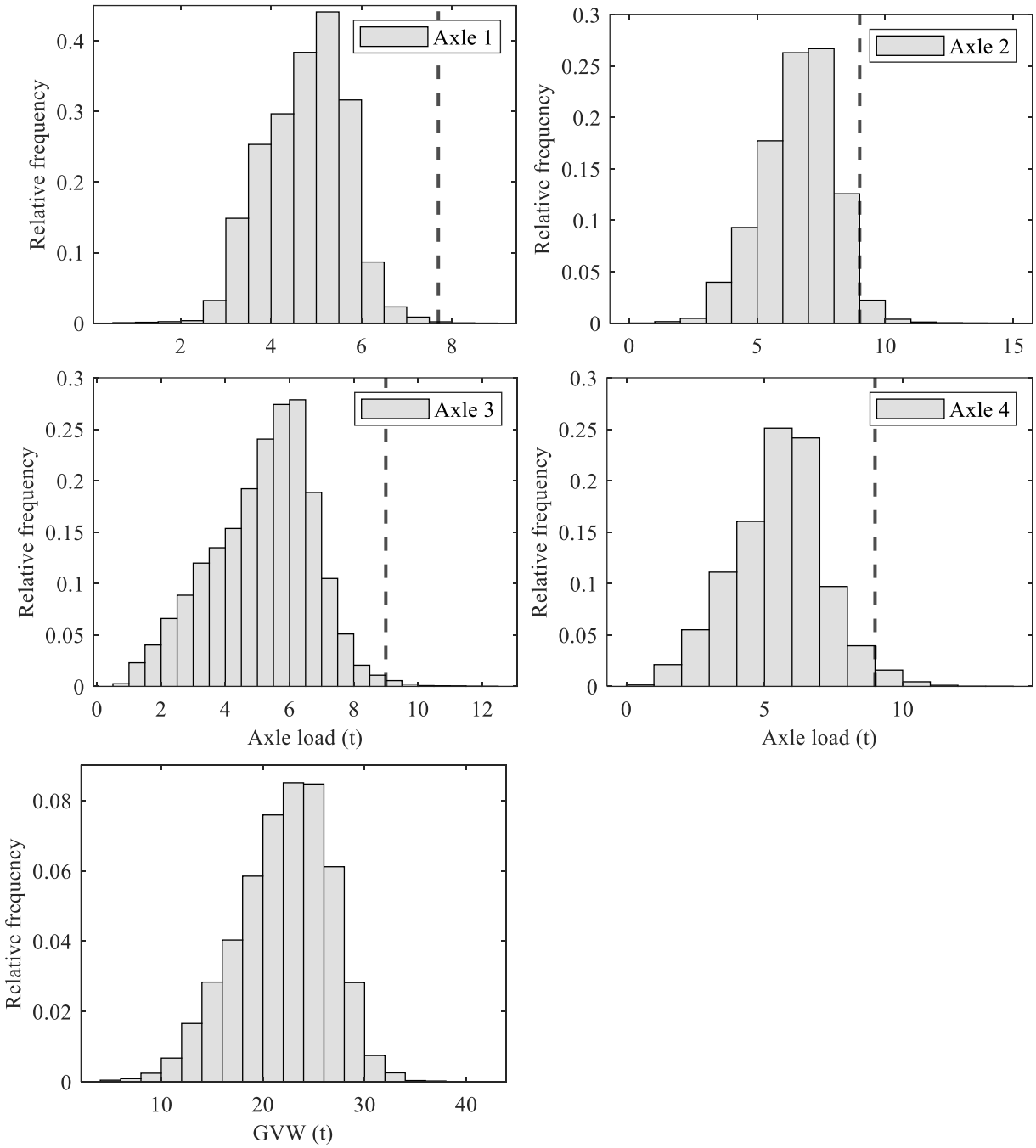

Figure A.15 Histograms of axle loads and GVW - four-axle vehicles.

- **Five axle vehicles:** GWV values lie between 7 t and 56 t, which is the maximum legal GVW in the country. The histogram of GVW presents a main peak around 33 t and two lower peaks at 18 t and 25 t. Front axle weight is unimodal with a minimum of 1 t and a maximum of 9 t with most of the values at 6 t. The rest of the individual axle loads are between 0.8 t and 14 t. Second axle is bimodal with peaks at 4 t and 7 t and third axle is unimodal showing a peak at 5 t. Rear two axles are trimodals with the highest at 6 t and the two lowest and 2.3 t and 0.9 t. Both tandems present values between 2 t and 25 t.

The first tandem present a clear peak at 14 t and the second tandem is trimodal with main peak at 13 t and two lower peak at 2 t and 5 t. The first tandem presents more stable values since it is more influenced by the weight of the truck tractor, however, the second tandem presents different peaks showing loaded and unloaded vehicles.

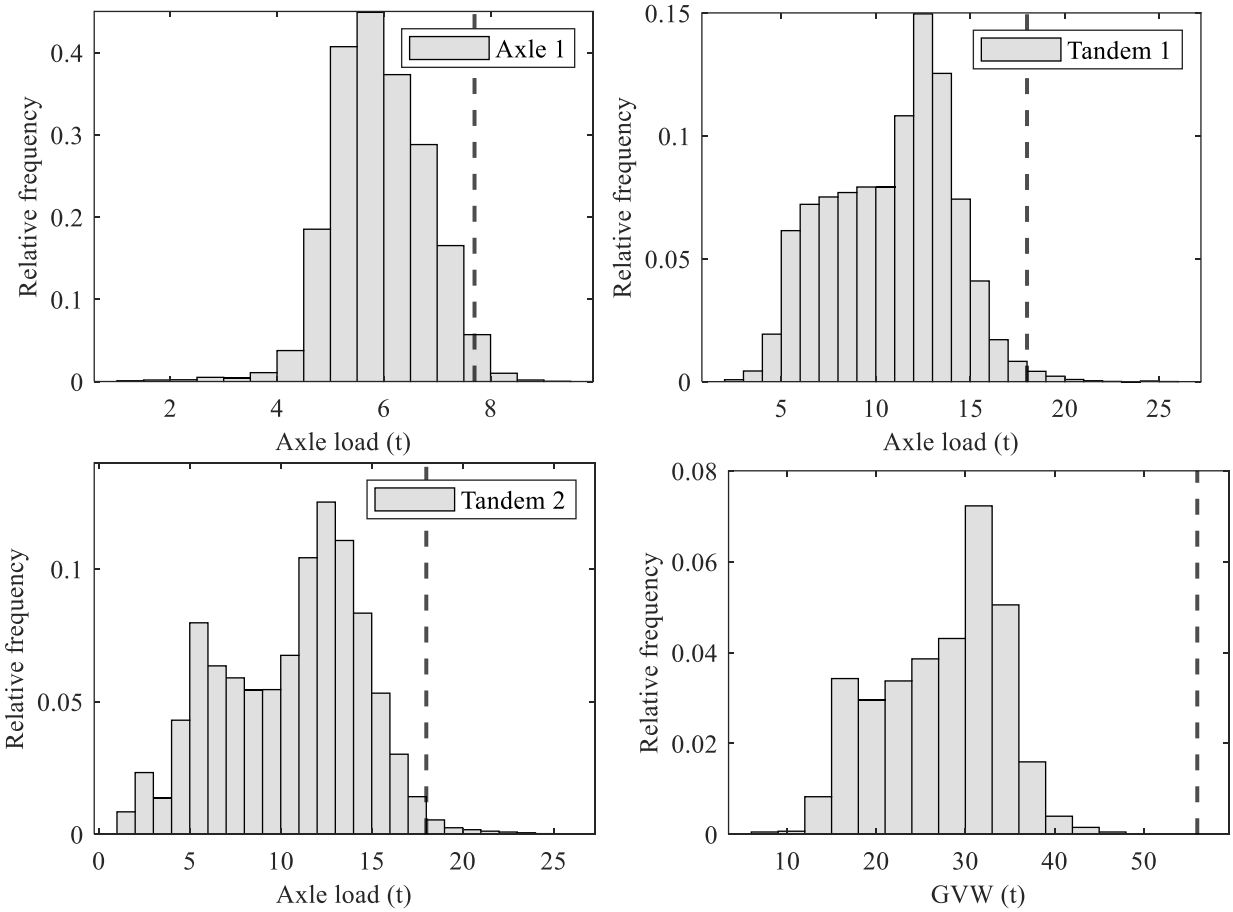

Figure A.16 Histograms of axle loads and GVW - five-axle vehicles.

- **Six axle vehicles** are those vehicles formed by truck tractor of single axle and read tandem plus one tridem at the back of the vehicle. The GVW recorded are between 8.1 t and 72.8 t. Distribution is bimodal with a clear peak at 46 t and a second peak around 30 t. Front single axle presents unimodal distribution with minimum of 1 t maximum of 10 t and most of the values around 6 t. The rest of the recorded single axles present minimum values of 0.8 t and maximums located around 15 t. Distributions are not clearly bimodal since the threshold between unloaded and loaded is not defined. The main peak is found at 7 t. The tandem weight lies between 2 t and 27 t with a peak at 17 t and the minimum tridem recorded is 3 t while the maximum is 41.7 t with a peak at 21 t.

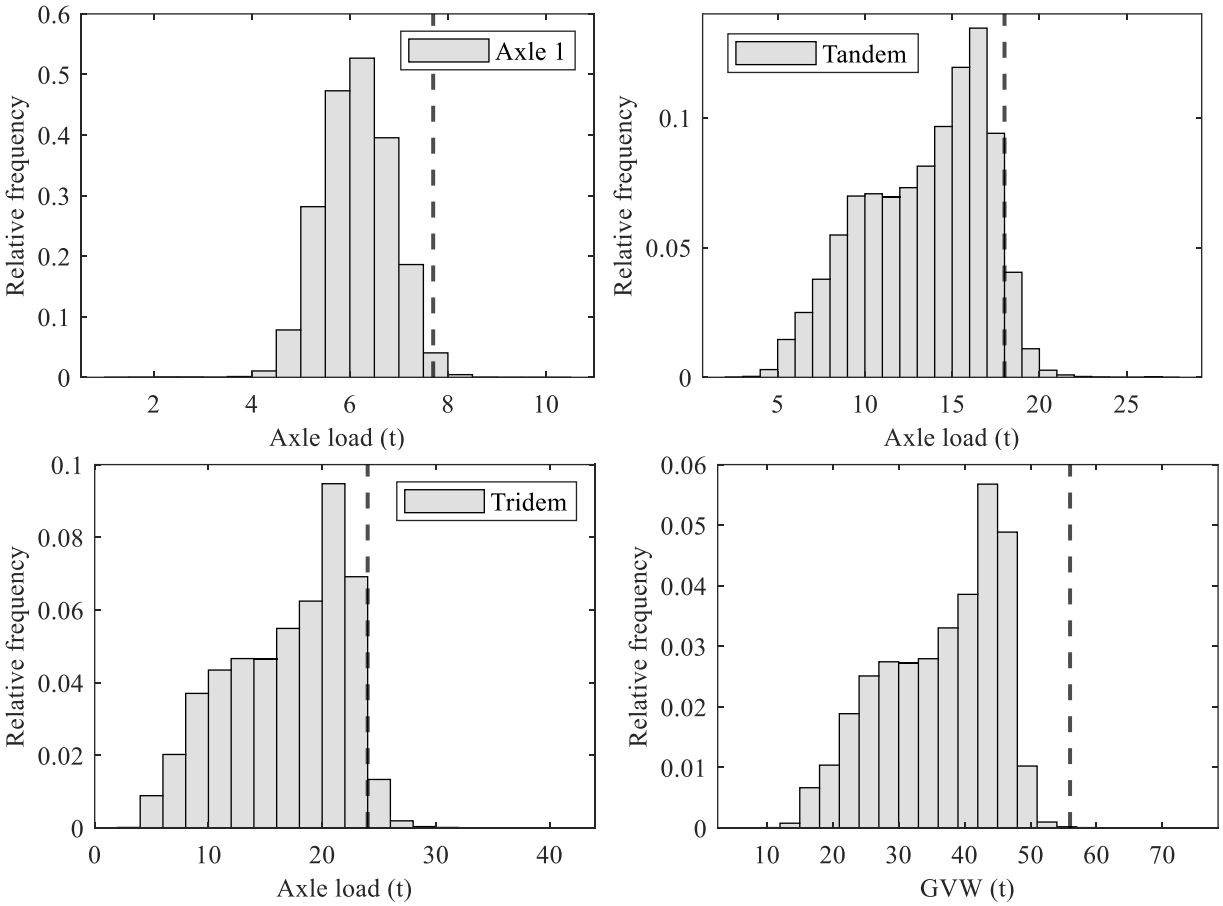

Figure A.17. Axle loads and GVW – six-axle vehicles.

- **Seven-axle vehicles** are those vehicles that consist of the truck tractor and two rear tandems. The GVWs recorded are from 9.2 t to 82 t. This shows a clear overloading of these larger vehicles. The histogram of GVW shows an important peak at 50 t. From this it can be inferred that most of the trucks are loaded while a few are unloaded since there is not a clear peak at lower weights. The single axle in the truck tractor again presents a unimodal shape with a peak value of 6 t. Minimum and maximum values of the rest of the axles are between 0.8 t and 15 t, similar values as the ones mentioned before. Distributions present an important peak at 7.5 t, while the lower peak is not clear since the number of unloaded vehicles is quite low. Tandems present values between 1.7 t and 29.7 t. Distributions are very similar with a significant peak at 15 t that represents the loaded tandems.

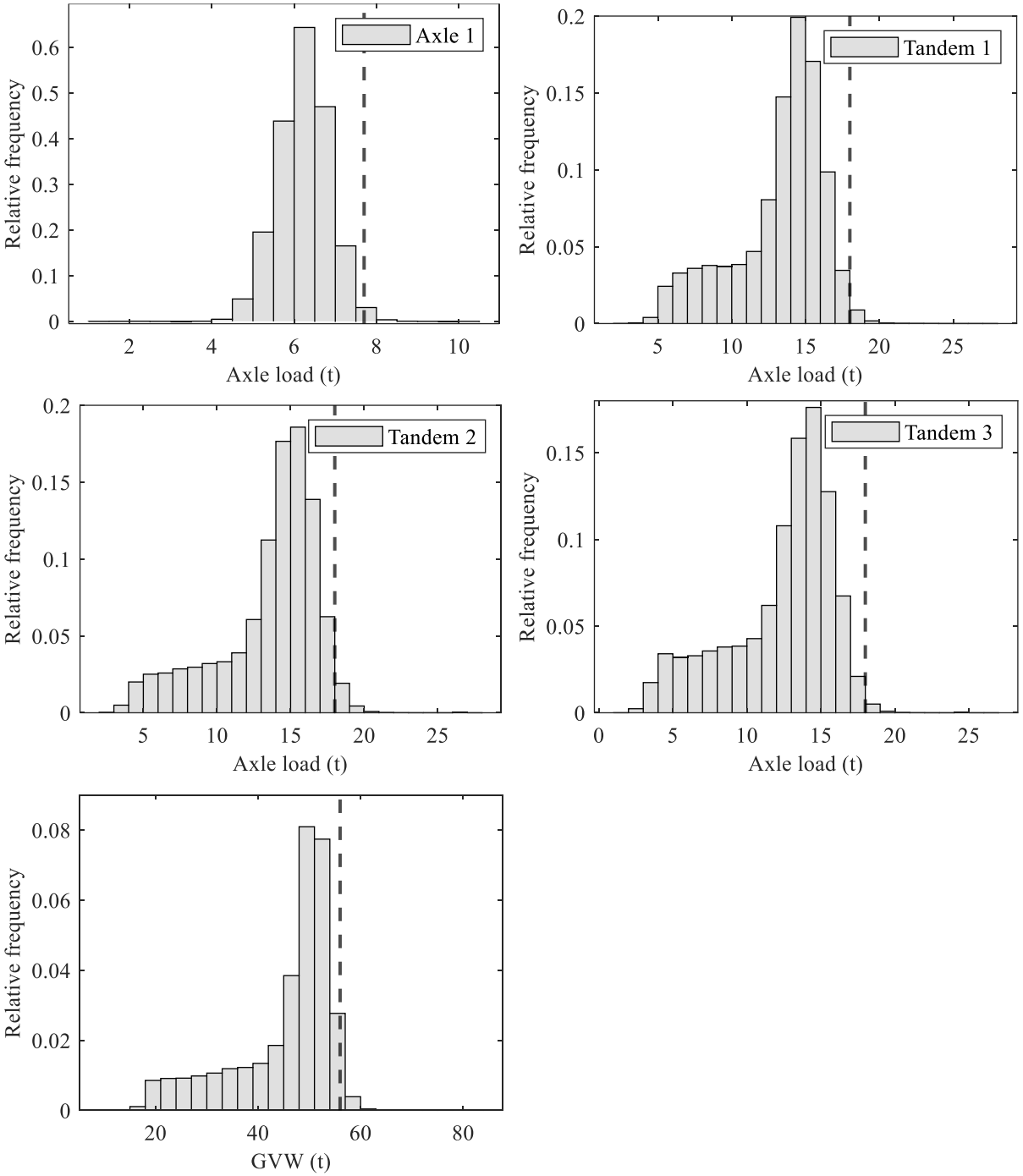

Figure A.18. Axle loads and GVW – seven-axle vehicles.

- **Eight axle vehicles:** the vehicle geometry consists of the typical truck tractor plus one tridem and one tandem. Recorded vehicular loads have a minimum value of 17.2 t and a maximum of 90.7 t. The distribution is bimodal with a small peak of unloaded vehicles at 22 t and a large peak of loaded vehicles at 52 t. Individual axles present weights between 0.9 t and 12 t and 13 t for the last axle. These values are slightly lower than for other vehicle classes but logical since the vehicle weight is distributed among more axles. First axle records have a minimum of 1 t and a maximum of 10 t with the peak at

6 t. Axles from 2 to 6 present bimodal distributions with a short peak at 2.5 t and a large peak at 6 t. The seventh- and eight-axle histogram of loads present a larger lower peak, however, the bimodal shape is not clearly visible. Semi-loaded vehicles tend to locate the goods in the central axles thus unloading the rear axle. This increases the unloaded part of this histogram. The first tandem presents a minimum weight of 2.6 t and a maximum of 22.3 t. Bimodal distribution with a low peak at 5.6 t and large peak at 14.5 t. The rear tandem minimum of 2.2 t and maximum of 24.2 t. As happened with its individual axle load the lower peak is larger, which is a consequence of a higher percentage of unloaded axles. The tridem has a minimum recorded value of 4 t and a maximum of 35.1 t. Distribution is bimodal with a peak at 7.5 t and a larger peak at 21 t.

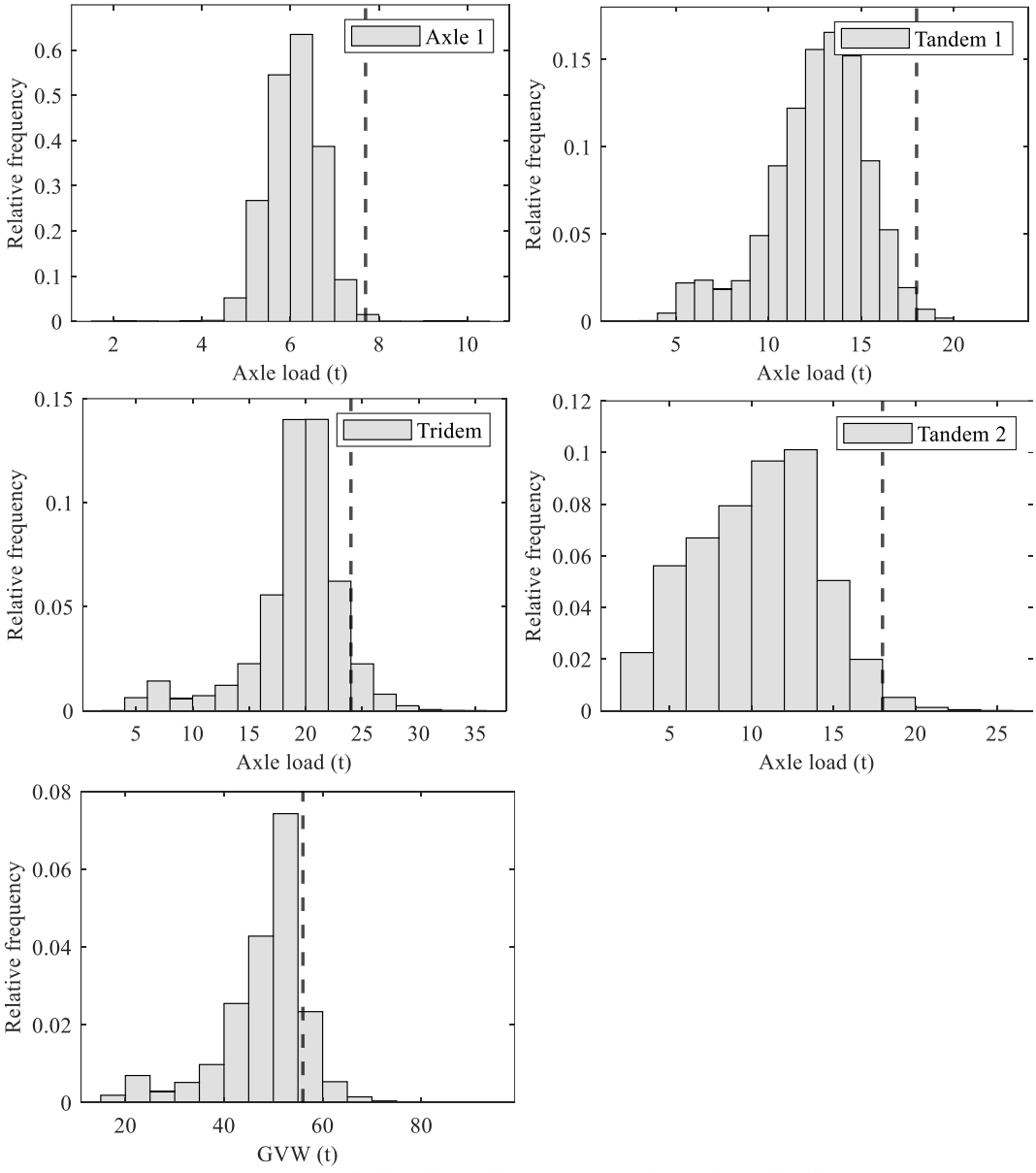

Figure A.19. Axle loads and GVW – eight-axle vehicles.

A.3 Generated and recorded axle load-GVW structure

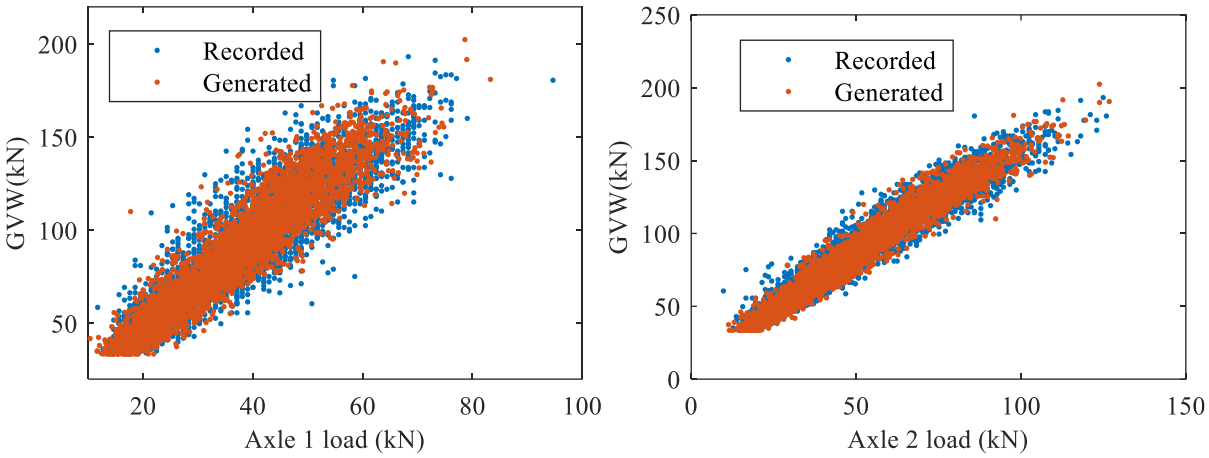

Figure A.20. Scatter plots of generated and recorded axle load-GVW – two-axle vehicles.

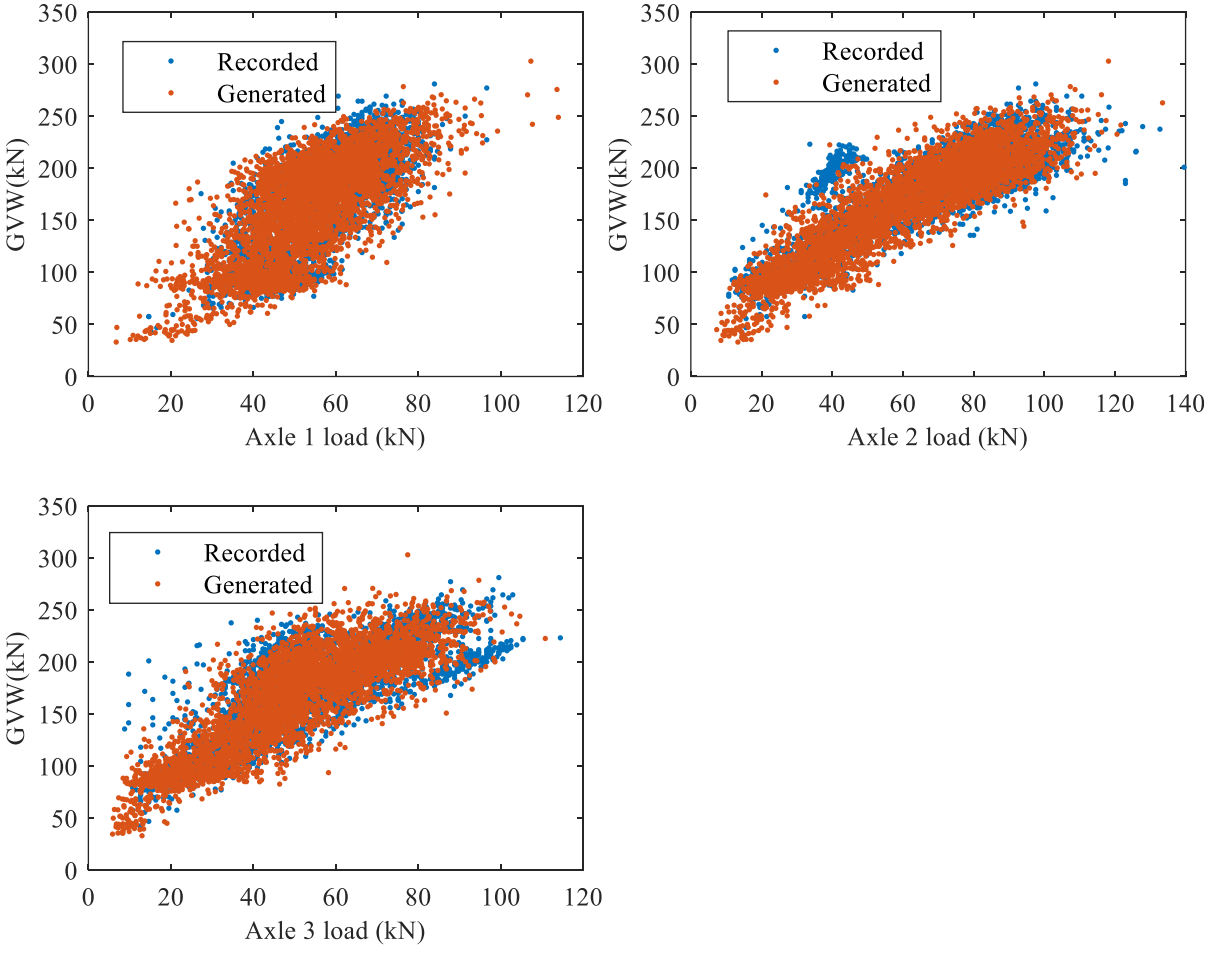

Figure A.21. Scatter plots of generated and recorded axle load-GVW – three-axle vehicles.

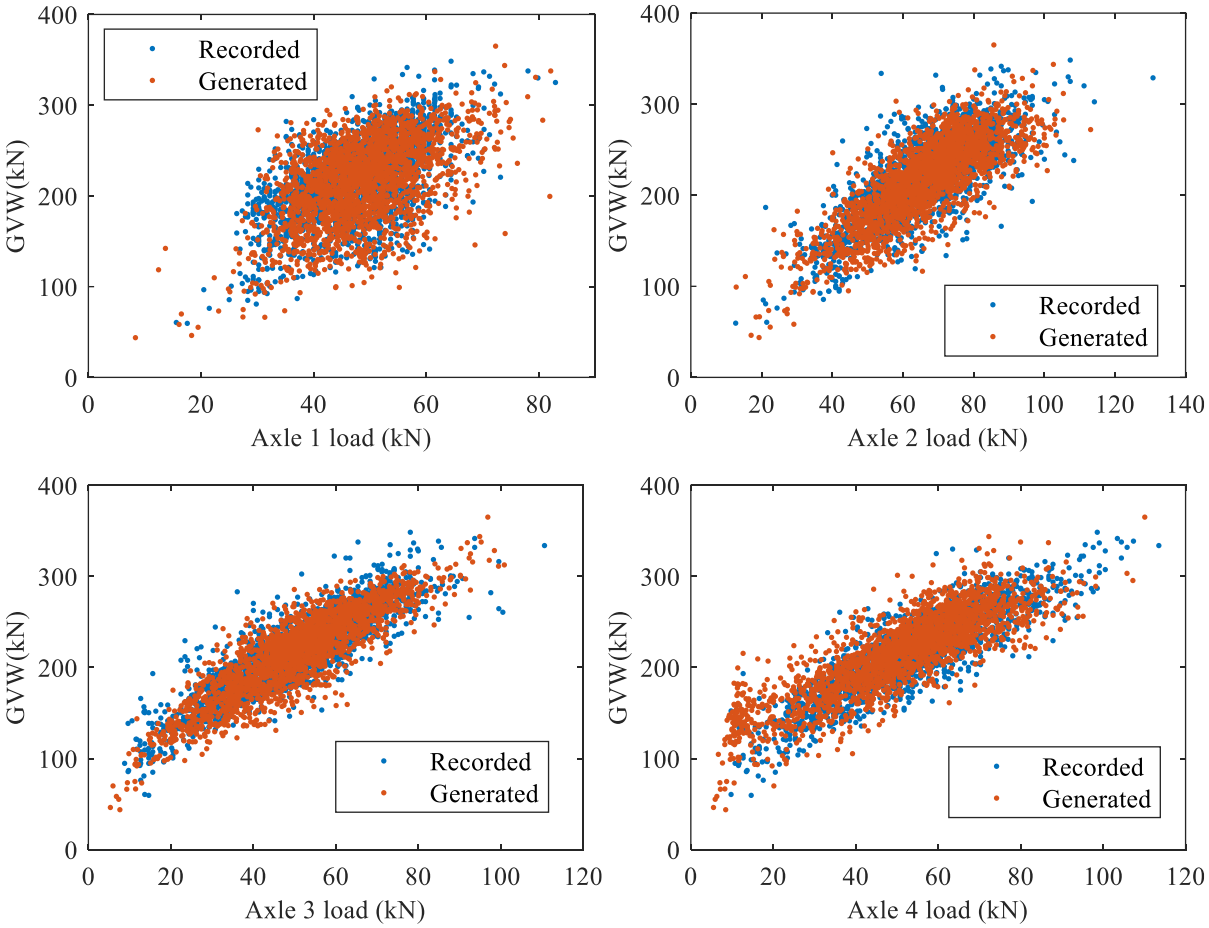

Figure A.22. Scatter plots of generated and recorded axle load-GVW – four-axle vehicles.

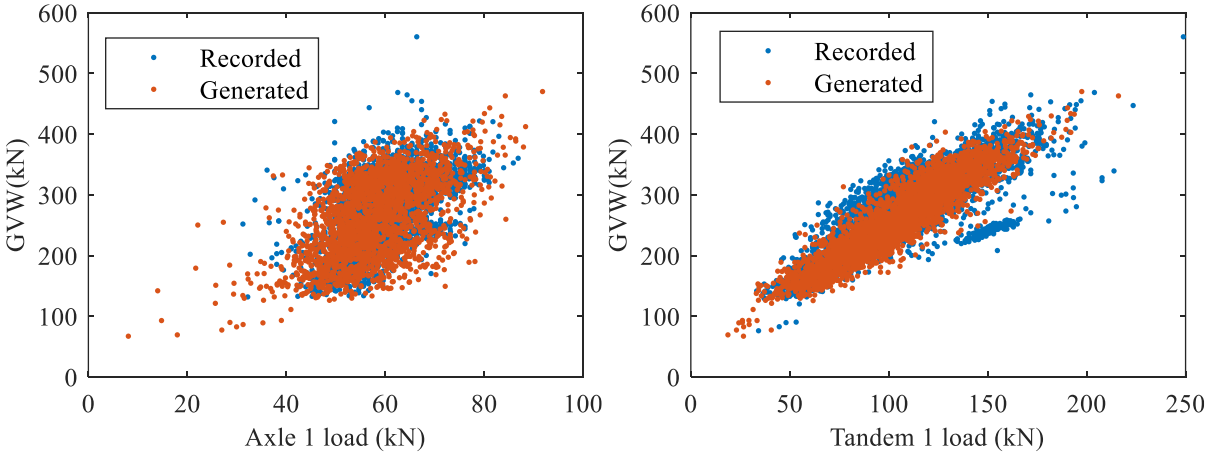

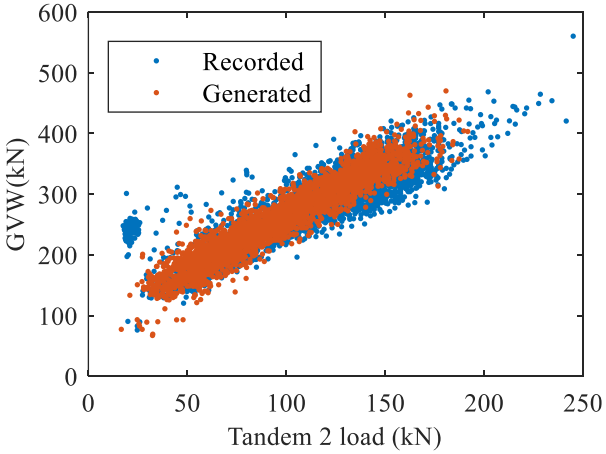

Figure A.23. Scatter plots of generated and recorded axle load-GVW – five-axle vehicles.

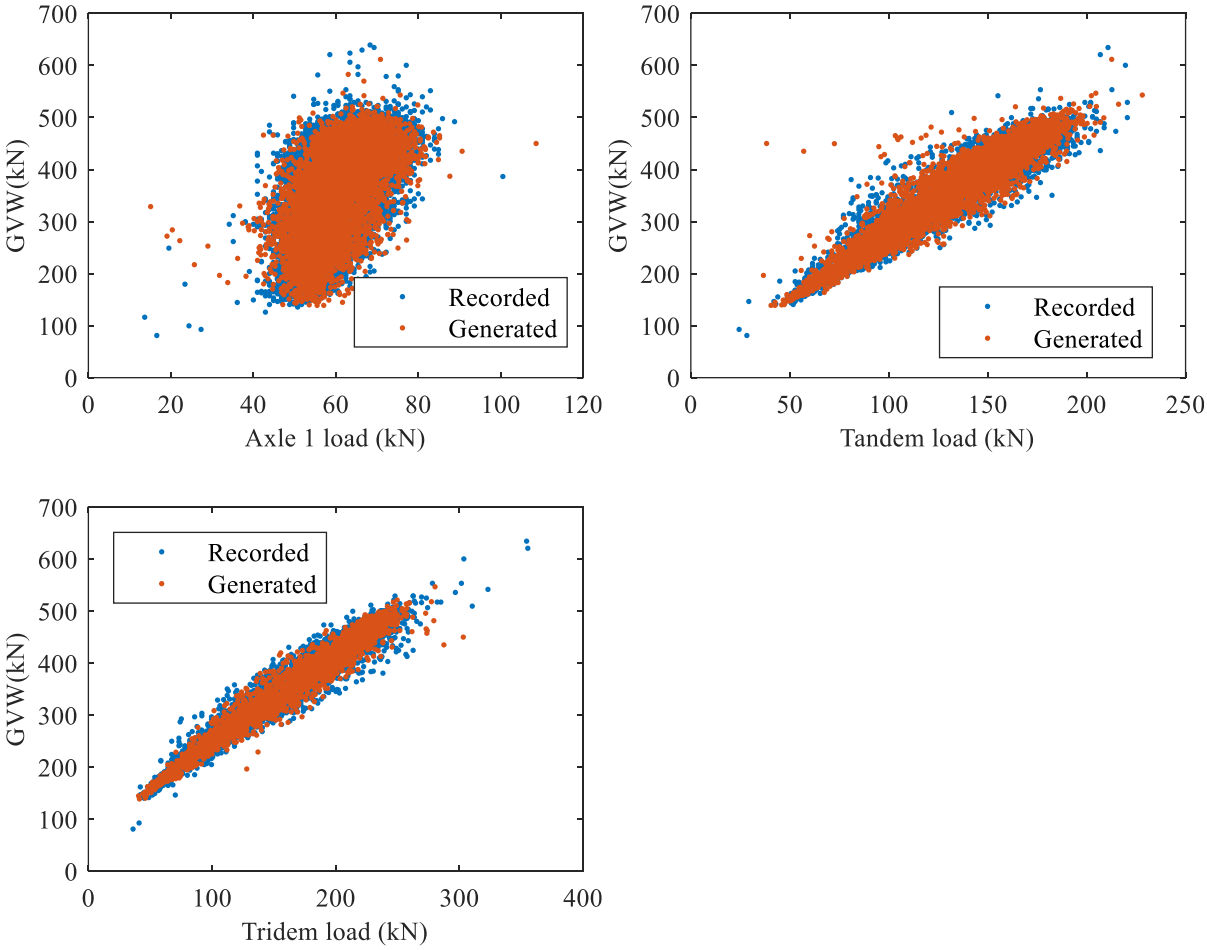

Figure A.24. Scatter plots of generated and recorded axle load-GVW – six-axle vehicles.

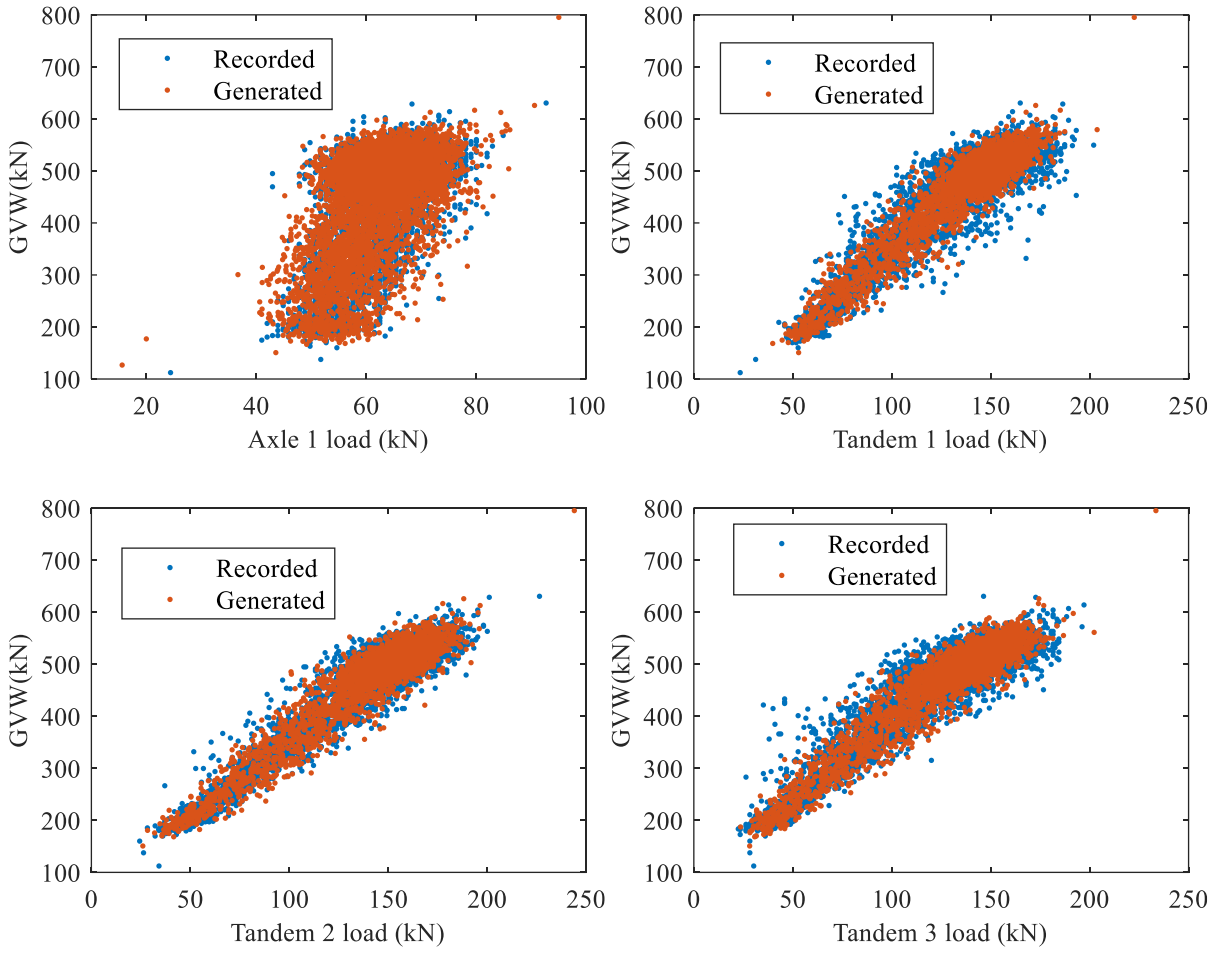

Figure A.25. Scatter plots of generated and recorded axle load-GVW – seven-axle vehicles.

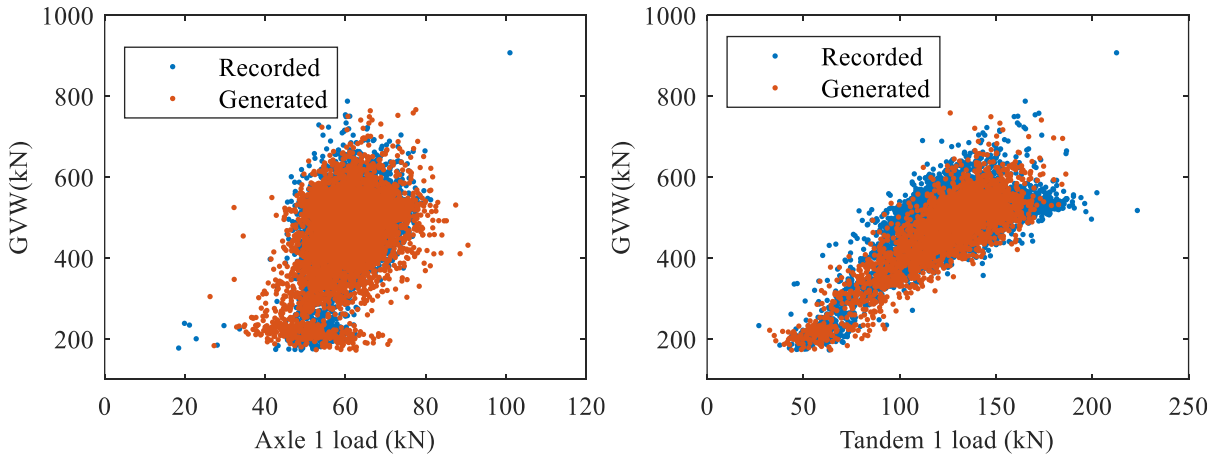

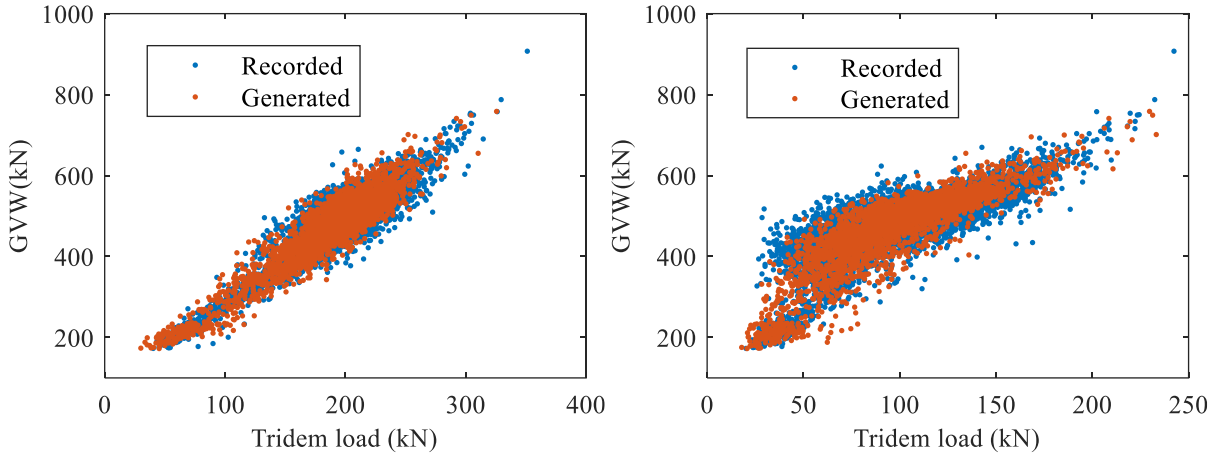

Figure A.26. Scatter plots of generated and recorded axle load-GVW – eight-axle vehicles.

A.4 Normal fit to tail of the GVW

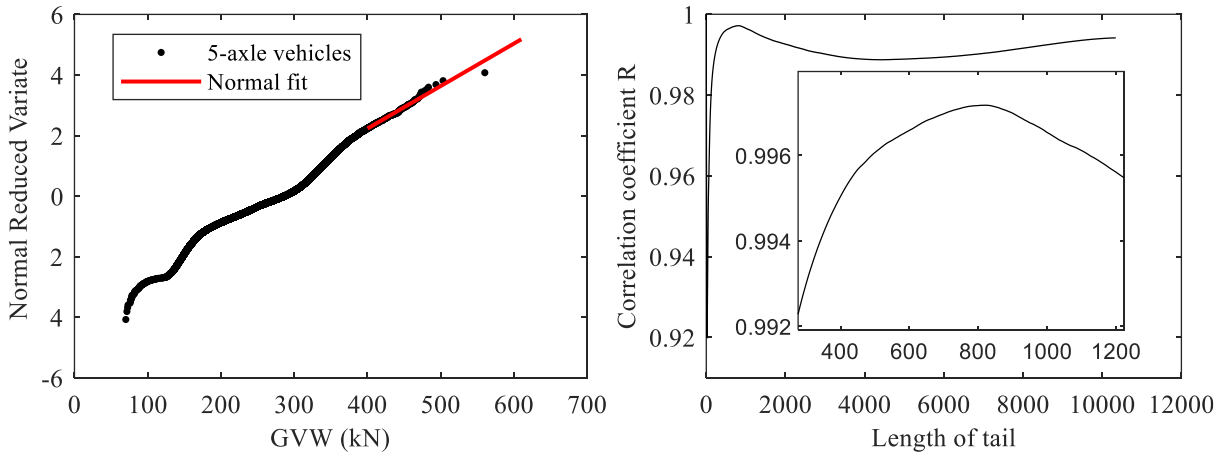

Figure A.27. Normal fit to the tail of the GVW – five-axle vehicles.

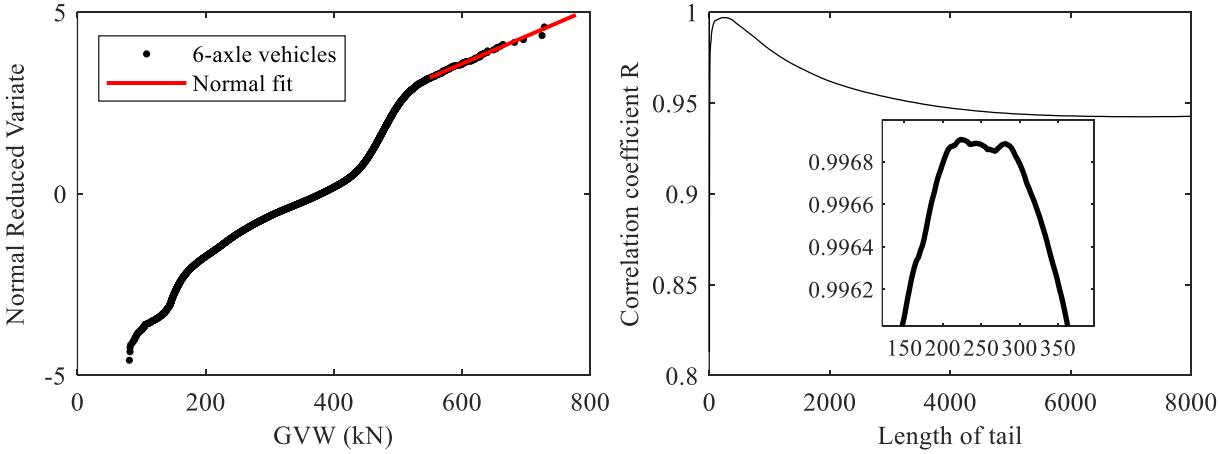

Figure A.28. Normal fit to the tail of the GVW – six-axle vehicles.

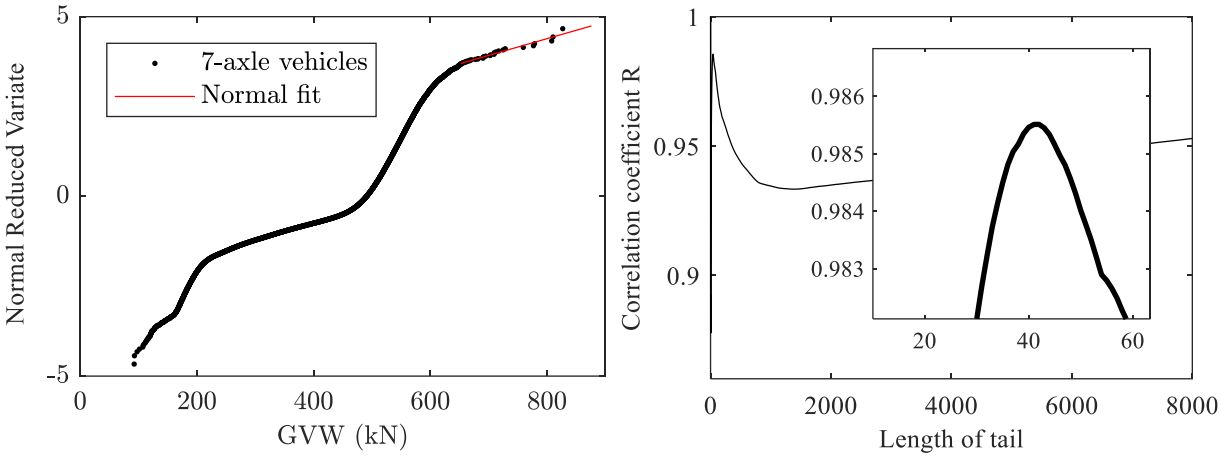

Figure A.29. Normal fit to the tail of the GVW – seven-axle vehicles.

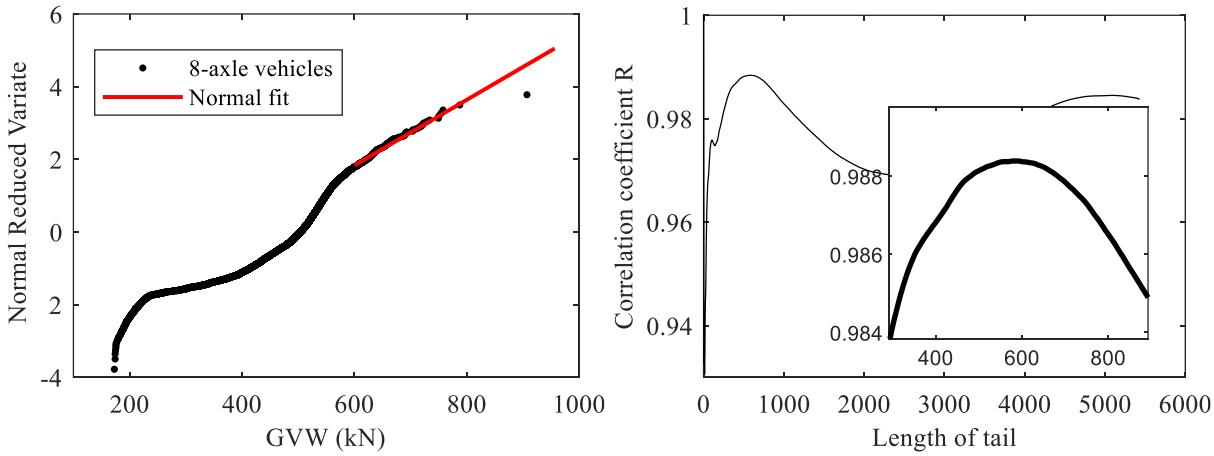

Figure A.30. Normal fit to the tail of the GVW – eight-axle vehicles.

A.5 Comparison recorded and simulated load effects.

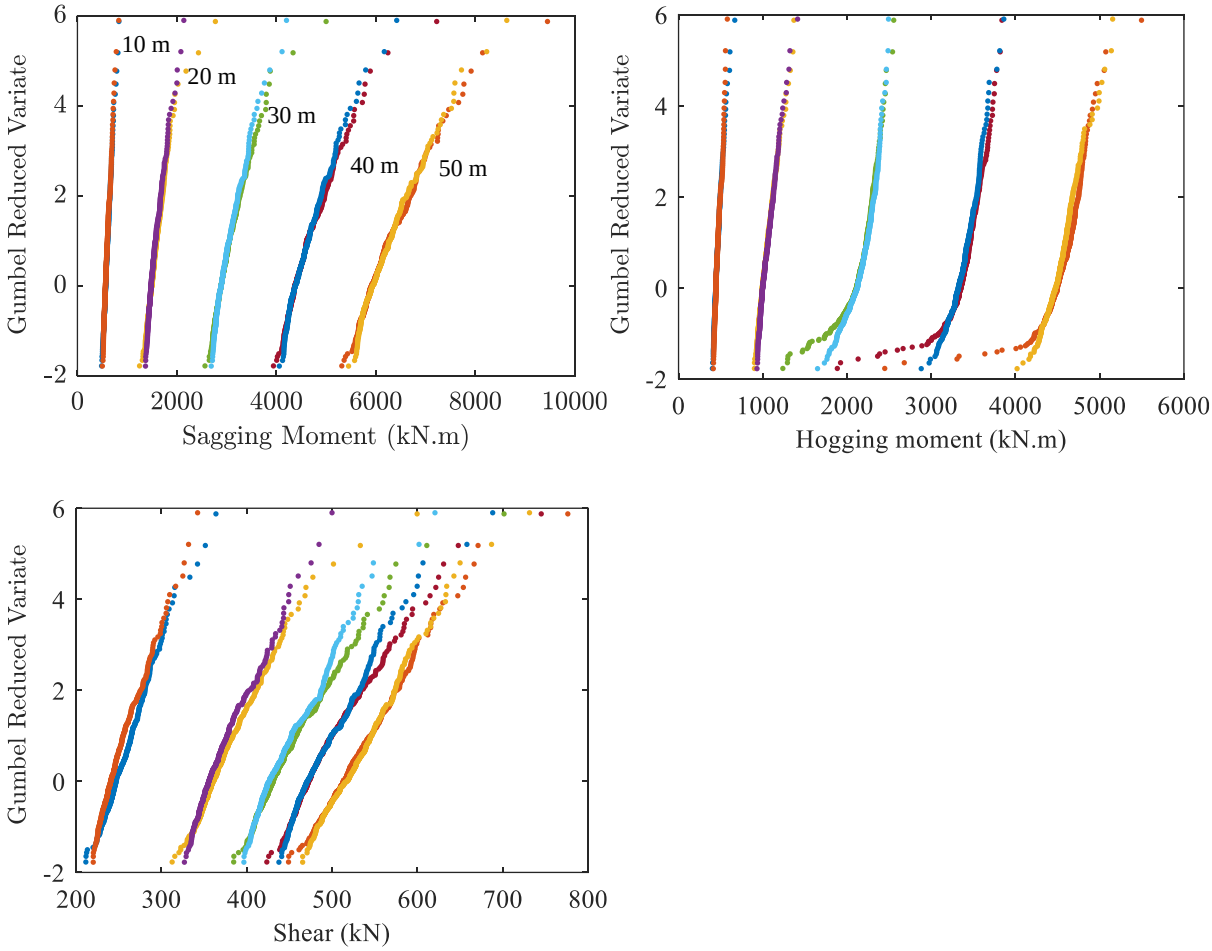

Figure A.31. Roosboom recorded and generated load effects on Gumbel probability paper – all span lenghts.

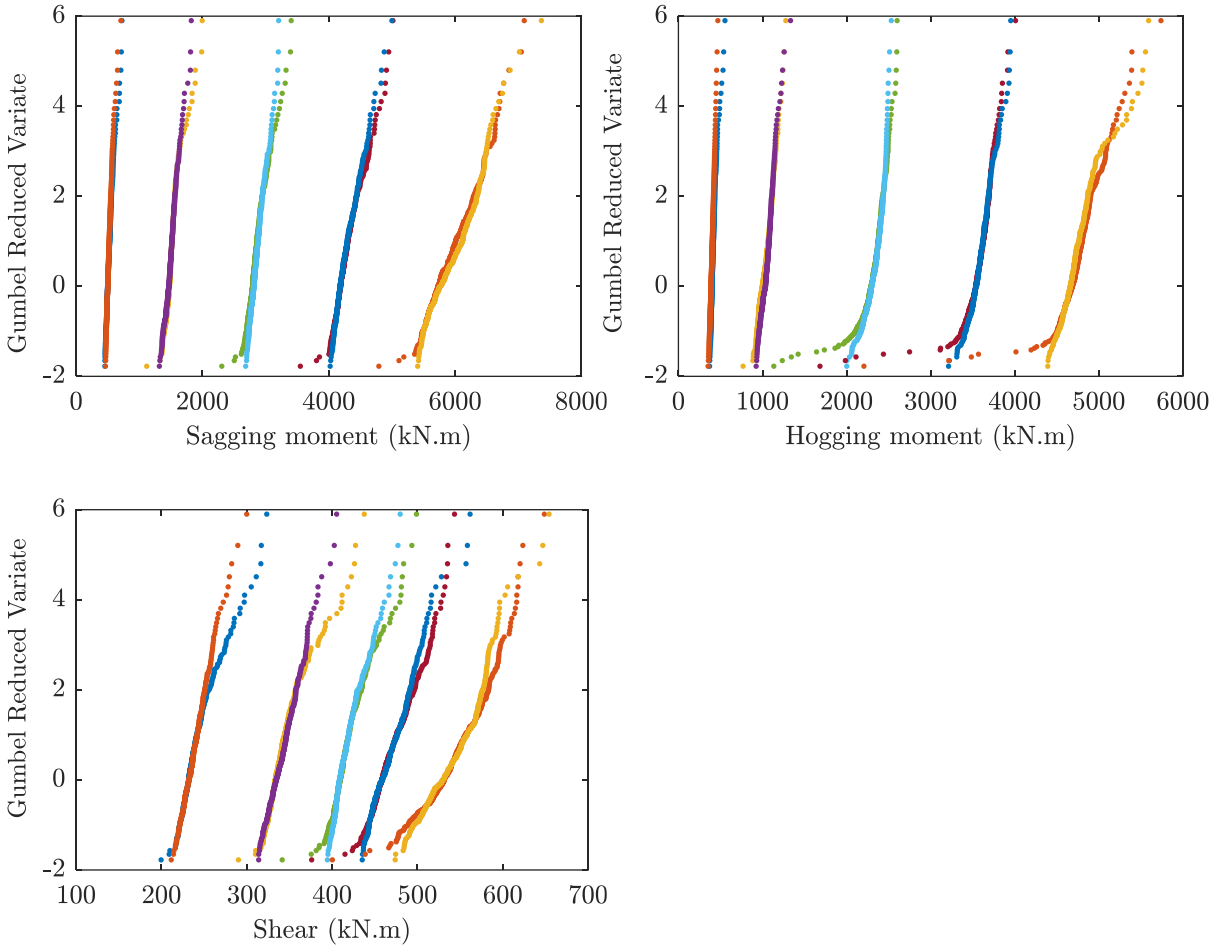

Figure A.32. Kaapmuiden recorded and generated load effects on Gumbel probability paper – all span lengths.

A.6 Influence of the traffic descriptors on the load effects.

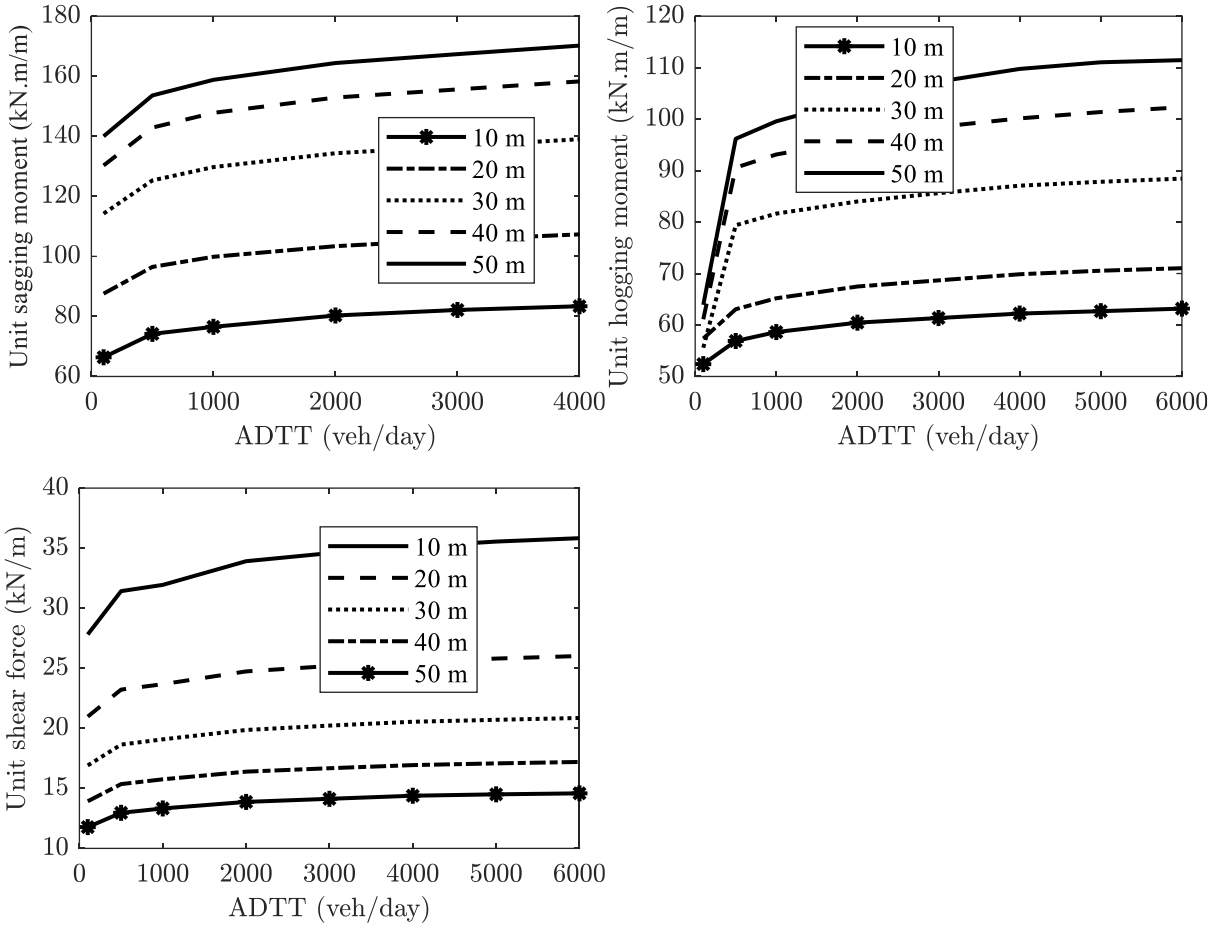

Figure A.33. Influence of the ADTT on the load effects.

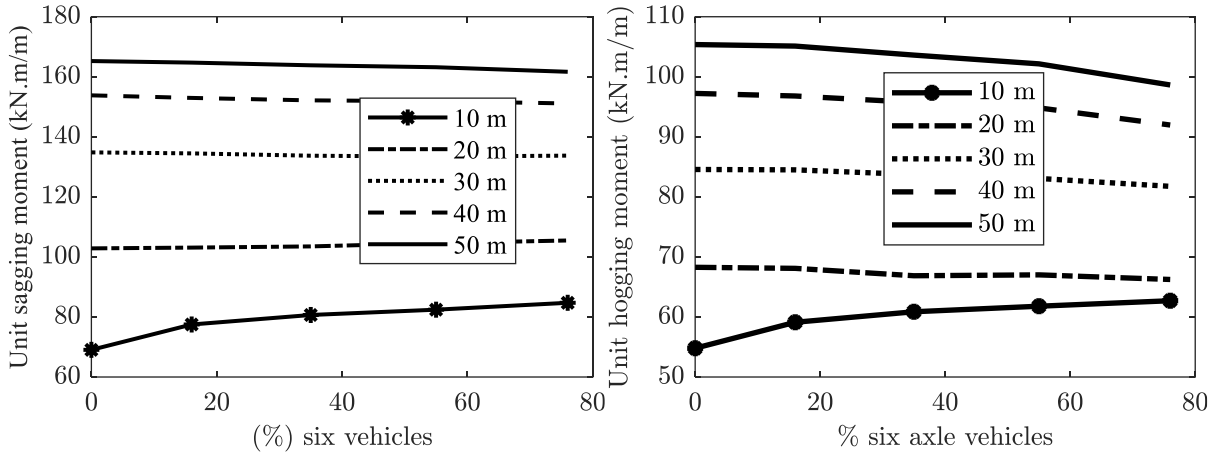

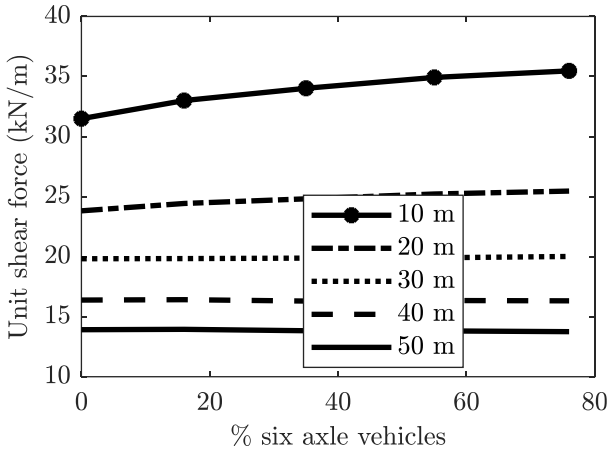

Figure A.34. Influence of the ratio six to seven axle vehicles on the load effects.

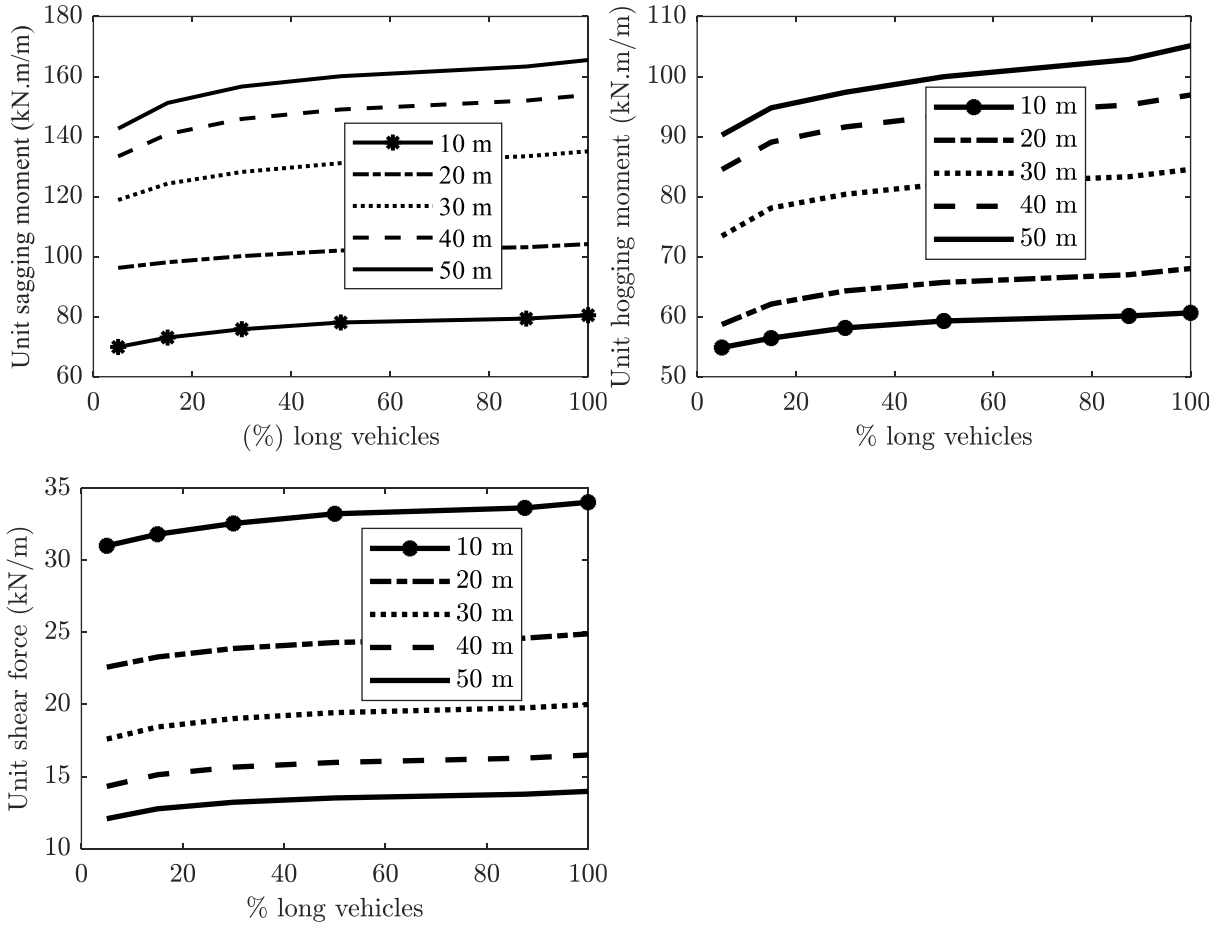

Figure A.35. Influence of the percentage of long vehicles on the load effects.

Appendix B

B.1 Extrapolation of load effects.

The extrapolation of the load effects for all the span lengths and simulations are shown hereafter. The dashed line represents the 975 years return period.

Extrapolations are performed on Gumbel probability paper and the value of the y-axis for the daily maxima characteristic load effects is calculated using the following equation:

$$y = -\ln\left(-\ln\left(1 - \frac{1}{d \cdot Y}\right)\right)$$

where d is the number of days in a year and Y the return period of the characteristic load effect in years. For instance, the y daily maxima value for the return period 975 years with 365 days per year is 12.78. The assumption of 365 days per year is conservative as mentioned in Section 4.5. If 250 days per year were considered the previous equation would yield a value of $y = 12.43$, consequently reducing the characteristic values obtained.

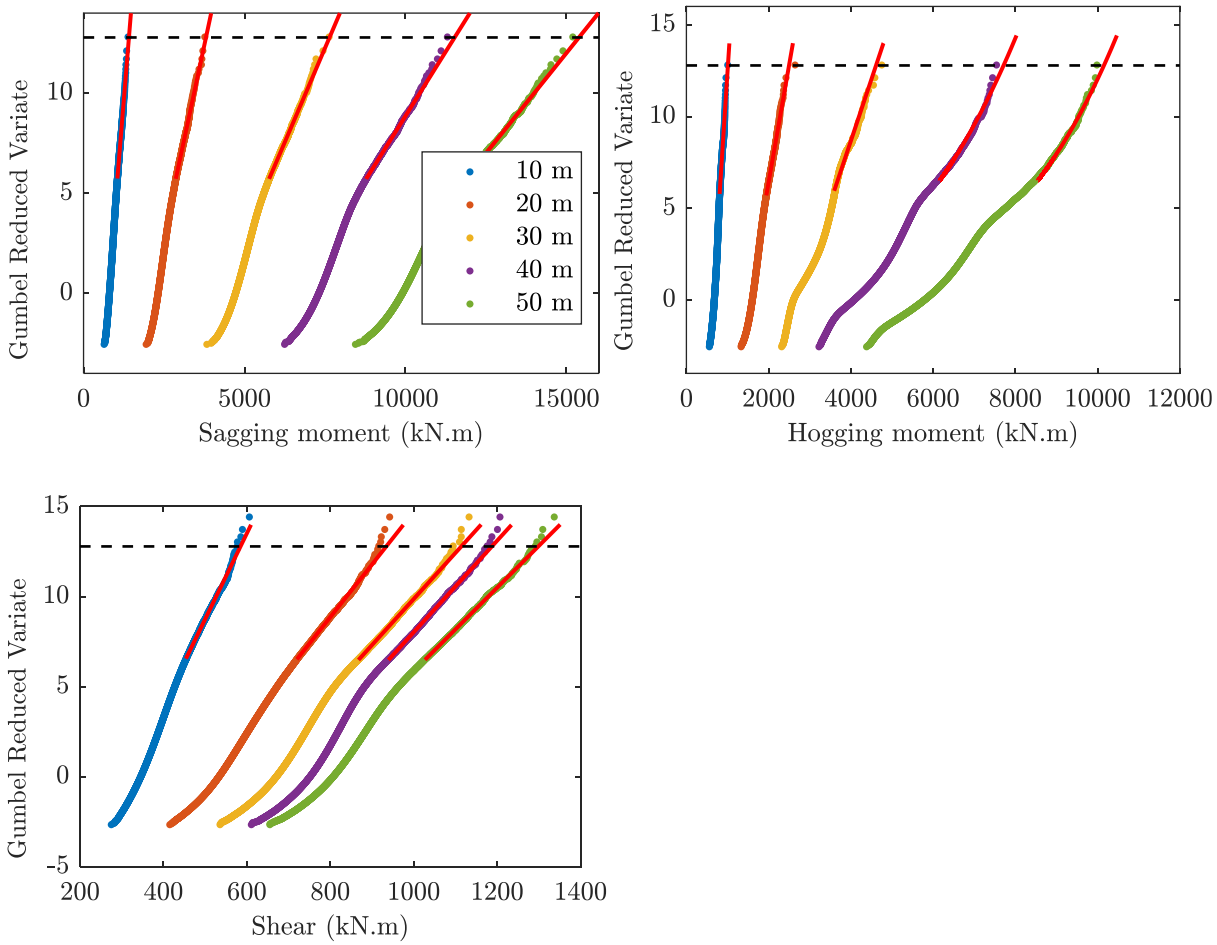

Figure B.1. Extrapolation of load effects on Gumbel probability paper – reference station.

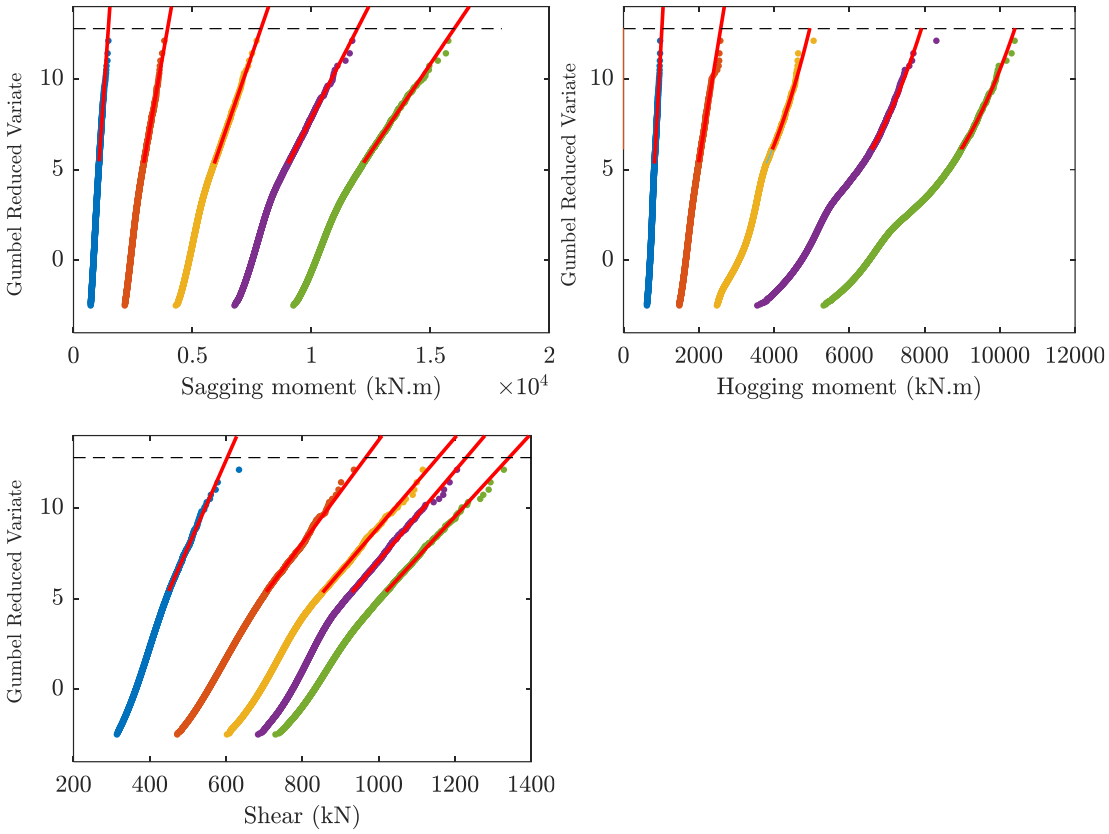

Figure B.2. Extrapolation of load effects on Gumbel probability paper – 4000 veh/day.

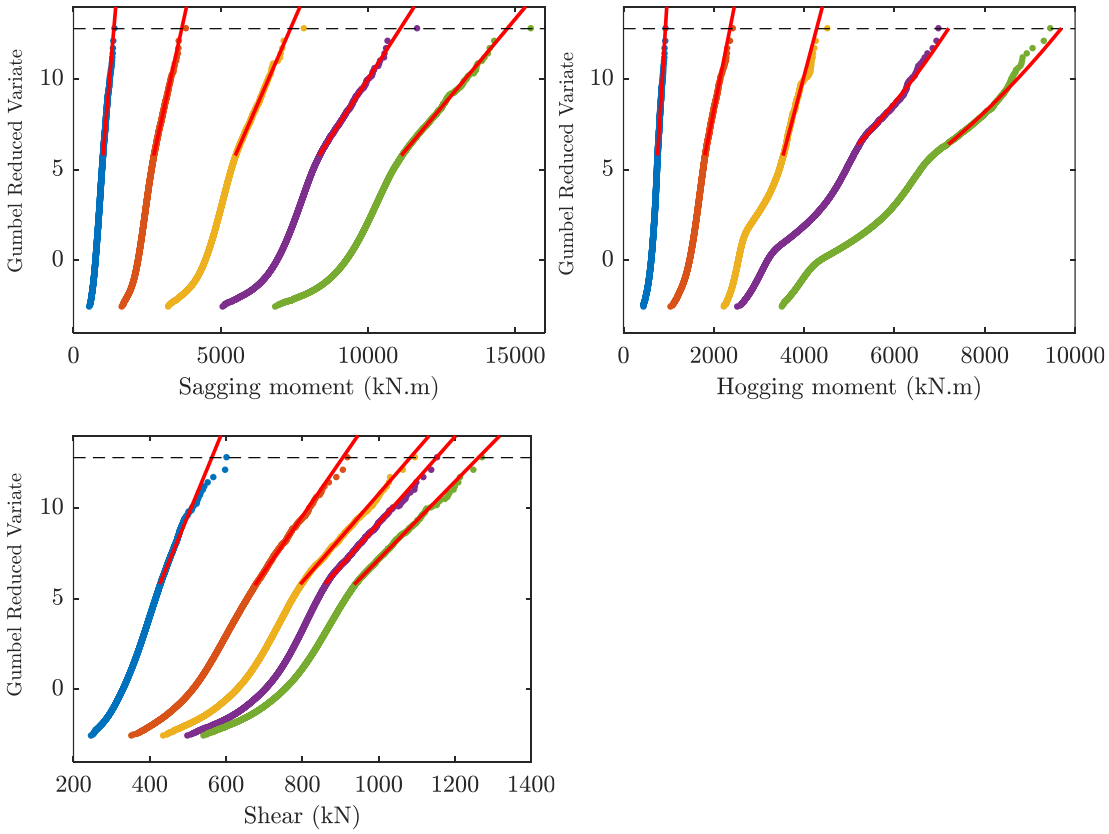

Figure B.3. Extrapolation of load effects on Gumbel probability paper – 1000 veh/day.

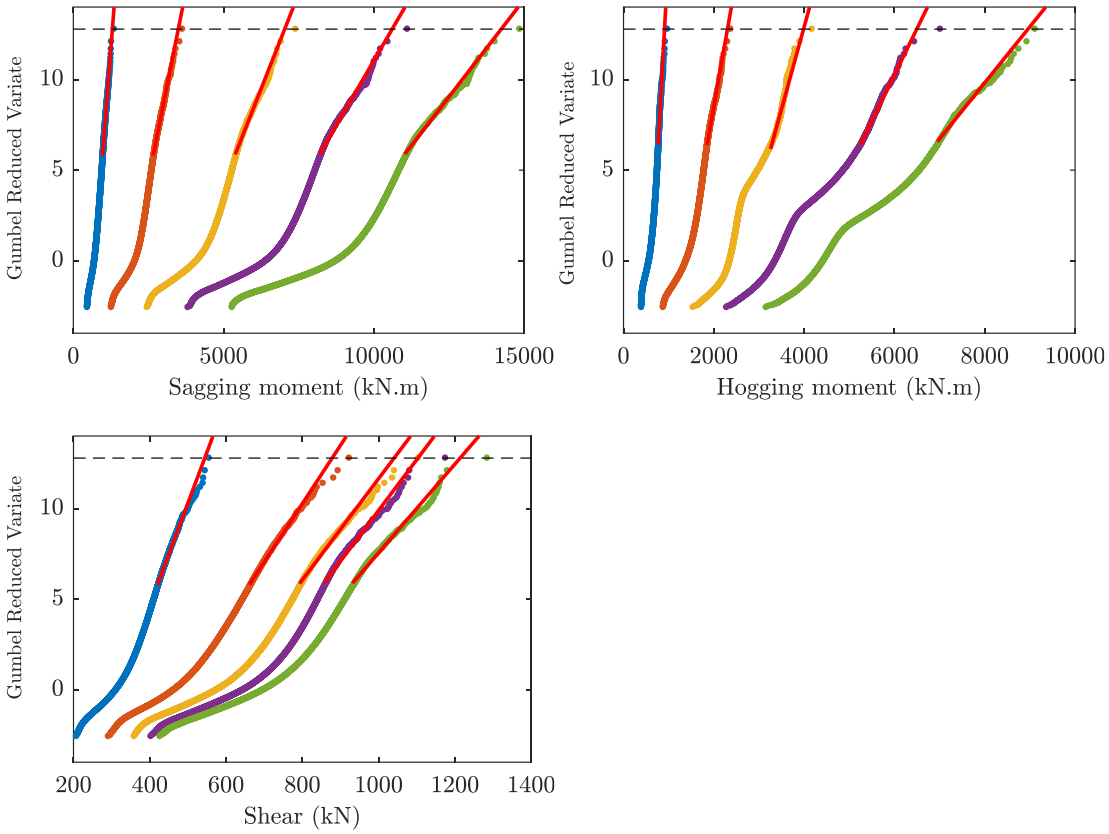

Figure B.4. Extrapolation of load effects on Gumbel probability paper – 500 veh/day.

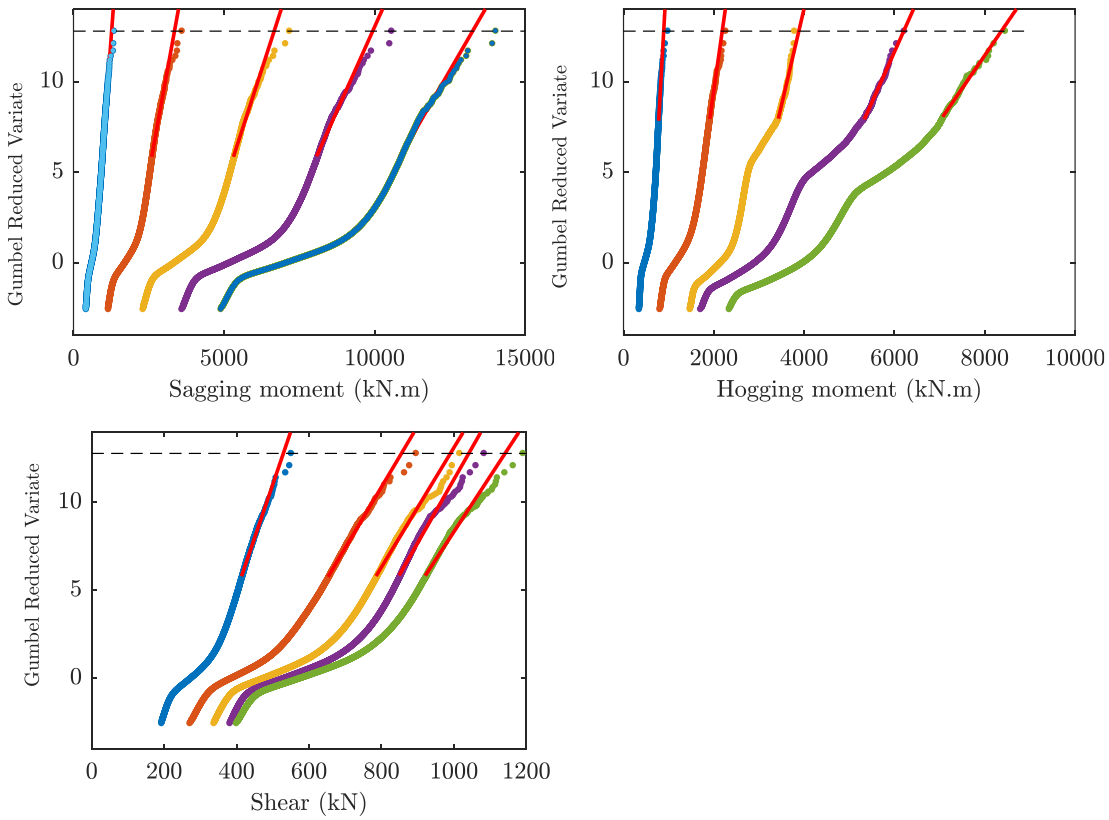

Figure B.5. Extrapolation of load effects on Gumbel probability paper – 100 veh/day.

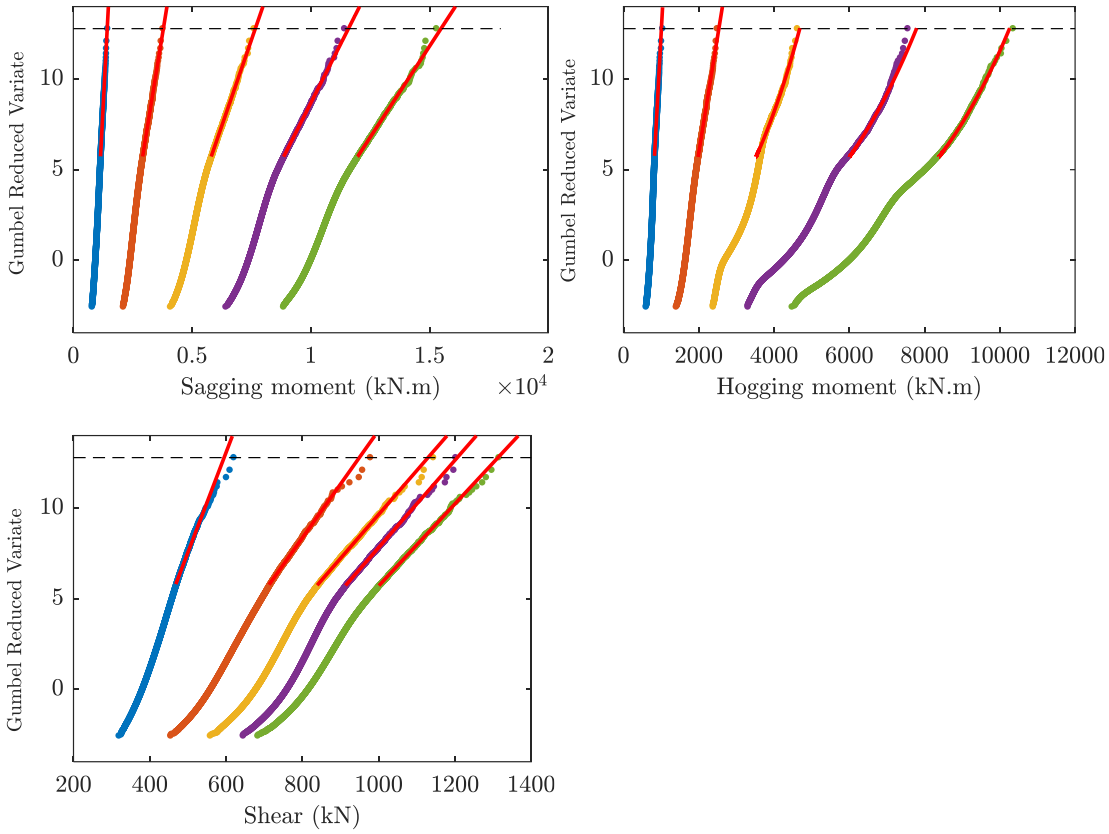

Figure B.6. Extrapolation of load effects on Gumbel probability paper – 100% long vehicles.

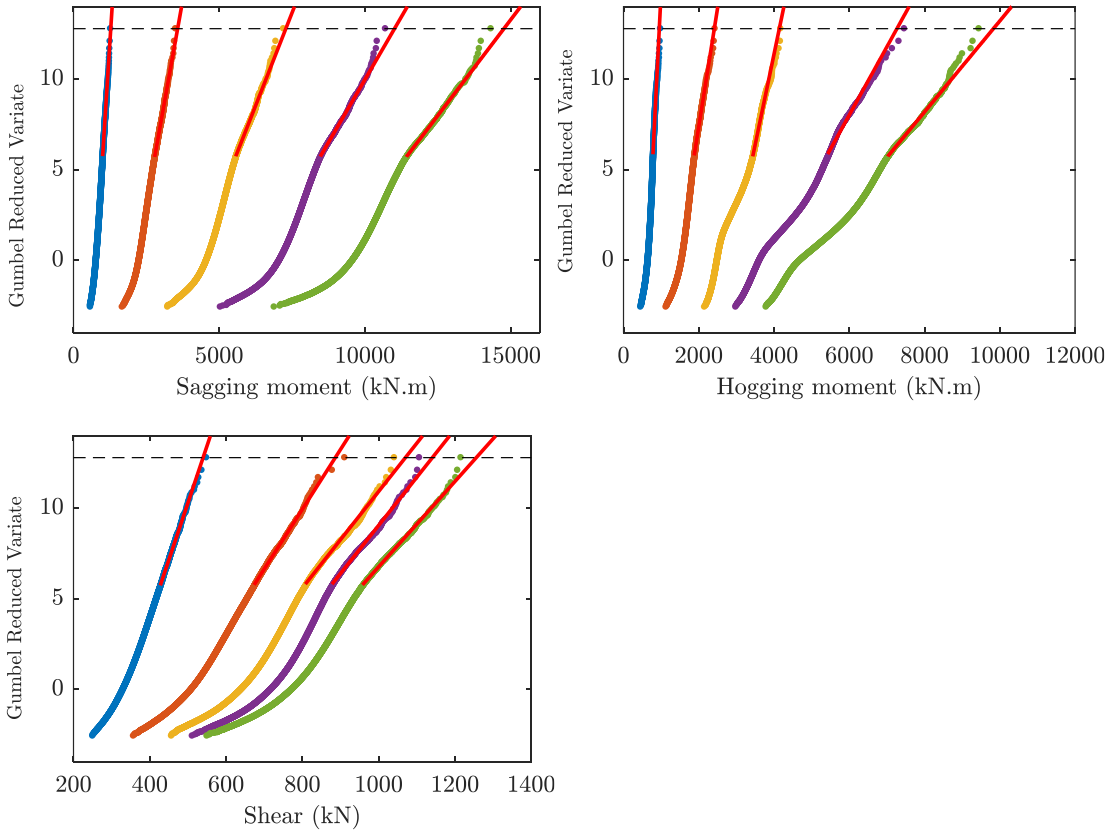

Figure B.7. Extrapolation of load effects on Gumbel probability paper – 50% long vehicles.

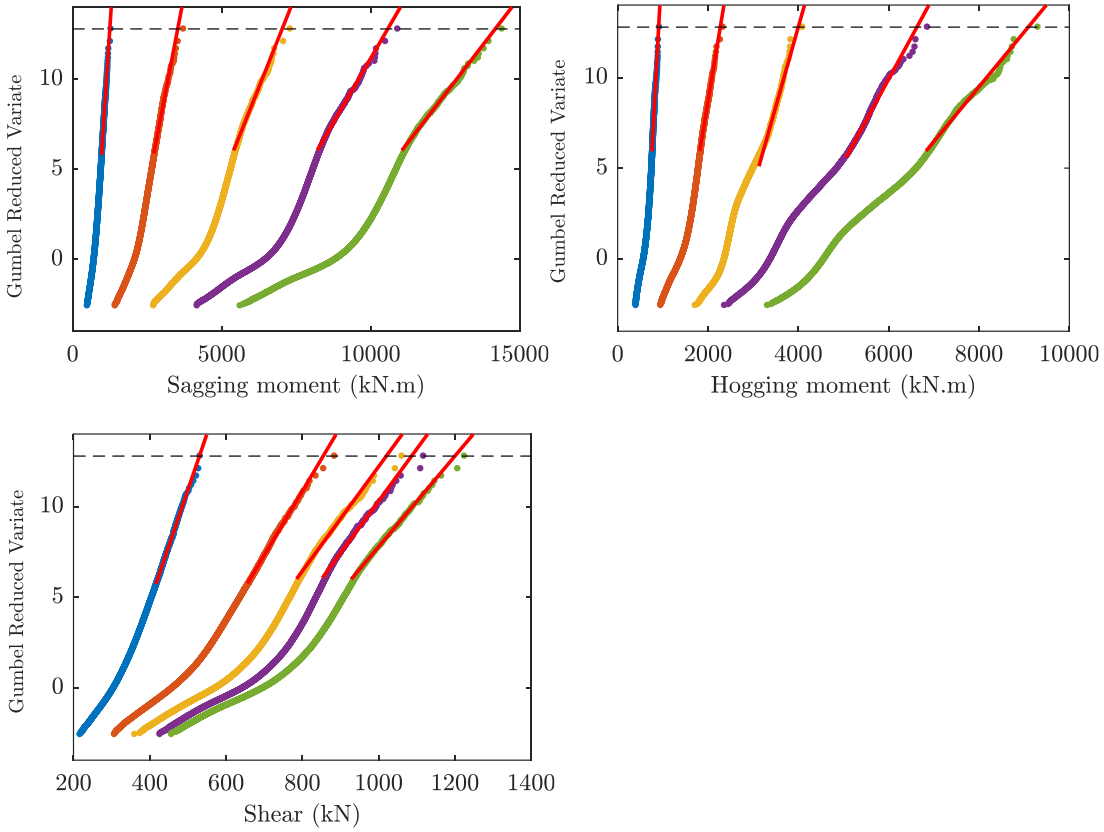

Figure B.8. Extrapolation of load effects on Gumbel probability paper – 25% long vehicles.

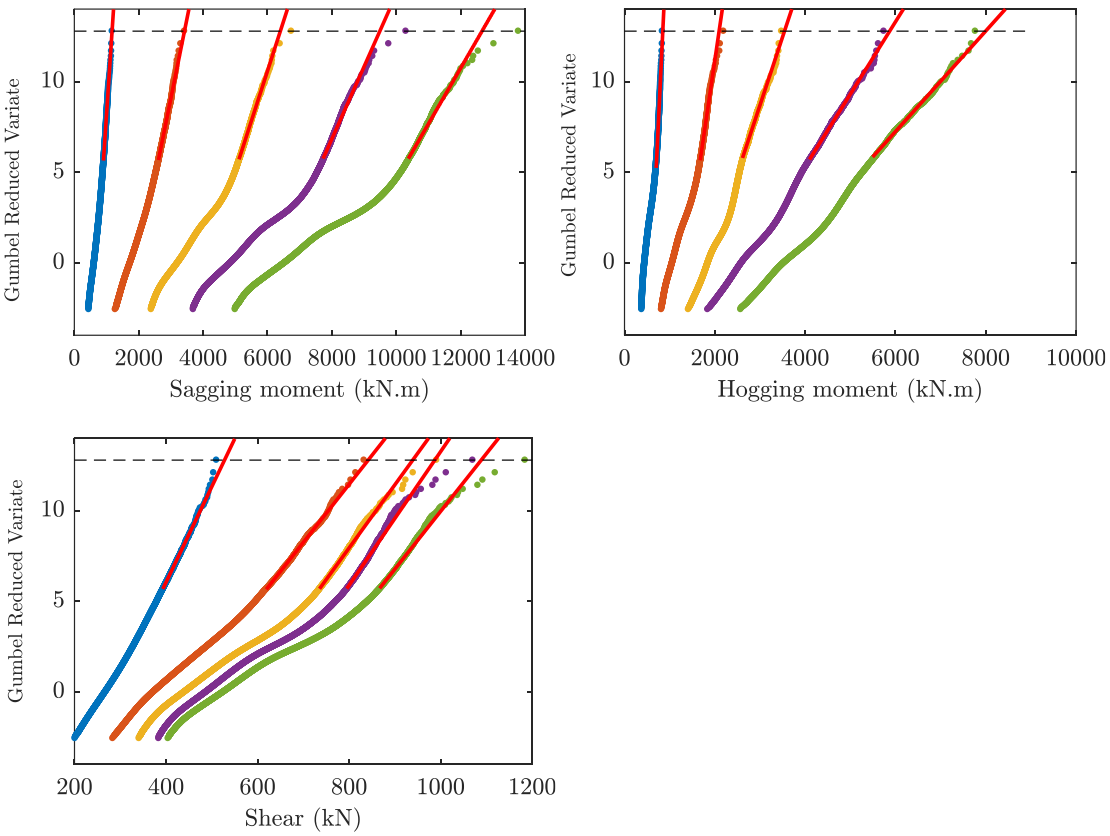

Figure B.9. Extrapolation of load effects on Gumbel probability paper – 5% long vehicles.

Table B.1. Bias and CV of extrapolated load effects using Gumbel distribution.

Gumbel fit	Bias			CV (%)			Bias	CV (%)
Span length (m)	Block size in years (daily max)						Block size (annual max)	
	100	500	1000	100	500	1000	1000	
	Sagging moment							
10	0.65	0.23	0.27	1.82	1.17	1.63	1.66	1.74
20	1.20	1.28	1.16	1.80	1.08	1.42	0.60	1.34
30	1.02	1.43	1.47	1.85	1.19	0.49	1.16	1.65
40	1.51	1.63	1.53	1.60	0.74	0.31	0.64	1.49
50	1.61	1.70	1.61	2.10	1.25	0.79	1.03	1.84
	Hogging moment							
10	0.89	0.14	0.07	1.61	0.59	0.50	0.19	2.49
20	0.92	0.63	0.57	1.94	0.99	0.31	0.57	0.98
30	3.79	2.22	1.42	2.38	1.93	1.57	0.83	2.72
40	8.73	9.07	8.28	1.94	1.17	0.89	2.27	3.31
50	10.78	7.12	5.79	1.53	0.95	0.38	1.30	1.25
	Shear force							
10	0.08	0.66	0.97	2.07	1.97	0.20	2.13	2.50
20	1.70	1.92	0.84	2.48	1.69	0.64	2.23	1.55
30	1.25	1.58	1.49	2.03	1.57	0.58	1.88	0.52
40	1.16	1.64	1.58	2.10	1.24	0.21	1.27	1.97
50	1.08	1.09	0.98	1.65	1.29	0.66	1.10	1.74

Table B.2. Bias and CV of extrapolated load effects using Weibull distribution.

Gumbel fit	Bias			CV (%)			Bias	CV (%)
Span length (m)	Block size in years (daily max)						Block size (annual max)	
	100	500	1000	100	500	1000	1000	
	Sagging moment							
10	-6.84	-4.83	-4.03	1.70	1.38	1.22	-0.70	1.06
20	-5.48	-3.59	-2.96	1.82	1.19	0.84	-1.56	1.63
30	-4.57	-2.66	-2.03	1.48	1.14	0.33	-0.99	1.45
40	-4.98	-3.11	-2.51	1.65	0.81	0.34	-1.32	0.80
50	-4.64	-2.89	-2.31	1.47	0.85	0.67	-0.62	2.21
	Hogging moment							
10	-5.73	-3.85	-3.16	1.39	0.84	0.59	-1.14	1.58
20	-6.84	-4.95	-4.32	1.77	0.58	0.92	-1.63	2.68
30	-8.75	-6.00	-4.87	2.37	0.83	0.67	-1.10	1.35
40	-0.04	-2.42	-1.39	1.62	0.85	0.76	-1.02	2.41
50	-1.99	-1.65	-1.37	1.12	0.55	0.47	-0.13	0.65
	Shear force							
10	-6.33	-4.06	-3.21	1.75	1.00	1.00	1.47	1.05
20	-5.27	-3.16	-2.42	1.70	0.76	0.77	1.09	1.84
30	-4.82	-2.70	-2.02	1.54	1.30	0.38	1.03	1.74
40	-5.28	-3.17	-2.57	1.68	0.78	0.64	0.58	0.50
50	-5.51	-3.67	-3.07	1.64	1.09	0.46	1.31	1.11

The tables of characteristic load effects for all ADTT simulations and reference periods follow:

Table B.3. Characteristic load effects 50 years reference period.

Span length (m)	ADTT (veh/day)				
	100	500	1000	2000	4000
	Sagging moment				
10	1267	1299	1371	1418	1463
20	3353	3493	3675	3762	3953
30	6663	7034	7368	7564	7877
40	9936	10612	11094	11426	11930
50	13253	14241	14728	15306	15999
	Hogging moment				
10	880	908	927	1001	1019
20	2186	2302	2357	2503	2582
30	3882	3986	4276	4654	4950
40	6205	6493	7196	7713	7917
50	8367	8956	9692	10134	10401
	Shear force				
10	529	544	563	585	603
20	855	878	906	934	966
30	990	1040	1083	1114	1155
40	1041	1103	1151	1187	1229
50	1141	1213	1261	1299	1342

Table B.4. Characteristic load effects 40 years reference period.

Span length (m)	ADTT (veh/day)				
	100	500	1000	2000	4000
	Sagging moment				
10	1257	1288	1359	1406	1451
20	3329	3467	3645	3737	3923
30	6620	6981	7309	7518	7818
40	9875	10533	11006	11359	11842
50	13176	14137	14613	15219	15884
	Hogging moment				
10	885	903	922	995	1013
20	2173	2286	2339	2485	2564
30	3861	3962	4252	4618	4923
40	6165	6450	7136	7668	7883
50	8305	8884	9618	10088	10364
	Shear force				
10	525	540	558	581	598
20	849	871	898	928	958
30	984	1032	1073	1107	1146
40	1035	1095	1142	1180	1220
50	1134	1204	1251	1290	1332

Table B.5. Characteristic load effects 30 years reference period.

Span length (m)	ADTT (veh/day)				
	100	500	1000	2000	4000
	Sagging moment				
10	1244	1275	1343	1391	1436
20	3298	3432	3606	3701	3884
30	6564	6912	7231	7444	7742
40	9798	10432	10893	11251	11729
50	13076	14003	14465	15077	15736
	Hogging moment				
10	879	897	915	987	1006
20	2157	2266	2317	2462	2542
30	3834	3930	4222	4572	4888
40	6113	6393	7059	7609	7838
50	8226	8791	9523	10029	10316
	Shear force				
10	521	535	553	575	592
20	840	862	889	918	948
30	975	1022	1062	1095	1135
40	1027	1085	1130	1168	1209
50	1125	1193	1238	1277	1319

Table B.6. Characteristic load effects 20 years reference period.

Span length (m)	ADTT (veh/day)				
	100	500	1000	2000	4000
	Sagging moment				
10	1226	1256	1322	1369	1414
20	3253	3383	3551	3650	3829
30	6485	6816	7123	7341	7635
40	9689	10290	10733	11099	11571
50	12935	13814	14257	14878	15527
	Hogging moment				
10	869	888	905	976	995
20	2134	2237	2284	2430	2510
30	3796	3885	4178	4507	4839
40	6041	6314	6948	7525	7773
50	8115	8660	9386	9944	10247
	Shear force				
10	514	528	545	566	584
20	829	850	876	904	934
30	963	1008	1045	1079	1118
40	1015	1070	1113	1152	1193
50	1112	1176	1219	1260	1302

Table B.7. Characteristic load effects 10 years reference period.

Span length (m)	ADTT (veh/day)				
	100	500	1000	2000	4000
	Sagging moment				
10	1195	1224	1285	1333	1378
20	3178	3300	3457	3562	3735
30	6350	6651	6937	7164	7452
40	9502	10048	10460	10838	11299
50	12694	13492	13901	14538	15170
	Hogging moment				
10	854	873	887	957	977
20	2094	2188	2229	2375	2455
30	3731	3809	4125	4395	4721
40	5916	6178	6753	7375	7658
50	7925	8436	9145	9792	10124
	Shear force				
10	502	516	531	551	570
20	809	828	853	880	909
30	943	983	1016	1052	1090
40	996	1045	1084	1125	1165
50	1090	1148	1187	1230	1272

The tables of characteristic load effects for all the percentage of long vehicles simulations and reference periods follow:

Table B.8. Characteristic load effects 50 years reference period.

Span length (m)	Long vehicles (%)				
	5	25	50	87.5	100
	Sagging moment				
10	1172	1247	1279	1418	1427
20	3421	3526	3573	3762	3791
30	6399	7033	7286	7564	7662
40	9490	10577	11015	11426	11584
50	12663	14184	14769	15306	15483
	Hogging moment				
10	848	908	951	1001	1007
20	2095	2272	2413	2503	2534
30	3543	3998	4140	4654	4684
40	5871	6625	7265	7713	7786
50	7996	9089	9829	10134	10257
	Shear force				
10	528	530	540	585	595
20	842	854	886	934	949
30	939	1020	1070	1114	1129
40	987	1086	1141	1187	1206
50	1089	1200	1256	1299	1313

Table B.9. Characteristic load effects 40 years reference period.

Span length (m)	Long vehicles (%)				
	5	25	50	87.5	100
	Sagging moment				
10	1164	1238	1270	1406	1418
20	3395	3500	3549	3737	3763
30	6358	6979	7231	7518	7603
40	9434	10499	10935	11359	11498
50	12591	14080	14663	15219	15372
	Hogging moment				
10	523	527	536	581	591
20	835	848	879	928	942
30	932	1012	1062	1107	1120
40	981	1078	1132	1180	1197
50	1082	1191	1246	1290	1303
	Shear force				
10	843	903	945	995	1001
20	2082	2257	2396	2485	2516
30	3513	3973	4118	4618	4678
40	5815	6576	7206	7668	7742
50	7916	9015	9740	10088	10212

Table B.10. Characteristic load effects 30 years reference period.

Span length (m)	Long vehicles (%)				
	5	25	50	87.5	100
	Sagging moment				
10	1153	1227	1259	1391	1406
20	3362	3467	3517	3701	3728
30	6306	6910	7161	7444	7528
40	9362	10397	10831	11251	11386
50	12497	13946	14527	15077	15229
	Hogging moment				
10	838	897	938	987	994
20	2065	2238	2374	2462	2494
30	3475	3940	4089	4572	4632
40	5743	6514	7129	7609	7684
50	7812	8920	9625	10029	10153
	Shear force				
10	518	522	532	575	586
20	826	840	871	918	932
30	924	1002	1051	1095	1108
40	973	1068	1121	1168	1185
50	1072	1179	1234	1277	1290

Table B.11. Characteristic load effects 20 years reference period.

Span length (m)	Long vehicles (%)				
	5	25	50	87.5	100
	Sagging moment				
10	1138	1211	1242	1369	1390
20	3316	3420	3471	3650	3678
30	6232	6812	7062	7341	7421
40	9260	10255	10685	11099	11230
50	12365	13758	14335	14878	15027
	Hogging moment				
10	830	888	928	976	983
20	2041	2211	2343	2430	2462
30	3421	3895	4048	4507	4569
40	5642	6425	7022	7525	7602
50	7666	8786	9463	9944	10068
	Shear force				
10	510	515	525	566	578
20	813	829	858	904	918
30	913	988	1036	1079	1092
40	962	1054	1106	1152	1168
50	1060	1163	1217	1260	1272

Table B.12. Characteristic load effects 10 years reference period.

Span length (m)	Long vehicles (%)				
	5	25	50	87.5	100
	Sagging moment				
10	1112	1183	1215	1333	1363
20	3238	3340	3394	3562	3592
30	6107	6645	6893	7164	7239
40	9087	10011	10434	10838	10963
50	12140	13436	14007	14538	14682
	Hogging moment				
10	817	873	912	957	965
20	2000	2165	2290	2375	2408
30	3329	3816	3979	4395	4459
40	5468	6274	6837	7375	7456
50	7416	8557	9257	9792	9918
	Shear force				
10	497	504	514	551	566
20	791	809	837	880	895
30	893	964	1010	1052	1063
40	943	1030	1080	1125	1139
50	1038	1135	1187	1230	1242

B.3 Site load factors.

Table B.13. ADTT site load factors LF_1.

Span length (m)	ADTT (veh/day)				
	100	500	1000	2000	4000
	Sagging moment				
10	0.89	0.92	0.97	1.00	1.03
20	0.89	0.93	0.98	1.00	1.05
30	0.88	0.93	0.97	1.00	1.04
40	0.87	0.93	0.97	1.00	1.04
50	0.87	0.93	0.96	1.00	1.05
	Hogging moment				
10	0.88	0.91	0.93	1.00	1.02
20	0.87	0.92	0.94	1.00	1.03
30	0.83	0.86	0.92	1.00	1.06
40	0.80	0.84	0.93	1.00	1.03
50	0.83	0.88	0.96	1.00	1.03
	Shear force				
10	0.90	0.93	0.96	1.00	1.03
20	0.92	0.94	0.97	1.00	1.03
30	0.89	0.93	0.97	1.00	1.04
40	0.88	0.93	0.97	1.00	1.04
50	0.88	0.93	0.97	1.00	1.03

Table B.14. Percentage of long vehicles site load factors LF_2.

Span length (m)	Long vehicles (%)				
	5	25	50	87.5	100
	Sagging moment				
10	0.83	0.89	0.91	1.00	1.02
20	0.91	0.94	0.95	1.00	1.01
30	0.85	0.93	0.96	1.00	1.01
40	0.84	0.92	0.96	1.00	1.01
50	0.84	0.92	0.96	1.00	1.01
	Hogging moment				
10	0.85	0.91	0.95	1.00	1.01
20	0.84	0.91	0.96	1.00	1.01
30	0.76	0.87	0.91	1.00	1.01
40	0.74	0.85	0.93	1.00	1.01
50	0.76	0.87	0.95	1.00	1.01
	Shear force				
10	0.90	0.91	0.93	1.00	1.03
20	0.90	0.92	0.95	1.00	1.02
30	0.85	0.92	0.96	1.00	1.01
40	0.84	0.92	0.96	1.00	1.01
50	0.84	0.92	0.97	1.00	1.01

Table B.15. Reference period site load factors LF_3 (global).

Span length (m)	Reference period				
	10	20	30	40	50
	Sagging moment				
10	0.55	0.57	0.57	0.58	0.59
15	0.53	0.54	0.55	0.56	0.56
20	0.55	0.56	0.57	0.58	0.58
30	0.60	0.62	0.63	0.63	0.64
40	0.58	0.60	0.61	0.61	0.62
50	0.55	0.56	0.57	0.57	0.58
	Hogging moment				
10	0.67	0.68	0.69	0.70	0.70
15	0.66	0.68	0.68	0.69	0.70
20	0.56	0.58	0.58	0.59	0.59
30	0.53	0.54	0.55	0.56	0.56
40	0.54	0.55	0.55	0.56	0.56
50	0.48	0.49	0.49	0.49	0.50
	Shear force				
10	0.55	0.57	0.57	0.58	0.58
15	0.60	0.60	0.59	0.59	0.58
20	0.66	0.68	0.69	0.70	0.70
30	0.66	0.68	0.69	0.69	0.70
40	0.60	0.62	0.63	0.63	0.64
50	0.58	0.59	0.60	0.61	0.61

Table B.16. Reference period site load factors LF_3 (lane 1).

Span length (m)	Reference period				
	10	20	30	40	50
	Sagging moment				
10	0.74	0.76	0.77	0.78	0.79
15	0.70	0.72	0.73	0.74	0.75
20	0.70	0.72	0.73	0.74	0.74
30	0.74	0.76	0.77	0.77	0.78
40	0.72	0.73	0.74	0.75	0.76
50	0.67	0.69	0.70	0.70	0.71
	Hogging moment				
10	0.89	0.91	0.93	0.93	0.94
15	0.92	0.94	0.96	0.97	0.97
20	0.71	0.72	0.73	0.74	0.75
30	0.62	0.64	0.64	0.65	0.65
40	0.59	0.60	0.61	0.61	0.62
50	0.53	0.54	0.55	0.55	0.56
	Shear force				
10	0.75	0.77	0.78	0.79	0.80
15	0.80	0.82	0.83	0.84	0.85
20	0.81	0.82	0.83	0.84	0.85
30	0.81	0.82	0.83	0.84	0.85
40	0.76	0.78	0.79	0.80	0.80
50	0.70	0.72	0.73	0.74	0.74

Table B.17. Reference period site load factors LF_3 (lane 2).

Span length (m)	Reference period				
	10	20	30	40	50
	Sagging moment				
10	0.30	0.30	0.31	0.31	0.31
15	0.31	0.31	0.31	0.31	0.31
20	0.34	0.35	0.36	0.36	0.36
30	0.43	0.44	0.44	0.45	0.45
40	0.41	0.42	0.42	0.43	0.43
50	0.38	0.39	0.39	0.40	0.40
	Hogging moment				
10	0.37	0.38	0.38	0.38	0.38
15	0.32	0.32	0.32	0.32	0.32
20	0.37	0.38	0.38	0.38	0.39
30	0.40	0.42	0.43	0.43	0.44
40	0.47	0.48	0.49	0.49	0.49
50	0.41	0.41	0.42	0.42	0.42
	Shear force				
10	0.29	0.29	0.30	0.30	0.30
15	0.29	0.30	0.30	0.30	0.30
20	0.49	0.51	0.52	0.52	0.53
30	0.47	0.48	0.49	0.50	0.50
40	0.40	0.41	0.41	0.42	0.42
50	0.41	0.42	0.42	0.43	0.43

B.4 Validation load effects.

The following tables present the characteristic load effects at a return period of 975 years obtained using the recorded traffic from different stations and the values obtained modifying the reference station load effects (values in previous section) with the site load factor approach. The percentages represent the difference between the recorded values and the modified load effects (upper rows of the table) and the reduction achieved with the proposed method (lower rows of the table).

Table B.18. Kaapmuiden station.

			Recorded traffic			
Span length (m)	Sagging (kN.m)	%	Hogging (kN.m)	%	Shear (kN)	%
10	968	26.36	858	6.09	425	22.04
20	2762	23.29	1940	16.84	652	26.55
30	6115	15.84	4216	-2.84	893	16.29
40	9887	9.69	6433	8.86	953	15.98
50	13362	8.18	8474	11.77	1058	15.10
			Modified load effects			
Span length (m)	Sagging (kN.m)	%	Hogging (kN.m)	%	Shear (kN)	%
10	1315	7.31	913	8.78	545	6.78
20	3601	4.27	2333	6.79	888	4.99
30	7265	3.95	4099	11.92	1066	4.28
40	10948	4.18	7058	8.49	1135	4.44
50	14552	4.93	9604	5.23	1246	4.03

Table B.19. Zeerust station.

			Recorded traffic			
Span length (m)	Sagging (kN.m)	%	Hogging (kN.m)	%	Shear (kN)	%
10	1230	-0.52	837	4.65	545	-5.15
20	2685	20.42	1993	10.88	656	22.82
30	5557	18.62	2805	24.76	806	20.12
40	8616	16.25	4302	31.03	932	12.74
50	11687	15.30	7207	17.22	997	15.42
			Modified load effects			
Span length (m)	Sagging (kN.m)	%	Hogging (kN.m)	%	Shear (kN)	%
10	1224	13.71	878	12.29	519	11.32
20	3374	10.30	2237	10.64	850	9.07
30	6829	9.73	3729	19.89	1009	9.41
40	10287	9.96	6238	19.12	1069	10.01
50	13798	9.86	8707	14.08	1179	9.21

Table B.20. Komatiport station.

Recorded traffic						
Span length (m)	Sagging (kN.m)	%	Hogging (kN.m)	%	Shear (kN)	%
10	967	25.01	804	11.06	435	19.51
20	2879	17.47	2019	12.09	688	21.37
30	5841	16.95	4047	-2.21	876	15.74
40	8721	17.79	6639	-1.97	958	13.09
50	11595	18.48	9346	-3.96	998	17.72
Modified load effects						
Span length (m)	Sagging (kN.m)	%	Hogging (kN.m)	%	Shear (kN)	%
10	1290	9.04	904	9.68	541	7.54
20	3489	7.26	2297	8.24	875	6.32
30	7033	7.03	3959	14.93	1039	6.72
40	10609	7.15	6511	15.59	1102	7.19
50	14224	7.07	8990	11.29	1213	6.60

Table B.21. Wilge station.

Recorded traffic						
Span length (m)	Sagging (kN.m)	%	Hogging (kN.m)	%	Shear (kN)	%
10	1390	0.90	939	4.51	568	1.72
20	3813	-2.06	2450	0.76	841	9.23
30	6882	8.39	4048	11.12	1041	5.87
40	10551	6.96	6415	15.45	1145	2.83
50	14516	4.27	9782	2.46	1244	3.47
Modified load effects						
Span length (m)	Sagging (kN.m)	%	Hogging (kN.m)	%	Shear (kN)	%
10	1403	1.09	984	1.75	578	1.11
20	3736	0.68	2469	1.37	926	0.84
30	7512	0.69	4555	2.14	1106	0.75
40	11340	0.75	7587	1.64	1178	0.79
50	15164	0.93	10029	1.04	1289	0.73

Table B.22. Witbank station.

Recorded traffic						
Span length (m)	Sagging (kN.m)	%	Hogging (kN.m)	%	Shear (kN)	%
10	1321	-0.71	848	8.30	573	-5.11
20	3364	6.59	2120	10.03	748	15.88
30	6212	14.69	3960	4.14	919	14.05
40	9692	11.73	6439	9.65	1010	11.20
50	13043	10.82	8232	14.87	1070	14.44
Modified load effects						
Span length (m)	Sagging (kN.m)	%	Hogging (kN.m)	%	Shear (kN)	%
10	1311	7.54	925	7.67	546	6.71
20	3601	4.26	2356	5.87	889	4.82
30	7281	3.75	4131	11.25	1069	4.05
40	10980	3.90	7127	7.61	1138	4.17
50	14626	4.45	9670	4.57	1250	3.73

B.5 Traffic partial factors.

Table B.23. Traffic partial factors γ_t – all load effects and lengths measured.

	Sagging					
	Length measured (days)					
Span length	1	5	10	30	60	90
10	1.04	1.03	1.02	1.02	1.01	1.01
20	1.05	1.03	1.03	1.02	1.02	1.02
30	1.06	1.03	1.03	1.02	1.02	1.02
40	1.06	1.03	1.03	1.02	1.02	1.02
50	1.07	1.04	1.03	1.02	1.02	1.02
	Hogging					
Span length	1	5	10	30	60	90
10	1.15	1.06	1.06	1.04	1.03	1.03
20	1.09	1.05	1.04	1.03	1.03	1.03
30	1.15	1.06	1.05	1.04	1.04	1.04
40	1.12	1.05	1.04	1.04	1.03	1.03
50	1.08	1.03	1.03	1.02	1.02	1.02
	Shear					
Span length	1	5	10	30	60	90
10	1.04	1.03	1.02	1.02	1.01	1.01
20	1.05	1.03	1.02	1.02	1.01	1.01
30	1.05	1.03	1.02	1.02	1.02	1.02
40	1.05	1.03	1.02	1.02	1.02	1.02
50	1.05	1.03	1.02	1.02	1.02	1.02

B.6 Reliability based partial factors.

Table B.24. Reliability based partial factor γ_q. Design 50 years reference period.

Span length (m)	ADTT (veh/day)					Long vehicles (%)				
	100	500	1000	2000	4000	5	25	50	87.5	100
Sagging moment										
10	1.04	1.04	1.04	1.04	1.04	1.03	1.03	1.03	1.04	1.03
20	1.03	1.04	1.04	1.03	1.04	1.03	1.03	1.03	1.03	1.03
30	1.03	1.04	1.04	1.04	1.03	1.03	1.04	1.04	1.04	1.04
40	1.03	1.03	1.04	1.03	1.03	1.03	1.03	1.03	1.03	1.03
50	1.03	1.03	1.04	1.03	1.03	1.03	1.03	1.03	1.03	1.03
Hogging moment										
10	1.03	1.03	1.03	1.03	1.03	1.02	1.02	1.03	1.03	1.03
20	1.03	1.03	1.04	1.03	1.03	1.03	1.03	1.03	1.03	1.03
30	1.03	1.03	1.03	1.04	1.02	1.04	1.03	1.03	1.04	1.03
40	1.03	1.03	1.04	1.03	1.02	1.04	1.03	1.04	1.03	1.03
50	1.03	1.04	1.03	1.02	1.02	1.05	1.04	1.04	1.02	1.02
Shear force										
10	1.03	1.03	1.04	1.04	1.04	1.04	1.03	1.03	1.04	1.03
20	1.04	1.04	1.04	1.04	1.04	1.04	1.03	1.04	1.04	1.04
30	1.03	1.04	1.04	1.04	1.04	1.03	1.04	1.04	1.04	1.04
40	1.03	1.03	1.04	1.03	1.03	1.03	1.03	1.03	1.03	1.04
50	1.03	1.04	1.04	1.03	1.03	1.03	1.03	1.04	1.03	1.04

Table B.25. Reliability based partial factor γ_q. Design 40 years reference period.

Span length (m)	ADTT (veh/day)					Long vehicles (%)				
	100	500	1000	2000	4000	5	25	50	87.5	100
Sagging moment										
10	1.04	1.04	1.05	1.04	1.04	1.04	1.04	1.04	1.04	1.03
20	1.04	1.04	1.04	1.04	1.04	1.04	1.04	1.04	1.04	1.04
30	1.03	1.04	1.04	1.04	1.04	1.03	1.04	1.04	1.04	1.04
40	1.03	1.04	1.04	1.04	1.04	1.03	1.04	1.04	1.04	1.04
50	1.03	1.04	1.04	1.04	1.04	1.03	1.04	1.04	1.04	1.04
Hogging moment										
10	1.03	1.03	1.03	1.03	1.03	1.03	1.03	1.03	1.03	1.03
20	1.03	1.04	1.04	1.04	1.04	1.03	1.03	1.04	1.04	1.04
30	1.03	1.03	1.03	1.04	1.03	1.04	1.03	1.03	1.04	1.03
40	1.03	1.04	1.04	1.03	1.02	1.05	1.04	1.04	1.03	1.03
50	1.04	1.04	1.04	1.02	1.02	1.05	1.04	1.05	1.02	1.02
Shear force										
10	1.04	1.04	1.04	1.04	1.04	1.04	1.04	1.03	1.04	1.04
20	1.04	1.04	1.04	1.04	1.04	1.04	1.04	1.04	1.04	1.04
30	1.03	1.04	1.04	1.04	1.04	1.04	1.04	1.04	1.04	1.04
40	1.03	1.04	1.04	1.04	1.04	1.03	1.04	1.04	1.04	1.04
50	1.03	1.04	1.04	1.04	1.04	1.03	1.04	1.04	1.04	1.04

Table B.26. Reliability based partial factor γ_q. Design 30 years reference period.

Span length (m)	ADTT (veh/day)					Long vehicles (%)				
	100	500	1000	2000	4000	5	25	50	87.5	100
Sagging moment										
10	1.05	1.05	1.05	1.05	1.05	1.04	1.04	1.04	1.05	1.04
20	1.04	1.05	1.05	1.04	1.05	1.04	1.04	1.04	1.04	1.04
30	1.04	1.05	1.05	1.04	1.04	1.04	1.05	1.04	1.04	1.05
40	1.04	1.04	1.05	1.04	1.04	1.04	1.04	1.04	1.04	1.04
50	1.03	1.04	1.05	1.04	1.04	1.03	1.04	1.04	1.04	1.04
Hogging moment										
10	1.03	1.03	1.04	1.04	1.03	1.03	1.03	1.03	1.04	1.03
20	1.03	1.04	1.05	1.04	1.04	1.04	1.04	1.04	1.04	1.04
30	1.03	1.04	1.03	1.05	1.03	1.05	1.04	1.03	1.05	1.04
40	1.04	1.04	1.05	1.03	1.03	1.06	1.04	1.05	1.03	1.03
50	1.04	1.05	1.04	1.03	1.02	1.06	1.05	1.05	1.03	1.03
Shear force										
10	1.04	1.04	1.05	1.05	1.05	1.05	1.04	1.04	1.05	1.04
20	1.05	1.05	1.05	1.05	1.05	1.05	1.04	1.05	1.05	1.05
30	1.04	1.05	1.05	1.05	1.05	1.04	1.05	1.05	1.05	1.05
40	1.04	1.04	1.05	1.04	1.04	1.04	1.04	1.04	1.04	1.05
50	1.04	1.05	1.05	1.04	1.04	1.04	1.04	1.05	1.04	1.05

Table B.27. Reliability based partial factor γ_q. Design 20 years reference period.

Span length (m)	ADTT (veh/day)					Long vehicles (%)				
	100	500	1000	2000	4000	5	25	50	87.5	100
	Sagging moment									
10	1.06	1.06	1.06	1.06	1.06	1.05	1.05	1.05	1.06	1.04
20	1.05	1.05	1.06	1.05	1.05	1.05	1.05	1.05	1.05	1.05
30	1.05	1.05	1.06	1.05	1.05	1.04	1.05	1.05	1.05	1.05
40	1.04	1.05	1.06	1.05	1.05	1.04	1.05	1.05	1.05	1.05
50	1.04	1.05	1.06	1.05	1.05	1.04	1.05	1.05	1.05	1.05
	Hogging moment									
10	1.04	1.04	1.04	1.04	1.04	1.04	1.04	1.04	1.04	1.04
20	1.04	1.05	1.05	1.05	1.05	1.04	1.05	1.05	1.05	1.05
30	1.04	1.04	1.04	1.05	1.04	1.06	1.04	1.04	1.05	1.04
40	1.05	1.05	1.06	1.04	1.03	1.07	1.05	1.06	1.04	1.04
50	1.05	1.06	1.05	1.03	1.02	1.07	1.06	1.06	1.03	1.03
	Shear force									
10	1.05	1.05	1.05	1.06	1.05	1.04	1.04	1.04	1.04	1.04
20	1.05	1.06	1.06	1.06	1.06	1.04	1.05	1.05	1.05	1.05
30	1.05	1.05	1.06	1.06	1.06	1.06	1.04	1.04	1.05	1.04
40	1.04	1.05	1.06	1.05	1.05	1.07	1.05	1.06	1.04	1.04
50	1.04	1.05	1.06	1.05	1.05	1.07	1.06	1.06	1.03	1.03

Table B.28. Reliability based partial factor γ_q. Design 10 years reference period.

Span length (m)	ADTT (veh/day)					Long vehicles (%)				
	100	500	1000	2000	4000	5	25	50	87.5	100
Sagging moment										
10	1.07	1.07	1.08	1.07	1.07	1.06	1.06	1.06	1.07	1.06
20	1.06	1.07	1.07	1.07	1.07	1.07	1.07	1.06	1.07	1.07
30	1.06	1.07	1.07	1.07	1.07	1.06	1.07	1.07	1.07	1.07
40	1.05	1.07	1.07	1.07	1.07	1.05	1.07	1.07	1.07	1.07
50	1.05	1.07	1.07	1.06	1.06	1.05	1.07	1.06	1.06	1.06
Hogging moment										
10	1.05	1.05	1.05	1.05	1.05	1.04	1.05	1.05	1.05	1.05
20	1.05	1.06	1.07	1.06	1.06	1.06	1.06	1.06	1.06	1.06
30	1.05	1.05	1.05	1.07	1.05	1.08	1.06	1.05	1.07	1.06
40	1.06	1.06	1.08	1.05	1.04	1.09	1.07	1.07	1.05	1.05
50	1.07	1.07	1.07	1.04	1.03	1.09	1.07	1.08	1.04	1.04
Shear force										
10	1.06	1.07	1.07	1.07	1.07	1.07	1.06	1.06	1.07	1.06
20	1.07	1.07	1.07	1.07	1.07	1.07	1.07	1.07	1.07	1.07
30	1.06	1.07	1.08	1.07	1.07	1.06	1.07	1.07	1.07	1.07
40	1.05	1.06	1.07	1.07	1.07	1.05	1.06	1.07	1.07	1.07
50	1.05	1.07	1.07	1.07	1.06	1.06	1.07	1.07	1.07	1.07

Table B.29. Reliability based partial factor γ_q. Assessment 50 years reference period.

Span length (m)	ADTT (veh/day)					Long vehicles (%)				
	100	500	1000	2000	4000	5	25	50	87.5	100
	Sagging moment									
10	0.98	0.98	0.98	0.98	0.98	0.98	0.98	0.98	0.98	0.99
20	0.98	0.98	0.98	0.98	0.98	0.98	0.98	0.98	0.98	0.98
30	0.99	0.98	0.98	0.98	0.98	0.99	0.98	0.98	0.98	0.98
40	0.99	0.98	0.98	0.98	0.98	0.99	0.98	0.98	0.98	0.98
50	0.99	0.98	0.98	0.98	0.98	0.99	0.98	0.98	0.98	0.98
	Hogging moment									
10	0.99	0.99	0.99	0.99	0.99	0.99	0.99	0.99	0.99	0.99
20	0.99	0.98	0.98	0.98	0.98	0.99	0.99	0.98	0.98	0.98
30	0.99	0.99	0.99	0.98	0.99	0.98	0.99	0.99	0.98	0.99
40	0.99	0.99	0.98	0.99	0.98	0.98	0.98	0.98	0.99	0.99
50	0.98	0.98	0.98	0.99	0.98	0.98	0.98	0.98	0.99	0.99
	Shear force									
10	0.98	0.98	0.98	0.98	0.98	0.98	0.98	0.99	0.98	0.98
20	0.98	0.98	0.98	0.98	0.98	0.98	0.98	0.98	0.98	0.98
30	0.99	0.98	0.98	0.98	0.98	0.98	0.98	0.98	0.98	0.98
40	0.99	0.98	0.98	0.98	0.98	0.99	0.98	0.98	0.98	0.98
50	0.99	0.98	0.98	0.98	0.98	0.99	0.98	0.98	0.98	0.98

Table B.30. Reliability based partial factor γ_q. Assessment 40 years reference period.

Span length (m)	ADTT (veh/day)					Long vehicles (%)				
	100	500	1000	2000	4000	5	25	50	87.5	100
Sagging moment										
10	0.99	0.99	0.99	0.99	0.99	0.99	0.99	0.99	0.99	0.99
20	0.99	0.99	0.99	0.99	0.99	0.99	0.99	0.99	0.99	0.99
30	0.99	0.99	0.99	0.99	0.99	0.99	0.99	0.99	0.99	0.99
40	0.99	0.99	0.99	0.99	0.99	0.99	0.99	0.99	0.99	0.99
50	0.99	0.99	0.99	0.99	0.99	0.99	0.99	0.99	0.99	0.99
Hogging moment										
10	0.99	0.99	0.99	0.99	0.99	0.99	0.99	0.99	0.99	0.99
20	0.99	0.99	0.99	0.99	0.99	0.99	0.99	0.99	0.99	0.99
30	0.99	0.99	0.99	0.99	0.99	0.99	0.99	0.99	0.99	0.99
40	0.99	0.99	0.99	0.99	0.99	0.98	0.99	0.99	0.99	0.99
50	0.99	0.99	0.99	0.99	0.99	0.98	0.99	0.98	0.99	0.99
Shear force										
10	0.99	0.99	0.99	0.99	0.99	0.99	0.99	0.99	0.99	0.99
20	0.99	0.99	0.99	0.99	0.99	0.99	0.99	0.99	0.99	0.99
30	0.99	0.99	0.99	0.99	0.99	0.99	0.99	0.99	0.99	0.99
40	0.99	0.99	0.99	0.99	0.99	0.99	0.99	0.99	0.99	0.99
50	0.99	0.99	0.99	0.99	0.99	0.99	0.99	0.99	0.99	0.99

Table B.31. Reliability based partial factor γ_q. Assessment 30 years reference period.

Span length (m)	ADTT (veh/day)					Long vehicles (%)				
	100	500	1000	2000	4000	5	25	50	87.5	100
	Sagging moment									
10	0.99	0.99	0.99	0.99	0.99	0.99	0.99	0.99	0.99	0.99
20	0.99	0.99	0.99	0.99	0.99	0.99	0.99	0.99	0.99	0.99
30	0.99	0.99	0.99	0.99	0.99	0.99	0.99	0.99	0.99	0.99
40	0.99	0.99	0.99	0.99	0.99	0.99	0.99	0.99	0.99	0.99
50	0.99	0.99	0.99	0.99	0.99	0.99	0.99	0.99	0.99	0.99
	Hogging moment									
10	0.99	0.99	0.99	0.99	0.99	1.00	0.99	0.99	0.99	0.99
20	0.99	0.99	0.99	0.99	0.99	0.99	0.99	0.99	0.99	0.99
30	0.99	0.99	0.99	0.99	0.99	0.99	0.99	0.99	0.99	0.99
40	0.99	0.99	0.99	0.99	1.00	0.99	0.99	0.99	0.99	0.99
50	0.99	0.99	0.99	1.00	1.00	0.99	0.99	0.99	1.00	1.00
	Shear force									
10	0.99	0.99	0.99	0.99	0.99	0.99	0.99	0.99	0.99	0.99
20	0.99	0.99	0.99	0.99	0.99	0.99	0.99	0.99	0.99	0.99
30	0.99	0.99	0.99	0.99	0.99	0.99	0.99	0.99	0.99	0.99
40	0.99	0.99	0.99	0.99	0.99	0.99	0.99	0.99	0.99	0.99
50	0.99	0.99	0.99	0.99	0.99	0.99	0.99	0.99	0.99	0.99

Table B.32. Reliability based partial factor γ_q. Assessment 20 years reference period.

Span length (m)	ADTT (veh/day)					Long vehicles (%)				
	100	500	1000	2000	4000	5	25	50	87.5	100
Sagging moment										
10	1.00	1.00	1.00	1.00	1.00	1.00	1.00	1.00	1.00	1.00
20	1.00	1.00	1.00	1.00	1.00	1.00	1.00	1.00	1.00	1.00
30	1.00	1.00	1.00	1.00	1.00	1.00	1.00	1.00	1.00	1.00
40	1.00	1.00	1.00	1.00	1.00	1.00	1.00	1.00	1.00	1.00
50	1.00	1.00	1.00	1.00	1.00	1.00	1.00	1.00	1.00	1.00
Hogging moment										
10	1.00	1.00	1.00	1.00	1.00	1.00	1.00	1.00	1.00	1.00
20	1.00	1.00	1.00	1.00	1.00	1.00	1.00	1.00	1.00	1.00
30	1.00	1.00	1.00	1.00	1.00	1.00	1.00	1.00	1.00	1.00
40	1.00	1.00	1.00	1.00	1.00	1.00	1.00	1.00	1.00	1.00
50	1.00	1.00	1.00	1.00	1.00	1.00	1.00	1.00	1.00	1.00
Shear force										
10	1.00	1.00	1.00	1.00	1.00	1.00	1.00	1.00	1.00	1.00
20	1.00	1.00	1.00	1.00	1.00	1.00	1.00	1.00	1.00	1.00
30	1.00	1.00	1.00	1.00	1.00	1.00	1.00	1.00	1.00	1.00
40	1.00	1.00	1.00	1.00	1.00	1.00	1.00	1.00	1.00	1.00
50	1.00	1.00	1.00	1.00	1.00	1.00	1.00	1.00	1.00	1.00

Table B.33. Reliability based partial factor γ_q. Assessment 10 years reference period.

Span length (m)	ADTT (veh/day)					Long vehicles (%)				
	100	500	1000	2000	4000	5	25	50	87.5	100
Sagging moment										
10	1.01	1.01	1.02	1.02	1.02	1.01	1.01	1.01	1.02	1.01
20	1.01	1.01	1.02	1.01	1.01	1.01	1.01	1.01	1.01	1.01
30	1.01	1.01	1.02	1.01	1.01	1.01	1.01	1.01	1.01	1.01
40	1.01	1.01	1.01	1.01	1.01	1.01	1.01	1.01	1.01	1.01
50	1.01	1.01	1.01	1.01	1.01	1.01	1.01	1.01	1.01	1.01
Hogging moment										
10	1.01	1.01	1.01	1.01	1.01	1.01	1.01	1.01	1.01	1.01
20	1.01	1.01	1.01	1.01	1.01	1.01	1.01	1.01	1.01	1.01
30	1.01	1.01	1.01	1.01	1.01	1.02	1.01	1.01	1.01	1.01
40	1.01	1.01	1.02	1.01	1.01	1.02	1.01	1.02	1.01	1.01
50	1.01	1.02	1.01	1.01	1.01	1.02	1.02	1.02	1.01	1.01
Shear force										
10	1.01	1.01	1.01	1.01	1.01	1.01	1.01	1.01	1.01	1.01
20	1.01	1.01	1.02	1.02	1.02	1.02	1.01	1.01	1.02	1.01
30	1.01	1.01	1.02	1.01	1.01	1.01	1.01	1.01	1.01	1.02
40	1.01	1.01	1.02	1.01	1.01	1.01	1.01	1.01	1.01	1.01
50	1.01	1.01	1.02	1.01	1.01	1.01	1.01	1.01	1.01	1.01

B.7 Reliability analysis

The values of the variables used in the reliability analysis in Section 7.6 are detailed in the following tables. Values from in are also used in the first FORM analysis to evaluate the importance of the uncertainties. The resulting sensitivity factors from the FORM analysis in Section 7.6.2 are shown in Table B.37.

Table B.34. Properties of variables in FORM verification scenario 1.

Scenario 1: 500 veh/day 25% long	Span length (m)	Distribution E_Q	$\mu\ (E_Q)$	$CV\ (E_Q)$	γ_Q^*	γ_e	LF_1	LF_2	LF_3	E_{kd}	β
Sagging	10	Gumbel	1033	0.05	1.14	1.01	0.92	0.89	0.55	2420	1.83
	20	Gumbel	2864	0.05	1.14	1.01	0.93	0.94	0.55	6489	2.12
	30	Gumbel	5643	0.04	1.14	1.01	0.93	0.93	0.60	11870	2.24
	40	Gumbel	8492	0.03	1.14	1.01	0.93	0.92	0.58	18564	2.21
	50	Gumbel	11374	0.03	1.14	1.01	0.93	0.92	0.55	26570	2.34
Shear	10	Gumbel	449	0.04	1.14	1.01	0.93	0.92	0.55	1001	1.81
	20	Gumbel	704	0.05	1.14	1.01	0.94	0.92	0.66	1329	2.03
	30	Gumbel	835	0.04	1.14	1.01	0.93	0.92	0.66	1592	2.11
	40	Gumbel	886	0.03	1.14	1.01	0.93	0.92	0.60	1863	2.18
	50	Gumbel	967	0.03	1.14	1.01	0.93	0.92	0.58	2131	2.29
Hogging	10	Gumbel	761	0.03	1.14	1.01	0.91	0.91	0.67	1426	1.80
	20	Gumbel	1875	0.03	1.14	1.01	0.92	0.91	0.56	4219	1.95
	30	Gumbel	3044	0.07	1.14	1.01	0.86	0.87	0.53	8312	1.86
	40	Gumbel	4603	0.08	1.14	1.01	0.84	0.85	0.54	13716	2.14
	50	Gumbel	6509	0.06	1.14	1.01	0.88	0.87	0.48	20429	2.42

Table B.35. Variables in FORM verification scenario 2.

Scenario 2: 100 veh/day 87% long	Span length (m)	Distribution E_Q	$\mu(E_Q)$	$CV\ (E_Q)$	γ_Q^*	γ_e	LF_1	LF_2	LF_3	E_{kd}	β
Sagging	10	Gumbel	1083	0.05	1.22	1.01	0.89	1	0.55	2420	2.69
	20	Gumbel	2921	0.05	1.22	1.01	0.89	1	0.55	6489	2.62
	30	Gumbel	5861	0.05	1.22	1.01	0.88	1	0.6	11870	2.56
	40	Gumbel	8823	0.04	1.22	1.01	0.87	1	0.58	18564	2.53
	50	Gumbel	11824	0.04	1.22	1.01	0.87	1	0.55	26570	2.69
Shear	10	Gumbel	464	0.05	1.22	1.01	0.9	1	0.55	1001	2.54
	20	Gumbel	737	0.05	1.22	1.01	0.92	1	0.66	1329	2.69
	30	Gumbel	873	0.05	1.22	1.01	0.89	1	0.66	1592	2.58
	40	Gumbel	928	0.04	1.22	1.01	0.88	1	0.6	1863	2.54
	50	Gumbel	1014	0.04	1.22	1.01	0.88	1	0.58	2131	2.61
Hogging	10	Gumbel	792	0.03	1.22	1.01	0.88	1	0.67	1426	2.68
	20	Gumbel	1955	0.04	1.22	1.01	0.87	1	0.56	4219	2.5
	30	Normal	3491	0.04	1.22	1.01	0.83	1	0.53	8312	2.44
	40	Normal	5458	0.04	1.22	1.01	0.8	1	0.54	13716	2.71
	50	Gumbel	7256	0.05	1.22	1.01	0.83	1	0.48	20429	2.89

Table B.36. Variables in FORM verification scenario 3.

Scenario 3: 2000 veh/day 87% long	Span length (m)	E_Q	$\mu\ (E_Q)$	$CV\ (E_Q)$	γ_Q^*	γ_e	LF_1	LF_2	LF_3	E_{kd}	β	θ_t	$\mu\ (\theta_t)$	$CV\ (\theta_t)$
Sagging	10	Gumbel	1298	0.05	1.17	1.01	1	1	0.59	2420	2.35	Neg. Gumb.	1407	0.009
	20	Gumbel	3453	0.04	1.17	1.01	1	1	0.58	6489	2.40	Neg. Gumb.	3797	0.009
	30	Gumbel	6934	0.04	1.17	1.01	1	1	0.64	11870	2.40	Neg. Gumb.	7535	0.008
	40	Gumbel	10482	0.04	1.17	1.01	1	1	0.62	18564	2.39	Neg. Gumb.	11505	0.008
	50	Gumbel	14019	0.03	1.17	1.01	1	1	0.58	26570	2.50	Neg. Gumb.	15369	0.009
Shear	10	Gumbel	536	0.05	1.17	1.01	1	1	0.58	1001	2.32	Neg. Gumb.	577	0.009
	20	Gumbel	852	0.05	1.17	1.01	1	1	0.7	1329	2.39	Neg. Gumb.	934	0.008
	30	Gumbel	1019	0.05	1.17	1.01	1	1	0.7	1592	2.41	Neg. Gumb.	1117	0.007
	40	Gumbel	1096	0.04	1.17	1.01	1	1	0.64	1863	2.35	Neg. Gumb.	1190	0.008
	50	Gumbel	1194	0.04	1.17	1.01	1	1	0.61	2131	2.37	Neg. Gumb.	1300	0.007
Hogging	10	Gumbel	933	0.03	1.17	1.01	1	1	0.7	1426	2.30	Neg. Gumb.	998	0.006
	20	Gumbel	2308	0.04	1.17	1.01	1	1	0.59	4219	2.29	Neg. Gumb.	2499	0.008
	30	Gumbel	4281	0.05	1.17	1.01	1	1	0.56	8312	2.36	Neg. Gumb.	4636	0.015
	40	Gumbel	7164	0.04	1.17	1.01	1	1	0.56	13716	2.35	Neg. Gumb.	7682	0.008
	50	Gumbel	9596	0.03	1.17	1.01	1	1	0.5	20429	2.24	Neg. Gumb.	10114	0.006

The statistical uncertainty in the determination of the load effects θ_e is modelled in every case a Normal distribution with mean $\mu = 1$ and coefficient of variation $CV = 0.02$ as indicated previously in Section 7.1.

Table B.37. Sensitivity factors from FORM analysis.

Loading CV=0.02	α sensitivity factors										
κ	θ_R	d	A_s	f_y	$\theta_{E,G}$	E_G	$\theta_{E,Q}$	E_Q	α_Q	α_G	α_R
0.30	0.50	0.17	0.17	0.51	-0.15	-0.11	-0.61	-0.13	-0.63	-0.19	0.75
0.40	0.52	0.18	0.18	0.53	-0.22	-0.16	-0.55	-0.12	-0.56	-0.27	0.79
0.50	0.54	0.18	0.19	0.54	-0.28	-0.21	-0.46	-0.10	-0.47	-0.35	0.81
0.60	0.55	0.19	0.19	0.55	-0.35	-0.26	-0.36	-0.07	-0.36	-0.44	0.82
0.70	0.55	0.19	0.19	0.55	-0.41	-0.31	-0.25	-0.05	-0.26	-0.51	0.82
0.80	0.54	0.18	0.19	0.54	-0.45	-0.34	-0.15	-0.03	-0.16	-0.57	0.81
Loading CV=0.06	α sensitivity factors										
κ	θ_R	d	A_s	f_y	$\theta_{E,G}$	E_G	$\theta_{E,Q}$	E_Q	α_Q	α_G	α_R
0.30	0.42	0.14	0.14	0.42	-0.12	-0.09	-0.52	-0.56	-0.76	-0.15	0.63
0.40	0.45	0.15	0.16	0.45	-0.18	-0.13	-0.49	-0.51	-0.70	-0.22	0.68
0.50	0.49	0.17	0.17	0.49	-0.25	-0.19	-0.43	-0.41	-0.60	-0.31	0.74
0.60	0.53	0.18	0.18	0.53	-0.34	-0.25	-0.34	-0.28	-0.45	-0.42	0.79
0.70	0.54	0.18	0.19	0.54	-0.41	-0.31	-0.24	-0.17	-0.29	-0.51	0.81
0.80	0.54	0.18	0.19	0.54	-0.46	-0.35	-0.15	-0.09	-0.17	-0.57	0.80

$$\alpha_Q = \sqrt{{\alpha_{EQ}}^2 + {\alpha_{\theta EQ}}^2}; \quad \alpha_G = \sqrt{{\alpha_{EG}}^2 + {\alpha_{\theta EG}}^2}; \quad \alpha_R = \sqrt{{\alpha_{\theta R}}^2 + {\alpha_d}^2 + {\alpha_{A_s}}^2 + {\alpha_{f_y}}^2};$$